

# Highly Reactive Beryllium and Bismuth Complexes: Structure Analysis, Chemical Bonding, and Redox Chemistry

Jacob E. Walley

B.S. Chemistry, Gardner-Webb University, 2017

A Dissertation presented to the Graduate Faculty  
of the University of Virginia in Candidacy for the degree of  
Doctor of Philosophy

Department of Chemistry

University of Virginia  
October 2021

## Abstract

The field of catalysis is dominated by transition metals. In industry, these metals are often used as catalysts for the transformation of simple small molecules into value-added commodities. Many of these catalytic systems feature expensive and geologically scarce precious metals such as platinum, palladium, rhodium, and iridium. Therefore, there is a growing synthetic effort to develop the chemistry of geologically abundant and inexpensive main-group elements. Such well-defined processes are difficult to many main-group elements, thus mimicking the reactivity of transition metals is an enormous synthetic challenge. Access to *d*-orbitals allows for multiple coordination sites and variable redox states for transition metals, while main-group elements are limited to *s*- and *p*-orbitals. Therefore, it is important to study fundamental reaction pathways for main-group elements to discover chemistry that both mimics and diverges those known for transition metals. Herein, beryllium and bismuth chemistry is studied through the scope of neutral carbene and carbene ligands. This research uses a neutral carbon-based ligand (i.e., carbenes and carbenes) scaffolding as an approach to develop new bonding modes, oxidation states, and reactivity for main-group elements.

Beryllium, the lightest member of the alkaline earth series, is one of the least explored elements on the periodic table. This is, in part, due to the presumed toxicity of its complexes. Nevertheless, studying beryllium is important for developing a better understanding of periodic trends and synthetic strategies for the alkaline earth elements. Chapter 2 discusses the isolation and study of the first examples of carbodicarbene beryllium complexes. The isolation of these compounds led to the first example of a beryllium mediated C(sp<sup>3</sup>)-H activation event, which is promoted by either a base or a one-electron reducing agent. A new class of five-membered beryllacycles was also developed, and the coordination chemistry of carbenes led to the first example of a

beryllacycle ring-expansion reaction mechanism. A series of carbene-beryllium complexes were also developed and is discussed in chapter 3. These include carbene-supported aryl- and alk-oxo beryllium complexes and doubly reduced carbene-beryllium( $\alpha$ -diamide) molecules.

The chemistry of bismuth has exhibited a remarkable transition-metal-like reactivity profile in recent years. For example, bismuth is capable of both Bi(III/V) and Bi(I/III) redox cycles. Chemists are also interested in bismuth cations for their applications in Lewis acid catalysis. In chapter 4, a new class of bismuth cations (bismaalkene cations) were developed by the complexation of carbodicarbene, followed by halide abstractions. These molecules were studied using X-ray crystallography, NMR spectroscopy, and DFT to investigate the bonding. In chapter 5, the first reactions of organometallic bismuth complexes with sodium 2-phosphaethynolate, the P-analogue of cyanate, were studied. In this study, carbene transfer and thermal reduction of the bismuth center (Bi<sup>III</sup> to Bi<sup>II</sup>) was observed. The same reactivity profile was observed for analogous antimony complexes.

## Copyright Information

Chapters 1–5 contain modified versions of published work which have been reproduced in accordance with the American Chemical Society Journal Publishing Agreement, John Wiley and Sons Publication Agreement, Royal Society of Chemistry Publication Agreement, MDPI Publication Agreement, and De Gruyter Publication Agreement. Proper citation for each chapter is given below and on the first page of each of the chapters within this thesis.

### Chapter 1:

- Walley, J. E.; Gilliard, R. J., *EIBC* **2021**. Accepted and Pending Publication.

### Chapter 2:

- Walley, J. E.; Breiner, G.; Wang, G.; Dickie, D. A.; Molino, A.; Dutton, J. L.; Wilson, D. J. D.; Gilliard, J. R. J., *Chem. Commun.* **2019**, 55, 1967-1970. DOI: [10.1039/c8cc10022e](https://doi.org/10.1039/c8cc10022e)
- Walley, J. E.; Obi, A. D.; Breiner, G.; Wang, G.; Dickie, D. A.; Molino, A.; Dutton, J. L.; Wilson, D. J. D.; Gilliard, R. J., Jr., *Inorg. Chem.* **2019**, 58, 11118-11126. DOI: [10.1021/acs.inorgchem.9b01643](https://doi.org/10.1021/acs.inorgchem.9b01643)
- Walley, J. E.; Dickie, D. A.; Gilliard, R. J., *Z. Naturforsch. B* **2020**, 75, 497. DOI: [10.1515/znb-2020-0033/html](https://doi.org/10.1515/znb-2020-0033/html)

### Chapter 3:

- Freeman, L. A.; Walley, J. E.; Obi, A. D.; Wang, G.; Dickie, D. A.; Molino, A.; Wilson, D. J. D.; Gilliard, R. J., Jr., *Inorg. Chem.* **2019**, 58, 10554-10568. DOI: [10.1515/znb-2020-0033/html](https://doi.org/10.1515/znb-2020-0033/html)
- Walley, J. E.; Wong, Y. -O.; Freeman, L. A.; Dickie, D. A.; Gilliard, R. J., Jr. *Catalysts* **2019**, 9, 934. DOI: [10.3390/catal9110934](https://doi.org/10.3390/catal9110934)

#### Chapter 4:

- Walley, J. E.; Warring, L.; Wang, G.; Dickie, D. A.; Pan, S.; Frenking, G.; Gilliard, R. J., *Angew. Chem., Int. Ed.* **2021**, *60*, 6682-6690. [DOI: 10.1002/anie.202014398](https://doi.org/10.1002/anie.202014398)

#### Chapters 5:

- Walley, J. E.; Warring, L. S.; Kertesz, E.; Wang, G.; Dickie, D. A.; Benko, Z.; Gilliard, R. J., Jr., *Inorg. Chem.* **2021**, *60*, 4733-4743. [DOI: 10.1021/acs.inorgchem.0c03683](https://doi.org/10.1021/acs.inorgchem.0c03683)

## **Acknowledgements**

To my friends Kyle Cooper and Chris Coffey, college would have not been the same without you guys. Kyle, we have been through so much together. I have known you since 7th grade and we have been friends since the 9th grade. We share so many memories. I remember playing cards with you, Thomas, Jarrett, Gurwinder, a few other guys, and we would gamble things like twinkies, Debbie cakes, and cheese danishes. You, Thomas, and I would get our guitars and go jam for hours on the weekend. My favorite aspect about our friendship is how we can always find humor in whatever we are doing! Even when I threw you under the bus senior year of high school in anatomy and physiology (you know what I'm referring to). After starting our freshmen year at Gardner-Webb, we eventually met Chris Coffey. I remember my first interaction with you, Chris. I was playing my guitar with our dorm room open and Chris came walking by and poked his head in. He said something on the lines of "Hey, you play guitar too! We should jam sometime." All three of us started hanging out more and more and we would jam together. We even wrote a few songs and made some music videos. I had so much fun in college and have so many wonderful memories and they are all thanks to you two. You are some of the best men that I have ever had the pleasure of knowing.

Throughout elementary and middle school, I was very much regarded as trouble to my teachers. I made it an effort to hang out with people who were disruptive because I thought it was cool to be the class clown. Towards the end of the eighth grade, I remember that I was on the verge of being expelled from my school based on something horrible that I did not do, but I was in the wrong place at the wrong time. The person who did this horrible thing blamed me and the school administration tried to expel me based on the fact that they did not want to believe me. The high school principal at the time (Dr. Becky Friend) came to ask me about this incident and I am so

lucky that she had faith in my word that I did not do it and gave me the chance I desperately needed. Once high school started, I made an effort to focus more on my studies and stay out of trouble. Although, I still hung out with the wrong people and found myself in trouble and Dr. Friend's office at times. Instead of getting me into serious trouble, she would give me the second chance that I needed. To Dr. Becky Friend, I am so grateful to you for giving me all the second chances and believing in me when I needed it.

To my high school chemistry teacher, the late Mr. Bryson. Thank you so much for sparking my interest in chemistry. Before taking your class, I had virtually zero chemical knowledge of chemistry, but you sparked my interest. While taking your class, I became driven to excel and was excited to learn new concepts. I ended up doing so well, that you allowed me to teach the next semester's chemistry course under the supervision of a teacher. This opportunity gave me a solid foundation of general chemistry knowledge that set me up to excel in my general chemistry classes in college. I am greatly appreciative of all you have done for me.

To my chemistry professors at Gardner-Webb University, thank you all so much for preparing me to take on the challenges of graduate school. At the beginning of my undergraduate career at Gardner-Webb, graduate school was not even on my radar, I was considering going into nursing or PA school. I remember having a conversation with Dr. Totten about graduate school and that changed my entire perspective. I was shocked when you told me that you get paid, being paid to go to school seemed like a wild thought to me at the time. Funny enough, now I have the perspective that graduate students are underpaid! After attending an REU program, I was for sure going to graduate school, I just needed to decide on a subject. Dr. Brooks made this easy, I thoroughly enjoyed your inorganic chemistry class (as well as your organic chemistry classes) and had a strong desire to further study the subject. I am so grateful that you encouraged me to apply

to UVA, I would never have been here if it was not for you. Dr. Eddins, though I never got to take your environmental chemistry class, you helped me so much with writing applications for both my REU and for graduate school. I remember spending hours rewriting drafts until you gave me the thumbs up. You helped me put my best foot forward and I am so grateful for that.

To my Principal Investigator, Prof. Robert J. Gilliard, Jr., graduate school has been some of the most difficult years of my life, but joining your group was one of the best decisions I have made. There is no assortment of words that I can use to portray how grateful I am towards you. You have truly made my entire graduate school experience a rich and rewarding one. I remember nearly 4 years ago sitting in your office when I was considering joining your group and you asked me what my goals were. I responded with something on lines of "If this doesn't work out, I will probably try something computational." Despite having little to no synthetic experience and barely knowing what I was doing you still decided to take me on as your graduate student and I am so grateful for that. Not only have you taught me how to be a good scientist, but you have shown me how to be a good leader because you are an exceptional leader. You are 110% invested in all projects and the future of every student you take on. I remember when we were in the big office that has now been renovated, and you would spend a lot of your day in there asking every one of us what we were doing in the lab. You would also slack off and joke around with us, which adds a friendly and fun element to our group. I remember when I was struggling to synthesize the carbodicarbene ligand that we initially agreed upon making, you would come into the lab and get your hands dirty with the reaction to help me figure out the hidden details that weren't discussed in the published procedure. Even though you are becoming increasingly busier over the years because of the great success you have had as a PI, you will still find time to come into the lab and run a reaction with a struggling student and that is an extremely admirable gesture. There are not

many PIs out there that will find the time to do this, but you always make time. Again, thank you so much for always standing by my side and helping me through some of the biggest challenges that I have ever faced. You are truly an amazing person.

To the current members of the Gilliard Lab, it has been an absolute pleasure working alongside you guys, all of you are brilliant scientists and I am so proud to have been a part of this team. To Kelsie and Luke, we are what remains of the first generation of the Gilliard lab, and guess what? We made it! We have pioneered the path towards graduation and that is something to be proud of. It has been a great journey learning, collaborating, and hanging out with you guys. To AC, I have always enjoyed our conversations about chemistry and other things, you always have new ideas and maintain a passion for what you are doing. I appreciate everything you have done to help me with my projects. You have done so well for yourself in graduate school and I am excited to see where you end up on the job market. To the third-year students Levi, Kim, Haleigh, and Caleb, I am very impressed by all of you. Despite the COVID-19 setback, you all have first-author papers which are in the works or about to be published. Kim, I am so impressed with what you have done with the CDC-borafluorene project, this is by far one of the most complicated systems our lab has seen. You have done an outstanding job elucidating the equilibrium process we were observing. Levi, you are one of the best synthetic chemists I have met and it was such a pleasure to work alongside you. I remember the summer you arrived you were doing the base bath one day and I approached you asking if you wanted an easy paper, you said "yeah!" You helped me not with one, but two bismuth papers, these would not have been published so quickly if it wasn't for your efforts. I am so appreciative of your help. To the younger members of the Gilliard Lab, Eric and Nathan, you guys are so bright and I have been impressed with how fast you are grasping things. Keep up the good work, you guys are paving the road for successful careers!

To Guocang Wang (Wilson), it was an absolute luxury to have you in the lab when we all first started. You paved the foundation of chemistry in our laboratory and set all of us up for success, you have been greatly missed ever since you left. I am so appreciative of all your guidance with the beryllium chemistry, even though you would scare me on how toxic the element is. I remember when you showed me how to synthesize beryllium dichloride dietherate, you weighed out 500 mg of Be and said “can kill 100 people” (or something of that nature). When the beryllium project was shut down after a series of unrelated events, you helped me get started on bismuth chemistry before you left. Since then, this project has taken off and we have had two high-quality publications. You were always there to answer my questions, even if they were stupid, and that is exactly what I needed. Thank you so much for all of your guidance!

There are many other people around the chemistry department to whom I owe acknowledgment. To our X-ray crystallographer, Diane Dickie. Crystallography is one of the most interesting aspects of the research we do and learning how to mount crystals and solve them (in some cases) has been a lot of fun. You are such a great teacher and I wish I had the opportunity to take your class. To Dr. Xiaofan Jia and Dr. Nichole Liebov, with being in a new lab, I did not have any older graduate students to look up to and seek guidance, but you guys made yourselves available for us. I am so appreciative of all your encouragement, helping prepare us for candidacy, and helping with chemistry in some cases at the beginning. Your guidance gave me a jumpstart to help me succeed as a graduate student. Kaeleigh, I greatly enjoyed all of our chats in the hall to procrastinate getting back to work. You are so much fun to be around and I will miss hanging out with you!

I have met many good friends and colleagues in my time at the University of Virginia. To my friend Paul Miller, it was not too long after we arrived at UVA that we became friends. I would

say our friendship was started when we were playing Black Ops Zombies daily after work. When we would manage to get ourselves away from the TV, we went for runs. You are someone who always has been there, listens, and knows how to keep a conversation going. You are also a really smart and talented organic chemist, and I am excited for your future at NCSU, you are doing so well! I am grateful to have made such a great friend like you and I am looking forward to more adventures together.

To the game night crew, Snigdha, Paul, Cait, Daniel, Joe, Anna, and Angela, hanging out with you guys and playing board games was so much fun. I thoroughly enjoy all of the social deception games we played! Daniel, I appreciate all that you have done for Snigdha and I, especially agreeing to be the officiant who married us. You are one of the smartest guys I have ever met and it is always a joy talking with you. I must say that when I was first meeting you I was thoroughly impressed with your vast knowledge of alcohol (and just everything in general!). Joe, I believe the first time we met was at the Bebedero when Snigdha introduced me to all of her economics friends. Since then, we would see each other and talk at various parties. Over the past year and a half, we have grown closer through playing video games, which we play nearly every single day. I am always looking forward to playing online and hanging out with you and everyone else at the end of the day. Spending time with everyone in this group of friends is always, without a doubt, so much fun and it has been a huge stress release in this final year of my Ph.D. I am looking forward to more adventures with you guys!

To the undergrad (now recent graduate), Grace Breiner, who I had the pleasure of mentoring. I lucked out on being your mentor, you are so bright and caught on fast to the chemistry we were doing. Because of your efforts put towards synthesizing the carbodicarbene ligand, I was able to focus on the new coordination chemistry and that set us up for success. I am so appreciative

of all your efforts and I am so proud of the scientist that you became. Even though you are no longer pursuing chemistry, you will always find success wherever you are because of your strong work ethic and diligence in your work. I am so proud of you!

To the amazing woman who was responsible for raising me to be the man I am today, my mother. Mom, you have sacrificed so much of your time, money, and energy to make sure I had a bright future. Raising a child by yourself and maintaining a full-time job to keep food on the table is such a difficult task, and I cannot begin to imagine the effort you put forth. I am so grateful for everything you have done, because I know it was all for me. You raised me while you were attending college, we were so poor I remember there were weeks we would eat oatmeal every day because we had nothing else. I remember there was a Christmas charity at Curious Minds where parents would donate gifts for a child in poverty, I was the recipient one year. All this to say that even though we were broke, I never had any clue because any extra penny you had you would usually spend it on something for me. After you graduated, you moved us to my grandparents' house in North Carolina so we could be closer to family. Growing up around my grandparents was an amazing experience. You made sure I went to a good school and got me involved in extracurricular activities (basketball, boy scouts, guitar). Even though our family does not have a big educational background, you always said "when you go to college" and never said "if you go to college," this is such a simple use of language that had a huge impact on my life decision. Thank you for all of your love and support. I appreciate everything you have done for me, mom.

To grandma and papaw, thank you for always being there for me. Whether it be to pick me up from school or to make me dinner, you guys always made time for me and included me in what you were doing. You are the epitome of what grandparents should be and I love both of you so much. To my grandmother, you are full of historical knowledge and are so good at telling me

stories. I have learned so much about American history and the history of our family just by talking to you. Thank you for always feeding me whenever I said I was hungry even if I had already eaten and was just bored. To my late grandfather, I greatly enjoyed all the time we spent together. From simple things like hauling the trash to the dump, to helping you out in the yard, I truly cherish every memory I have with you. I remember going to the wither's place and helping you mop the floors so you could get free steaks, which were amazing by the way. I also enjoyed you picking me up from school every day where we would then proceed to the Brevard station museum to pick up grandma. If she wasn't ready to go, you would cut off all of the lights in the building even if they were still working. I love and miss you so much. Thanks for everything papaw.

While there were so many people that played a role in my life in getting me to graduate school, there is only one person that helped get me through graduate school. To my amazing and gorgeous wife Snigdha Das, thank you for being there for me during the hardest times of graduate school. When my grandfather died, you were there for me. When I was going through my candidacy exam, you were there for me. When I was under pressure from deadlines, you were there for me. Whenever I talk myself down, you are always there to talk me back up. I am so lucky to have snagged a woman like you four years ago, and I am happy to say that these past four years have been the best years of my life. Despite being poor graduate students, we still find time to take vacations and go out and have fun. For instance, our annual pre-COVID New York trips have been nothing less than amazing. I remember our first time in New York, we were walking around central park and sat down on a bench next to an old man playing an accordian. It was such a simple moment, but it felt so good because it was with you, the love of my life. We do not compromise on fun and I love that about us. We have only just started our life together and I am super excited to see what our future has in store for us. I love you so much.

# Table of Contents

Abstract .....	2
Copyright Information .....	4
Acknowledgements .....	6
List of Abbreviations .....	17
List of Figures .....	18
List of Schemes .....	20
List of Tables .....	21
Chapter 1: Introduction .....	22
<b>1.1 Introduction to Beryllium</b> .....	23
<i>1.1.1 Origin and Isolation of Beryllium</i> .....	23
<i>1.1.2 Physical and Chemical Properties of Beryllium</i> .....	24
<i>1.1.3 Applications of Beryllium</i> .....	24
<i>1.1.4 Toxicity of Beryllium</i> .....	25
<i>1.1.5 <sup>9</sup>Be NMR Spectroscopy</i> .....	26
<b>1.2 Introduction to Bismuth</b> .....	27
<i>1.2.1 Origin and Isolation of Bismuth</i> .....	27
<i>1.2.2 Physical and Chemical Properties of Bismuth</i> .....	28
<i>1.2.3 Applications of Bismuth</i> .....	28
<b>1.3 Ligand Design for Main-Group Complexes</b> .....	29
<i>1.3.1 Anionic vs. Neutral Ligands</i> .....	29
<i>1.3.2 Brief History and Electronic Nature of Carbenes and Carbones</i> .....	30
<i>1.3.3 Synthetic Procedure for Carbodicarbene Ligand</i> .....	31
Chapter 2: Carbodicarbene Beryllium Chemistry .....	35
<b>2.1 Introduction to Carbene Beryllium Chemistry</b> .....	36
<i>2.1.1 Synthesis of Monodentate Carbodiphosphorane Beryllium Complexes</i> .....	36
<i>2.1.1 Synthesis of a Tridentate Carbodiphosphorane Beryllium Complex</i> .....	37
<b>2.2 Synthesis of Carbodicarbene-Supported Beryllium Dichloride and Salt Metathesis Reactions</b> .....	38
<i>2.2.1 Synthesis of Carbodicarbene Beryllium Dichloride</i> .....	38
<i>2.1.2 Salt Metathesis Reactions of Carbodicarbene Beryllium Dichloride</i> .....	40

2.1.3 Crystallographic Analysis of Carbodicarbene Beryllium Complexes 2.5 – 2.8.....	42
2.1.4 Theoretical Analysis of Carbodicarbene Beryllium Complexes 2.5 and 2.6.....	44
<b>2.3 Intramolecular CH Activation of (CDC)BeCl[N(SiMe<sub>3</sub>)<sub>2</sub>]</b> .....	47
2.3.1 Beryllium Mediated C(sp <sup>3</sup> )–H Activation and Cyclization Reaction .....	47
2.3.2 Crystallographic Analysis of Carbodicarbene Beryllacycle 2.9 .....	49
2.3.3 <sup>9</sup> Be NMR Comparison of Compounds 2.5, 2.6, and 2.9 .....	50
<b>2.4 Carbodicarbene Beryllacycle and Ring Expansion Chemistry</b> .....	51
2.4.1 Synthesis of Carbodicarbene(Chloro)Beryllacycle 2.10 .....	51
2.4.2 Crystallographic Analysis of Beryllacycle 2.10 .....	52
2.4.3 Carbene Coordination Chemistry to Beryllacycle 2.10 .....	52
2.4.4 <sup>9</sup> Be NMR Analysis of Beryllacycles 2.10 – 2.12 .....	55
2.4.5 Theoretical Analysis for the Ring Expansion Reaction of 2.10 .....	56
<b>2.5 Summary of Carbodicarbene Beryllium Chemistry</b> .....	61
Chapter 3: Carbene Beryllium Chemistry.....	63
<b>3.1 Introduction to Carbene Beryllium Chemistry</b> .....	64
3.1.1 N-Heterocyclic Carbene Beryllium Complexes.....	64
3.1.2 Cyclic(Alkyl)Amino Carbene Beryllium Complexes.....	66
<b>3.2 Carbene-Supported Beryllium Aryl- and Alkoxide Complexes</b> .....	72
3.2.1 Introduction to Alkaline Earth Oxides.....	72
3.2.2 Synthesis and Isolation of Beryllium Aryl- and Alkoxides .....	73
3.2.3 Crystallographic Analysis of Beryllium Aryl- and Alkoxides.....	75
<b>3.3 Reduction of Carbene–Beryllium Dihalides in the Presence of a Redox Non-Innocent Bipyridene</b> .....	77
3.3.1 Introduction to Beryllium Complexes with Redox Non-Innocent Ligands .....	77
3.3.2 Synthesis and Characterization of Double Reduced Carbene-Beryllium Bipyridene Complexes.....	78
3.3.3 Crystallographic Study of Double Reduced Carbene-Beryllium Bipyridene Complexes .....	82
<b>3.4 Summary of Carbene Beryllium Chemistry</b> .....	84
Chapter 4: Carbodicarbene-Stabilized Bismaalkene Cations: Unravelling the Complexities of Carbene versus Carbene in Heavy Pnictogen Chemistry .....	85
<b>4.1 Introduction to Bismuth Cation Chemistry</b> .....	86
4.1.1 Carbene-Bismuth Complexes and other Bismuth Cations .....	86

4.1.2 <i>The Potential of Carbodicarbenes in Pnictaalkene Cation Chemistry</i> .....	88
<b>4.2 Synthesis of NHC-Supported Bismuthenium Complexes</b> .....	90
4.2.1 <i>Synthesis of Carbene-Supported Pseudo Monocations</i> .....	90
4.2.2 <i>Carbene vs Carbone in Stabilizing Phenylbismuth Dichloride</i> .....	92
<b>4.3 Synthesis of CDC-Stabilized Mono-, Di-, and Tri-Positive Bismuthenium Ions</b> .....	95
4.3.1 <i>Synthesis of CDC-Stabilized Phenylbismuth Bismaalkene Mono- and Dications</i> .....	95
4.3.1 <i>Synthesis of CDC-Stabilized Bismaalkene Mono-, Di- and Trications</i> .....	97
<b>4.4 Bonding Analysis of Bismuth and Bismuthenium Complexes</b> .....	102
<b>4.5 Summary of Carbodicarbene Bismaalkene Cations</b> .....	105
Chapter 5: Indirect Access to Carbene Adducts of Bismuth and Antimony Substituted Phosphaketene and their Unusual Thermal Transformation to Dipnictines and [(NHC) <sub>2</sub> OCP][OCP] .....	106
<b>5.1 Introduction to Phosphaketene Chemistry</b> .....	107
5.1.1 <i>The Diverse Reactivity of the 2-Phosphaethynolate Anion</i> .....	107
5.1.2 <i>Select Examples in Main-Group Phosphaketene Chemistry</i> .....	108
<b>5.2 Synthesis of NHC Diphenylpnictogen Halide Complexes</b> .....	110
5.2.1 <i>Synthesis of NHC-Supported Diphenylpnictogen Chloride Dimers</i> .....	110
5.2.2 <i>Crystallographic Analysis of NHC-Supported Diphenylpnictogen Chloride Dimers</i> .....	111
<b>5.3 Isolation of NHC-Phosphaketene Adducts of Diphenylpnictogen</b> .....	112
5.3.1 <i>Reaction of Na[OCP] with NHC-Supported Diphenylpnictogen Chloride Dimers</i> ...	112
5.3.2 <i>Crystallographic Analysis of NHC-Phosphaketene Adducts of Diphenylpnictogen</i> ..	113
<b>5.4 Thermal Reduction at Sb and Bi Centers</b> .....	115
5.4.1 <i>Thermal Reactivity of NHC-Phosphaketene Adducts of Diphenylpnictogen</i> .....	115
5.4.2 <i>Crystallographic Analysis of [(NHC)<sub>2</sub>OCP][OCP]</i> 5.5 .....	116
<b>5.5 Computational Analysis of Thermal Reduction at Sb and Bi</b> .....	117
<b>5.6 Summary of Sb and Bi Thermal Reduction Chemistry</b> .....	123
Appendix 1: Experimental .....	125
Appendix 2: Spectral Data .....	143
Appendix 3: Crystallographic Data .....	207
References .....	240

## List of Abbreviations

Ae	alkaline earth
Pn	pnictogen
LA	Lewis acid
LB	Lewis base
Dipp	2,6-diisopropylphenyl
Mes	mesityl (2,4,6-trimethylphenyl)
NHC	<i>N</i> -heterocyclic carbene
CAAC	cyclic(alkyl)amino carbene
CDC	carbodicarbene
CDP	carbodiphosphorane
sIme	1,3-dimethylimidazolin-2-ylidene
sIPr or <i>IPr</i>	1,3-diisopropylimidazolin-2-ylidene
IPr	1,3-bis(2,6-diisopropylphenyl)imidazolin-2-ylidene
IMes	1,3-bis(2,4,6-trimethylphenyl)imidazolin-2-ylidene
Bpy	2,2'-bipyridine
DAD	diazadiene
OCP <sup>-</sup>	2-phosphaethynolate
M-PCO	metal-phosphaketene
M-OCP	metal-oxyphosphaalkyne
2-py-in	2-(2-pyridyl)indole
(Et <sub>2</sub> O) <sub>2</sub> BeCl <sub>2</sub>	beryllium dichloride dietherate
Ph <sub>2</sub> BiCl	diphenylbismuth chloride
(THF)Bi(Ph)Cl <sub>2</sub>	tetrahydrofuran phenylbismuth dichloride
KC <sub>8</sub>	potassium graphite
K[N(SiMe <sub>3</sub> )]	potassium bis(trimethylsilyl)amide
AgSbF <sub>6</sub>	silver antimony hexafluoride
AgNTf <sub>2</sub>	silver bis(trifluoromethylsulfonyl)amide
THF	tetrahydrofuran
DCM	dichloromethane
ACN	acetonitrile
NMR	nuclear magnetic resonance

IR	infrared
UV-Vis	ultraviolet-visible
RER	ring expansion reaction
TS	transition state
HOMO	highest occupied molecular orbital
LUMO	lowest unoccupied molecular orbital
QTAIM	quantum theory for atoms in molecules
EDA	energy decomposition analysis
CBD	chronic beryllium disease

## List of Figures

**Figure 1.3.1** **A:** One halide abstraction from an anionic NacNac ligand metal halide; **B:** Two halide abstractions from a neutral carbene ligand metal dihalide.

**Figure 1.3.2** Carbenes: *N*-heterocyclic carbene and cyclic(alkyl)(amino) carbene and respective energies of frontier orbitals; carbene: carbodicarbene and respective energies of frontier orbitals.

**Figure 2.1.1** Isolation of carbodiphosphorane beryllium dichloride adducts.

**Figure 2.1.2** Isolation of an s-block–carbon double bond using carbodiphosphorane.

**Figure 2.2.1** Molecular structures of **2.5**, **2.6**, **2.7**, and **2.8**.

**Figure 2.2.2** Plots of the HOMO of **2.5** and **2.6**, indicating a lone pair MO on the central carbene carbon.

**Figure 2.2.3** Plot of EDA-NOCV deformation densities ( $\Delta\rho_1$ ) of the largest sigma donation orbital interaction in **2.5** (left) and **2.6** (right). The charge flows from red to blue.

**Figure 2.3.1** Reaction of pure compound **2.6** reaction with 1 equivalent of  $\text{KC}_8$  at different time intervals.

**Figure 2.3.2** Molecular structure of **2.9**.

**Figure 2.4.1** Molecular structure of **2.10**, **2.11**, and **2.12**.

**Figure 2.4.2** Ring expansion pathway for **2.10** with  $\text{MeNHC}$  and  $\text{MeCAAC}$ . Calculated relative free energies ( $\Delta G$ ,  $\text{kJ mol}^{-1}$ ) at the B3LYP-D3(BJ)/def2-TZVPP/B3LYP-D3(BJ)/def2-SVP (SMD, toluene) level of theory.

**Figure 2.4.3** Plots of HOMO (left) and LUMO (right) of **2.9** (a) and **2.10** (b).

**Figure 2.4.4** Plots of the deformation densities of the interactions for the pair-wise orbital interactions of the two strongest orbital interactions with the associated interaction energies for

(a) theoretical compound **2.13** (interaction between <sup>Me</sup>CAAC and **2.10**), and (b) **TS1b**. Charge flow is from red to blue.

**Figure 3.1.1** Illustration of orbital overlap involved in (CAAC)<sub>2</sub>Be<sup>0</sup>.

**Figure 3.1.2** Bond length comparison for CAAC–Be<sup>II</sup>Cl<sub>2</sub> (top left), [(CAAC)<sub>2</sub>Be<sup>I</sup>]<sup>+</sup> (top right), (CAAC)<sub>2</sub>Be<sup>0</sup> (bottom left), and (CAACH)Be<sup>I</sup>(CAAC) (bottom right).

**Figure 3.2.1** <sup>1</sup>H NMR spectrum (500.13 MHz, C<sub>6</sub>D<sub>6</sub>, 298 K) of compound **3.19** reaction with one equivalent of LiODipp. Free sIPr methine (3.96 ppm).

**Figure 3.2.2** Molecular structure of **3.19**, **3.20**, and **3.21**.

**Figure 3.3.1** **A.** Synthesis of a (DAD)<sub>2</sub>Be complex and equilibrium with THF; **B.** synthesis of an electroluminescent (2-py-in)<sub>2</sub>Be compound.

**Figure 3.3.2** Plot of HOMOs for compound **3.27**<sup>NMe</sup> (left) and **3.28**<sup>NMe</sup> (right).

**Figure 3.3.3** Molecular structures of **3.26**, **3.27**, and **3.28** with H atoms omitted for clarity.

**Figure 4.1.1** Representative examples of bismuth cations (**4.1-4.5**).

**Figure 4.1.2** Structurally characterized examples of neutral and cationic pnictaalkenes.

**Figure 4.2.1** Molecular structures of **4.8**, **4.9**, and **4.10**.

**Figure 4.2.2** Molecular structures of **4.11** and **4.12** (thermal ellipsoids at 50% probability; H atoms omitted for clarity).

**Figure 4.3.1** Molecular structures of **4.13** and **4.14** (thermal ellipsoids at 50% probability; H atoms were omitted for clarity).

**Figure 4.3.2** Molecular structures of **4.15-4.18** (thermal ellipsoids at 50% probability; H atoms, counteranions and non-coordinating solvent omitted for clarity).

**Figure 5.1.1** (A) OCP to OPC rearrangement; (B) phosphine-promoted CO dissociation; (C) Thermal loss of CO from NHC-phosphaketene adducts of triphenyl-germanium or -tin to form NHC-phosphinidenes.

**Figure 5.2.1** Molecular structures of **5.1** and **5.2**.

**Figure 5.3.1** Molecular structures of **5.3** and **5.4**.

**Figure 5.4.1** Molecular structure of **5.5** (thermal ellipsoids at 50% probability; H atoms omitted for clarity, only one orientation of the symmetry disordered [OCP]<sup>−</sup> anion is shown.).

**Figure 5.5.1** LUMO and HOMO of Ph<sub>2</sub>BiPCO.

**Figure 5.5.2** Resonance structures for compounds **5.3** / **5.4** (A) and the cation of **5.5** (B).

**Figure 5.5.3** Molecular electrostatic potential for the cationic moiety of **5.5**.

**Figure 5.5.4** Proposed mechanism for the formation of [NHC<sub>2</sub>OCP]<sup>+</sup>[OCP]<sup>−</sup>.

## List of Schemes

**Scheme 1.3.3** Synthetic route to carbodicarbene ligand with isopropyl groups.

**Scheme 2.2.1** Synthesis of carbodicarbene-beryllium dichloride, (CDC)BeCl<sub>2</sub>.

**Scheme 2.2.2** Synthesis of carbodicarbene-beryllium compounds, (CDC)BeCl[N(SiMe<sub>3</sub>)<sub>2</sub>] (**2.6**), (CDC)BeCl(BH<sub>4</sub>) (**2.7**), and (CDC)Be(CH<sub>3</sub>)<sub>2</sub> (**2.8**).

**Scheme 2.3.1** Synthesis of carbodicarbene-beryllium metallacycle.

**Scheme 2.4.1** Beryllacycle salt metathesis with (Et<sub>2</sub>O)<sub>2</sub>BeCl<sub>2</sub>.

**Scheme 2.4.2** CAAC-promoted ring expansion and NHC coordination to beryllium.

**Scheme 3.1.1** **A.** Synthesis of the first NHC-beryllium complex, [(NHC)<sub>3</sub>BeCl]Cl. **B.** Synthesis of the first NHC supported organoberyllium complex, (NHC)BePh<sub>2</sub>. **C.** Reaction of dimethylberyllium with phenylsilane leads to beryllium insertion into the C–N bonds of an imidazole ring. IPr (R = 2,6-diisopropylphenyl); IMes (R = 2,4,6-trimethylphenyl).

**Scheme 3.1.2** Synthesis of CAAC stabilized beryllium(0) species.

**Scheme 3.1.3** Reactivity of (Me<sup>2</sup>CAAC)<sub>2</sub>Be<sup>0</sup> towards CO<sub>2</sub> and selenium (Se).

**Scheme 3.1.4** (Et<sup>2</sup>CAAC)<sub>2</sub>Be<sup>0</sup> as a soluble reducing agent.

**Scheme 3.1.5** Synthesis of (CAAC)<sub>2</sub>Be<sup>I</sup> by oxidation of (CAAC)<sub>2</sub>Be<sup>0</sup>

**Scheme 3.2.1** Synthesis of a complex containing two untethered NHCs bound to a mononuclear beryllium halide (**3.19**). Reactions of **3.19** with LiODipp and NaOEt to produce (sIPr)Be(ODipp)<sub>2</sub> (**3.20**) and [(sIPr)BeCl(EtO)]<sub>2</sub> (**3.21**), respectively.

**Scheme 3.3.2** Synthesis of doubly-reduced beryllium complexes.

**Scheme 4.2.1** Synthesis of bismuth cations supported by *N*-heterocyclic carbenes and a cyclic(alkyl)amino carbene.

**Scheme 4.2.2** Synthesis of NHC- and CDC- supported phenylbismuth dichloride (NHC = 4,5-dimethyl-1,3-diisopropylimidazolin-2-ylidene; CDC = bis(1-isopropyl-3-methyl-benzimidazol-2-ylidene)methane).

**Scheme 4.3.1** Synthesis of CDC-stabilized bismuth mono- and di-cations with increasing bismaalkene character.

**Scheme 4.3.2** Synthesis of a *bis*-CDC-supported tribromobismuth dimer.

**Scheme 4.3.3** Synthesis of CDC mono-, di-, and tri-positive bismuthenium ions. Note: similar to compound **4.14**, compounds **4.17** and **4.18** can be represented as resonance structures with their respective zwitterions analogous to those shown in Scheme 4.3.1.

**Scheme 5.2.1** Synthesis of diphenylpnictogen halide *N*-heterocyclic carbene complexes.

**Scheme 5.3.1** Synthesis of bismuth and antimony phosphaketene adducts.

**Scheme 5.4.1** Thermal reduction at Sb or Bi center to tetraphenyldipnuctogen compounds.

## List of Tables

**Table 2.2.1:** EDA calculations at BP86-D3(BJ)/TZ2P (kJ mol<sup>-1</sup>).

**Table 2.4.1** B3LYP-D3(BJ)/def2-SVP (toluene) calculated MO energies (eV) and vertical singlet-triplet gap (kcal/mol).

**Table 2.4.2** EDA analysis of carbene adducts **2.12** and **2.13**, and transition state structures **TS1** (kcal/mol). Transition state structures **TS1** (kcal/mol).

**Table 5.5.1** Complex formation energies ( $\Delta E$ ) and Gibbs free energies ( $\Delta G$ ) in kcal/mol, geometrical parameters (bond length in Å/Wiberg Bond Indices), NPA partial charges of Pn ( $q$ ) in electrons and net charge transfer in electrons ( $\Delta q$ ) at the  $\omega$ B97XD/def2-TZVP level.

# Chapter 1: Introduction

- Walley, J. E. and Gilliard, R. J., *EIBC 2021*. Accepted and Pending Publication.

## 1.1 Introduction to Beryllium

### 1.1.1 Origin and Isolation of Beryllium

The beautiful shades of gemstones such as emerald green or the blue of aquamarine have long captivated mankind. Although the colors of these gems differ, they are both made of the same mineral, beryl, which is composed of beryllium aluminum cyclosilicate. Beryl is colorless in its purest form, but impurities in its composition give it a variety of colors, as seen in these stones. Emerald green, for example, results from chromium and vanadium impurities,<sup>1</sup> while iron impurities give aquamarine its blue color.<sup>2</sup>

Louis Nicolas Vauquelin, a French pharmacist, studied beryl in 1798 and successfully separated the beryllium salts from aluminum salts.<sup>3</sup> Because of the sweet taste of the beryllium-containing salts, he proposed the term glucinium (Gl), but German scientists replaced it with beryllium (Be). It was subsequently discovered that the consumption of beryllium can lead to serious health risks. Indeed, beryllium has been classified as the most toxic non-radioactive element on the periodic table (*vide infra*).<sup>4</sup> In 1828, Friedrich Wöhler and Antoine Bussy isolated beryllium metal by the reduction of beryllium dichloride with potassium.<sup>3</sup> Currently, elemental beryllium is made from heating a mixture of  $\text{BeF}_2$  with magnesium metal at 1300 °C, or by electrolysis of  $\text{BeCl}_2$ .<sup>1</sup>

In comparison to the heavier alkaline earth metals such as magnesium, the number of commercially available beryllium reagents are extremely limited. Therefore, beryllium chemists initially focused on synthesizing necessary reagents directly from beryllium metal, with the most common reagents being beryllium halides.<sup>5-6</sup> The most popular beryllium starting material,  $\text{BeCl}_2$ ,

can be synthesized using a small amount of metal with the addition of two molar equivalents of HCl in diethyl ether. This cleanly generates the crystalline dietherate complex  $(\text{Et}_2\text{O})_2\text{BeCl}_2$ .<sup>7</sup>

### *1.1.2 Physical and Chemical Properties of Beryllium*

The reactivity of beryllium is fascinating as its atomic properties set it apart from the rest of the alkaline earth metals. Beryllium dichloride, for example, reacts vigorously with water to give  $\text{Be}(\text{OH})_2$  and 2 HCl. The heavier alkaline earth dichlorides  $\text{MCl}_2$  ( $\text{M} = \text{Mg}, \text{Ca}, \text{Sr}, \text{Ba}$ ) dissolve and ionize into  $\text{M}^{2+}$  and 2  $\text{Cl}^-$  in water. Beryllium possesses the highest electronegativity ( $\text{Be}: 1.57; \text{Mg}: 1.31; \text{Ca}: 1.00; \text{Sr}: 0.95; \text{Ba}: 0.89$ )<sup>8</sup> and the smallest ionic radius of group 2 ( $\text{Be}^{2+}: 0.34 \text{ \AA}; \text{Mg}^{2+}: 0.78 \text{ \AA}; \text{Ca}^{2+}: 1.06 \text{ \AA}; \text{Sr}^{2+}: 1.27 \text{ \AA}; \text{Ba}^{2+}: 1.43 \text{ \AA}$ ).<sup>9</sup> Therefore,  $\text{Be}^{2+}$  is regarded as the most charge dense metal ion. As a result, while  $\text{Mg}^{2+}$ – $\text{Ba}^{2+}$  form ionic interactions with chloride, beryllium produces polar covalent bonds with chlorine. Beryllium also has the highest reduction potential of the alkaline earth metals ( $\text{Be}^{2+}/\text{Be}^0 -1.85 \text{ eV}$ ),<sup>10</sup> therefore, beryllium is the easiest group 2 element to reduce to subvalent states. Perhaps resulting from the latter property, two new formal oxidation states ( $\text{Be}^0$  and  $\text{Be}^{\text{I}}$ ) have been uncovered within the last five years.<sup>11-</sup>

12

### *1.1.3 Applications of Beryllium*

Beryllium has several industrial applications. When alloyed with other metals, materials with improved properties can be obtained. For instance, when copper is mixed with 2% beryllium, the resulting alloy has sixfold-increased strength with respect to unadulterated copper as well as non-sparking and non-magnetic properties.<sup>1, 3</sup> Because they do not produce sparks, beryllium-copper alloys are used to make tools for explosive atmospheres such as oil rigs. Beryllium-copper tools are also used for maintenance of magnetic resonance imaging devices because of their non-

magnetic properties.<sup>3</sup> Beryllium-aluminum alloys have found applications in the aerospace industry because of their high strength and light weight.<sup>13</sup> Beryllium also serves as a neutron reflector in nuclear fission power plants and nuclear weapons.<sup>3</sup> Because of its transparency to X-rays, beryllium is used to construct radiation windows in X-ray tubes.<sup>3</sup> Due to the relatively unexplored nature of this element, it is likely that many of beryllium's applications have yet to be discovered. As such, pioneering research in this field is imperative for realizing new chemistry and applications for beryllium. In the past 5 years, there have been several review articles discussing the structure and reactivity of beryllium coordination complexes.<sup>4, 14-15</sup>

#### 1.1.4 Toxicity of Beryllium

Handling beryllium and its compounds requires additional safety precautions including ensuring proper disposal of waste, the utilization of a well-ventilated fume hood during synthetic operations, and possibly respirators or masks depending on the specific applications. Chemists should always check reputable safety data sheets before using any beryllium-containing compound. Inhalation of small amounts of beryllium compounds ( $2 \mu\text{g m}^{-3}$ ) may result in chronic beryllium disease (CBD), which can develop within one to twenty years after exposure.<sup>16</sup> Reports suggest that after lung cells are exposed to beryllium, an autoimmune response is initiated, which may result in respiratory damage by scarring the lungs because the body is unable to get rid of the beryllium particulates.<sup>17-19</sup>

Currently, it is not well understood how beryllium coordinates to biomolecules inside the body. In order to better understand how  $\text{Be}^{2+}$  binds with biomolecules *in vivo*, Buchner performed a study where the coordination of biomimetic ligands to beryllium was assessed.<sup>20</sup> The results in this work showed that only  $\kappa^3$  and  $\kappa^4$  ligating sites in peptides and polysaccharides can reversibly coordinate beryllium. It was found that multinuclear beryllium complexes (i.e., more than one

beryllium atom in a single molecular complex) frequently formed. Therefore, it was postulated that the latency time for CBD could result from the necessity to form such multinuclear complexes with low concentrations of beryllium. Furthermore, beryllium coordination increases the concentration of Brønsted acids, which is a possible cause for beryllium-induced cell death.

### 1.1.5 $^9\text{Be}$ NMR Spectroscopy

One of the most useful techniques for characterizing organometallic beryllium compounds is indubitably  $^9\text{Be}$  NMR spectroscopy. Beryllium's spin active nuclei ( $s = 3/2$ ) is quadrupolar, thus, its coordination environment affects the  $^9\text{Be}$  NMR peak width. In general, highly symmetric coordination environments around beryllium result in sharp peaks in a  $^9\text{Be}$  NMR spectrum.<sup>21</sup> Beryllium tends to adopt either trigonal planar (three-coordinate) or tetrahedral (four-coordinate) geometries, with the latter being the most symmetric. Distortions from these geometries that compromise symmetry result in peak broadening.

In 2004, John et al. published a table of  $^9\text{Be}$  NMR chemical shifts for beryllium complexes that were categorized by coordination environment.<sup>22</sup> These categories are, cyclopentadienyl complexes ( $\delta = -27.7$  to  $-20.8$  ppm), four-coordinate complexes ( $\delta = -1.2$  to  $12.3$  ppm), and two/three-coordinate complexes ( $\delta > 5.8$  ppm). Nearly 16 years later, Plieger published an update to these trends to include more than 54 publications containing NMR data for beryllium complexes.<sup>21</sup> The respective ranges for  $^9\text{Be}$  NMR shifts have increased for cyclopentadienyl complexes ( $-27.7$  to  $-14.8$  ppm), four-coordinate ( $-5.3$  to  $13.7$  ppm), and two/three-coordinate complexes ( $0.93$  to  $44$  ppm). There is now significant overlap between these three trends, which is likely due to the utilization of a range of new ligands (*vide infra*) which has resulted in compounds with unusual electronic structures. Nevertheless, the peak width at half height is a good

indication of the coordination number with three-coordinate complexes being broad and four-coordinate compounds showing sharp signals.

## 1.2 Introduction to Bismuth

### 1.2.1 Origin and Isolation of Bismuth

Bismuth, derived from the German word 'wismuth' (white mass), is one of the most unique main-group metals on the periodic table. Elemental bismuth can often be found as crystals with elegant colors that result from a reflective oxide layer over the surface. Bismuth can be obtained from the ores bismuthinite and bismute, which chemically is bismuth sulfide and bismuth oxide, respectively. In earlier times, people would often confuse bismuth with lead and tin. A French chemist by name of Claude François Geoffroy eventually demonstrated that bismuth is distinct from these elements and is credited with the discovery of bismuth in 1753.<sup>23</sup>

Bismuth starting materials are widely available for purchase through chemical vendors. One of the most popular bismuth starting materials used in the work described herein is bismuth trichloride,  $\text{BiCl}_3$ , which is highly moisture sensitive. As a result,  $\text{BiCl}_3$  purchased from chemical vendors usually contains trace amounts of its water product, bismuth oxychloride. Bismuth trichloride can be purified by refluxing in in toluene to make the crystalline toluene adduct  $(\text{toluene})\text{BiCl}_3$ , which can then be used as a pure form of bismuth trichloride. In addition, THF supported phenylbismuth dichloride  $(\text{THF})\text{Bi}(\text{Ph})\text{Cl}_2$  and diphenylbismuth chloride  $\text{Ph}_2\text{BiCl}$  can be synthesized from 1:2 and 2:1 mixtures of triphenylbismuth and bismuth trichloride, respectively.<sup>24</sup>

### 1.2.2 Physical and Chemical Properties of Bismuth

Due to its position on the periodic table, bismuth, a 6<sup>th</sup> period element, exhibits a remarkable reactivity profile and has demonstrated transition-metal-like behavior in recent years.<sup>25-26</sup> This is important to the main-group community because the low toxicity and respectable geological abundance of bismuth renders it a promising candidate for green industrial catalysis. Bismuth is electronically limited in its frontier orbitals as it cannot access *d*-orbitals and is restricted to its 6*s* and three 6*p* orbitals, thus, the isolation of redox active organometallic bismuth complexes requires clever synthetic design. The 6*s* orbital is usually occupied by a lone pair, resulting in the ubiquitous +3 oxidation state seen in many of its complexes, while the three 6*p* orbitals are largely responsible for facilitating the molecular geometry around the bismuth metal center. These valence orbitals are large, diffuse, and polarizable, leading to weak bonds (single and multiple) between Bi and 2<sup>nd</sup> period atoms.

Compared to its lighter group 15 congeners (N, P, As, Sb), bismuth is the only metal. Bismuth is the most diamagnetic metal known, as it is highly repelled by a magnetic field. Although its naturally occurring isotope bismuth-209 is notably stable it is nevertheless slightly radioactive, with a half-life of  $1.9 \times 10^{19}$  years.<sup>23</sup> Possessing the lowest electronegativity (N: 3.04; P: 2.19; As: 2.18; Sb: 2.05; Bi: 2.02) and largest ionic radius (N<sup>3+</sup>: 0.16 Å; P<sup>3+</sup>: 0.44 Å; As<sup>3+</sup>: 0.58 Å; Sb<sup>3+</sup>: 0.76 Å; Bi<sup>3+</sup>: 1.03 Å)<sup>9</sup> out of group 15, the Bi<sup>3+</sup> ion exhibits a charge/radius ratio of 2.91 Å<sup>-1</sup> and has found significant applications in Lewis acid catalysis.<sup>26-27</sup>

### 1.2.3 Applications of Bismuth

There are numerous applications of bismuth due to its non-toxic profile and diverse chemical properties. Bismuth subsalicylate is the primary component of the common over-the-

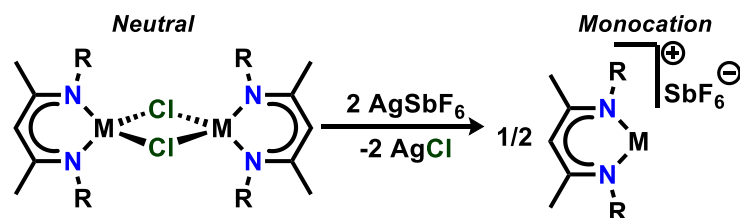
counter heartburn medication, Pepto-Bismol. Due to its exceptionally good diamagnetic properties (*vide supra*), bismuth has found use in maglev trains, which can reach speeds to 250+ mph. Bismuth oxide is used in dragon egg fireworks to make the crackling sound upon explosion, this used to be lead oxide before knowledge of its toxicity. Bismuth oxide is perhaps the most industrially important synthon, which is used to make a variety of bismuth compounds. Recent efforts from the chemical community to push non-toxic main-group elements towards catalytic activity reminiscent of the transition-metals has uncovered several redox catalytic pathways with bismuth, including Bi(I/III) and Bi(III/V) catalysis.

## 1.3 Ligand Design for Main-Group Complexes

### 1.3.1 Anionic vs. Neutral Ligands

At the roots of synthesizing highly reactive main-group complexes is ligand design. For decades, synthetic chemists have focused largely on designing bulky anionic ligands such as  $\beta$ -diketiminate (NacNac),<sup>28</sup> amidinate,<sup>29</sup> or *meta*-terphenyl derivatives<sup>30</sup> that can provide steric and electronic stability towards highly reactive motifs. These ligands can be tuned (i.e., sterically and electronically) by interchanging their functional groups. However, a major limitation of complexes containing anionic ligands is that one-electron is consumed in metal-ligand bonding. When neutral ligands are used, there is potential to increase the reactivity at the main-group center, since no electrons are consumed in metal-ligand binding. For example, as there is only one M–Cl motif per metal center, only one halide can be abstracted from the generic NacNac-supported metal halide complex [(NacNac)M( $\mu$ -Cl)]<sub>2</sub> to give a monocationic complex (Figure 1.3.1A). When neutral ligands such as *N*-heterocyclic carbenes (*vide infra*) are coordinated to metal dihalides, the

**A: Single halide abstraction at anionic NacNac supported metal chloride**



**B: Double halide abstraction at neutral N-heterocyclic carbene supported metal dichloride**

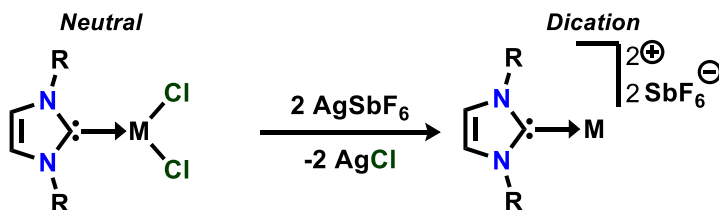


**Figure 1.3.1** A: One halide abstraction from an anionic NacNac ligand metal halide; **B**: Two halide abstractions from a neutral carbene ligand metal dihalide. abstraction of two M–Cl units becomes a possibility allowing for the formation of a dicationic complex (Figure 1.3.1B).

### 1.3.2 Brief History and Electronic Nature of Carbenes and Carbones

Our lab is particularly interested in utilizing neutral carbon-based ligands (i.e. carbenes and carbones) with unique electron morphologies (Figure 1.3.2). *N*-heterocyclic carbenes (NHCs), isolated in 1991 by Arduengo,<sup>31</sup> are one of the most ubiquitous ligands in organometallic chemistry. NHCs have been heavily utilized in stabilizing a plethora of low-coordinate, low-oxidation state main-group compounds, owing to NHCs  $\sigma$ -donating (HOMO) and  $\pi$ -accepting (LUMO) frontier orbitals.<sup>32-33</sup> Fourteen years after the isolation of NHCs, cyclic(alkyl)amino carbenes (CAAC) were synthetically realized by Bertrand in 2005.<sup>34</sup> Replacing a nitrogen on NHC with a quaternary carbon makes CAACs better  $\sigma$ -donors and  $\pi$ -acceptors.<sup>33</sup> CAACs have proven their ability in stabilizing subvalent elements which traditional NHCs could not. For example, Braunschweig demonstrated that two CAACs were sufficient in stabilizing subvalent Be(0),<sup>11</sup>

while initial computational reports proposed three NHCs.<sup>10,35</sup> Nearly three years after synthesizing CAACs, Bertrand synthesized the first carbodicarbene (CDC) in 2008.<sup>36</sup> CDCs are superior  $\sigma$ -donors to NHCs and CAACs, and are  $\pi$ -donating rather than  $\pi$ -accepting. CDCs are formally considered C(0) complexes stabilized by two flanking NHCs,<sup>37</sup> thus accounting for two lone pairs of electrons localized on the central carbon atom. Prior to the work described herein, there were examples of NHC and CAAC complexes with group 2 elements and bismuth, however, there were no examples with CDCs. Hence, we used the unique electronic nature of CDCs to develop a novel class of beryllacycles and bismaalkene cations.

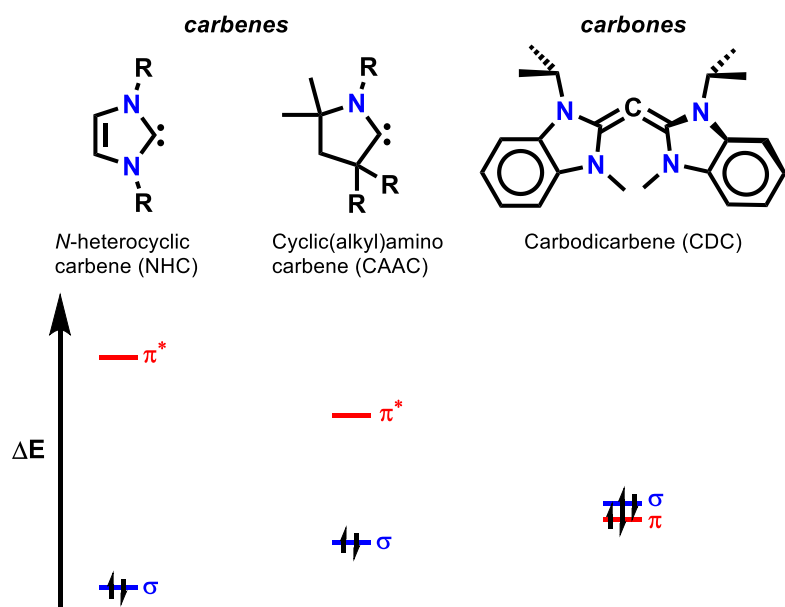
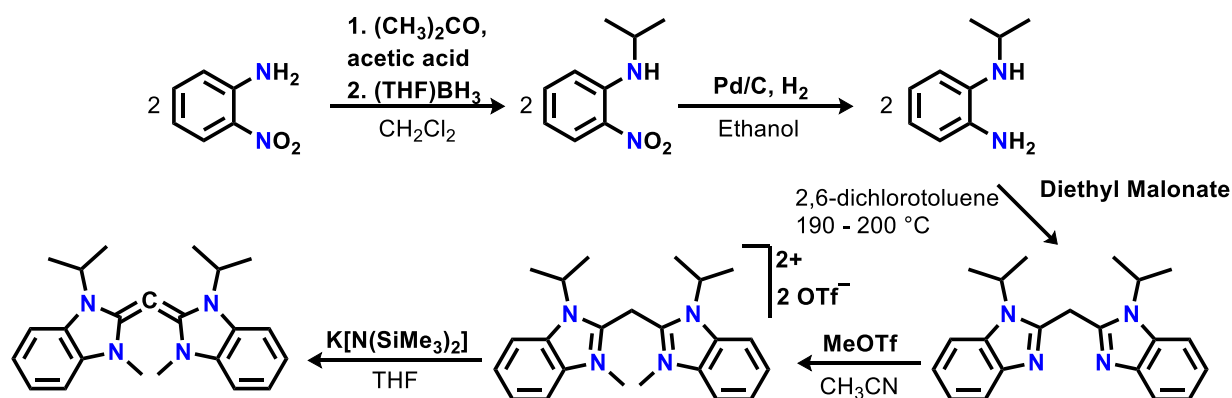


**Figure 1.3.2** Carbenes: *N*-heterocyclic carbene and cyclic(alkyl)(amino) carbene and respective energies of frontier orbitals; Carbone: carbodicarbene and respective energies of frontier orbitals.

### 1.3.3 Synthetic Procedure for Carbodicarbene Ligand

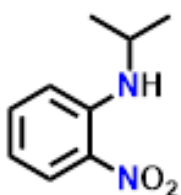
The decision was made to synthesize the CDC ligand with sterically demanding side arms in order to provide steric protection to the coordinating metal center. The synthesis of this ligand

is shown in Scheme 1.3.3. Alkylation of the amine group in 2-nitroaniline followed by hydrogenation affords N-isopropyl-1,2-phenylenediamine in nearly quantitative yield. Refluxing this compound with diethyl malonate produces *bis*(benzimidazole-2-yl)methane in 60% yield. *Bis*-methylation forms the corresponding triflate salt. After the deprotonation of the methylene protons, the free CDC ligand is produced in good yield. This procedure is discussed in detail below.



**Scheme 1.3.3** Synthetic route to carbodicarbene ligand with isopropyl groups.

**Synthesis of N-isopropyl-2-nitroaniline:** To a 3000



mL Schlenk flash, 2-nitroaniline was added (92.08 g, 667 mmol).

Subsequently, 200 mL dichloromethane, 750 mL glacial acetic acid, and acetone (150 mL, 2043 mmol) were added. (**Note:** the isopropyl group comes from the conjugate acid of acetone in the equilibrium of acetone and acetic acid.)

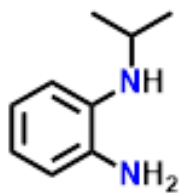
The solution was stirred for 5 minutes, then cooled to  $0^\circ\text{C}$ .  $\text{BH}_3(\text{THF})$  (800 mL, 800 mmol) was added dropwise for 3 hours. (**Note:** in order to avoid decomposition with air,  $\text{BH}_3(\text{THF})$  is canula



dropwise for 3 hours. (**Note:** in order to avoid decomposition with air,  $\text{BH}_3(\text{THF})$  is canula

transferred over argon to the addition funnel.) The final product was obtained by extracting with DCM, then drying *in vacuo*.

**Synthesis of N-isopropylbenzene-1,2-diamine:** To a stainless-

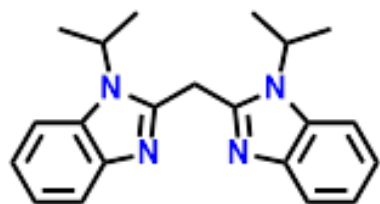


steel reactor, N-isopropyl-2-nitroaniline (114.2 g, 57.5 mmol) was dissolved in ethanol (200 mL). 0.5 g of Pd/C was added to the reactor

along with a stir bar. The reaction proceeded over a course of 1 to 2 weeks under hydrogen pressure (700 PSI). (**Note:** please refer to proper safety protocols when using the high-pressure line.) After the reaction was complete (indicated by a loss of yellow color), the solution was filtered, the dried *in vacuo*.



**Synthesis of bis(1-isopropyl-benzimidazol-2-yl)methane:** A 2-necked round bottom flask was fitted



with a dean-stark apparatus and a dripping funnel. N-

isopropyl-1,2-phenylenediamine (30 g, 167 mmol) dissolved in 100 mL 2,6-dichlorotoluene was added to the flask, and stirred. The attached dripping funnel was charged with diethyl malonate (36 grams, 167 mmol).

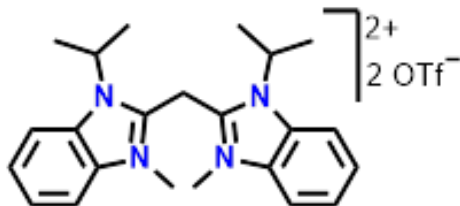
The reaction mixture was heated to 170 °C, then the

diethyl malonate was added dropwise to the stirring mixture. The dripping process proceeded while the temperature was allowed to increase to and maintained between 190 and 200 °C for 16



hours. Upon cooling to room temperature, a purple precipitate formed from solution. This precipitate was collected via filtration and washed with hexanes before drying under reduced pressure.

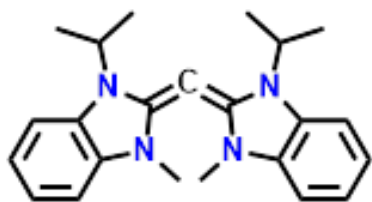
**Synthesis of 2,2'-methylenebis(1-isopropyl-3-methyl-benzimidazolium)trifluoromethanesulfonate:** To a 250 mL Schlenk flask bis(1-isopropyl-benzimidazole-2-yl)methane (20.0 grams,



60.2 mmol) was added and dissolved in 100 mL of anhydrous acetonitrile, then stirred. Methyl triflate (31.9 grams, 19.4 mmol) was added dropwise to the flask. The

reaction continued to stir for 1 hour. The product was obtained as a white powder by precipitation with ether.

**Synthesis of bis(1-isopropyl-3-methyl-benzimidazol-2-ylidene)methane:** To a 100 mL round bottom flask, 2,2'-methylenebis(1-isopropyl-3-methyl-



benzimidazolium) trifluoromethanesulfonate (10 g, 15 mmol) was dissolved in 40 mL THF. A slight excess of  $K[N(SiMe_3)_2]$  (6.60

g, 33.1 mmol) dissolved in 20 mL THF was added dropwise to the stirring solution. The solution was stirred for 3 hours, the volume was reduced to approximately 10-20 mL THF and filtered. The crude product was washed in diethyl ether, then dried *in vacuo* to give pure CDC ligand.

## Chapter 2: Carbodicarbene Beryllium Chemistry

- Walley, J. E.; Breiner, G.; Wang, G.; Dickie, D. A.; Molino, A.; Dutton, J. L.; Wilson, D. J. D.; Gilliard, J. R. J., *Chem. Commun.* **2019**, 55, 1967-1970.
- Walley, J. E.; Obi, A. D.; Breiner, G.; Wang, G.; Dickie, D. A.; Molino, A.; Dutton, J. L.; Wilson, D. J. D.; Gilliard, R. J., Jr., *Inorg Chem* **2019**, 58, 11118-11126.
- Walley, J. E.; Dickie, D. A.; Gilliard, R. J., *Z. Naturforsch. B* **2020**, 75, 497.

## 2.1 Introduction to Carbene Beryllium Chemistry

### 2.1.1 Synthesis of Monodentate Carbodiphosphorane Beryllium Complexes

When compared to carbene–beryllium chemistry (discussed in chapter 3), the analogous chemistry with carbones is in its infancy. Indeed, the first carbene–beryllium complex was synthesized in 2011,<sup>38</sup> whereas the first carbene-beryllium complex [(NHC)<sub>3</sub>BeCl]Cl was synthesized 26 years ago by Herrmann.<sup>39</sup> In their 2011 report, Petz, Frenking, and Neumüller aimed to answer the question “how does the double Lewis base (LB) hexaphenylcarbodiphosphorane (Ph<sub>3</sub>P)<sub>2</sub>C react with a double Lewis acid (LA) BeCl<sub>2</sub>?” The LA–LB adduct (Ph<sub>3</sub>P)<sub>2</sub>C–BeCl<sub>2</sub> (**2.1**) was isolated from the reaction of CDP with BeCl<sub>2</sub> (Figure 2.1.1). It was reported that **2.1** is unstable in DCM and THF,<sup>38</sup> leading to both mono- and di-protonated CDP ligand. However, isolation of **2.1** is feasible with the halogenated solvent 2-bromofluorobenzene. The <sup>CDP</sup>C–Be bond length (1.742 Å) of **2.1** is notably shorter than those of <sup>carbene</sup>C–Be bonded complexes (1.773–1.779 Å). Calculations demonstrate that the <sup>CDP</sup>C–Be bond mostly comes from the σ-donor lone pair on CDP, while π-donation is weak. It was also calculated that the coordination of two BeCl<sub>2</sub> should be possible as the second lone pair is only partially involved in the binding interactions with just one BeCl<sub>2</sub>.

Braunschweig and coworkers considered that geminal coordination of two BeCl<sub>2</sub> units could be a result of steric hindrance.<sup>40</sup> Therefore, two smaller carbodiphosphorane ligands, (Ph<sub>2</sub>MeP)<sub>2</sub>C and (Cy<sub>2</sub>MeP)<sub>2</sub>, were prepared and initially reacted with with equimolar amounts of BeCl<sub>2</sub> to give [(Ph<sub>2</sub>MeP)<sub>2</sub>C–BeCl<sub>2</sub>] (**2.2**) and [(Cy<sub>2</sub>MeP)<sub>2</sub>–BeCl<sub>2</sub>] (**2.3**), respectively. The addition of an additional equivalent of BeCl<sub>2</sub> to **2.2** or **2.3** did not result in geminal coordination. The <sup>CDP</sup>C–Be bond lengths are 1.742(9) Å (**2.2**) and 1.720(3) Å (**2.3**), which is comparable to that of **2.1**. The

torsion angles between the  $\text{BeCl}_2$  and  $\text{CP}_2$  planes are  $43^\circ$  (**2.2**) and  $60^\circ$  (**2.3**), suggesting nominal  $\pi$ -interaction similar to that in  $(\text{Ph}_3\text{P})_2\text{C}-\text{BeCl}_2$ .

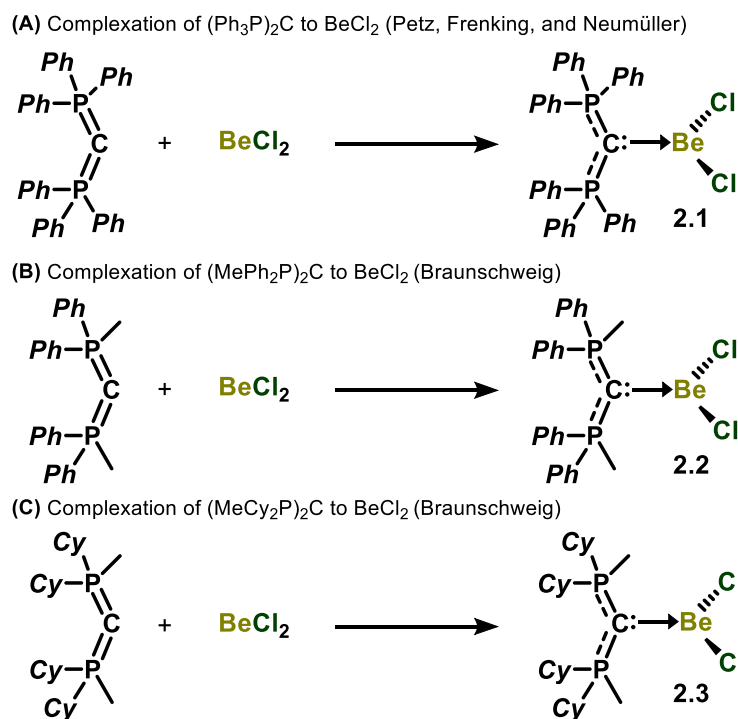


**Figure 2.1.1** Isolation of carbodiphosphorane beryllium dichloride adducts.

### 2.1.1 Synthesis of a Tridentate Carbodiphosphorane Beryllium Complex

In order to force  $p$ -orbital overlap between carbodiphosphorane (CDP) and beryllium, Buchner and coworkers aimed to decrease the torsion angle between  $\text{R}_3\text{P}=\text{C}=\text{PR}_3$  and beryllium.<sup>41</sup> Hexaphenylcarbodiphosphorane was reacted with two equivalents of *n*-butyllithium, which leads to the formation of *ortho*-lithiated carbodiphosphorane.<sup>42</sup> The reaction of *ortho*-lithiated carbodiphosphorane with one equivalent of  $\text{BeCl}_2$  yields the di-*ortho*-beryllated CDP complex (**2.4**), where the beryllium is bound by two phenyl groups and the carbene carbon (Figure 2.1.2). Compound **2.4** exhibits a short  $^{\text{CDC}}\text{C}-\text{Be}$  bond distance ( $1.704 \text{ \AA}$ ), which is comparable to  $^{\text{CAAC}}\text{C}-\text{Be}$  bond in beryllium(I) radical cations ( $1.691 - 1.694 \text{ \AA}$ ) and shorter than those in  $\text{CDP}-\text{BeCl}_2$

complexes **2.1–2.3**. A broad signal at 26.3 ppm was observed by  $^9\text{Be}$  NMR spectroscopy, which is characteristic of a three-coordinate beryllium system. The double bond character of **2.4** was studied using computational methods.<sup>41</sup>

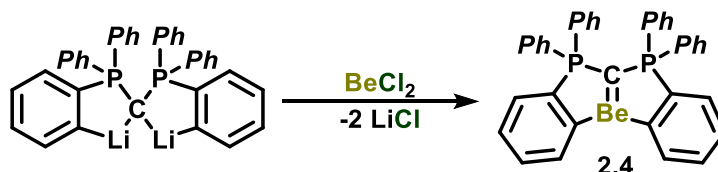


**Figure 2.1.2** Isolation of an s-block-carbon double bond using carbodiphosphorane.

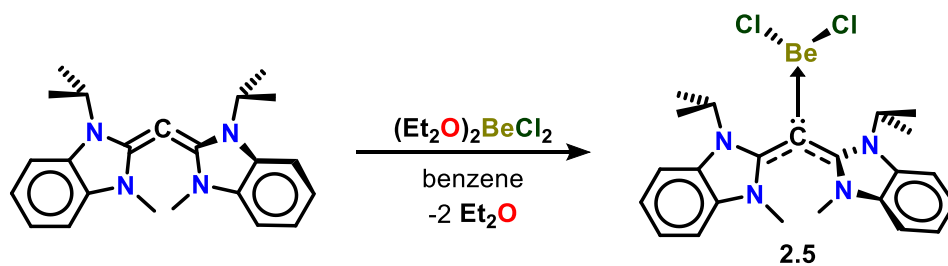
While group 2 carbodicarbene complexes have been studied computationally by Frenking,<sup>43</sup> there have been no molecular examples of organoberyllium compounds that feature a carbodicarbene. Herein, the first examples of CDC *s*-block complexes are described. Notably, a heteroleptic  $(\text{CDC})\text{BeCl}[\text{N}(\text{SiMe}_3)_2]$  complex undergoes a formal C–H bond activation to form a five-membered beryllacycle, which is the first examples of beryllium formally activating a C–H bond. This new class of carbodicarbene beryllacycles were shown to undergo a ring expansion reaction from five- to six-membered beryllacycles.

## 2.2 Synthesis of Carbodicarbene-Supported Beryllium Dichloride and Salt Metathesis Reactions

### 2.2.1 Synthesis of Carbodicarbene Beryllium Dichloride

The addition of a benzene solution of  $(\text{Et}_2\text{O})_2\text{BeCl}_2$  to a solution of CDC at room temperature resulted in the formation of a yellow solid, which immediately precipitated from solution. Apart from dichloromethane (DCM), the yellow solid was insoluble in most organic solvents. The  $^1\text{H}$  NMR spectrum in  $\text{CD}_2\text{Cl}_2$  revealed a heptet at 4.71 ppm, which was attributed to the methine protons on  $\text{CDC-BeCl}_2$  (**2.5**) (Scheme 2.2.1). Compound **2.5** was isolated in 97%

yield. The  $^{13}\text{C}$  NMR showed a shift at 160.34 ppm attributed to the carbene carbons on the CDC ligand. There was no shift observed for the the carbone carbon in the  $^{13}\text{C}$  NMR spectrum. While **2.5** is relatively stable in DCM, free CDC ligand decomposes as ascertained by an unintelligible  $^1\text{H}$  NMR spectrum. Notably, unlike the carbodiphosphorane (CDP) analogues  $[(\text{PPh}_3)_2\text{C}-\text{BeCl}_2]$ ,<sup>38, 40</sup> the CDC- $\text{BeCl}_2$  complex is stable in halogenated solvents which allowed for spectroscopic analysis by NMR.



**Scheme 2.2.1** Synthesis of carbodicarbene-beryllium dichloride,  $(\text{CDC})\text{BeCl}_2$ .

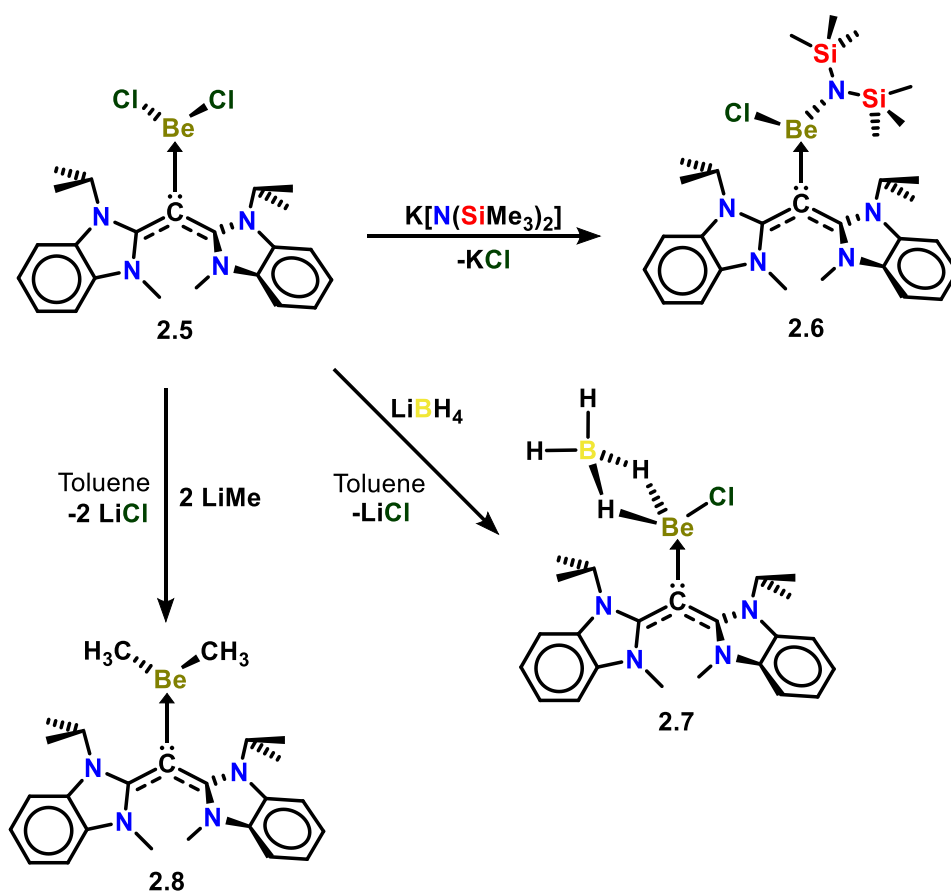
Yellow block-shaped single crystals of compound **2.5** suitable for a single crystal X-ray diffraction study were obtained from a DCM/hexanes mixture (1:1) at  $-37\text{ }^\circ\text{C}$ . The structure reveals CDC bound to monomeric beryllium dichloride, and the tricoordinate beryllium atom adopts trigonal planar molecular geometry (Figure 2.2.1). The C1–Be1 bond distance of **2.5** [1.748(6) Å] is shorter than the comparable  $^{\text{carbene}}\text{C}-\text{Be}$  bond in known carbene- $\text{BeCl}_2$  adducts (1.773–1.779 Å),<sup>11, 40, 44</sup> but slightly longer than those known for carbodiphosphorane- $\text{BeCl}_2$  (1.720–1.743 Å).<sup>38, 40</sup> The Be1–C11 bond in **2.5** [1.941(3) Å] is longer than the Be–Cl bonds in the NHC- $\text{BeCl}_2$  complex (1.881–1.884 Å)<sup>44</sup> and CAAC- $\text{BeCl}_2$  complexes (1.901–1.912 Å)<sup>11</sup>, but marginally shorter than the Be–Cl bonds in  $(\text{PPh}_3)_2\text{C}-\text{BeCl}_2$  (1.947–1.961 Å).<sup>38</sup> This suggests substantial activation of beryllium chloride facilitated by the CDC, an overall superior donor ligand relative to NHCs and CAACs. The C2–C1–C2' allenic moiety of **2.5** is significantly

elongated (1.405(3) Å) with respect to the free CDC (1.335(5) Å),<sup>45</sup> indicating electron donation from the central allenic carbon to an electrophilic beryllium center. DFT calculations for **2.5** yield a geometry that is consistent with the crystal structure, with Be–C<sub>carbone</sub> and Be–Cl bond distances (Wiberg bond index, WBI) of 1.764 Å (0.200) and 1.925 Å (0.348), respectively. Compound **2.5** with equivalent isopropyl groups is the lowest energy conformation; a structure with inequivalent isopropyl groups was found to be 4.5 kJ mol<sup>-1</sup> higher in energy. The B3LYP-D3(BJ)/def2-TZVP calculated  $\Delta G$  binding energy of BeCl<sub>2</sub> in **2.5** is 145.1 kJ mol<sup>-1</sup>, which is comparable to 151.3 kJ mol<sup>-1</sup> in the [(PPh<sub>3</sub>)<sub>2</sub>C–BeCl<sub>2</sub>].

### 2.1.2 Salt Metathesis Reactions of Carbodicarbene Beryllium Dichloride

One equivalent of potassium bis(trimethylsilyl)amide (K[N(SiMe<sub>3</sub>)<sub>2</sub>]) was added dropwise to a suspension of **2.5** in toluene (Scheme 2.2.2). The <sup>1</sup>H NMR spectrum revealed a broad septet at 4.80 ppm for the methine proton and the appearance of a N(SiMe<sub>3</sub>) group at 0.33 ppm, which was consistent with compound **2.6**. The <sup>13</sup>C NMR showed a shift at 160.8 ppm which was attributed to the carbene carbon. There was also no chemical shift for the carbone atom for this compound. Compound **2.6** was obtained in 75% isolated yield. The formation of heteroleptic tricoordinate compound **2.6** occurs in a 100% conversion. Broad bands representative of the allene asymmetric stretching frequency were observed at 1483 cm<sup>-1</sup> and 1481 cm<sup>-1</sup> for compounds **2.5** and **2.6** respectively. Yellow air- and moisture-sensitive block-shaped crystals of **2.6** suitable for a single crystal X-ray diffraction study were obtained from a hexanes/toluene (3:1) mixture at room temperature. The lack of ligand scrambling can be attributed to a combination of sterics from the bulky [N(SiMe<sub>3</sub>)<sub>2</sub>]<sup>-</sup> group and the CDC ligand. In a similar fashion, compound **2.5** can be reacted with one equivalent of LiBH<sub>4</sub> to synthesize (CDC)BeCl(BH<sub>4</sub>) (**2.7**). After the reaction was allowed to stir overnight, the product was extracted with toluene and concentrated. Yellow block-like

crystals of **2.7** suitable for X-ray diffraction were obtained from the concentrated solution at  $-37$  °C. We attempted this reaction with two equivalents and a large excess of  $\text{LiBH}_4$ , however, only one  $\text{Cl}^-$  is exchanged for a  $[\text{BH}_4]^-$ . Both halides in **2.5** can be substituted by using anionic ligands less sterically demanding than  $[\text{N}(\text{SiMe}_3)_2]^-$  and  $[\text{BH}_4]^-$ . The salt metathesis of **2.5** with two equivalents of methyllithium in toluene gives the bis-substituted CDC-supported dimethylberyllium,  $(\text{CDC})\text{BeMe}_2$  (**2.8**). Crystals of **2.8** suitable for X-ray diffraction can be obtained from a concentrated benzene solution.



**Scheme 2.2.2** Synthesis of carbodicarbene-beryllium compounds,  $(\text{CDC})\text{BeCl}[\text{N}(\text{SiMe}_3)_2]$  (**2.6**),  $(\text{CDC})\text{BeCl}(\text{BH}_4)$  (**2.7**), and  $(\text{CDC})\text{Be}(\text{CH}_3)_2$  (**2.8**).

### 2.1.3 Crystallographic Analysis of Carbodicarbene Beryllium Complexes **2.5** – **2.8**

The structure of **2.6** shows a tricoordinate beryllium atom in a trigonal planar environment (Figure 2.2.1). The C1–Be1 bond in **2.6** [1.766(3) Å] is longer than that in **2.5** [1.748(6) Å]. The C1–Be1 [1.766(3) Å] and C11–Be1 [1.996(2) Å] bonds in **2.6** are each slightly longer than those in **2.5** [1.748(6) and 1.941(3) Å, respectively]. The C2–C1 [1.409(2) Å] and C1–C13 [1.385(2) Å] bonds of the allenic moiety in **2.6** is in accordance with the related C2–C1 bond in **2.5** (1.405(3) Å). The allenic C2–C1–C13 angle in **2.6** is 117.60(14)°, representing less electron donation from C1 to Be1 compared to that of **2.5** [(C2–C1–C2') is 116.6(3)°]. DFT calculations for **2.6** yield Be–C<sub>carbone</sub> and Be–Cl bond distances (WBI) of 1.779 Å (0.196) and 1.983 Å (0.312), respectively. Both Be–C<sub>carbone</sub> and Be–Cl bond distances are longer, with smaller WBIs, in **2.6** compared to **2.5**. The calculated  $\Delta G$  binding energy of BeCl(HDMS) in **2.6** is 93.2 kJ mol<sup>-1</sup>, which is less than the binding energy of BeCl<sub>2</sub> in **2.5** [145.1 kJ mol<sup>-1</sup>].

The crystal structure of **2.7** revealed a distorted tetrahedral beryllium center (Figure 2.2.1), with the largest deviations from the idealized 109.5° being C1–Be1–C11 [123.6(3)°] and H1A–Be1–H1B [72.7(19)°]. There are two three-center two-electron bonds (B1–H1A–Be1 and B1–H1B–Be1) between boron and beryllium. Surprisingly, there is no statistically significant difference in the bond lengths between the bridging B–H bonds [B1–H1A = 1.13(3) Å; B1–H1B = 1.23(4) Å] and the terminal B–H bonds [B1–H1C = 1.14(5) Å; B1–H1D = 1.07(5) Å]. The CDC–beryllium bond, C1–Be1, is 1.750(6) Å, which is within the known range for other carbone–Be bonded compounds [1.742(9)–1.862(4) Å].<sup>38, 40, 46-47</sup> The carbodicarbene allene bond lengths C1–C2 [1.388(5) Å] and C1–C13 [1.414(5) Å] have elongated from its starting material (1.335 Å),<sup>45</sup> which results from electron donation from the carbone carbon (C1) to beryllium and lessened back-donation to the flanking carbene carbons (C2 and C13).

The crystal structure of **2.8** features beryllium in a trigonal planar geometry. The CDC–beryllium bond distance, Be1–C1, is 1.817(2) Å, which is considerably longer than those in **2.5** (1.748(6) Å), **2.6** (1.766(3) Å), and **2.7** (1.750(6) Å). This longer bond length is a result of the better  $\sigma$ -donor capabilities of the methyl groups compared to the chloride, hexamethyldisilazide, and borohydride ligands in **2.5–2.7**. The lessened electron donation from CDC is corroborated by the allenic bond lengths (1.3949(19) and 1.386(2) Å), which are shorter than those in **2.5–2.7**.

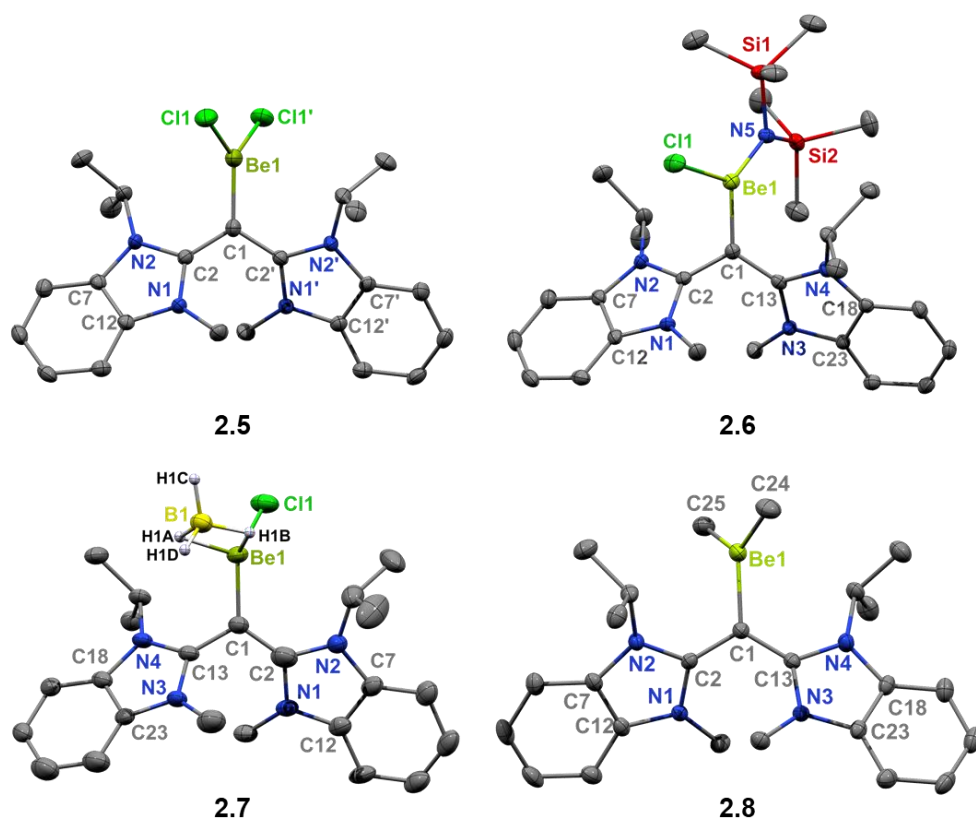


**Figure 2.2.1** Molecular structures of **2.5**: (thermal ellipsoids at 50% probability; H atoms were omitted for clarity). Selected bond distances (Å) and angles (deg): Be1–C1: 1.748(6); Be1–Cl1: 1.941(3); N1–C2: 1.375(3); N2–C2: 1.383(3); C1–C2: 1.405(3). C1–Be1–Cl1': 121.39(13); Cl1–Be1–Cl1: 117.2(3). C2–C1–C2': 116.6(3); C2–C1–Be1: 121.72(16); Cl1–Be1–C1–C2: 57.24(12). **2.6**: (thermal ellipsoids at 50% probability; H atoms and a non-coordinated toluene

solvent were omitted for clarity). Selected bond distances (Å) and angles (deg): N5–Be1: 1.605(2); Cl1–Be1: 1.996(2); C1–Be1: 1.766(3); C1–C2: 1.409(2); C1–C13: 1.385(2); N2–C2: 1.372(2); N1–C2: 1.372(2); N4–C13: 1.391(2); N3–C13: 1.3867(19). C13–C1–C2: 117.60(14); C13–C1–Be1: 124.09(14); C2–C1–Be1: 118.29(13); N5–Be1–C1: 129.51(14); N5–Be1–Cl1: 120.77(13); C1–Be1–Cl1: 109.71(12); C2–C1–Be1–Cl1: 46.07(18). **2.7:** (thermal ellipsoids at 30% probability; H atoms (except B-H) and non-coordinating solvent omitted for clarity). Selected bond distances (Å) and angles (deg): Be1–Cl1: 1.933(5); Be1–C1: 1.750(6); C1–C2: 1.388(5); C2–N1: 1.386(5); N1–C3: 1.443(5); C1–C13: 1.414(5). C1–Be1–H1A: 109.7(12); C1–Be1–H1B: 118.0(15); C1–Be1–Cl1: 123.6(3); C2–C1–C13: 115.0(3). **2.8:** (thermal ellipsoids at 50% probability; H atoms and a non-coordinated toluene solvent were omitted for clarity). Selected bond distances (Å) and angles (deg): Be1–C25: 1.756(3); Be1–C24: 1.758(3); Be1–C1: 1.817(2); C1–C2: 1.3949(19); C1–C13: 1.386(2); N1–C2: 1.3801(18); N2–C2: 1.3842(18); N3–C13: 1.3834(18); N4–C13: 1.3949(19). C25–Be1–C24: 124.18(14); C25–Be1–C1: 116.04(13); C24–Be1–C1: 119.78(14).

#### *2.1.4 Theoretical Analysis of Carbodicarbene Beryllium Complexes 2.5 and 2.6*

The electronic structure and bonding of **2.5** and **2.6** were investigated with DFT calculations. In both complexes, the HOMO (Figure 2.2.2) is associated with a lone-pair on the carbene carbon from CDC, which suggests that CDC is acting as a 2-electron donor to the Be species with a remaining  $\pi$  lone-pair from the central C(0) carbene carbon atom. The torsion angle of Cl1–Be1–C1–C2 in **2.5** is 57.3°, which supports unfavorable  $\pi$  overlap. Due to the steric crowding of the isopropyl groups on **2.6**, the torsion angle is greater than Cl1–Be1–C1–P1 in the reported (PPh<sub>3</sub>)<sub>2</sub>C–BeCl<sub>2</sub> complex (43.8°).<sup>38</sup>

Bader's QTAIM analysis supports a closed-shell donor-acceptor description of the Be-C bond (minimal electron density  $\rho$  at the bond critical point (BCP) and positive values of the Laplacian of  $\rho$  at the BCP). The nature of the <sup>carbonyl</sup>C-Be bonding was also analyzed with energy decomposition analysis (EDA) combined with natural orbitals of chemical valence (EDA-NOCV) calculations using BeClR (R = Cl, HDMS) and the ligand (L) as interacting fragments at the BP86-D3(BJ)/TZ2P level of theory. CDP-BeCl<sub>2</sub> was included for comparison. The L-Be bonding in **2.5**, **2.6** and CDP-BeCl<sub>2</sub> is best described as a donor-acceptor interaction. The numerical results (Table 2.2.1) give total interaction energies  $\Delta E_{\text{int}}$  between the fragments within the frozen geometry of the complexes **2.5** and **2.6** of  $-319.2$  and  $-332.0$  kJ mol<sup>-1</sup>, respectively. The orbital contribution  $\Delta E_{\text{orb}}$  is greater in **2.5** ( $-304.5$  kJ mol<sup>-1</sup>, 41.3%) than in **2.6** ( $-296.3$  kJ mol<sup>-1</sup>, 37.0%), both in absolute and percentage terms. This is consistent with the allenic C2-C1-C13 angle in **2.6**, which is greater than in **2.5** (less Be-C electron donation in **2.6**). While the electrostatic interaction energy  $\Delta E_{\text{elstat}}$  is smaller in **2.6**, the greater dispersion interaction  $\Delta E_{\text{dispersion}}$  in **2.6** ensures that the total interaction energy  $\Delta E_{\text{int}}$  in **2.6** is greater than in **2.5**. The EDA results for CDP-BeCl<sub>2</sub> are consistent with published work, noting that dispersion was not previously considered.<sup>38</sup> The  $\Delta E_{\text{int}}$  contribution in **2.5** is smaller than in CDP-BeCl<sub>2</sub> due to a smaller  $\Delta E_{\text{orb}}$  and  $\Delta E_{\text{disp}}$ , and larger  $\Delta E_{\text{Pauli}}$  contribution. In percentage attractive contributions, the difference between **2.5** and CDP-BeCl<sub>2</sub> largely arises from the greater  $\Delta E_{\text{disp}}$  in CDP-BeCl<sub>2</sub>. From EDA-NOCV results (Figure 2.2.3), the stabilization in **2.5** and **2.6** arises principally from C to Be  $\sigma$ -donation (65-69%), with minimal  $\pi$ -back donation (8-9%). There is a minor contribution from Be to C  $\sigma$ -donation (5%).



**Figure 2.2.2** Plots of the HOMO of **2.5** (left) and **2.6** (right), indicating a lone pair MO on the central carbone carbon.

	<b>2.5</b>	<b>2.6</b>	CDP-BeCl <sub>2</sub>
$\Delta E_{\text{int}}$	-319.2	-332.0	-344.9
$\Delta E_{\text{Pauli}}$	418.4	469.4	407.6
$\Delta E_{\text{Elstat}}^{\text{a}}$	-375.4 (50.9%)	-385.4 (48.1%)	-363.8 (48.3%)
$\Delta E_{\text{orb}}^{\text{a}}$	-304.5 (41.3%)	-296.3 (37.0%)	-310.0 (41.2%)
$\Delta E_{\text{disp}}^{\text{a}}$	-57.6 (7.8%)	-119.7 (14.9%)	-78.7 (10.5%)

**Table 2.2.2:** EDA calculations at BP86-D3(BJ)/TZ2P (kJ mol<sup>-1</sup>).

<sup>[a]</sup> The values in parentheses are the percentage contributions to the total attractive interactions  $\Delta E_{\text{elsat}} + \Delta E_{\text{orbital}} + \Delta E_{\text{dispersion}}$ .

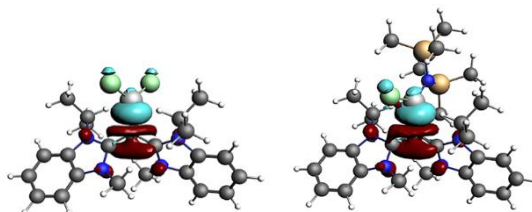
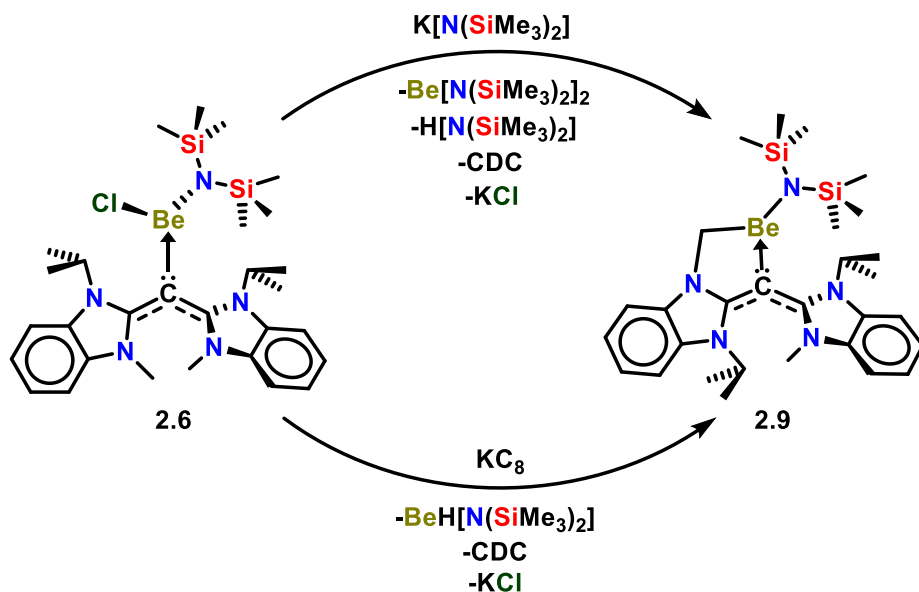


**Figure 2.2.3** Plot of EDA-NOCV deformation densities ( $\Delta\rho_1$ ) of the largest sigma donation orbital interaction in **2.5** (left) and **2.6** (right). The charge flows from red to blue.

## 2.3 Intramolecular CH Activation of (CDC)BeCl[N(SiMe<sub>3</sub>)<sub>2</sub>]

### 2.3.1 Beryllium Mediated C(sp<sup>3</sup>)-H Activation and Cyclization Reaction

The reaction of **2.6** with one equivalent of K[N(SiMe<sub>3</sub>)<sub>2</sub>] (Scheme 2.3.1) resulted in the emergence of two new septet environments (5.57 and 3.36 ppm) by <sup>1</sup>H NMR. These peaks are characteristic of the methine protons of an unsymmetrical CDC-containing product. Along with these compounds, peaks that correspond to free CDC ligand, Be[N(SiMe<sub>3</sub>)<sub>2</sub>]<sub>2</sub>,<sup>48</sup> K[N(SiMe<sub>3</sub>)<sub>2</sub>], and H[N(SiMe<sub>3</sub>)<sub>2</sub>] were also observed. We independently prepared Be[N(SiMe<sub>3</sub>)<sub>2</sub>]<sub>2</sub> and reacted it with free CDC in C<sub>6</sub>D<sub>6</sub> at temperatures up to 60 °C, however, no reaction was observed. Compound **2.9** can be obtained in 51% yield by the direct reaction of **2.5** with two equivalents of K[N(SiMe<sub>3</sub>)<sub>2</sub>]. Interestingly, a broad band at 1552 cm<sup>-1</sup> is attributed to the allene asymmetric stretching frequency in compound **2.9**. This higher frequency may be a result of the added ring strain.



**Scheme 2.3.1** Synthesis of carbodicarbene-beryllium metallacycle.

Though the exact mechanism for the formation of compound **2.9** is unknown, it may proceed by C(sp<sup>3</sup>)–H deprotonation where the protons of the methyl group are rendered more acidic due to close proximity to a highly polarizing Be<sup>2+</sup> center. Subsequent cyclization and metathesis of the chloride gives compound **2.9** where the isopropyl groups are inequivalent. The reaction also forms bis(trimethylsilyl)amine, H[N(SiMe<sub>3</sub>)<sub>2</sub>], the expected product for a reaction involving deprotonation. The formation of Be[N(SiMe<sub>3</sub>)<sub>2</sub>]<sub>2</sub> in the reaction is likely a result of the N(SiMe<sub>3</sub>)<sub>2</sub> anion outcompeting coordinated CDC ligand.

Due to the formal loss of a chloride, we reasoned that the cyclization could also be initiated by a one-electron reducing agent. Therefore, we reacted pure compound **2.6** with potassium graphite (KC<sub>8</sub>) and observed a greater conversion to compound **2.9** by NMR, negating the necessity of a strong base (Figure 2.3.1). This suggests that the conversion of **2.6** to **2.9** can also proceed via a radical based cyclization initiated by the formation of a highly reactive Be(I) intermediate. We also observed peaks at 4.34 and 0.49 ppm, which integrate to a ratio of 1H and 18H, respectively. These peaks were tentatively assigned to BeH[N(SiMe<sub>3</sub>)<sub>2</sub>], which was not isolated. The side product can be explained by a hydrogen radical obtained from cyclization combining with a Be[N(SiMe<sub>3</sub>)<sub>2</sub>] radical. Substantially less ligand dissociation was observed in the presence of KC<sub>8</sub> compared to K[N(SiMe<sub>3</sub>)<sub>2</sub>].

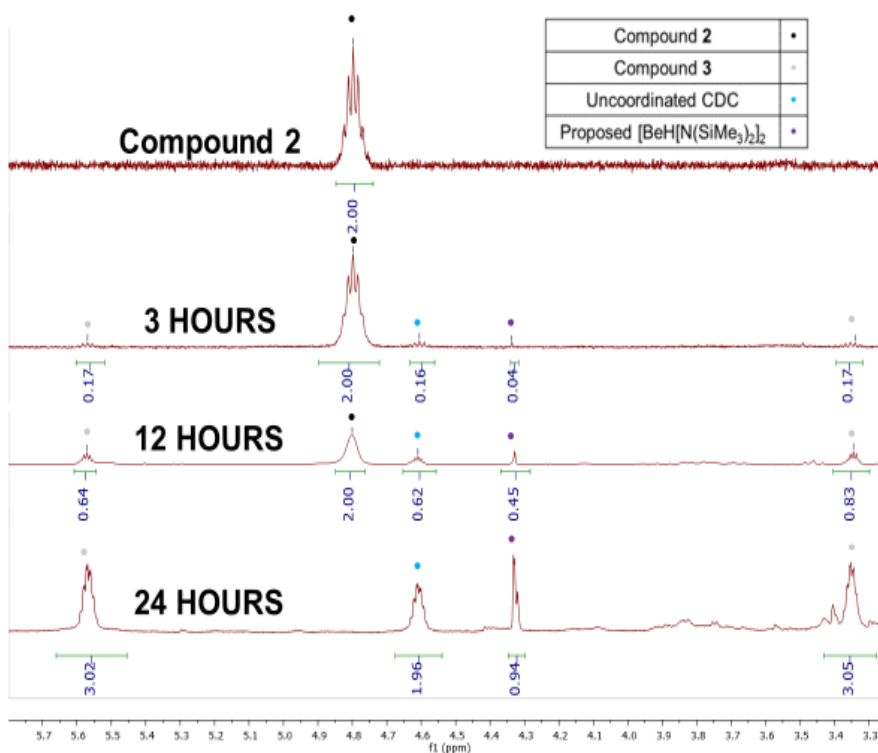


**Figure 2.3.1** Reaction of pure compound **2.6** reaction with 1 equivalent of  $\text{KC}_8$  at different time intervals.

### 2.3.2 Crystallographic Analysis of Carbodicarbene Beryllacycle **2.9**

Yellow rod-shaped crystals of **2.9** suitable for X-ray diffraction were obtained from a hexanes/toluene (10:1) solution of the reaction mixture at  $-37^\circ\text{C}$ . The molecular structure reveals a five-membered beryllium metallacycle (Figure 2.3.2). The beryllium atom resides in a distorted trigonal planar environment with two carbon–beryllium bonds [C3–Be1: 1.790(5) Å] and one nitrogen–beryllium bond [N5–Be1: 1.615(5) Å]. The C1–Be1 bond in **2.9** [1.796(5) Å] is slightly longer than in **2.6** [1.766(3) Å]. While the C2–C1–Be1 angle in **2.6** is [118.29(13)], the C3–Be1–C1 angle is significantly smaller [97.4(3)°] as the Be atom is incorporated into a five-membered ring. The C2–C1–C13 allenic angle in **2.9** is 126.7(3)°, which is larger than the comparable angle in both **2.5** [116.6(3)] and **2.6** [117.60(14)]. DFT calculations for **2.9** yield

Be1–C1 and Be1–C3 bond distances (WBI) of 1.785 (0.184) and 1.792 (0.254) Å, respectively. The Be1–C1 bond distance is slightly longer than in both **2.5** and **2.6**. Bader’s QTAIM analysis supports a closed-shell donor-acceptor description of the Be1–C1 bond, but a covalent Be1–C3 bond. The larger WBI for the Be1–C3 bond compared to Be1–C1 is consistent with an electron-sharing Be1–C3 description.

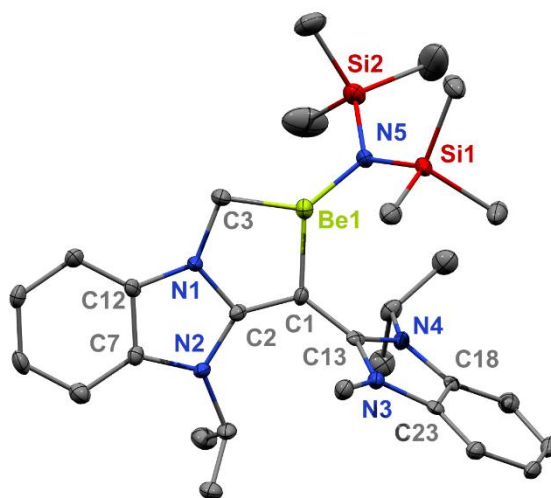


**Figure 2.3.2** Molecular structure of **2.9** (thermal ellipsoids at 50% probability; H atoms and co-crystallized  $\text{K}[\text{N}(\text{SiMe}_3)_2] \cdot 0.5\text{toluene}$  omitted for clarity). Selected bond distances (Å) and angles (deg): N5–Be1: 1.615(5); C1–C2: 1.373(4); C1–C13: 1.412(4); C1–Be1: 1.796(5); C3–Be1: 1.790(5); N1–C2: 1.374(4); N1–C3: 1.462(4); N2–C2: 1.395(4); N3–C14: 1.460(4); N4–C13: 1.366(4). N5–Be1–C3: 131.3(3); N5–Be1–C1: 131.0(3); C3–Be1–C1: 97.4(3); C2–C1–C13: 126.7(3); C2–C1–Be1: 104.7(3).

### 2.3.3 $^9\text{Be}$ NMR Comparison of Compounds **2.5**, **2.6**, and **2.9**

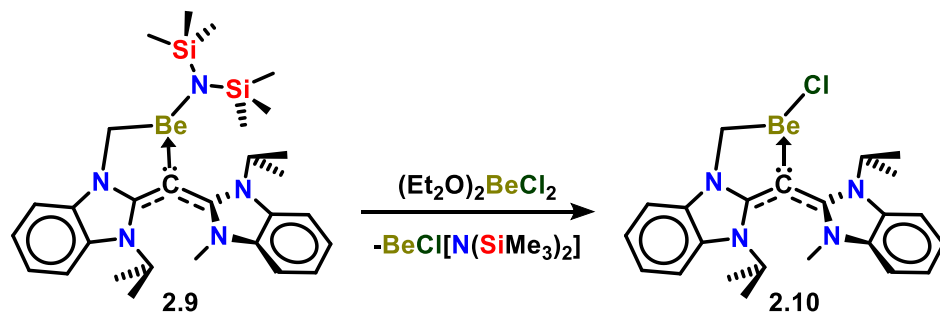
Analysis of the  $^9\text{Be}$  NMR chemical shifts for compounds **2.5** (11.39 ppm), **2.6** (10.41 ppm), and **2.9** (17.73 ppm) reveal that the peaks become more broad, respectively (Figures A2S3, A2S6, and A2S9). This line broadening is due to the trigonal planar geometry around the beryllium nuclei becoming less symmetric and more distorted. The  $^9\text{Be}$  NMR resonances of **2.5**, **2.6**, and **2.9** are in

the range of tricoordinate (NHC)BeR<sub>2</sub> compounds (10.95 ppm, 21.05 ppm),<sup>49-51</sup> (R<sub>3</sub>P)<sub>n</sub>Be<sup>n</sup>Bu<sub>2</sub> complexes (18.4 ppm, 23.2 ppm),<sup>52</sup> and the [Be<sup>n</sup>Bu<sub>2</sub>]<sub>2</sub> dimer (18.3 ppm).<sup>52</sup> It is noteworthy that the <sup>9</sup>Be chemical shift of compound **2.9** is one of the first reported for a five-membered beryllia heterocycle.

## 2.4 Carbodicarbene Beryllacycle and Ring Expansion Chemistry

### 2.4.1 Synthesis of Carbodicarbene(Chloro)Beryllacycle **2.10**

NHC and CAAC do not react with compound **2.9** due to the larger steric bulk, therefore a solution of compound **2.9** in a toluene/hexanes mixture was treated with beryllium dichloride dietherate, (Et<sub>2</sub>O)<sub>2</sub>BeCl<sub>2</sub>, and allowed to stir (Scheme 2.4.1). This metathesis reaction formed BeCl[N(SiMe<sub>3</sub>)<sub>2</sub>],<sup>7</sup> which was confirmed by <sup>9</sup>Be NMR (Figure A2S28). After two days, compound **2.10** was isolated as a yellow solid in 76% yield. The <sup>1</sup>H NMR in C<sub>6</sub>D<sub>6</sub> showed two heptets at 5.58 and 3.31 ppm, which were shifted slightly from the starting material **2.9** (5.57 and 3.36 ppm).<sup>46</sup> Interestingly, the two doublets (2.84 and 2.79 ppm), attributed to the enantiotopic methylene protons on the carbon atom adjacent to beryllium, were shifted downfield from **2.9** (2.75 and 2.60 ppm) and had merged significantly (Figure A2S19).<sup>46</sup> This can be explained by the less sterically demanding chloride allowing for facile rotation of the *N*-heterocyclic carbene (NHC) moiety in compound **2.10** with respect to **2.9**, which is hindered by the bulky [N(SiMe<sub>3</sub>)<sub>2</sub>]<sup>-</sup> group. The <sup>13</sup>C NMR showed a singlet at 164.9 ppm which was attributed to the carbene carbon. This is consistent with our previously reported CDC beryllium complexes (160.3-164.4 ppm).<sup>46</sup>



**Scheme 2.4.1** Beryllacycle salt metathesis with  $(\text{Et}_2\text{O})_2\text{BeCl}_2$ .

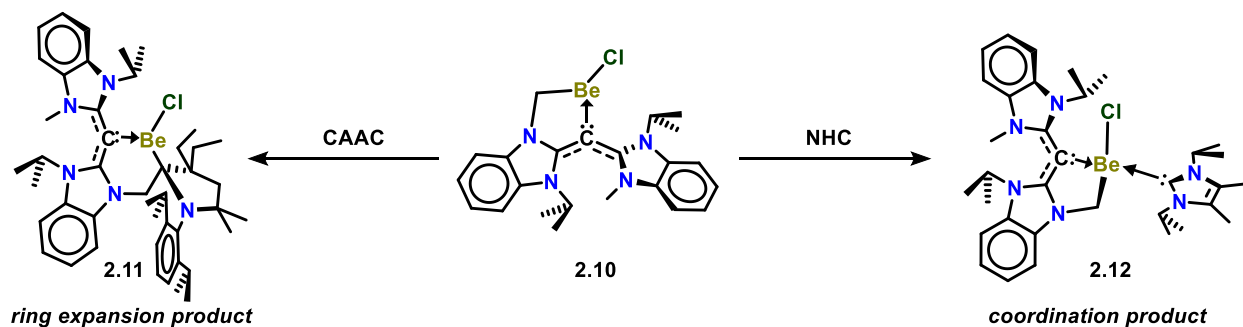
#### 2.4.2 Crystallographic Analysis of Beryllacycle **2.10**

Yellow block-shaped crystals of compound **2.10** suitable for X-ray diffraction were obtained from a toluene/hexanes mixture at  $-37\text{ }^\circ\text{C}$  (Figure 2.4.1). The beryllium atom resides in a distorted trigonal planar environment with two carbon–beryllium bonds [Be1–C3:  $1.769(3)\text{ \AA}$  and Be1–C1:  $1.743(3)\text{ \AA}$ ] and one beryllium–chloride bond [Be1–Cl1:  $1.916(2)\text{ \AA}$ ]. The C1–Be1 bond in **2.10** [ $1.743(3)\text{ \AA}$ ] is significantly shorter than that in **2.9** [ $1.796(5)\text{ \AA}$ ] suggesting a stronger carbone<sup>carbone</sup>C–Be interaction for **2.10**. In support of this greater electronic contribution from the carbone to the beryllium, the C1–C2 bond distance in **2.10** [ $1.391(2)\text{ \AA}$ ] is longer than that in **2.9** [ $1.373(4)\text{ \AA}$ ].

#### 2.4.3 Carbene Coordination Chemistry to Beryllacycle **2.10**

Due to the open coordination site on compound **2.10**, we were motivated to explore its coordination chemistry with carbenes. In toluene, a solution of  $\text{Et}^2\text{CAAC}$  was added to a stirring suspension of **2.10** (Scheme 2.4.2). Immediately upon addition, a yellow product formed in solution. After workup, compound **2.11** was isolated as a yellow solid in 84% yield. The  $^1\text{H}$  NMR showed two doublets at 2.98 and 2.25 ppm, attributed to diastereotopic methylene protons of the five-membered CAAC ring. This is in contrast to a singlet at 1.71 ppm for free  $\text{Et}^2\text{CAAC}$ .

Interestingly, two heptets at 4.96 and 4.79 ppm for the methine protons of the diisopropylphenyl (Dipp) moiety suggest that the rotation of the Dipp group is hindered by steric crowding.



**Scheme 2.4.2** CAAC-promoted ring expansion and NHC coordination to beryllium.

Yellow rod-shaped crystals of **2.11** were obtained by slow evaporation of toluene. The structure revealed that the  $\text{Et}^2\text{CAAC}$  carbene carbon (C24) inserted into the Be1–C3 bond of **2.10** to form a six-membered beryllacycle (Figure 2.4.1). The trigonal planar geometry surrounding beryllium is significantly less distorted than in **2.10** with a C1–Be1–C24 angle of  $114.46(17)^\circ$ , compared to  $101.01(14)^\circ$  for **2.10** (C1–Be1–C3). The Be1–C1 bond ( $1.754(3) \text{ \AA}$ ) is longer than that of **2.10**, indicating less electron donation from  $\text{carbonyl}^{\text{C}}$  to Be. While CAAC has been shown to insert into d-block metal–carbon bonds,<sup>53-54</sup> this is the first example where CAAC inserts into an s-block metal–carbon bond.

We considered that the carbene insertion into the Be1–C1 bond of compound **2.10** might be related to the enhanced electrophilicity of  $\text{Et}^2\text{CAAC}$ . Therefore, we reacted **2.10** with sIPr, a traditional NHC. A solution of sIPr was added to a stirring suspension of **2.10** in toluene. Immediately upon addition, a yellow product formed in solution. After workup, compound **2.12** was isolated as a yellow solid in 86% yield. The peaks in the  $^1\text{H}$  NMR of compound **2.12** in  $\text{C}_6\text{D}_6$  were broadened significantly; therefore, the  $^1\text{H}$  NMR spectrum was obtained in  $\text{CD}_2\text{Cl}_2$ . Two heptets at 5.35 and 3.77 ppm are attributed to the methine protons of the isopropyl groups on the CDC moiety. A heptet at 5.16 ppm was attributed to the methine protons of the isopropyl groups

for a coordinated sIPr ligand. The  $^{13}\text{C}$  NMR revealed a peak at 181.5 ppm which was attributed to the carbene carbon of the coordinated sIPr, which is comparable to the tetrahedral  $[(\text{sIme})_3\text{BeCl}]\text{Cl}$  (sIme = 1,3-dimethylimidazolin-2-ylidene) and  $[\text{BeCl}_2(\text{IPr})_2]$  (IPr = 1,3-diisopropylimidazolin-2-ylidene) (174.9 and 176.6 ppm, respectively).<sup>39-40</sup>

Yellow rod-shaped crystals of **2.12** were obtained by slow evaporation of a toluene/hexanes mixture (Figure 2.4.1). The structure features a beryllium atom in a distorted tetrahedral geometry, with the C1–Be1–C3 angle ( $94.65(17)^\circ$ ) being the largest deviation from  $109.5^\circ$ . The  $^{\text{carbene}}\text{C–Be}$  bond of **2.12** is  $1.862(4)$  Å, which is significantly longer than those of the beryllacycles **2.9–2.11**. In support of this significantly elongated  $^{\text{carbene}}\text{C–Be}$  dative bond, the allenic bond lengths C1–C2 and C1–C13 ( $1.387(3)$  Å and  $1.373(4)$  Å, respectively) are in agreement with greater  $^{\text{carbene}}\text{C}$  to  $^{\text{carbene}}\text{C}$   $\pi$ -donation. The Be1–C11 bond distance is  $2.084(3)$  Å, which is close to  $2.091$  Å for  $[(\text{sMe})_3\text{BeCl}]\text{Cl}$ .<sup>39</sup> The C24–Be1 bond distance in **2.12** ( $1.856(4)$  Å) is the longest reported  $^{\text{carbene}}\text{C–Be}$  bond to date, while previously reported  $^{\text{carbene}}\text{C–Be}$  bonds are within the range of  $1.765$ – $1.822$  Å.<sup>55</sup>

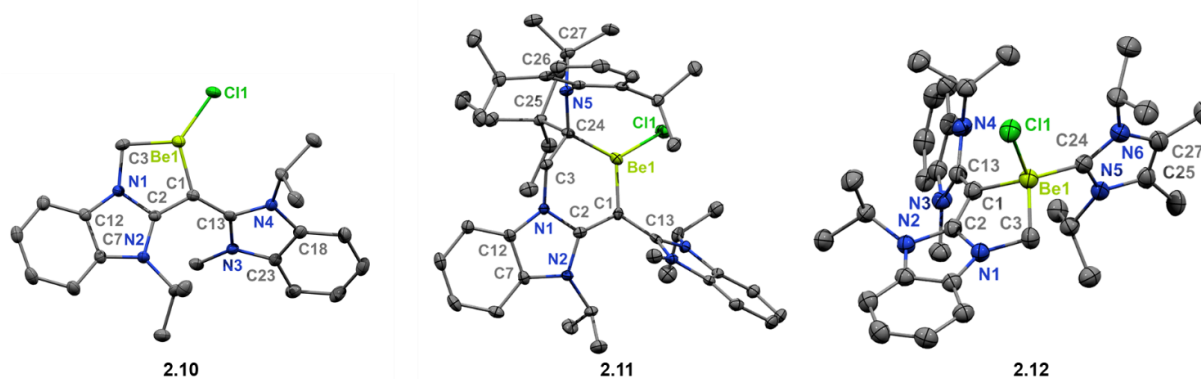


**Figure 2.4.1** Molecular structure of **2.10** (thermal ellipsoids at 50% probability; H atoms and non-coordinating solvent omitted for clarity). Selected bond distances (Å) and angles (deg): Be1–C11:  $1.916(2)$ ; Be1–C1:  $1.743(3)$ ; C1–C2:  $1.391(2)$ ; C2–N1:  $1.378(2)$ ; N1–C3:  $1.471(2)$ ; Be1–C3:  $1.769(3)$ ; C1–C13:  $1.403(2)$ . C1–Be1–C3:  $101.01(14)$ ; C1–Be1–C11:  $129.41(14)$ ; C3–Be1–C11:

129.56(14); C2–C1–C13: 125.28(15) C2–C1–Be1: 103.55(14). **2.11** (thermal ellipsoids at 50% probability; H atoms omitted for clarity). Selected bond distances (Å) and angles (deg): Be1–Cl1: 1.973(3); Be1–C1: 1.754(3); C1–C2: 1.387(3); C2–N1: 1.392(2); N1–C3: 1.467(2); C3–C24: 1.531(3); Be1–C24: 1.791(3); C1–C13: 1.428(3). C1–Be1–C24: 114.46(17); C1–Be1–Cl1: 119.13(16); C24–Be1–Cl1: 126.13(16); C2–C1–C13: 118.63(17); C2–C1–Be1: 115.70(18). **2.12** (thermal ellipsoids at 50% probability; H atoms omitted for clarity). Selected bond distances (Å) and angles (deg): Be1–Cl1: 2.084(3); Be1–C24: 1.856(4); Be1–C1: 1.862(4); C1–C2: 1.387(3); C2–N1: 1.361(3); N1–C3: 1.474(3); Be1–C3: 1.833(4); C1–C13: 1.373(3). C1–Be1–C3: 94.65(17); C1–Be1–Cl1: 106.38(15); C3–Be1–Cl1: 106.89(16); C3–Be1–C24: 113.08(18); C24–Be1–C1: 118.46(19); C24–Be1–Cl1: 115.07(16); C2–C1–C13: 125.3(2).

Compounds **2.10–2.12** were also analyzed by infrared spectroscopy (Figures A2S29–A2S31). Broad bands representative of the allene asymmetric stretching frequency were observed at 1548 cm<sup>-1</sup> and 1541 cm<sup>-1</sup> for compounds **2.10** and **2.12**, which is only slightly less than 1552 cm<sup>-1</sup> for compound **2.9**.<sup>46</sup> A broad band at 1518 cm<sup>-1</sup> was assigned to the allene asymmetric stretching mode for compound **2.11**. This shift to lower wavenumbers is a result of decreased ring strain. It is noteworthy that these trends were reproduced by calculations at the B3LYP-D3(BJ)/def2-TZVP level of theory.<sup>47</sup>

#### 2.4.4 <sup>9</sup>Be NMR Analysis of Beryllacycles **2.10 – 2.12**

The <sup>9</sup>Be NMR data were obtained for the tricoordinate compounds **2.10** and **2.11**, as well as the tetracoordinate compound **2.12**. These gave resonances at 18.2, 14.0, and 5.3 ppm, respectively. The <sup>9</sup>Be NMR spectra for compounds **2.10** and **2.11** show broad signals, which are consistent with reported tricoordinate beryllium complexes.<sup>11, 40, 46, 49-50, 56-57</sup> The <sup>9</sup>Be NMR signal

for compound **2.12** falls within the range of known tetrahedral beryllium compounds (0.8–5.5 ppm),<sup>39-40, 57-60</sup> and is notably sharper than the tricoordinate complexes **2.10** and **2.11**. This broadening is attributed to the quadrupolar coupling effect associated with the anisotropic <sup>9</sup>Be nuclei, which is expected to be zero for perfectly symmetric tetrahedral beryllium complexes.<sup>57</sup> Distortion from this ideal geometry or lower coordination numbers results in broadened chemical shifts.

#### 2.4.5 Theoretical Analysis for the Ring Expansion Reaction of **2.10**

A theoretical exploration of the mechanism for the ring expansion of **2.10** with both CAAC (observed) and NHC (unobserved) was carried out. Model NHC and CAAC ligands with N–Me substituents (labelled <sup>Me</sup>NHC and <sup>Me</sup>CAAC, Figure 2.4.2) were utilized for computational efficiency, which has been demonstrated to yield equivalent results to bulky substituents.<sup>61-62</sup>

The expected difference in reactivity between NHC and CAAC is shown in the reaction energy profile for the ring expansion reaction (RER) of **2.10** (Figure 2.4.2). Initial adduct formation is favorable between **2.10** and both <sup>Me</sup>NHC **2.12** and <sup>Me</sup>CAAC **5** ( $\Delta G = -24.5$  and  $-33.2$  kJ mol<sup>-1</sup>, respectively). However, the barrier for Be–C bond activation with <sup>Me</sup>NHC **TS1<sub>NHC</sub>** is 199.1 kJ mol<sup>-1</sup>, which was inaccessible under the given experimental conditions. Moreover, the ring expanded product with <sup>Me</sup>NHC is 58.3 kJ mol<sup>-1</sup> higher in free energy relative to the free reactants (**2.10** and <sup>Me</sup>NHC). Clearly, RER of **2.10** by NHC is both kinetically and thermodynamically unfavorable, which is consistent with the lack of observed RER with NHC. In contrast, with <sup>Me</sup>CAAC the **TS1<sub>CAAC</sub>** barrier for Be–C bond activation is low (14.0 kJ mol<sup>-1</sup>), which readily leads to the thermodynamically favorable ring expanded product **2.11** ( $-40.9$  kJ mol<sup>-1</sup>). The low barrier is consistent with non-forcing experimental conditions for the reaction to produce **2.11**.

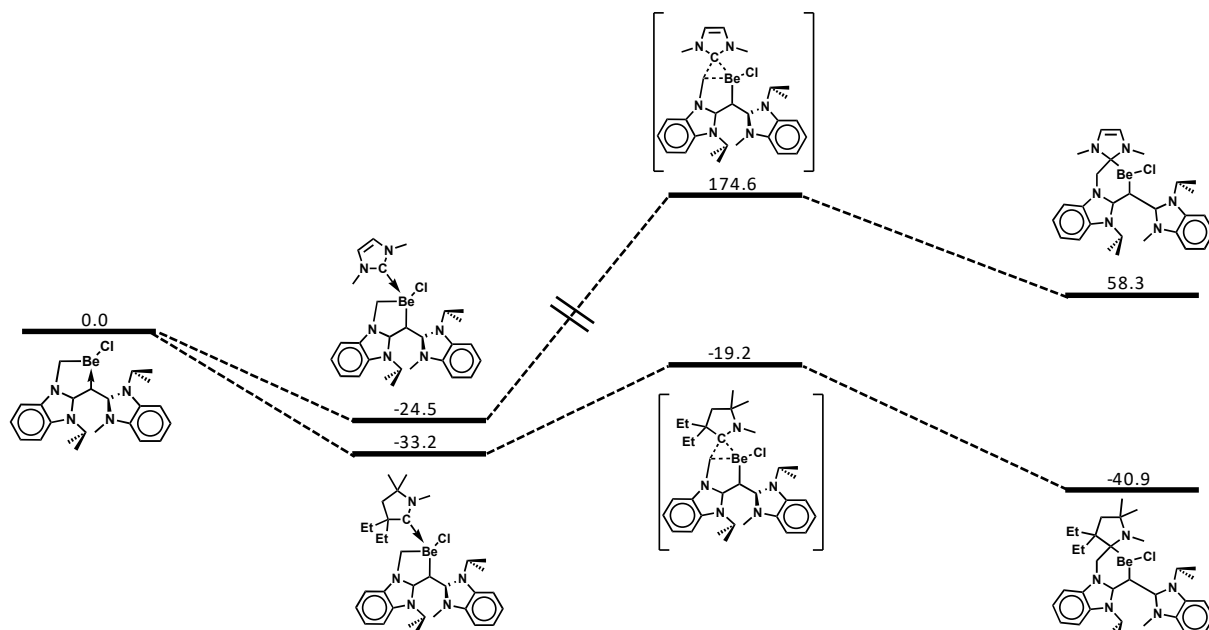


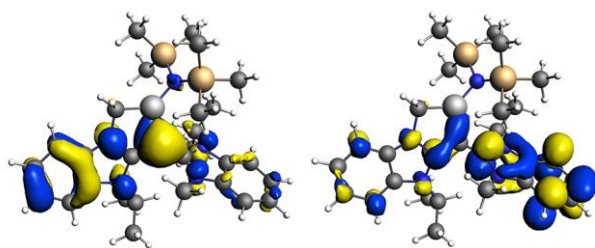
**Figure 2.4.2** Ring expansion pathway for **2.10** with  $\text{Me}^{\text{NHC}}$  and  $\text{Me}^{\text{CAAC}}$ . Calculated relative free energies ( $\Delta G$ ,  $\text{kJ mol}^{-1}$ ) at the B3LYP-D3(BJ)/def2-TZVPP/B3LYP-D3(BJ)/def2-SVP (SMD, toluene) level of theory.

Consideration of the molecular and electronic structure provides further insight into the observed reactivity. The B3LYP-D3(BJ)/def2-SVP (SMD, toluene) optimized geometries are consistent with the crystal structures, with C1–Be1 bond distances of 1.801 Å (**2.9**), 1.760 Å (**2.10**), 1.751 Å (**2.11**) and 1.865 Å (**2.12**). The shorter C1–Be1 bond in **2.10** compared to **2.9** is reflected in the NBO Wiberg bond index (WBI) values of 0.18 (**2.9**) and 0.20 (**2.10**). Quantum theory of atoms in molecules (QTAIM) analysis also supports the stronger interaction in **2.10**, with the electron density at the C1–Be1 bond critical point (BCP) being greater in **2.10** ( $0.073 \text{ e}/\text{Å}^3$ ) compared to **2.9** ( $0.069 \text{ e}/\text{Å}^3$ ). The QTAIM charge on the carbene carbon is also higher in **2.10** (-0.54) than in **2.9** (-0.50), reflecting a larger contribution from the carbene in **2.10** that is consistent with the analysis described above.

For compounds **2.9** and **2.10** the HOMO is a  $\pi$ -symmetric lone-pair centered on the carbene carbon (Figure 2.4.3), which is suggestive of a dative  $\text{carbene}^{\text{C}}\text{--Be}$  bonding interaction. The LUMO

of **2.10** is situated primarily on the NHC moiety of the CDC with sizable coefficients at the carbene C, which suggests potential for  $\pi$ -accepting behavior on the carbene C, and is consistent with recent experimental observations with CDC.<sup>63</sup> The LUMO of **2.9** is calculated to be 0.17 eV higher in energy than for **2.10** (Table 2.4.1), making **2.9** less electrophilic and less reactive towards the carbenes. Indeed, both the electronic structure and the steric repulsion of the bulky  $\text{N}(\text{SiMe}_3)_2$  group opposes the potential for reactivity of **2.9** with carbenes. Similarly, the lower energy LUMO of  $^{\text{Me}}\text{CAAC}$  compared to  $^{\text{Me}}\text{NHC}$  results in the interaction between **2.10** and  $^{\text{Me}}\text{CAAC}$  being more favorable, as expected.

(a)



(b)

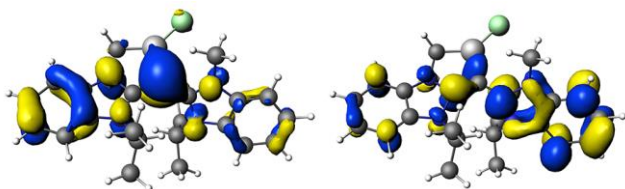


**Figure 2.4.3** Plots of HOMO (left) and LUMO (right) of **2.9** (a) and **2.10** (b).

Compound	HOMO	LUMO	HOMO-LUMO	$\Delta E_{ST}$
NHC <sup>Me</sup>	-6.07	0.42	6.49	93.1
CAAC <sup>Me</sup>	-5.35	0.11	5.25	56.6
CDC	-4.32	-0.42	3.91	65.2
2.9	-4.62	-1.00	3.62	60.3
2.10	-4.87	-1.17	3.70	47.3
2.11	-4.09	-1.26	2.83	45.5
2.12	-4.39	-0.90	3.49	40.3
2.13	-4.37	-0.95	3.42	39.0

**Table 2.4.1** B3LYP-D3(BJ)/def2-SVP (toluene) calculated MO energies (eV) and vertical singlet-triplet gap (kcal/mol).

It is instructive to compare the nature of the carbene adducts, **2.12** (NHC) and **2.13** (CAAC), to explore why the RER is observed for **2.13** but not for **2.12**. While the HOMO and LUMO energies of both carbene adducts are similar in character, both the HOMO-LUMO gap and  $\Delta E_{ST}$  are larger in **2.12**, providing greater electronic stability in **2.12** compared to **2.13**. EDA and ETS-NOCV analysis of **2.12** and **2.13** highlights the interaction between the carbene and the beryllacycle (Table 2.4.2). The bonding interaction in both **2.12** and **2.13** is well-described by a dative bonding model, with 63-65% electrostatic character and 36% orbital character. The interaction energy of the carbene,  $\Delta E_{int}$ , is greater in **2.12** (NHC), which largely arises from reduced Pauli repulsion ( $\Delta E_{Pauli}$ ). ETS-NOCV analysis indicates that the dominant pairwise orbital interaction  $\Delta\rho_1$  arises from  $\sigma$ -donation from the carbene C to the Be atom, as illustrated in Figure 2.4.4. Back-donation to the empty  $p\pi$  orbital of the carbene C atom ( $\Delta\rho_2$ ) is significantly weaker in energy.

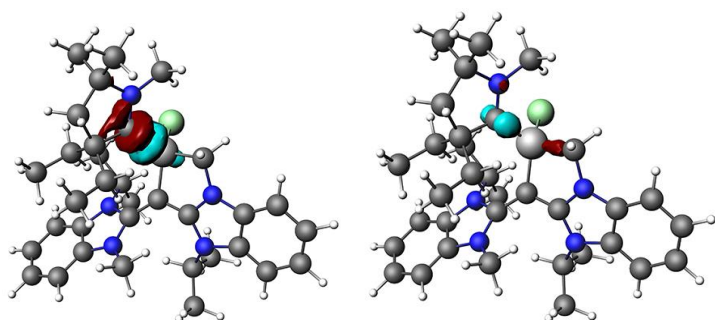
	<b>2.12 (NHC)</b>	<b>2.13 (CAAC)</b>	<b>TS1a NHC</b>	<b>TS1b CAAC</b>
$\square E_{\text{int}}$	-40.1	-36.2	-35.3	-36.6
$\square E_{\text{Pauli}}$	94.8	105.7	321.7	275.3
$\square E_{\text{elec}}^{\text{a}}$	-86.2 (63.9)	-90.4 (63.7)	-192.5 (53.9)	-172.2 (55.2)
$\square E_{\text{orb}}^{\text{a}}$	-48.7 (36.1)	-51.5 (36.3)	-164.4 (46.1)	-139.6 (44.8)
$\square E_1 (\sigma)^{\text{b}}$	-31.4 (64.6)	-32.8 (63.7)	-131.0 (79.7)	-103.6 (74.2)
$\square E_2 (\pi)^{\text{b}}$	-3.69 (7.6)	-4.61 (9.0)	-19.9 (12.1)	-21.6 (15.5)

**Table 2.4.2** EDA analysis of carbene adducts **2.12** and **2.13**, and transition state structures **TS1** (kcal/mol). Transition state structures **TS1** (kcal/mol).

<sup>a</sup>Values in parentheses give the percentage contribution to the attractive interactions,  $\Delta E_{\text{elec}} + \Delta E_{\text{orb}}$ .

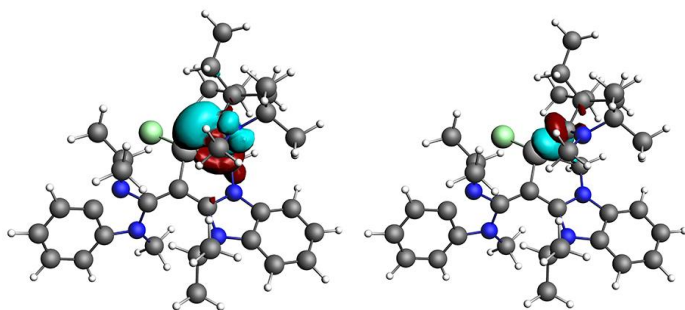
<sup>b</sup> Values in parentheses give the percentage contribution to the orbital interaction,  $\Delta E_{\text{orb}}$ .

(a)



$\Delta\rho_1, \Delta E_1 = -32.8$  kcal/mol     $\Delta\rho_2, \Delta E_2 = -4.61$  kcal/mol

(b)



$\Delta\rho_1, \Delta E_1 = -103.6$  kcal/mol     $\Delta\rho_2, \Delta E_2 = -21.6$  kcal/mol

**Figure 2.4.4** Plots of the deformation densities of the interactions for the pair-wise orbital interactions of the two strongest orbital interactions with the associated interaction energies for (a) theoretical compound **2.13** (interaction between <sup>Me</sup>CAAC and **2.10**), and (b) **TS1b**. Charge flow is from red to blue.

## 2.5 Summary of Carbodicarbene Beryllium Chemistry

The first carbene–beryllium complex was isolated in 2011. This chapter discusses the first examples of carbodicarbene beryllium complexes. CDC is reacted with BeCl<sub>2</sub> to give the LA–LB adduct (CDC)BeCl<sub>2</sub> (**2.5**). Salt metathesis reactions of **2.5** with K[N(SiMe<sub>3</sub>)<sub>2</sub>], LiBH<sub>4</sub>, and LiMe gave the corresponding products (CDC)BeCl[N(SiMe<sub>3</sub>)<sub>2</sub>] (**2.6**), (CDC)BeCl(BH<sub>4</sub>) (**2.7**), and (CDC)Be(CH<sub>3</sub>)<sub>2</sub> (**2.8**). Due to the steric crowding around **2.5**, the metathesis of two Be–Cl bonds was only possible with the small LiMe reagent.

The carbodicarbene–beryllium complex **2.6** forms a five-membered beryllium metallocycle (**2.9**) upon reaction with K[N(SiMe<sub>3</sub>)<sub>2</sub>] or KC<sub>8</sub>, highlighting the unprecedented C(sp<sup>3</sup>)–H activation and cyclization involving beryllium. Thus, this work illustrates an expansion of the emerging activation chemistry of the CDC ligand framework, demonstrating that CDC can be transformed from a neutral monodentate ligand to an anionic chelating ligand. C–H bond activation by the formation of a radical has shown to be a promising approach toward molecular construction with high atom- and step-economy. However, most examples exist only within the realm of transition metal chemistry. An example involving carbenes reported by Whittlesey showed that a Ru(IMes)(PPh<sub>3</sub>)<sub>3</sub>(CO)H<sub>2</sub> complex undergoes C–H activation on IMes during the reaction with (trimethylsilyl)ethane. The utilization of main group elements in C–H activation processes remains rather elusive and we are currently exploring methods to stabilize and isolate the Be(I) intermediate.

The beryllacycle **2.9** can be reacted with BeCl<sub>2</sub> to give the tricoordinate beryllacycle with a terminal chloride (**2.10**). This complex is less sterically hindered around the tricoordinate beryllium center and can easily coordinate a Lewis base. While a small carbene coordinated to Be gives a tetrahedral beryllium complex (**2.12**), <sup>Et</sup>CAAC inserted into a beryllium–carbon bond to form a ring expanded product (**2.11**). This represents the first example of CAAC promoting a ring expansion reaction. DFT calculations on the transition states for CAAC (14.0 kJ mol<sup>-1</sup>) and NHC (199.1 kJ mol<sup>-1</sup>) insertion corroborate the experimental data. In addition, the HOMO-LUMO gap for the NHC adduct **2.12** was found to be larger than that of a CAAC adduct. These results highlight a new bond activation event involving beryllium and the first example of a beryllium ring expansion reaction, which contributes to a better understanding of *s*-block CDC chemistry.

## Chapter 3: Carbene Beryllium Chemistry

- Freeman, L. A.; Walley, J. E.; Obi, A. D.; Wang, G.; Dickie, D. A.; Molino, A.; Wilson, D. J. D.; Gilliard, R. J., Jr., *Inorg Chem* **2019**, 58, 10554-10568.
- Walley, J. E.; Wong, Y.-O.; Freeman, L.A.; Dickie, D.A.; Gilliard, R.J., Jr. *Catalysts* **2019**, 9, 934.

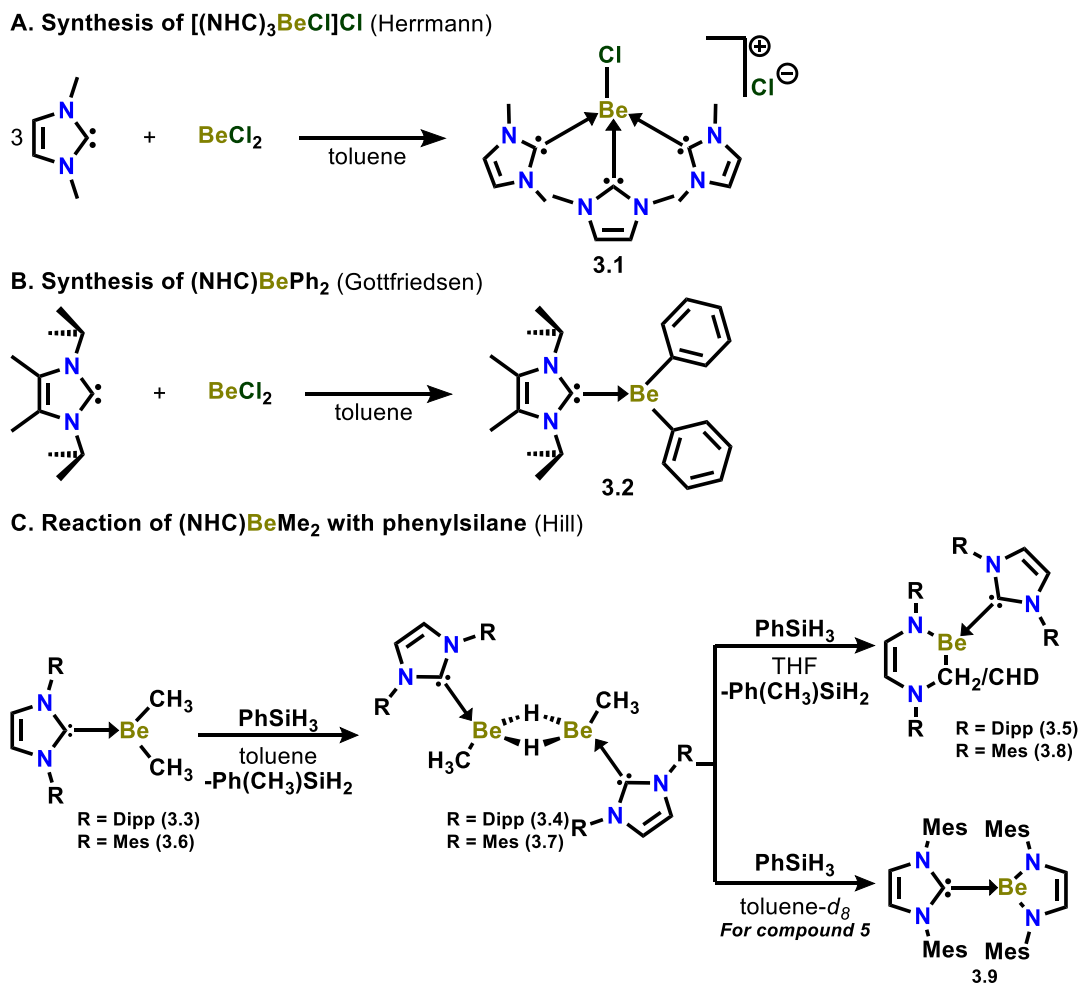
## 3.1 Introduction to Carbene Beryllium Chemistry

### 3.1.1 *N*-Heterocyclic Carbene Beryllium Complexes

As discussed in chapter 1, *N*-heterocyclic carbenes are some of the most ubiquitous ligands in organometallic main-group chemistry. The first example of a published NHC beryllium complex dates back to 1995, where Herrmann isolated the ionic [(NHC)<sub>3</sub>BeCl]Cl complex by the addition of three small NHC ligands to one equivalent of BeCl<sub>2</sub> (Scheme 3.1.1A). This complex contains <sup>NHC</sup>C–Be bonds (1.807(3) and 1.822(3) Å) that are within the range of other C–Be bonds. Nearly 10 years later, Gottfriedsen published the first example of an NHC-supported organoberyllium complex by the complexation reaction of NHC and diphenyl beryllium in toluene (Scheme 3.1.1B). The complex (NHC)BePh<sub>2</sub> exhibits a <sup>NHC</sup>C–Be bond length (1.807(4) Å) comparable to those in [(NHC)<sub>3</sub>BeCl]Cl.

In 2012, Hill and coworkers attempted to isolate an NHC-supported beryllium dihydride.<sup>50</sup> This was motivated by recent efforts towards synthesizing alkaline earth hydrides and utilizing these M–H motifs in metathesis reactions.<sup>64–66</sup> In this work, an NHC containing bulky diisopropylphenyl (Dipp) functional groups was used (IPr). The starting material (IPr)BeMe<sub>2</sub> (**3.3**) was synthesized by the addition of free IPr ligand to a stirring mixture of BeCl<sub>2</sub> followed by two equivalents of methyllithium in toluene (Scheme 3.1.1C). The insoluble LiCl precipitate was removed via filtration and crystals of **3.3** were obtained from a saturated toluene solution. Compound **3.3** was reacted with phenylsilane (PhSiH<sub>3</sub>) to give the bridging hydride complex [(IPr)Be(Me){μ-H}]<sub>2</sub> (**3.4**). When **3.4** was reacted with PhSiH<sub>3</sub> in THF, (IPr)BeH<sub>2</sub> was not observed. Instead, the ring expanded product **3.5** was obtained. The authors noted that while the precise mechanism is unknown, the conversion from **3.4** to **3.5** may occur through a putative

(IPr)BeH<sub>2</sub> intermediate. The reaction of **3.4** with PhSiD<sub>3</sub> was also performed and product **3.5** was obtained with a ‘CHD’ methylene motif.



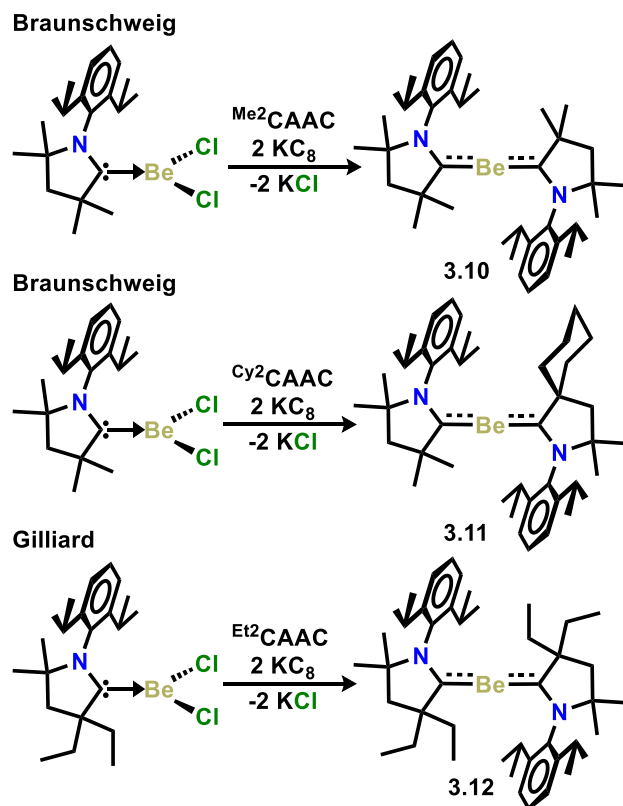
**Scheme 3.1.1** **A.** Synthesis of the first NHC-beryllium complex, [(NHC)<sub>3</sub>BeCl]Cl. **B.** Synthesis of the first NHC supported organoberyllium complex, (NHC)BePh<sub>2</sub>. **C.** Reaction of dimethylberyllium with phenylsilane leads to beryllium insertion into the C–N bonds of an imidazole ring. IPr (R = 2,6-diisopropylphenyl); IMes (R = 2,4,6-trimethylphenyl).

Nearly 3 years later, Hill published a mechanistic study for this reaction.<sup>49</sup> To better enhance solubility for NMR experiments a similar NHC ligand with mesityl groups (Mes) was utilized (IMes). The isostructural (IMes)BeMe<sub>2</sub> (**3.6**), [(IMes)Be(Me){μ-H}]<sub>2</sub> (**3.7**), and ring

expanded product (**3.8**) were synthesized in a similar fashion to compounds **3.3**, **3.4**, and **3.5**. Interestingly, use of the smaller IMes ligand resulted in the activation of both C–N bonds in the imidazole ring, forming Complex **3.9**, which was obtained from heating a toluene-*d*<sub>8</sub> solution of **5** for 1 week at 150 °C. After the *in situ* formation of (NHC)BeH<sub>2</sub>, it was found to be thermodynamically favorable for a second NHC to bind and form the intermediate (NHC)<sub>2</sub>BeH<sub>2</sub>. The next three steps involve: (1) hydride transfer from ‘BeH<sub>2</sub>’ to the carbenoid carbon of one of the NHCs, (2) insertion of beryllium hydride and activation of the C–N bond of the imidazole ring, (3) hydride transfer from beryllium to form the -CH<sub>2</sub>- motif.

### 3.1.2 Cyclic(Alkyl)Amino Carbene Beryllium Complexes

Over the past 15 years cyclic(alkyl)amino carbenes (CAAC) have demonstrated their utility in stabilizing an assortment of subvalent main-group complexes where traditional NHCs were unsuccessful. By utilizing the highly  $\pi$ -acidic nature of CAAC (<sup>Me2</sup>CAAC and <sup>Cy2</sup>CAAC), Braunschweig and coworkers successfully isolated the first examples of molecular beryllium(0) complexes (Scheme 3.1.2).<sup>11</sup> The reaction proceeds by reducing a mixture of (<sup>Me2</sup>CAAC)BeCl<sub>2</sub> and one equivalent of either <sup>Me2</sup>CAAC or <sup>Cy2</sup>CAAC with two equivalents of potassium graphite (KC<sub>8</sub>) to form, respectively, (<sup>Me2</sup>CAAC)<sub>2</sub>Be<sup>0</sup> (**3.10**) and (<sup>Cy2/Me2</sup>CAAC)Be<sup>0</sup> (**3.11**). Not only are these the first examples of beryllium in the oxidation state of zero, but **3.11** represents the first example of a *bis*(carbene) heteroleptic main-group complex.<sup>11</sup> Our lab has synthesized a derivative of this beryllium(0) complex by reducing a mixture of (<sup>Et2</sup>CAAC)BeCl<sub>2</sub> and <sup>Et2</sup>CAAC to synthesize (<sup>Et2</sup>CAAC)<sub>2</sub>Be<sup>0</sup> (**3.12**) and studied its utility as a 2 electron reductant (*vide infra*).



**Scheme 3.1.2** Synthesis of CAAC stabilized beryllium(0) species.

An interesting aspect of the geometric structure for  $(\text{CAAC})_2\text{Be}^0$  is that the two CAAC ligands are perfectly coplanar. Indeed, there is a torsion angle of  $180^\circ$  between the two CAAC ligand rings. This geometric feature can be explained by considering the electron configuration of the  $\text{Be}^0$  center, which was reported to be  $1s^22s^02p^2$ . The two electrons in beryllium's p orbital are involved in a three-center two-electron  $\pi$ -bond spanning the  $^{\text{CAAC}}\text{C}-\text{Be}-\text{C}^{\text{CAAC}}$  central framework. This bonding situation is illustrated in Figure 3.1.1. The  $\text{Be}-\text{C}_{\text{carbene}}$  bond lengths for  $(\text{CAAC})_2\text{Be}^0$  compounds range from  $1.657(4) \text{ \AA}$  to  $1.664(2) \text{ \AA}$ ,<sup>11, 56</sup> which is notably shorter than those known for  $(\text{CAAC})\text{Be}^{\text{II}}\text{Cl}_2$  ( $1.773\text{--}1.802(3) \text{ \AA}$ ).<sup>11, 40, 56</sup> This bond shortening can be explained by the partial double-bonding character of  $^{\text{carbene}}\text{C}-\text{Be}$  in  $(\text{CAAC})_2\text{Be}^0$ .

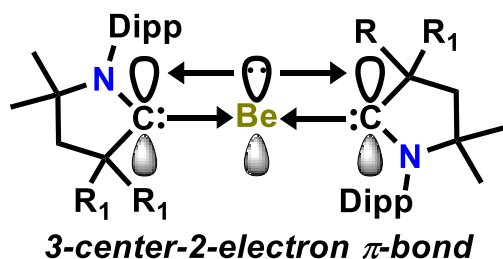
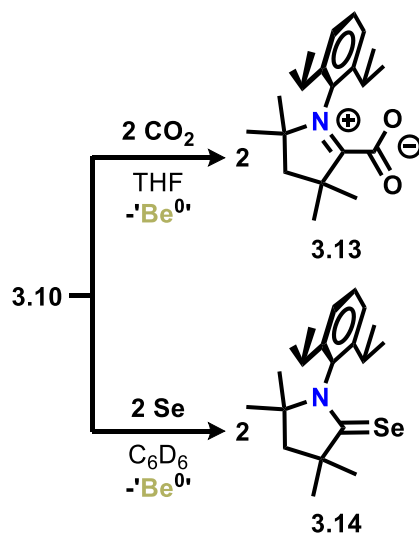


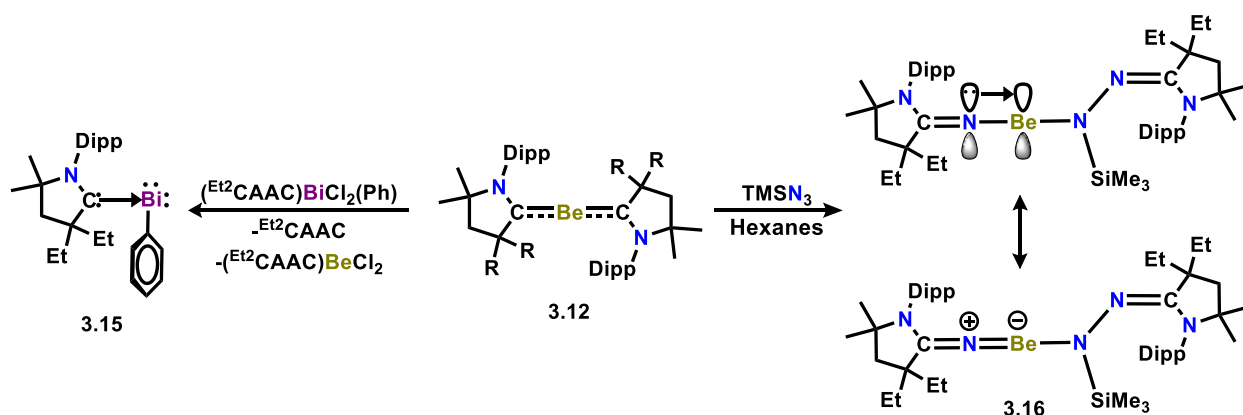
**Figure 3.1.1** Illustration of orbital overlap involved in  $(\text{CAAC})_2\text{Be}^0$ .

The reactivity of these *bis*-CAAC beryllium complexes reveals elemental beryllium behavior for the complex. For example it was found that **3.10** reacts with  $\text{CO}_2$  to yield the zwitterionic complex  $^{\text{Me}_2}\text{CAAC-CO}_2$  (**3.13**, Figure 3.1.3), which has been shown in other reports to form by the direct reaction of CAAC with  $\text{CO}_2$ .<sup>67-68</sup> The reaction of  $(^{\text{Me}_2}\text{CAAC})_2\text{Be}^0$  with elemental selenium (Se) forms the adduct  $^{\text{Me}_2}\text{CAAC-Se}$  (**3.14**, Figure 3.1.3), which is similarly known to form by the direct reaction of  $^{\text{Me}_2}\text{CAAC}$  with Se.<sup>69</sup> In both cases a black solid attributed to beryllium(0) metal precipitated from solution. As a result, the authors claimed that  $(^{\text{Me}_2}\text{CAAC})_2\text{Be}^0$ , as well as  $(^{\text{Cy}_2/\text{Me}_2}\text{CAAC})\text{Be}^0$ , can both be considered *bis*(CAAC) adducts of elemental beryllium.<sup>11</sup>



**Scheme 3.1.3** Reactivity of  $(^{\text{Me}_2}\text{CAAC})_2\text{Be}^0$  towards  $\text{CO}_2$  and selenium (Se).

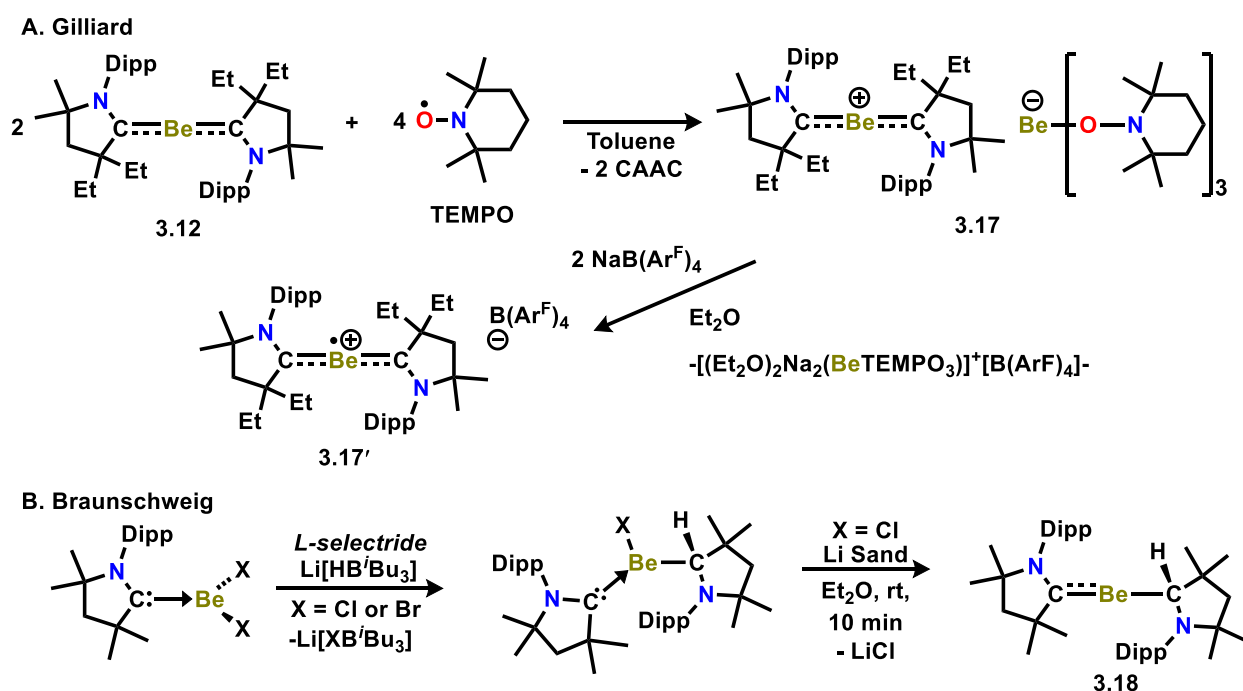
Our lab has further investigated the reactivity of beryllium(0) and discovered that **3.12** can reduce Bi(III) to Bi(I) to synthesize the first carbene–bismuthinidene complex (**3.15**, Scheme 3.1.4).<sup>56</sup> Because beryllium(0) is soluble in most organic solvents, it should exhibit a much different reactivity profile compared to surface area reducing agents such potassium graphite. While this soluble reductant chemistry has been well documented for sub-valent Mg(I)–Mg(I), this work represents beryllium(0) as a reducing agent for the first time. In this regard, we have also found that  $(\text{Et}^2\text{CAAC})_2\text{Be}^0$  will reduce trimethylsilyl azide ( $\text{TMSN}_3$ ) to give compound **3.16**. Featuring the shortest Be–N bond (1.464 Å), **3.16** represents the first *s*-block metal–nitrogen multiple bond and can be described best as a beryllium imido motif.



**Scheme 3.1.4**  $(\text{Et}^2\text{CAAC})_2\text{Be}^0$  as a soluble reducing agent.

In a similar context, chemists have been fascinated with the possibility of beryllium(I) species, mainly the elusive beryllium(I)–beryllium(I) bond which is discussed later in this review. It has already been demonstrated that a plausible beryllium(I) intermediate facilitates the activation of a  $\text{C}(\text{sp}^3)\text{--H}$  bond (**Chapter 2.3**), foreshadowing the reactivity of a beryllium radical species. In that case the beryllium(I) intermediate was not able to be isolated and immediately reacts upon formation. Other groups also report the reduction of certain Be(II) species fail to give Be(I).<sup>70-71</sup>

Contrasting the idea of reducing Be(II) to Be(I) is to oxidize the known  $(\text{CAAC})_2\text{Be}^0$  by one electron. Our lab succeeded with the strategy by oxidation of **3.12** with TEMPO (a one electron oxidizing agent), realizing the first beryllium(I) charged radical cation (**3.17**, Scheme 3.1.5A). The product  $[(\text{CAAC})_2\text{Be}^{\cdot+}][\text{Be}(\text{OR})_3]$  complex is completely insoluble in organic solvents, but can undergo anion exchange to with  $\text{Na}[\text{BAr}^{\text{F}}_4]$  to form the ether soluble complex  $[(\text{CAAC})_2\text{Be}^{\cdot+}][\text{BAr}^{\text{F}}_4]$  (**3.17'**).



**Scheme 3.1.5** Synthesis of  $(\text{CAAC})_2\text{Be}^{\cdot+}$  by oxidation of  $(\text{CAAC})_2\text{Be}^0$

Recently, Braunschweig reported the first *neutral* Be(I) radical (**3.18**, Scheme 3.1.5B).<sup>72</sup> The starting material  $(\text{CAAC}-\text{H})\text{BeX}(\text{CAAC})$  (X = Cl, Br) is synthesized by the reaction of  $\text{CAAC}-\text{BeX}_2$  with L-selectride in the presence of free CAAC. The reduction of  $(\text{CAAC}-\text{H})\text{BeCl}(\text{CAAC})$  to form the neutral Be(I) radical,  $(\text{CAAC}-\text{H})\text{Be}^{\cdot}(\text{CAAC})$  was achieved in  $\text{Et}_2\text{O}$  with Li sand, while the analogous reaction of  $(\text{CAAC}-\text{H})\text{BeBr}(\text{CAAC})$  with various reducing agents produced  $[\text{CAACH}]\text{Br}$ . The neutral radical is stabilized by both a protonated and neutral

CAAC ligand and possesses 23% spin density on the metal center. Interestingly, hyperfine coupling to  $^9\text{Be}$  (spin = 3/2) is observed in  $(\text{CAAC-H})\text{Be}^{\text{I}}(\text{CAAC})$  (4.1 G), which is not the case for **3.17'** (0.32 G).

A trend can be observed for the  $^{\text{CAAC}}\text{C}-\text{Be}$  bond lengths in the solid-state structure for all of the previously discussed CAAC-beryllium systems (Figure 3.1.2). The  $^{\text{CAAC}}\text{C}-\text{Be}$  bond lengths decreases in the order beryllium(II) (1.779 – 1.794 Å) > beryllium(I) cation (1.691 – 1.694 Å) > beryllium(0) (1.659 – 1.664 Å). This trend results from a greater  $\pi$ -interaction within the  $^{\text{CAAC}}\text{C}-\text{Be}$  bond for the reduced *bis*(CAAC) beryllium systems compared to the divalent  $(\text{CAAC})\text{BeCl}_2$ . The neutral beryllium(I) complex  $^{\text{CAAC}}\text{C}-\text{Be}$  bond (1.661 Å) is comparable to that of beryllium(0) because of a 2-center-1-electron interaction in **3.18**.

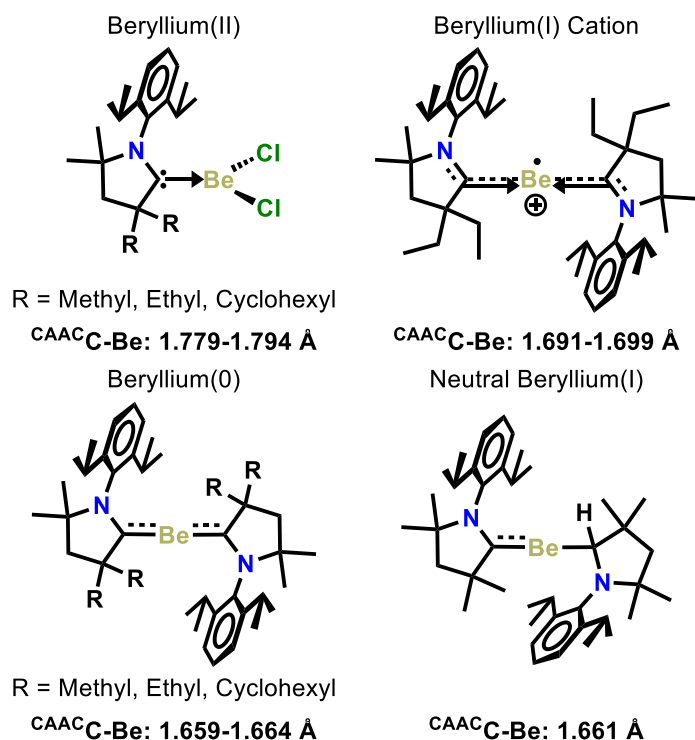


**Figure 3.1.2** Bond length comparison for  $\text{CAAC}-\text{Be}^{\text{II}}\text{Cl}_2$  (top left),  $[(\text{CAAC})_2\text{Be}^{\text{I}}]^+$  (top right),  $(\text{CAAC})_2\text{Be}^0$  (bottom left), and  $(\text{CAACH})\text{Be}^{\text{I}}(\text{CAAC})$  (bottom right).

## 3.2 Carbene-Supported Beryllium Aryl- and Alkoxide Complexes

### 3.2.1 Introduction to Alkaline Earth Oxides

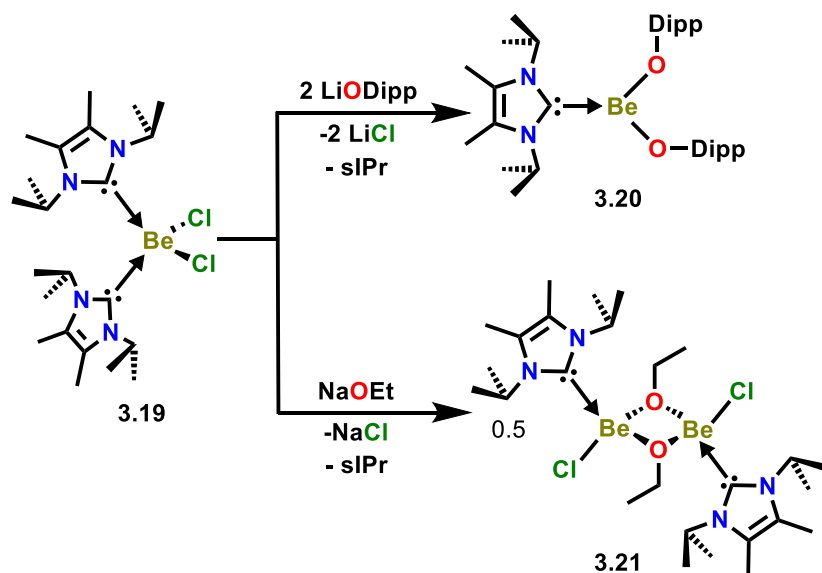
The chemistry of alkaline earth metal oxides has historically been associated with materials of high thermal stability and poor solubility.<sup>73</sup> For example, beryllium and magnesium oxide melt at extremely high temperatures (up to 2852 °C) and are completely insoluble in organic solvents.<sup>74</sup> Indeed, the inherent chemical and physical properties of Ae-O (Ae = alkaline earth) heterogeneous materials preclude the use of these types of compounds as precursors for molecular chemistry. As such, chemists routinely employ synthetic strategies to decorate Ae-O bonds with various aryl or alkyl functionalities and/or bulky ligands to impart both stability and solubility. Even under these strict conditions, Ae-O moieties have a propensity to form insoluble polymeric structures, particularly after loss of stabilizing ligands.<sup>15, 75</sup> Consequently, the literature contains a relatively small number of structurally characterized compounds containing Ae-O fragments beyond weakly bound Ae $\leftarrow$ O dative interactions resulting from coordination of ethereal solvents.<sup>76-80</sup>

Early work by Bell on the reactions of beryllium chloride with lithium salts led to the reactive beryllium alkoxide dimer (ClBeO<sup>t</sup>Bu•OEt)<sub>2</sub> and tetramer (ClBeO<sup>t</sup>Bu)<sub>4</sub>.<sup>77</sup> Power reported a beryllium aryloxide [Be(OMes\*)<sub>2</sub>(OEt<sub>2</sub>)] (Mes\* = 2,4,6-<sup>t</sup>Bu<sub>3</sub>C<sub>6</sub>H<sub>2</sub>) which is protected by sterically demanding groups.<sup>81</sup> More recently, Hill reported a series of beryllium aryl- and alkoxides (NacNac-BeOR; R = Me, <sup>t</sup>Bu, Ph) stabilized by the bulky  $\beta$ -diketiminato (NacNac) ligand, as well as the first tricoordinate beryllium hydroxide (NacNac-BeOH).<sup>70</sup> In a subsequent report, Hill detailed the synthesis of tricoordinate  $\beta$ -diketiminato beryllium alkoxide species, [NacNac-BeO(CH<sub>2</sub>)<sub>4</sub>I], which was generated by ring opening insertion of tetrahydrofuran into a beryllium-iodide bond.<sup>82</sup>

### 3.2.2 Synthesis and Isolation of Beryllium Aryl- and Alkoxides

The chemistry of beryllium continues to be severely understudied relative to the heavier group 2 elements and NHC-beryllium oxides are hitherto unknown. Herein, the synthesis of  $(\text{sIPr})_2\text{BeCl}_2$  (**3.19**),  $[(\text{sIPr})\text{Be}(\text{OEt})\text{Cl}]_2$  (**3.20**), and  $(\text{sIPr})\text{Be}(\text{ODipp})_2$  (**3.21**) is described. The reaction of 1,3-diisopropyl-4,5-dimethylimidazol-2-ylidene ( $\text{sIPr}$ ) and  $(\text{Et}_2\text{O})_2\text{BeCl}_2$  in THF produces a white suspension after stirring for 1 h at room temperature. After workup, compound **3.19** is isolated as a white solid in 84% yield. The  $^1\text{H}$  NMR spectrum revealed a new septet at 6.34 ppm which was attributed to the methine protons of compound **3.20**. Due to the strongly deshielding Be center, this peak is significantly downfield from free ligand (3.96 ppm).

Two equivalents of lithium diisopropylphenoxide ( $\text{LiODipp}$ ) were stirred with **3.19** in THF for 18 h at room temperature (Scheme 3.2.1). After workup,  $(\text{sIPr})\text{Be}(\text{ODipp})_2$  (**3.20**) was obtained as a white solid in 34% yield. The  $^1\text{H}$  NMR spectra shows two new heptets at 4.87 ppm and 3.55 ppm, representative of new methine environments for  $\text{sIPr}$  and  $\text{ODipp}$ , respectively. We also performed the reaction of **3.19** with one equivalent of  $\text{LiODipp}$ . The  $^1\text{H}$  NMR spectrum revealed peaks for **3.19**, **3.20**, and uncoordinated  $\text{sIPr}$  (Figure 3.2.1). It is clear that the reaction is highly selective for producing **3.20**, and therefore no heteroleptic monosubstituted molecules could be isolated.



**Scheme 3.2.1** Synthesis of a complex containing two untethered NHCs bound to a mononuclear beryllium halide (**3.19**). Reactions of **3.19** with LiODipp and NaOEt to produce  $(\text{sIPr})\text{Be}(\text{ODipp})_2$  (**3.20**) and  $[(\text{sIPr})\text{BeCl}(\text{EtO})]_2$  (**3.21**), respectively.

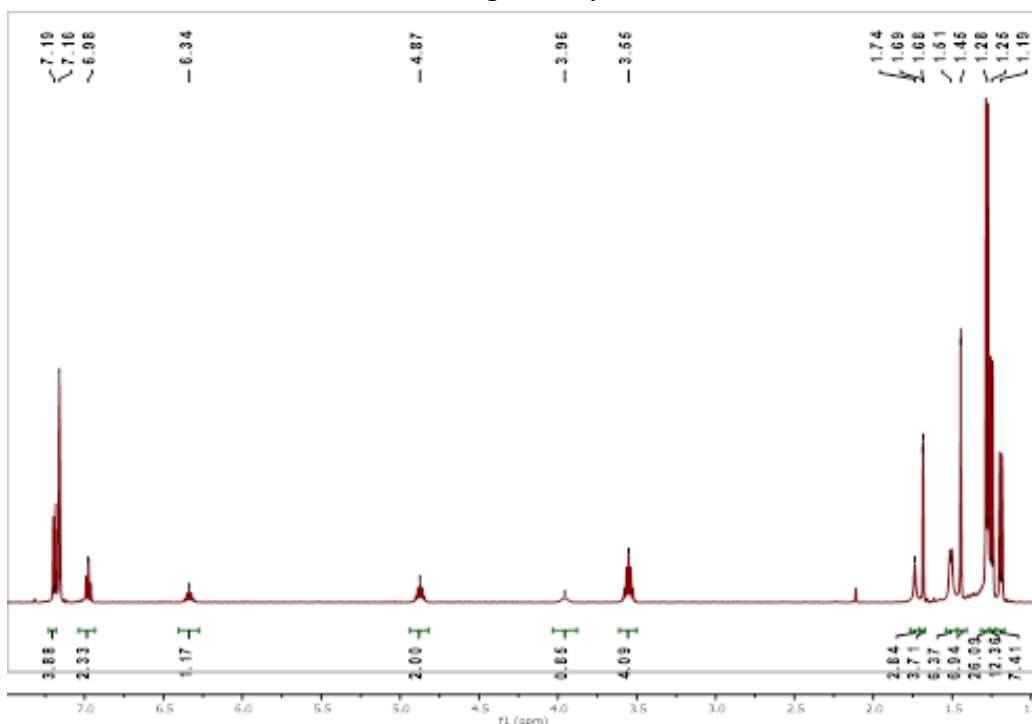


**Figure 3.2.1**  $^1\text{H}$  NMR spectrum (500.13 MHz,  $\text{C}_6\text{D}_6$ , 298 K) of compound **3.19** reaction with one equivalent of LiODipp. Free sIPr methine (3.96 ppm).

It was reasoned that the reaction of **3.19** with a less sterically demanding alkoxide salt would give the heteroleptic halo-beryllium alkoxide dimer. Therefore, **3.19** was reacted with sodium ethoxide in THF for two days. After removing insoluble NaCl and concentration of the filtrate, compound **3.21** was obtained as colorless block-like crystals at  $-37\text{ }^{\circ}\text{C}$  from a toluene solution. The  $^1\text{H}$  NMR spectra revealed a septet at 6.47 ppm for a methine environment of a new sIPr containing product, which is downfield from the starting material **3.19** (6.34 ppm). Due to very similar solubilities, crystals of compounds **3.19** and **3.21** were obtained in the bulk product and could not be separated despite considerable effort.

### 3.2.3 Crystallographic Analysis of Beryllium Aryl- and Alkoxides

Colorless crystals of compound **3.19** were obtained from toluene at  $-37\text{ }^{\circ}\text{C}$ . The structure features a unit of  $\text{BeCl}_2$  coordinated by two sIPr ligands. The beryllium atom is featured in a distorted tetrahedral environment with the widest bond angle being  $\text{C1}-\text{Be1}-\text{Cl1}$  at  $118.13(6)^{\circ}$ , with two NHC ligands bound to  $\text{BeCl}_2$  (Figure 3.2.2). The  $^{\text{carbene}}\text{C}-\text{Be}$  bond distance of **3.19** is  $1.849(3)\text{ \AA}$  falls within the range of other  $^{\text{carbene}}\text{C}-\text{Be}$  bonds ( $1.779-1.856(4)$ ).<sup>11, 39-40, 44, 47, 49, 56, 70</sup> Additionally, the  $^{\text{carbene}}\text{C}-\text{Be}$  bond of **3.19** is longer than those of  $(\text{CDC})\text{BeCl}_2$  ( $1.748\text{ \AA}$ ),<sup>46</sup> and  $(\text{CDP})\text{BeCl}_2$  ( $1.742\text{ \AA}$ ).<sup>38</sup> Compound **3.19** is structurally similar to the recently reported  $(\text{PMe}_3)_2\text{BeCl}_2$  and  $(\text{NHC})_2\text{BeCl}_2$  complexes.<sup>40, 83</sup>

Colorless, needlelike crystals of **3.20** were obtained at  $-37\text{ }^{\circ}\text{C}$  from a toluene solution (Figure 3.2.2). The crystal structure revealed one sIPr ligand bound to beryllium *bis*(diisopropylphenoxide),  $(\text{sIPr})\text{Be}(\text{ODipp})_2$ . The beryllium is centered in a distorted trigonal planar geometry, with the largest angle being  $\text{O1}-\text{Be1}-\text{C1}$  at  $124.99(17)^{\circ}$ . The  $^{\text{carbene}}\text{C}-\text{Be}$  bond ( $1.797\text{ \AA}$ ) falls within the range of known  $^{\text{carbene}}\text{C}-\text{Be}$  bond distances.<sup>39-40, 44</sup>

The crystal structure revealed a bridging ethoxide beryllium complex, **3.21**, where one chloride remains on each beryllium atom (Figure 3.2.2). These complexes represent the first examples of beryllium alkoxide species stabilized by a neutral carbene ligand. The beryllium atoms are each in a distorted tetrahedral environment. The <sup>carbene</sup>C–Be bond length is 1.855(4) Å, which is slightly longer than the starting material **1**. The Be–O bond distances (1.621(4) Å and 1.641(4) Å) are within the range of the Be–O bond distances of the known amidinate supported [Be(μ-OEt)]<sub>2</sub> dimer (1.602 Å and 1.631 Å),<sup>84</sup> and the ketiminate supported [Be(OEt)Cl]<sub>2</sub> dimer (1.631 Å and 1.666 Å).<sup>5</sup>

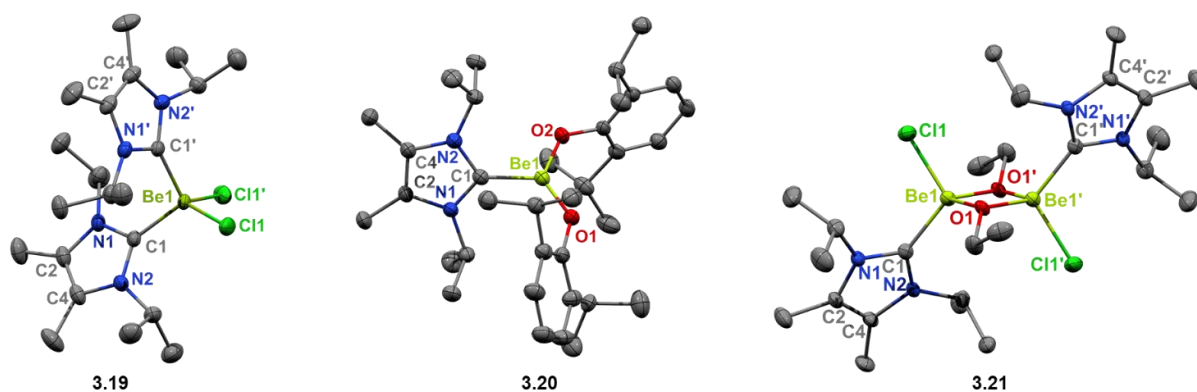


**Figure 3.2.2** Molecular structure of **3.19** (thermal ellipsoids at 50% probability; H atoms and toluene solvent molecules omitted for clarity). Selected bond distances (Å) and angles (deg): Cl1–Be1: 2.0445(19); C1–Be1: 1.849(3); N1–C1: 1.367(2); N1–C2: 1.397(2); C2–C4: 1.354(3); N2–C4: 1.397(2); N2–C1: 1.357(2). N2–C1–Be1: 132.29(14); N1–C1–Be1: 123.10(14); C1–Be1–C1: 105.37(19); C1–Be1–Cl1: 118.13(6); C1–Be1–Cl1: 103.79(6). **3.20** (thermal ellipsoids at 50% probability; H atoms omitted for clarity). Selected bond distances (Å) and angles (deg): Be1–O2: 1.497(3); Be1–O1: 1.507(3); Be1–C1: 1.797(3); N1–C2: 1.393(2); N1–C1: 1.353(2); N1–C2: 1.359(2); N2–C4: 1.391(2); C2–C4: 1.362(3). O2–Be1–O1: 122.34(17); O2–Be1–C1: 112.66(15); O1–Be1–C1: 124.99(17). **3.21** (thermal ellipsoids at 50% probability; H atoms omitted for clarity). Selected bond distances (Å) and angles (deg): Be1–O1: 1.621(4);

Be1–O1: 1.641(4); Be1–C1: 1.855(4); Be1–Cl1: 2.044(3); N1–C1: 1.362(3); N1–C2: 1.391(3); 1.362(3); N2–C4: 1.393(3); C2–C4: 1.355(4). O1–Be1–O1: 89.99(18); O1–Be1–C1: 113.9(2); O1–Be1–C1: 119.0(2); C1–Be1–Cl1: 109.11(18).

### 3.3 Reduction of Carbene–Beryllium Dihalides in the Presence of a Redox Non-Innocent Bipyridene

#### 3.3.1 Introduction to Beryllium Complexes with Redox Non-Innocent Ligands

As discussed in 3.1.2, The CAAC ligand system was ideal in stabilizing subvalent beryllium ( $\text{Be}^{\text{I}}$  and  $\text{Be}^0$ ). While reducing the beryllium metal center represents a difficult synthetic challenge, a more viable method is to reduce the beryllium complex, where a redox non-innocent ligand accepts the electrons instead of the metal. Thiele found that the treatment of beryllium chloride with diazadiene (DAD) and sodium produced the highly stable  $[\text{Be}(\text{DAD})_2]$  (**3.22**, Figure 3.3.1A), where each DAD ligand has been singly reduced.<sup>85</sup> When this paramagnetic complex is dissolved in THF an intramolecular disproportionation takes place, where one of the singly reduced anionic ligands transfers its electron to the other DAD ligand forming a doubly-reduced  $[(\text{THF})\text{Be}(\text{DAD})]_2$  complex (**3.23**). Wang showed that reacting beryllium dichloride with an unsymmetrical 2-(2-pyridyl)indole (2-py-in) ligand and butyllithium produces a non-radical bis( $N,N'$ -chelating)beryllium complex (**3.24**, Figure 3.3.1B), where  $N$  is bound as an amide and  $N'$  is a pendant datively bound pyridine.<sup>86</sup> Complex **3.24** was demonstrated as an efficient and promising emitter for electroluminescent devices. Moreover, paramagnetic character, as seen in **3.23**, can be avoided by utilizing an unsymmetric ligand, such as 2-py-in in **3.24**, which forces the charge to localize on one nitrogen.

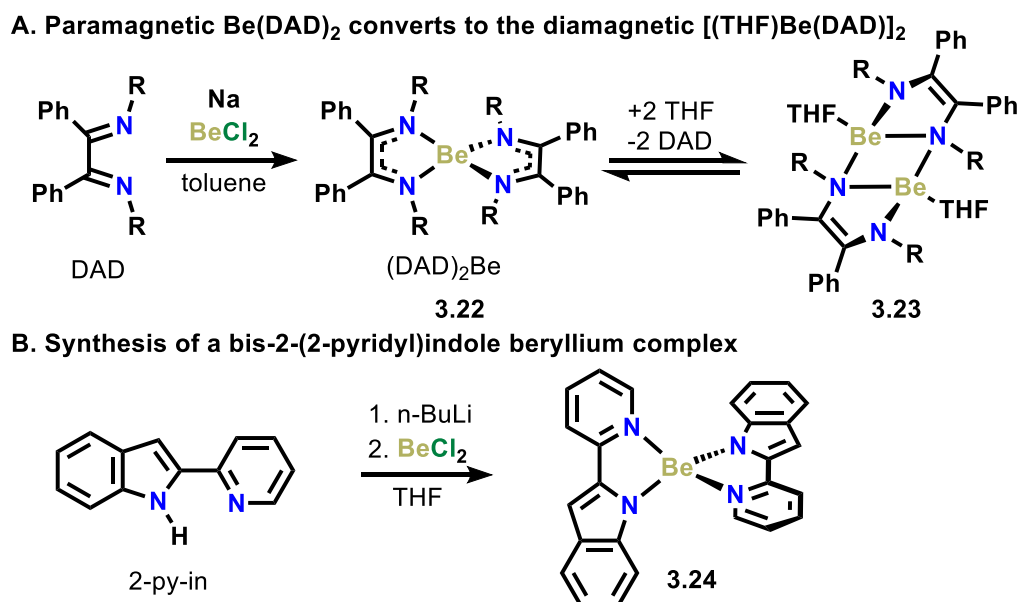


**Figure 3.3.1** **A.** Synthesis of a  $(\text{DAD})_2\text{Be}$  complex and equilibrium with THF; **B.** synthesis of an electroluminescent  $(2\text{-py-in})_2\text{Be}$  compound.

Hill found that heating  $(\text{IMes})\text{Be}(\text{CH}_3)_2$  ( $\text{IMes} = 1,3\text{-bis}(2,4,6\text{-trimethylphenyl})\text{imidazol-2-ylidene}$ ) with excess phenylsilane yields  $(\text{IMes})\text{Be}(\text{mesDAB})$  ( $\text{mesDAB} = \text{bis}(2,4,6\text{-trimethylphenyl})\text{-1,4-diazabutadiene}$ ), where  $\text{mesDAB}$  is a doubly reduced diamine ligand (compound **3.9**, 3.1.1).<sup>49</sup> An interesting geometric feature for the solid-state structure of  $(\text{IMes})\text{Be}(\text{mesDAB})$  is the near coplanarity of the NHC and  $\text{mesDAB}$  rings, with a torsion angle of nearly  $36^\circ$  between the two motifs. The sterically demanding mesityl group would lead one to suspect a torsion angle closer to  $90^\circ$ . Therefore, there must be an electronic reason for this geometric structure.

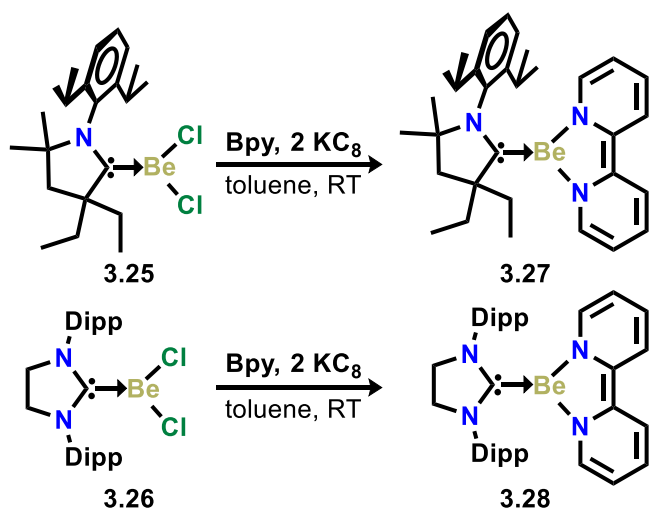
### 3.3.2 Synthesis and Characterization of Double Reduced Carbene-Beryllium Bipyridene Complexes

The starting material  $(\text{Et}^2\text{CAAC})_2\text{BeCl}_2$  (**3.25**) was previously reported by our lab. The SIPr adduct of  $\text{BeCl}_2$  was prepared under similar conditions, in which  $\text{BeCl}_2 \cdot 2(\text{Et}_2\text{O})$  was added to a

solution of free SIPr in dry toluene to yield the desired solvent-free coordination compound, **3.26**, as a white solid after 16 h at room temperature. The  $^1\text{H}$  NMR spectrum of **3.26** in  $\text{C}_6\text{D}_6$  showed a heptet at 3.26 ppm attributed to the methine proton of a new SIPr coordination compound, compared to 3.28 ppm for free SIPr. The  $\text{CH}_2$  protons of the five-membered heterocyclic ring were shifted from 3.37 to 3.51 ppm. The  $^{13}\text{C}$  NMR spectrum showed a shift at 188.1 ppm, attributed to the carbene carbon of coordinated SIPr. This is within the range of known NHC–beryllium dichloride complexes. The  $^9\text{Be}$  NMR spectrum showed a broad signal at 10.0 ppm, which is slightly upfield from the range of terphenyl–beryllium complexes reported by Power (11.4–17.4 ppm). The  $^9\text{Be}$  NMR shift of **3.26** is also slightly upfield from (MesDAC)BeCl<sub>2</sub> [MesDAC = bis(2,4,6-trimethylphenyl) cyclic diamidocarbene] which gives a resonance at 11.6 ppm. There are no  $^9\text{Be}$  NMR data reported for tricoordinate adducts of BeCl<sub>2</sub> with Arduengo-type NHCs for direct comparison. However, the  $^9\text{Be}$  NMR resonances for tetracoordinate (sIPr)<sub>2</sub>BeCl<sub>2</sub> (3.4 ppm) and [(sIMe)<sub>3</sub>BeCl]<sup>+</sup>[Cl]<sup>−</sup> (0.9 ppm) are both substantially upfield from that of **3.26** (sIPr = 1,3-diisopropylimidazol-2-ylidene, sIMe = 1,3-dimethylimidazol-2-ylidene). These differences are consistent with the general trends observed in the  $^9\text{Be}$  NMR data of tetracoordinate and tricoordinate beryllium complexes.

<sup>Ei2</sup>CAAC– and SIPr–beryllium congeners were synthesized by the addition of KC<sub>8</sub> (2 eq) to mixtures of bpy with either (<sup>Ei2</sup>CAAC)BeCl<sub>2</sub> or (SIPr)BeCl<sub>2</sub> (Scheme 3.3.2). The resulting mixtures were stirred vigorously for 16 hours, yielding the products (<sup>Ei2</sup>CAAC)Be(bpy) (**3.27**) and (SIPr)Be(bpy) (**3.28**) as dark blue and dark orange solids, respectively. The  $^1\text{H}$  NMR spectrum of **3.27** in  $\text{C}_6\text{D}_6$  revealed a characteristic singlet at 1.54 ppm for the  $\text{CH}_2$  protons of the five-membered heterocyclic ring, compared to 1.71 ppm for the free <sup>Ei2</sup>CAAC. The  $^9\text{Be}$  NMR showed a broad signal at 4.8 ppm, which is similar to that reported for (IMes)Be(<sup>Mes</sup>DAB) (4.4 ppm).<sup>87</sup> The  $^1\text{H}$

NMR spectrum of **3.28** in  $C_6D_6$  showed a septet at 3.11 ppm attributed to the methine proton of a new SIPr coordination compound, compared to 3.26 ppm for **3.26**. The  $CH_2$  protons of the five-membered heterocyclic ring were shifted from 3.51 ppm to 3.36 ppm. The  $^9Be$  NMR showed a broad signal at 4.50 ppm, which is within range of both **3.28** and  $(IMes)Be^{(Mes)DAB}$ .<sup>87</sup> Notably, both **3.27** and **3.28** gave  $^9Be$  NMR resonances substantially upfield for tricoordinate complexes. This is likely because of a positive electromeric contribution from the  $\pi$ -symmetric lone pairs of the diimine nitrogen atoms.



**Scheme 3.3.2** Synthesis of doubly-reduced beryllium complexes.

B3LYP-D3(BJ)/def2-TZVP calculations for **3.26** yield Be–C (1.779 Å) and Be–Cl (1.914 Å) bond distances. Natural bond orbital (NBO) and energy decomposition analysis (EDA) results are consistent with a donor–acceptor bonding description of  $^{NHC}C-Be$  (60% electrostatic, 35% orbital, and 4% dispersion contribution to Be–C bond). DFT similarly yields three-coordinate geometries for **3.27**<sup>NMe</sup> and **3.28**<sup>NMe</sup>, with Be–C bond distances of 1.731 and 1.747 Å, respectively (for further details see SI – Tables S7-S8). The HOMOs for **3.27**<sup>NMe</sup> and **3.28**<sup>NMe</sup> reveal  $\pi$ -symmetric delocalization over bpy and Be, with some contribution to a Be=C double bond.

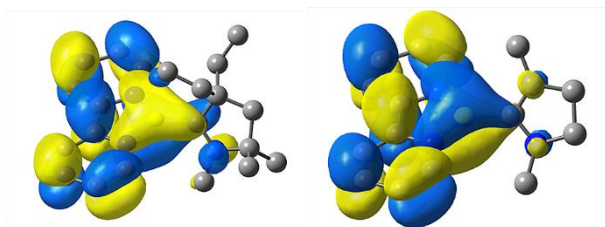


**Figure 3.3.2** Plot of HOMOs for compound **3.27**<sup>NMe</sup> (left) and **3.28**<sup>NMe</sup> (right).

The UV-Vis spectrum for **3.27** (Figure A2S51) in toluene showed a strong absorption band ( $\epsilon = 14931 \text{ M}^{-1}\text{cm}^{-1}$ ) at 385 nm, two weak signals at 482 nm, 507 nm ( $\epsilon = 5034 \text{ M}^{-1}\text{cm}^{-1}$  and  $4949 \text{ M}^{-1}\text{cm}^{-1}$ ), and a broad, weak absorption band ( $\epsilon = 2377 \text{ M}^{-1}\text{cm}^{-1}$ ) at 805 nm. The corresponding energy of the transition at 805 nm is low at 35.5 kcal/mol. The UV-Vis spectrum for **3.28** (Figure A2S52) in toluene showed a strong absorption band ( $\epsilon = 9183 \text{ M}^{-1}\text{cm}^{-1}$ ) at 385 nm, three weak bands at 483 nm, 509 nm, 552 nm ( $\epsilon = 4537 \text{ M}^{-1}\text{cm}^{-1}$ ,  $5154 \text{ M}^{-1}\text{cm}^{-1}$ , and  $3799 \text{ M}^{-1}\text{cm}^{-1}$ ), and a strong, broad band ( $\epsilon = 17075 \text{ M}^{-1}\text{cm}^{-1}$ ) at 1020 nm.

TD-DFT ( $\omega\text{B97XD/def2-TZVP}$ ) calculations of **3.27**<sup>NMe</sup> yield strong bands at 307 and 498 nm (LC  $\pi\text{-}\pi^*$  on bpy), with weaker bands at 381 nm (LMCT; bpy to Be) and 593 nm (LC  $\pi\text{-}\pi^*$  on bpy). The long wavelength band (732 nm) is associated with a HOMO-LUMO transition principally characterized as  $\pi\text{-}\pi^*$  LCT (bpy to CAAC). TD-DFT calculations of **3.28**<sup>NMe</sup> yield a strong band at 301 nm (LC  $\pi\text{-}\pi^*$  on bpy), with weaker bands at 387 nm (LMCT; bpy to Be), 489 nm (LC  $\pi\text{-}\pi^*$  on bpy), 495 nm (LCT  $\pi\text{-}\pi^*$  bpy to NHC), and 593 nm (LC  $\pi\text{-}\pi^*$  on bpy). No band was identified from the calculations that corresponded to the high-intensity band observed experimentally at 1020 nm.

### 3.3.3 Crystallographic Study of Double Reduced Carbene-Beryllium Bipyridene Complexes

Colorless plate-like crystals of **3.26** suitable for single crystal X-ray diffraction analysis were obtained from a toluene solution at  $-37\text{ }^{\circ}\text{C}$ . The molecular structure (Figure 3.3.3) shows a tricoordinate beryllium center adopting a trigonal planar geometry. The  $\text{NHC-C-Be}$  bond distance of **3.26** is  $1.786(3)\text{ \AA}$ , which is in agreement with the  $\text{NHC-C-Be}$  bonds of  $\text{IPrBeCl}_2$  ( $1.773\text{ \AA}$ ),<sup>44</sup> the  $[(\text{IME})_3\text{BeCl}]\text{Cl}$  salt ( $1.807$  and  $1.822\text{ \AA}$ ),<sup>39</sup> and  $(\text{sIPr})_2\text{BeCl}_2$  ( $1.839\text{ \AA}$ )<sup>40</sup> (IPr = 1,3-bis(2,6-diisopropylphenyl)imidazole-2-ylidene); IME = 1,3-dimethylimidazolin-2-ylidene; sIPr = 1,3-diisopropyl-4,5-dimethylimidazol-2-ylidene). The Be-Cl bond distances in **3.26** [ $1.888(2)\text{ \AA}$  and  $1.904(2)\text{ \AA}$ ] are longer than those of the isostructural three-coordinate  $\text{IPrBeCl}_2$  ( $1.881$  and  $1.884\text{ \AA}$ ), but shorter than those of the four-coordinate NHC compounds  $[(\text{IME})_3\text{BeCl}]\text{Cl}$  ( $2.091$  and  $2.076\text{ \AA}$ ) and  $(\text{sIPr})_2\text{BeCl}_2$  ( $2.039$  and  $2.052\text{ \AA}$ ). The shorter  $\text{NHC-C-Be}$  bond lengths in the tricoordinate complexes are a result of greater electron donation from NHC to Be when compared with fourcoordinate NHC-Be analogs.

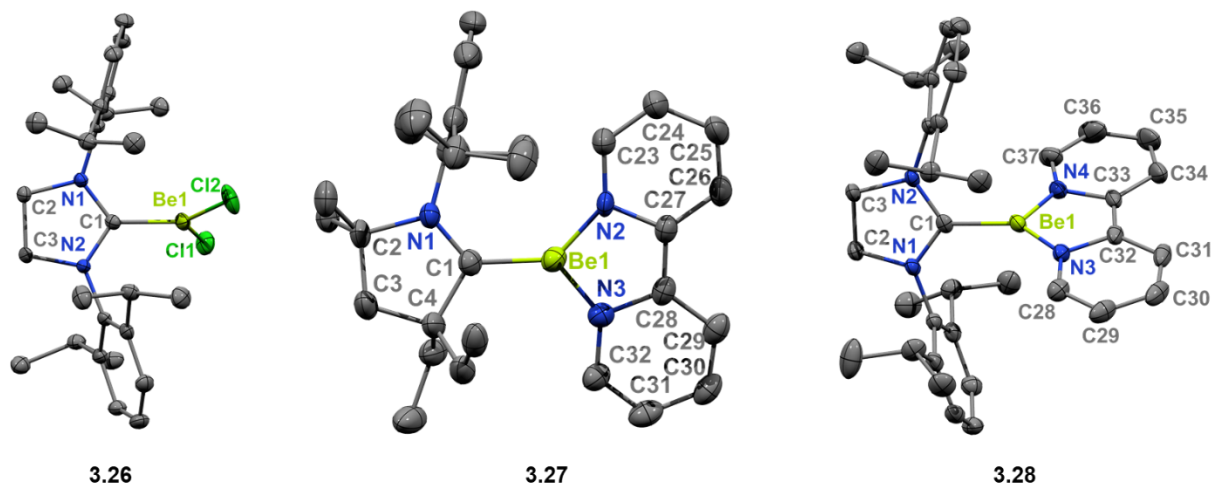


**Figure 3.3.3** Molecular structures of **3.26**, **3.27**, and **3.28** with H atoms omitted for clarity. Selected bond distances ( $\text{\AA}$ ) and angles ( $^{\circ}$ ) – **3.26**: C1–Be1:  $1.786(3)$ ; C1–N1:  $1.330(2)$ ; Be1–Cl1:  $1.904(2)$ ; Be1–Cl2:  $1.888(2)$ ; C1–Be1–Cl1:  $115.30(13)$ ; C1–Be1–Cl2:  $121.85(14)$ ; Cl1–Be1–Cl2:

122.82(11). **3.27**: Be1–C1: 1.799(6); Be1–N2: 1.631(6); N2–C27: 1.430(5); C27–C28: 1.382(5); N3–C28: 1.430(5); Be1–N3: 1.621(5); N1–C1: 1.321(5); N2–C23: 1.358(5); N3–C32: 1.383(5). N2–Be1–N3: 99.2(3); N3–Be1–C1: 128.6(3); N2–Be1–C1: 132.2(3); N1–C1–Be1: 128.8(3); C4–C1–Be1: 122.2(3). N1–C1–Be1–N2: 18.7(7); Be1–N3–C28–C27: 1.1(4). **3.28**: Be1–C1: 1.781(5); Be1–N3: 1.592(5); N3–C32: 1.429(4); C32–C33: 1.384(6); N4–C33: 1.429(4); Be1–N4: 1.581(5); N1–C1: 1.327(4); N2–C1: 1.346(4); N4–C37: 1.372(5); N3–C28: 1.374(5). N4–Be1–N3: 100.8(3); N3–Be1–C1: 135.0(3); N4–Be1–C1: 124.1(3); N2–C1–Be1: 124.8(3); N1–C1–Be1: 126.8(3). N2–C1–Be1–N4: 57.5(5); Be1–N3–C32–C33: 1.0(4).

Blue plate-like crystals suitable for X-ray diffraction were obtained from a saturated toluene solution of **3.27** at  $-37$  °C. The structure reveals a tricoordinate beryllium center in a distorted trigonal planar environment, where the N2–Be1–N3 angle is  $99.2(3)^\circ$ . Interestingly, the N2–Be1–C1–N1 torsion angle of **3.27** is smaller than expected ( $18.7(7)^\circ$ ). The <sup>CAAC</sup>C–Be bond distance is 1.799(6) Å, which is slightly longer than the starting material (<sup>Et<sup>2</sup></sup>CAAC)BeCl<sub>2</sub> (1.794 Å). The N2–C27 and N3–C28 bonds (both 1.430(5) Å) are single-bond-like, while C32–C33 (1.382(5) Å) is nearly the length of a C–C double bond. Orange plate-like crystals of **3.28** suitable for X-ray diffraction were obtained from a toluene solution at  $-37$  °C. The molecular structure of **3.28** reveals a tricoordinate beryllium center in a distorted trigonal planar environment, where the N3–Be–N4 angle is  $99.2(3)^\circ$ . The <sup>NHC</sup>C–Be bond distance of **3.28** is 1.781(5) Å, which is comparable to 1.768 Å for the isostructural (IMes)Be(<sup>Mes</sup>DAB)<sup>49</sup> (IMes = 1,3-bis(2,4,6-trimethylphenyl)imidazol-2-ylidene <sup>Mes</sup>DAB = *bis*(2,4,6-trimethylphenyl)-1,4-diazabutadiene)). The bond distances in the five-membered beryllacycle are in agreement with a doubly reduced bpy ligand coordinated to a Be(II) center. The N4–C33 and N3–C32 bonds (1.429(4) Å) are single bond like, while C32–C33 (1.384(6) Å) is nearly the length of a C–C double bond.

### 3.4 Summary of Carbene Beryllium Chemistry

A series of molecular alkoxo-bridged dimers of beryllium were prepared. The reaction of beryllium chloride dietherate with two equivalents of 1,3-diisopropyl-4,5-dimethylimidazol-2-ylidene resulted in the formation of a *bis*(*N*-heterocyclic carbene) (NHC) beryllium dichloride complex, (sIPr)<sub>2</sub>BeCl<sub>2</sub> (**3.19**). Compound **3.19** was reacted with lithium diisopropylphenoxide (LiODipp) or sodium ethoxide (NaOEt) to form the terminal aryloxo (sIPr)Be(ODipp)<sub>2</sub> (**3.20**) and alkoxide bridged dimer [(sIPr)Be(OEt)Cl]<sub>2</sub> (**3.21**), respectively. Compounds **3.20** and **3.21** represent the first beryllium alkoxo and aryloxo species coordinated by NHCs.

In order to expand the scope of redox chemistry known for beryllium, a set of reduced beryllium complexes were synthesized and their resulting structural and electronic properties were studied. The carbene-coordinated alkaline earth-halides, (<sup>Et2</sup>CAAC)BeCl<sub>2</sub> (**3.25**) and (SIPr)BeCl<sub>2</sub> (**3.26**), were combined with an  $\alpha$ -diimine 2,2-bipyridine (bpy) and a stoichiometric amount of potassium graphite to form the doubly-reduced compounds (<sup>Et2</sup>CAAC)Be(bpy) (**3.27**) and (SIPr)Be(bpy) (**3.28**). The doubly-reduced compounds **3.27** and **3.28** exhibit substantial  $\pi$ -bonding interactions across the diimine core, metal center, and  $\pi$ -acidic carbene. In the original manuscript these compounds were compared to magnesium analogues to highlight the differences in the organometallic chemistry of the lightest alkaline earth metals, magnesium and beryllium, in an otherwise identical chemical environment.

## **Chapter 4: Carbodicarbene-Stabilized Bismaalkene Cations: Unravelling the Complexities of Carbene versus Carbone in Heavy Pnictogen Chemistry**

- Walley, J. E.; Warring, L.; Wang, G.; Dickie, D. A.; Pan, S.; Frenking, G.; Gilliard, R. J.,  
*Angew. Chem., Int. Ed.* **2021**, *60*, 6682-6690.

## 4.1 Introduction to Bismuth Cation Chemistry

### 4.1.1 Carbene-Bismuth Complexes and other Bismuth Cations

The chemistry of bismuth has recently seen a surge in interest due in part to the stabilization of reactive bismuth complexes with novel electronic structure,<sup>88-89</sup> and the utilization of low-valent and/or low-coordinate bismuth compounds in catalysis.<sup>88-94</sup> Bismuth compounds have also been the subject of green chemistry efforts as its non-toxic nature sets it apart from the lighter pnictogen elements (i.e., P, As, Sb).<sup>23</sup>

In low-coordinate bismuth chemistry, the discovery of homometallic Bi=Bi bonds and monometallic Bi complexes has dominated the chemical literature.<sup>90-91, 94-107</sup> A number of groups have pursued stabilizing reactive Bi centers using carbenes to access both electrophilic and subvalent Bi complexes. It is noteworthy that while the carbene chemistry of the lighter pnictogen elements is well-established and continues to lead to new avenues of research, carbene-bismuth chemistry has presented significant experimental challenges.<sup>32</sup> Indeed, Dutton and coworkers reported the first *N*-heterocyclic carbene-bismuth complexes only six years ago, while those of phosphorus have been known for decades.<sup>108-109</sup> Recently, our laboratory has been exploring the coordination chemistry of bismuth with various carbene ligands, which led to the synthesis of the first cyclic (alkyl)(amino)carbene (CAAC)-coordinated Bi compounds.<sup>110</sup> While the reaction of CAAC-Bi(Ph)Cl<sub>2</sub> with traditional reducing agents (e.g., Na, K, KC<sub>8</sub>) resulted in rapid decomposition, utilization of the subvalent (CAAC)<sub>2</sub>Be complex afforded the first carbene-bismuthinidene.<sup>56</sup> The bonding interaction between the carbene carbon and the large Bi atom renders the carbene-bismuthinidene extremely reactive in solution, decomposing to Bi metal and

free carbene. The high reactivity of the complex largely results from the destabilization of the  $2p\pi$ - $6p\pi$  interaction (i.e., weak backdonation of the  $\pi$ -symmetric Bi lone pair to the carbene p-orbital).

Mebs and Beckmann recently described the synthesis of the first bismuthenium monocation, representing a bismuth carbene analogue (Figure 4.1.1, **4.1**).<sup>111</sup> The cation was formed by chloride abstraction with a silylium cation species generated *in situ*. Okuda showed that protonolysis of a *tris*(allyl)bismuth species results in the formation of a *bis*(allyl)bismuth monocation, which has been used as a stoichiometric allyl transfer reagent and inhibitor for controlled radical polymerization (Figure 4.1.1, **4.2**).<sup>112</sup> The first carbene-bismuthenium cation was reported by Goicoechea, which was formed by halide abstraction with  $\text{AlBr}_3$  (Figure 4.1.1, **4.3**).<sup>113</sup> A bismuthenium dication was isolated by Venugopal utilizing a multi-dentate hydrido*tris*(pyrazolyl)borate ligand (Figure 4.1.1, **4.4**).<sup>27</sup> The three orthogonally facing nitrogen donor atoms result in Lewis acid sites *trans* to the Bi–N bonds, affording a highly electrophilic bismuth center. Recently, Burford and coworkers reported a series of *bis*(bipyridine)pnictinium complexes. All of the pnictogen complexes were ionic with the exception of bismuth, which was described as a *bis*(bipyridine) adduct of bismuth trifluoromethanesulfonate (Figure 4.1.1, **4.5**).<sup>114</sup>

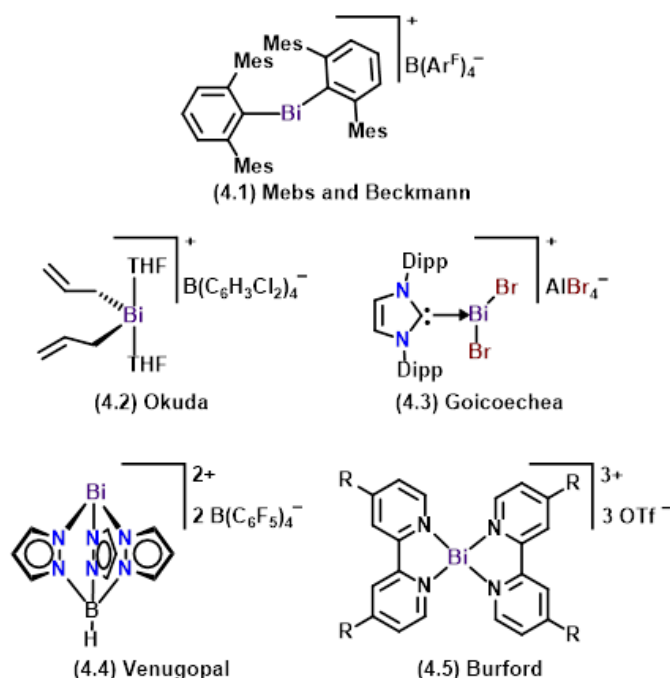


**Figure 4.1.1** Representative examples of bismuth cations (4.1-4.5).

#### 4.1.2 The Potential of Carbodicarbenes in Pnictaalkene Cation Chemistry

Carbodicarbenes,<sup>37, 115</sup> a type of carbene,<sup>43, 116-117</sup> are ideal ligands for stabilizing low-coordinate electrophilic bismuth cations because of their strong nucleophilic character, which is superior to both NHCs and CAACs.<sup>33</sup> Unlike carbenes, carbones can serve as two- or four-electron donors.<sup>118-119</sup> While the first carbene was isolated in 1961 by Ramirez,<sup>120</sup> CDCs were first theorized by Frenking<sup>37</sup> and their synthesis was achieved by Bertrand.<sup>115</sup> Since the original report the library of available CDC ligands has been expanded,<sup>45, 121</sup> however, the utilization of this ligand framework in main-group chemistry remains scarce.<sup>46-47, 122-125</sup> Herein, we describe the first complexation reactions of CDC with bismuth, namely phenylbismuth dichloride,  $\text{PhBiCl}_2$ , and bismuth tribromide,  $\text{BiBr}_3$ . These complexes undergo halide abstraction reactions to give mono-, di-, and tri-positive bismuthenium ions. Notably, the CDC-bismuth cations represent a new carbon–bismuth bonding motif, with a double dative bond from carbon to bismuth. To the best of our knowledge, the  $\text{C}\Rightarrow\text{Bi}$  interaction in compound **4.14** is the shortest known  $\text{C}-\text{Bi}^+$  bond,

representing an unprecedented cationic bismaalkene. Moreover, the formation of the dications and trication demonstrate a non-reductive method to achieve heteronuclear C=Bi double bond character. Neutral pnictaalkenes C=E (E = pnictogen) are well-established for C=P<sup>126-130</sup> and C=As<sup>131-137</sup> multiple bonds. However, for the heavier elements, compounds containing C=Sb<sup>138-142</sup> and C=Bi<sup>56, 102, 141, 143-144</sup> multiple bonds are rare and synthetically challenging. For pnictaalkene monocations there are reports for [C=P]<sup>+</sup> and [C=As]<sup>+</sup>,<sup>129, 145-151</sup> but to the best of our knowledge there are no structurally characterized examples pnictaalkene dications, [C=E]<sup>2+</sup> (Figure 4.1.2). Interestingly, there is one example of a phosphallene trication.<sup>123</sup> In this chapter, the first examples of [C=Bi]<sup>+</sup> (**4.13**, **4.16**), [C=Bi]<sup>2+</sup> (**4.14**, **4.17**), and [C=Bi=C]<sup>3+</sup> (**4.18**) bismaalkene cations have been synthesized.

In addition to the CDC-[Bi] complexes (**4.12-4.18**), we have prepared the first examples of carbene-supported di(organo)bismuthenium ions (**4.8-4.10**), which form through a THF-promoted rearrangement pathway, or by direct coordination of a sterically demanding carbene ligand. Experimental and theoretical analyses of NHC/CAAC- and CDC-bismuth cations clearly highlight the observed differences in stability and chemical bonding between carbene- and carbene-stabilized bismuth species.

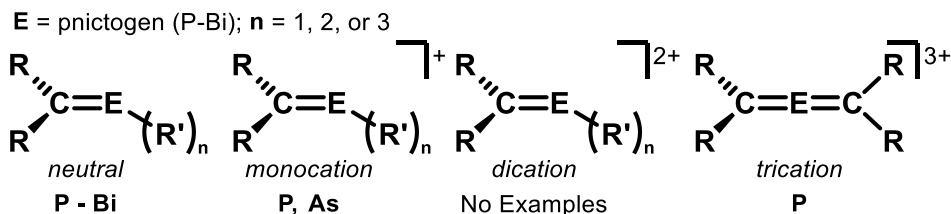
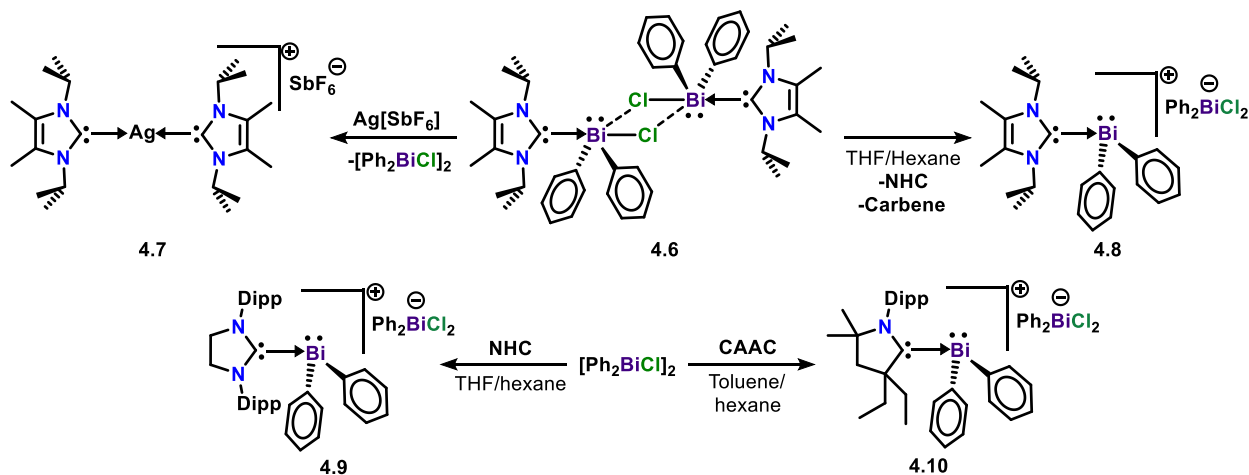


**Figure 4.1.2** Structurally characterized examples of neutral and cationic pnictaalkenes.

## 4.2 Synthesis of NHC-Supported Bismuthenium Complexes

### 4.2.1 Synthesis of Carbene-Supported Pseudo Monocations



**Scheme 4.2.1** Synthesis of bismuth cations supported by *N*-heterocyclic carbenes and a cyclic(alkyl)amino carbene.

We hypothesized that a strong monodentate neutral donor ligand would aid in the preparation of low-coordinate bismuth cations. Our group recently reported **4.6** (Compound **5.2** in preceding chapter), which is supported by two *N*-heterocyclic carbene (NHC) 4,5-dimethyl-1,3-diiisopropylimidazolin-2-ylidene ligands. In an effort to synthesize an NHC supported monocation, we reacted  $[(\text{NHC})(\text{Ph}_2)\text{Bi}(\mu\text{-Cl})]_2$  with silver hexafluoroantimonate ( $\text{AgSbF}_6$ ). Instead of the expected halide abstraction, the NHC transferred from Bi to Ag to give compound **4.7** (Scheme 4.2.1). Notably, this represents an unprecedented case of reverse-transmetalation,<sup>152</sup> where the carbene transfers to the silver halide abstracting reagent. The formation of compound **4.7** was ascertained by single-crystal X-ray diffraction and  $^1\text{H}$  NMR (Figure A3S15). Interestingly, recrystallization of  $[(\text{NHC})(\text{Ph}_2)\text{Bi}(\mu\text{-Cl})]_2$  from a THF/hexanes mixture lead to the formation of our target bismuthenium cation,  $[(\text{NHC})(\text{Ph}_2)\text{Bi}]^+$ , which contains a dichlorodiphenylbismuthate counteranion,  $[(\text{Ph}_2)\text{BiCl}_2]^-$  (**4.8**). Accordingly, THF allows for the rearrangement of **4.6** into **4.8** by facilitating NHC ligand dissociation and chloride abstraction to form the  $[(\text{Ph}_2)\text{BiCl}_2]^-$  anion.

The reaction of more sterically crowded carbene ligands, 1,3-bis(2,6-diisopropylphenyl)-4,5-dihydroimidazole-2-ylidene (SIPr) and (2,6-diisopropylphenyl)-4,4-diethyl-2,2-dimethylpyrrolidin-5-ylidene (CAAC), with  $[(\text{Ph}_2\text{Bi}(\mu\text{-Cl}))_2]$  lead to cationic complexes isostructural to that of compound **4.8**. Indeed, no reaction occurs when  $[(\text{SIPr})\text{Bi}(\text{Ph}_2)][(\text{Ph}_2)\text{BiCl}_2]$  (**4.9**) or  $[(\text{CAAC})\text{Bi}(\text{Ph}_2)][(\text{Ph}_2)\text{BiCl}_2]$  (**4.10**) is reacted with one extra equivalent of carbene.

The solid-state structures of compounds **4.8-4.10** are shown in Figure 4.2.1. Colorless crystals of **4.8** and **4.9** were grown from a THF/hexanes (2:1) layered mixture, while colorless crystals of **4.10** crystallized from toluene at  $-37\text{ }^\circ\text{C}$ . The structures reveal cationic  $[(\text{carbene})\text{Bi}(\text{Ph}_2)]^+$  units with an  $[(\text{Ph}_2)\text{BiCl}_2]^-$  anion coordinating through Cl to the Bi. These ionic interactions (Bi1---Cl1) increase in the order of **4.9** [3.0405(13) Å] < **4.10** [3.090(2) Å] < **4.8** [3.1092(8) Å]. Comparing these interactions to the sum of covalent radii for bismuth and chloride (2.5 Å),<sup>153</sup> compounds **4.8-4.10** can all be considered ionic. The longer Bi1---Cl1 interaction in **4.9** (3.0405(13) Å) compared to **4.8** (3.1092(8) Å) and **4.10** (3.090(2) Å) can be reasoned by the small size of the NHC ligand in **4.9**, which is in close proximity to the Bi center and thus exhibits stronger binding. The carbene–Bi bond distances decrease in the same order, **4.9** [2.431(5) Å] > **4.10** [2.393(9) Å] > **4.8** [2.383(2) Å], corroborating the observed ionic interactions.

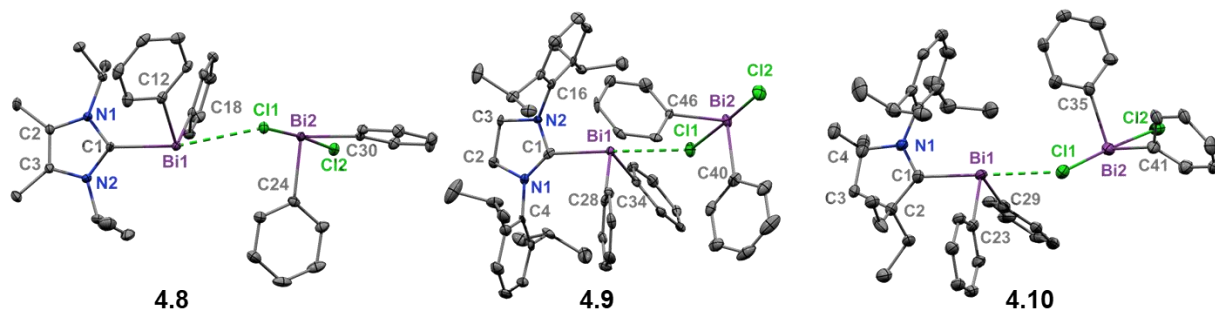
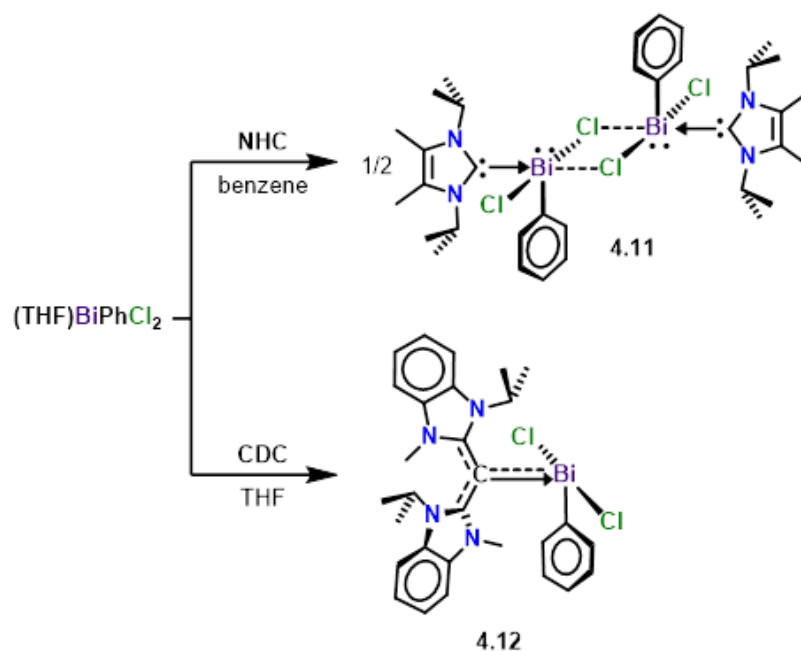


**Figure 4.2.1** Molecular structures – **4.8** (a): (thermal ellipsoids at 50% probability; H atoms omitted for clarity). Selected bond distances (Å) and angles (deg): C1–Bi1: 2.383(2); Bi1---Cl1: 3.1092(8); Cl1–Bi2: 2.8039(7); Bi2–Cl2: 2.6832(7). C1–Bi1–Cl1: 175.45(11); Cl2–Bi2–Cl1: 178.24(4). **4.9** (b): (thermal ellipsoids at 50% probability; H atoms were omitted for clarity). Selected bond distances (Å) and angles (deg): C1–Bi1: 2.431(5); Bi1---Cl1: 3.0405(13); Cl1–Bi2: 2.8347(13); Bi2–Cl2: 2.6392(14). C1–Bi1–Cl1: 167.194(66); Cl2–Bi2–Cl1: 176.258(18). **4.10** (b): (thermal ellipsoids at 30% probability; H atoms were omitted for clarity). Selected bond distances (Å) and angles (deg): C1–Bi1: 2.393(9); Bi1---Cl1: 3.090(2); Cl1–Bi2: 2.818(3); Bi2–Cl2: 2.649(3). C1–Bi1–Cl1: 179.2(2); Cl2–Bi2–Cl1: 174.12(8).

#### 4.2.2 Carbene vs Carbone in Stabilizing Phenylbismuth Dichloride

We hypothesized that the stronger electron donor properties of CDC compared to NHC would promote significant Bi–Cl bond elongation, allowing for facile halide abstraction. To draw comparisons between the two ligands and to test our hypothesis, we synthesized an NHC complex of phenylbismuth dichloride, [(NHC)Bi(Ph)Cl<sub>2</sub>]<sub>2</sub>, as well as the CDC analogue, (CDC)Bi(Ph)Cl<sub>2</sub>. NHC was allowed to react with (THF)Bi(Ph)Cl<sub>2</sub> for 1 hour at room temperature in benzene (Scheme 4.2.2). After purification, compound **4.11** was obtained as a white solid in 75% yield. The <sup>1</sup>H NMR spectrum revealed a well-defined heptet at 4.95 ppm (*J* = 7.0 Hz), representing the methine environment of a coordinated NHC ligand. Similarly, CDC was reacted with

(THF)Bi(Ph)Cl<sub>2</sub> in THF at room temperature, which forms a deep yellow precipitate upon addition. After filtration and drying under vacuum, (CDC)Bi(Ph)Cl<sub>2</sub> (**4.12**) is obtained in 69% yield. A broad peak at 5.22 ppm was observed in the <sup>1</sup>H NMR spectrum for **4.12** in CD<sub>2</sub>Cl<sub>2</sub>, representing the methine proton of a new CDC coordination environment. In the <sup>13</sup>C NMR, a sharp singlet at 189.3 ppm is representative of the carbene carbon atom, this is only slightly downfield of the carbene carbon in compound **4.11** (185.6 ppm).



**Scheme 4.2.2** Synthesis of NHC- and CDC- supported phenylbismuth dichloride (NHC = 4,5-dimethyl-1,3-diisopropylimidazol-2-ylidene; CDC = bis(1-isopropyl-3-methyl-benzimidazol-2-ylidene)methane).

Colorless single-crystals of compound **4.11** were obtained from a saturated benzene solution at room temperature, while yellow crystals of compound **4.12** were obtained from a THF/hexanes (1:2) layered mixture at room temperature (Figure 4.2.2). There are two notable differences between the solid-state structures of **4.11** and **4.12**. (1) The NHC-supported bismuth

complex **4.11** is dimeric and the CDC coordinated compound **4.12** is monomeric, suggesting that the strong electron donor properties of CDC negates the necessity for dimerization due to an electronically saturated bismuth atom. (2) The <sup>carbene</sup>C–Bi bond length in **4.12** [2.249(6) Å] is significantly shorter than the <sup>carbene</sup>C–Bi bond length in **4.11** [2.346(2) Å]. This is a result of a partial  $\pi$ -donation from CDC to Bi in the former. As predicted, the average Bi–Cl bond lengths for **4.12** (2.734 Å) are longer than those in **4.11** (2.694 Å). Due to the observed differences in the metrical data we reasoned that CDC should lead to bismuth compounds with multiple bond character and enhanced stability. Thus, CDC-Bi cations were targeted as a platform to access bismaalkene-type species, which unlike the lighter pnictogen congeners are extremely rare.

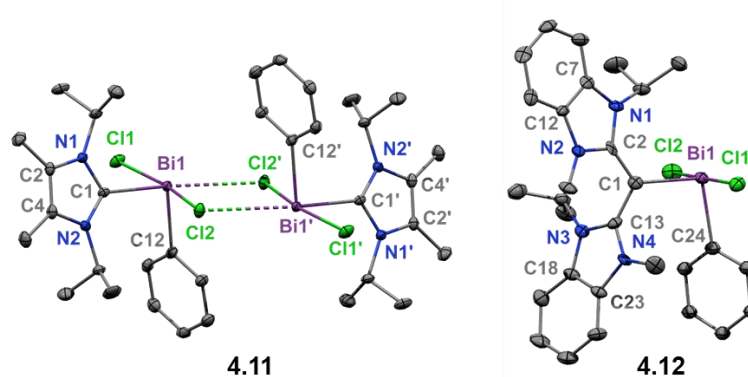
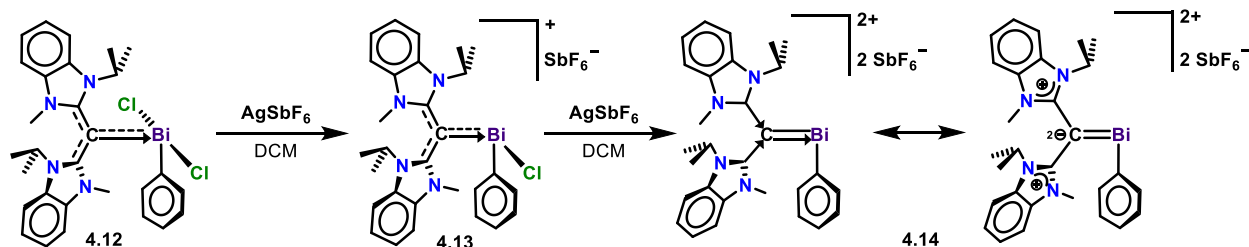


**Figure 4.2.2** Molecular structures of **4.11** and **4.12** (thermal ellipsoids at 50% probability; H atoms omitted for clarity). **4.11**: C1–Bi1: 2.346(2); Bi1---Cl2': 3.2473(7); Bi1–Cl1: 2.6857(6); Bi1–Cl2: 2.7031(6). Cl1–Bi1–Cl2: 166.081(18); Cl2–Bi1–C1: 99.21(8); Cl1–Bi1–C1: 84.96(5); C12–Bi1–Cl1: 92.21(6); C12–Bi1–Cl2: 91.65(6); C12–Bi1–C1: 99.21(8). **4.12**: C1–Bi1: 2.249(6); Bi1–Cl1: 2.7693(14); Bi1–Cl2: 2.6989(15); Bi1–C24: 2.275(12); C1–C2: 1.393(8); C1–C13: 1.445(8). Cl1–Bi1–Cl2: 176.21(5); Cl2–Bi1–C1: 90.52(15); Cl1–Bi1–C1: 93.23(15); C24–Bi1–Cl1: 89.8(5); C24–Bi1–Cl2: 89.2(5); C24–Bi1–C1: 97.2(6).

## 4.3 Synthesis of CDC-Stabilized Mono-, Di-, and Tri-Positive Bismuthenium Ions

### 4.3.1 Synthesis of CDC-Stabilized Phenylbismuth Bismaalkene Mono- and Dications

In order to test our hypothesis that CDC would enable the formation of electropositive bismuth cations with increasing double bond character, we probed the reaction of **4.12** with one equivalent of  $\text{AgSbF}_6$  in dichloromethane (DCM) (Scheme 4.3.1). Orange needle-like X-ray quality crystals of the monocation (**4.13**) were obtained in 78% yield from a THF/hexanes (1:1) layered mixture at room temperature. The  $^1\text{H}$  NMR spectrum of **4.13** in  $\text{THF-}d_8$  revealed a broad resonance at 5.03 ppm for the methine proton of the coordinated CDC ligand which is slightly downfield compared to its starting material **4.12**. Due to the more deshielding electrophilic bismuth center, the  $^{13}\text{C}$  NMR spectrum reveals a singlet downfield from that in **4.12** at 191.6 ppm attributed to the carbene carbon of **4.13**. In pursuit of a dicationic species via a second halide abstraction, we added in an additional equivalent of  $\text{AgSbF}_6$  to **4.13** in DCM. Dark red X-ray quality crystals of the bismuthenium complex **4.14** were obtained in 43% yield from a DCM/hexanes (1:1) layered mixture at room temperature. A broad resonance attributed to the methine proton of coordinated CDC ligand in **4.14** is observed at 4.57 ppm in  $\text{CD}_2\text{Cl}_2$ , which is consistent with the trend observed for complexes **4.12** and **4.13**. In this respect, the  $^{13}\text{C}$  NMR shows a peak at 209.7 ppm for the carbene carbon of **4.14**, which is downfield from that of both **4.12** and **4.13**, supporting substantial electron donation from CDC to bismuth.



**Scheme 4.3.1** Synthesis of CDC-stabilized bismuth mono- and di-cations with increasing bismaalkene character.

The solid-state structures of cations **4.13** and **4.14** are shown in Figure 4.3.1. Both cations contain coordinating  $[\text{SbF}_6]^-$  counter anions, with Bi---F interaction distances of 2.904(2) Å (**4.13**) and 2.603(8) - 2.740(7) Å (**4.14**). The CDC–bismuth bond length decreases in the order of **4.12** [2.249(6) Å] > **4.13** [2.226(3) Å] > **4.14** [2.157(11) Å], and these data support an increase in  $\pi$ -donor character from CDC as the bismuth center becomes increasingly electrophilic. Notably, the C1–Bi1 bonds are significantly shorter than those in their NHC-bismuthenium congeners. Since carbenes are  $\pi$ -basic rather than  $\pi$ -acidic, and the bismuth center is electrophilic, the C–Bi bond lengths are shortened due to substantial  $\pi$ -donation from the  $\text{carboneC}$  to Bi. The  $\text{carboneC}$ –Bi bond length in **4.14** is shorter than the  $\text{CAAC}$ C–Bi bond in the subvalent carbene-bismuthindene [2.199(2) Å] and even rivals that of the bismuthio ylide (2.16 Å),<sup>102</sup> and the aromatic C–Bi bonds of a bismabenzene (2.154 - 2.160(4) Å).<sup>143</sup> Thus, **4.14** may be regarded a stabilized dicationic bismaalkene, which is unprecedented. It is noteworthy that while phosphalkene species have been widely studied,<sup>127-128, 154</sup> structurally characterized examples of heavy bismuth analogues are virtually unexplored.

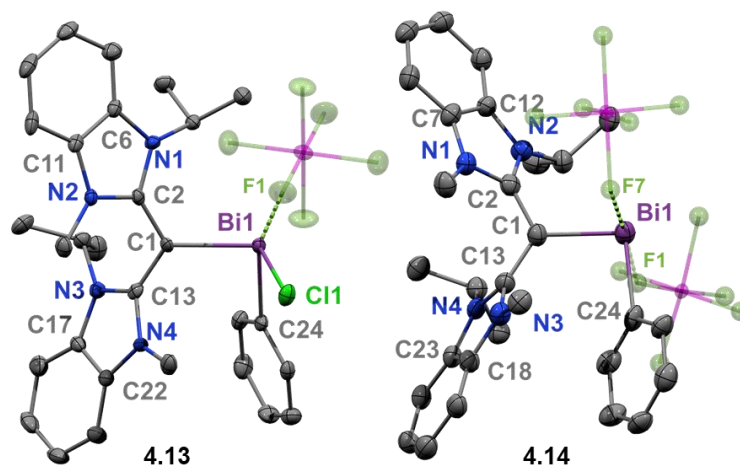


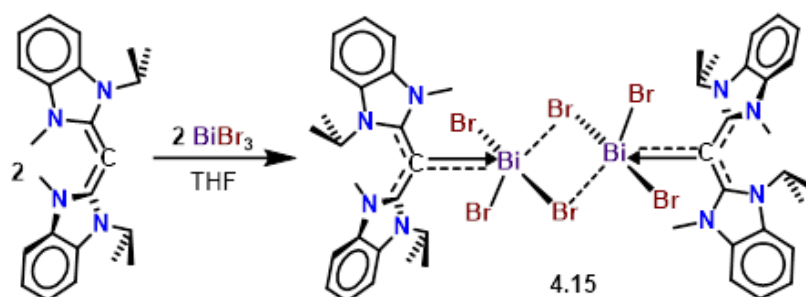
**Figure 4.3.1** Molecular structures of **4.13** and **4.14** (thermal ellipsoids at 50% probability; H atoms were omitted for clarity). **4.13**: C1–Bi1: 2.226(3); Bi1–Cl1: 2.5573(9); C24–Bi1: 2.242(3); C1–C2: 1.417(5); C1–C13: 1.427(5); Bi1---F1: 2.904(2). C1–Bi1–Cl1: 102.82(9); C1–Bi1–C24: 93.60(13); C24–Bi1–Cl1: 93.86(10). **4.14**: C1–Bi1: 2.157(11); Bi1–C24: 2.223(12); C1–C2: 1.444(15); C1–C13: 1.426(15); Bi1---F1: 2.603(8); Bi1---F7: 2.740(7); C1–Bi1–C24: 96.7(4).

#### 4.3.1 Synthesis of CDC-Stabilized Bismaalkene Mono-, Di- and Trications

In order to synthesize bismuthenium ions without weakly coordinating anion contacts, we reacted CDC with bismuth tribromide in THF overnight (Scheme 4.3.2). After workup, compound **4.15** was obtained as a red solid in 86 % yield. The  $^1\text{H}$  NMR spectrum of **4.15** shows a well-defined heptet ( $J = 6.7$  Hz) at 5.01 ppm representative of a sterically unrestricted CDC coordination environment; this is in contrast to the broad signals observed for **4.12**, **4.13**, and **4.14**. Red single crystals of **4.15** suitable for X-ray diffraction analysis were obtained from a THF/hexanes (2:1) layered mixture at room temperature.

The solid-state structure of compound **4.15** shows a dimeric  $[(\text{CDC})\text{BiBr}_3]_2$  complex with bridging bromides (Figure 4.3.2). Each bismuth atom has adopted a distorted square pyramidal

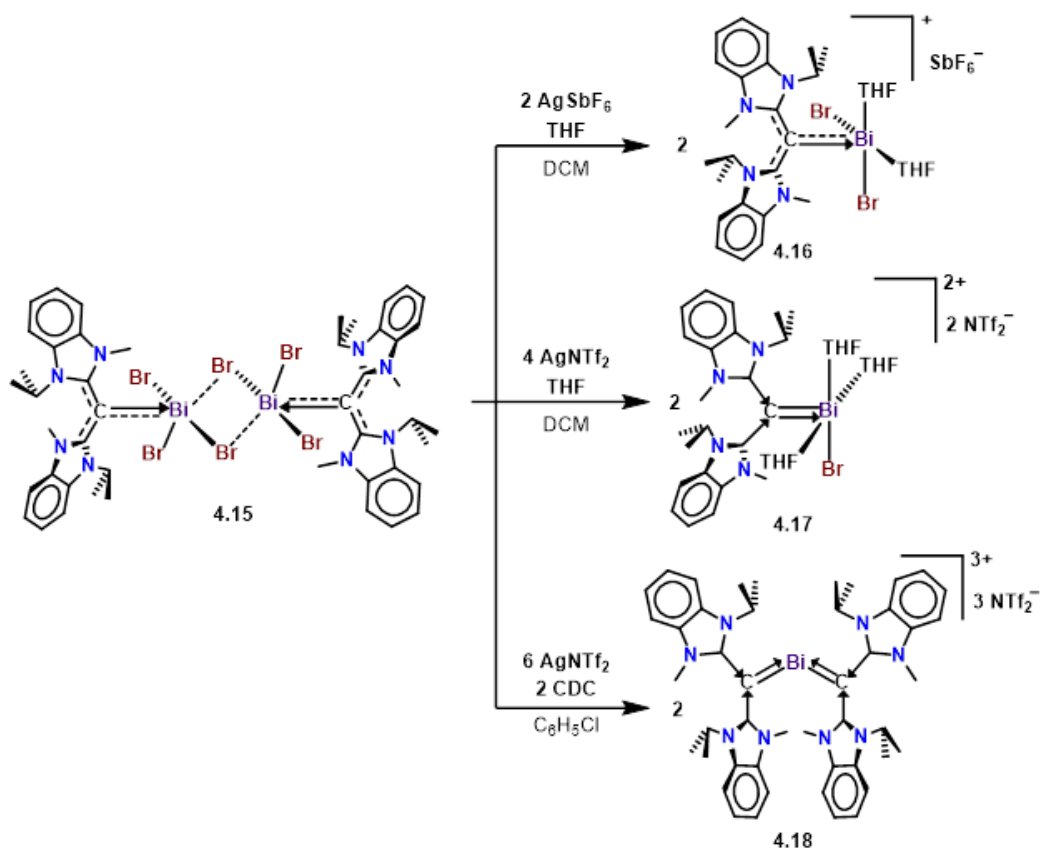
geometry when considering the bromide contacts. The CDC–bismuth bond [C1–Bi1: 2.292(9) Å] is shorter than that in compound **4.12** [2.249(6) Å]. The bismuth–bromide bond in the apical position of **4.15**, [Bi1–Br2: 2.6629(16) Å], is shorter than the sum of ionic radii for Bi and Br (2.68 Å).<sup>153</sup> The other two bismuth–bromide bonds are substantially longer [Bi1–Br1: 2.9196(12) Å and Bi1–Br3: 2.8390(12) Å], which support weaker Bi–Br interactions.



**Scheme 4.3.2** Synthesis of a *bis*-CDC-supported tribromobismuth dimer.

While halide abstraction from compound **4.12** will only yield mono- and di-positive bismuthenium ions (**4.13** and **4.14**), compound **4.15** is a suitable starting material for synthesizing a tri-positive bismuthenium ion. Our initial synthetic approach involved the use of THF, which would provide additional support to the bismuth center by readily filling the coordination sphere upon halide abstraction. Interestingly, when compound **4.15** is reacted with  $\text{AgSbF}_6$ , THF solvent polymerized into a tough insoluble solid material uncharacterizable by traditional spectroscopic methods. In an effort to circumvent this polymerization process, but still allow for THF coordination, we performed the reaction of **4.15** with two equivalents of  $\text{AgSbF}_6$  in DCM and added an aliquot of THF *in situ* (Scheme 4.3.3). Thus, the monocation **4.16** was isolated in 67% yield. Unlike the monocation **4.13**, compound **4.16** does not contain any anion interactions due to the coordination of THF solvent molecules to Bi. Attempts to form the dicationic product from the reaction of **4.15** with four equivalents of  $\text{AgSbF}_6$  and a variety of other halide abstraction reagents proved to be

unsuccessful. This is in accordance with the observed difference in Bi–Br bond distances, which suggest that one Br atom is more tightly bound to Bi. However, facile halide abstraction was observed to generate the dication **4.17** when four equivalents of silver (*bis*-trifluoromethylsulfonyl)imide (AgNTf<sub>2</sub>) were reacted with **4.15**. Similar to **4.16**, compound **4.17** does not contain any anion contacts to the bismuth center. The <sup>1</sup>H NMR integrations suggested that a third equivalent of THF coordinated to bismuth with respect to the monocation **4.16**, to give a 1:3 THF to CDC ratio. Several attempts were made to synthesize a trication using this THF addition method, but all proved to be unsuccessful. We therefore hypothesized that the coordination of a second CDC ligand would render the last Bi–Br bond more labile due to the strong donor effect, thus weakening the Bi–Br bond. As such, the reaction **4.15** and two equivalents of CDC with six equivalents of AgNTf<sub>2</sub> successfully gave the *bis*(CDC)bismuthenium trication **4.18** in 73% yield. The shift pattern in the <sup>1</sup>H NMR spectrum of **4.18** closely resembles that of a *bis*(CDC) dicationic(hydrido)boron complex,<sup>125</sup> further supporting that two CDC ligands have coordinated to the Bi center.



**Scheme 4.3.3** Synthesis of CDC mono-, di-, and tri-positive bismuthenium ions. Note: similar to compound **4.14**, compounds **4.17** and **4.18** can be represented as resonance structures with their respective zwitterions analogous to those shown in Scheme 4.3.1.

Red needle-like crystals of **4.16** suitable for X-ray diffraction were obtained from a THF/hexanes (1:1) layered mixture at room temperature. The crystal structure reveals a monocationic  $[(\text{CDC})\text{BiBr}_2(\text{THF})_2]^+$  core, and the bismuth center has adopted a square pyramidal geometry. The  $^{\text{carbone}}\text{C}$ -bismuth bond of **4.16** [C1-Bi1: 2.226(12) Å] is slightly longer than that of **4.13**, which is expected for a higher coordination number. Red plate-like crystals of compound **4.17** were obtained from a DCM/ether (2:1) mixture at room temperature. Similar to **4.16**, the structure reveals a square pyramidal dicationic  $[(\text{CDC})\text{BiBr}(\text{THF})_3]^{2+}$  core, with an additional THF occupying a coordination site. As a result of three coordinating THF molecules, the  $^{\text{carbone}}\text{C}$ -Bi

bond of **4.17** [C1–Bi1: 2.199(5) Å] is longer than **4.14** [C1–Bi1: 2.157(11) Å]. Dark blue plate-like crystals of compound **4.18** were obtained from a chlorobenzene/hexanes (10:1) mixture. The crystal structure of **4.18** revealed two CDC ligands coordinated to a Bi<sup>III</sup> center, with three [NTf<sub>2</sub>]<sup>-</sup> counter anions. The <sup>carbone</sup>C–bismuth bonds [Bi1–C24: 2.166(2) and Bi1–C1: 2.197(2) Å] are only slightly shorter than that in **4.17**. The average allenic bond length has increased from 1.335 Å in the free ligand to 1.437 Å suggesting substantial electron donation from the carbone carbon to Bi<sup>III</sup>, and less back donation to the NHC moiety.

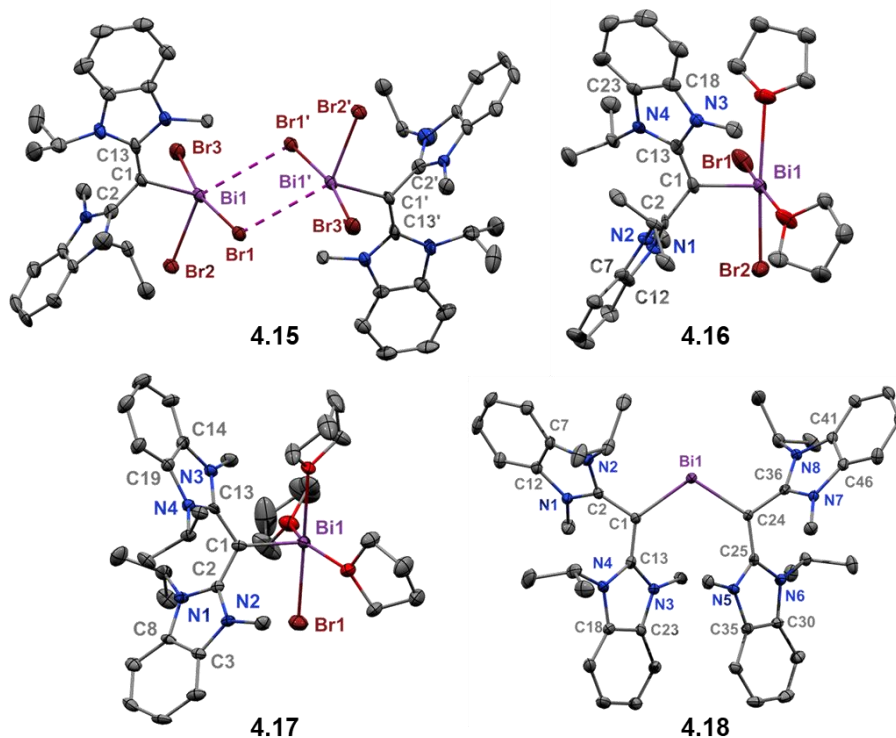


**Figure 4.3.2** Molecular structures of **4.15-4.18** (thermal ellipsoids at 50% probability; H atoms, counteranions and non-coordinating solvent omitted for clarity). **4.15**: Bi1–C1: 2.292(9); Bi1–Br1: 2.9196(12); Bi1–Br2: 2.6483(11); Bi1–Br3: 2.8390(12); Bi1---Br1': 3.4829(15); C1–C13: 1.367(13); C1–C2: 1.438(12). **4.16**: Bi1–C1: 2.226(12); Bi1–Br2: 2.6629(16); Bi1–Br1: 2.7052(18); C1–C13: 1.395(17); C1–C2: 1.447(15). **4.17**: Bi1–Br1: 2.6439(6); Bi1–C1: 2.199(5);

C1–C2: 1.441(6); C1–C13: 1.433(6). **4.18**: Bi1–C24: 2.166(2); Bi1–C1: 2.197(2); C1–C13: 1.424(3); C1–C2: 1.443(3); C24–C25: 1.436(3); C24–C36: 1.444(3). C24–Bi1–C1: 111.23(9).

#### 4.4 Bonding Analysis of Bismuth and Bismuthenium Complexes

CDC-stabilized bismuthenium complexes **4.12-4.18** were calculated with quantum chemical methods using density functional theory (DFT) at the BP86-D3(BJ)/def2-TZVPP level.<sup>155-160</sup> The nature of the chemical bonds between the CDC ligand and the remaining bismuthenium fragments [Bi] was investigated with energy decomposition analysis (EDA)<sup>161</sup> in conjunction with natural orbitals for chemical valence (NOCV).<sup>162-163</sup> The EDA-NOCV method<sup>161-163</sup> has been proven to give deep insights into the nature of the chemical bond in a variety of main-group compounds and transition metal complexes.<sup>164-171</sup>

The calculated and experimental geometries of **4.12-4.18** are in agreement except for some Bi---F distances for the weakly coordinating anions in **4.13** and **4.14**, which are considerably shorter than the experimental distances.<sup>172</sup> This is also observed when the M06-2X functional is used for the geometry optimization.<sup>173</sup> These differences are most likely due to intermolecular forces in the solid state. Therefore, the bonding analysis was carried out with the EDA-NOCV method using the calculated and the experimental geometries.<sup>172</sup> The computed bond dissociation free energy ( $\Delta G^{298}$ ) of the CDC–Bi bond at 298 K ranges from 27.2-62.3 kcal/mol, which indicates that the molecules are thermodynamically quite stable. The geometries of compound **4.18** (CDC)<sub>2</sub>Bi[NTf<sub>2</sub>]<sub>3</sub> and the free trication [(CDC)<sub>2</sub>Bi]<sup>3+</sup> were optimized. The agreement of the theoretical values of (CDC)<sub>2</sub>Bi[NTf<sub>2</sub>]<sub>3</sub> with the experimental data is reasonably good, the deviation between the calculated and X-ray values is likely to be caused by solid-state forces. The calculated geometry of the free trication [(CDC)<sub>2</sub>Bi]<sup>3+</sup> is only slightly different from the geometry in the

presence of the counter ions in  $(\text{CDC})_2\text{Bi}[\text{NTf}_2]_3$ . The bond strength of the CDC ligands to bismuth in  $(\text{CDC})_2\text{Bi}[\text{NTf}_2]_3$  has been estimated by calculating the bond dissociation energy for the reaction  $(\text{CDC})_2\text{Bi}[\text{NTf}_2]_3 \rightarrow 2\text{CDC} + \text{Bi}[\text{NTf}_2]_3$ . The computed value of  $D_0$  ( $\Delta G^{298}$ ) = 128.6 (88.2) kcal/mol suggests that the bonds are quite strong.

The calculated intrinsic interaction energy ( $\Delta E_{\text{int}}$ ) values are similar except for structures **4.13**, **4.14** and **4.17**, where the energy values using the experimental geometries are somewhat larger. However, the percentage contributions of the four components to the CDC-[Bi] interaction, i.e., Pauli repulsion  $\Delta E_{\text{Pauli}}$ , dispersion forces  $\Delta E_{\text{disp}}$ , electrostatic attraction  $\Delta E_{\text{elstat}}$  and orbital (covalent) interaction  $\Delta E_{\text{orb}}$  are very similar. This indicates that the bonding analysis using the calculated structures may safely be used for the experimentally observed species. The breakdown of the  $\Delta E_{\text{orb}}$  term into pairwise interactions  $\Delta E_{\text{orb}(1)} - \Delta E_{\text{orb}(3)}$  shows that the major contribution  $\Delta E_{\text{orb}(1)}$  comes from the  $\sigma$  donation of the CDC ligand  $[\text{CDC}] \rightarrow [\text{Bi}]$ . The donation  $\Delta E_{\text{orb}(2)}$  of the  $\pi$  lone pair of the CDC ligand<sup>14</sup>  $[\text{CDC}] \rightarrow [\text{Bi}]$  is significantly weaker. It becomes stronger when the experimental geometries are used, because the measured carbon-bismuth distances are shorter than the calculated values.<sup>172</sup> The largest contribution of the  $[\text{CDC}] \rightarrow [\text{Bi}]$   $\pi$  donation is found for **4.14** where it amounts to 19% of the total orbital interactions when the experimental geometry is used. The third pairwise orbital contribution  $\Delta E_{\text{orb}(3)}$  is due to weak  $[\text{CDC}] \leftarrow [\text{Bi}]$   $\sigma$  backdonation. This is the complementary part of the overall  $\sigma$  bond. For the trication **4.18**, the lowest values were provided by using the triplet states of  $[(\text{CDC})_2]^{2+}$  and  $\text{Bi}^+$  with the electron configuration  $(6s^2 6p_y^1 6p_z^1)$  for the atomic ion.

The results of the bonding analysis suggest that the  $\text{NHC}^{\text{Ph}}$  substituents of the CDC ligand serve as a sink for the electronic charge, because they are rotated out of the molecular frame so that the vacant  $\pi$  orbitals of  $\text{NHC}^{\text{Ph}}$  can interact with the occupied orbitals of the [Bi] donor. The

related molecular orbitals representing double dative interaction is provided in the supporting information of the original paper.<sup>172</sup> Note that in moving from **4.12**→**4.13**→**4.14** or **4.15**→**4.16**→**4.17**, with the increase in electrophilic character of Bi, both the absolute values of [CDC]→[Bi]  $\sigma$  and  $\pi$  donation gradually increases (from **4.15**→**4.16** the  $\sigma$  donation remains essentially the same), which agrees with the increasingly shorter <sup>carbone</sup>C–Bi bond lengths.

The pairwise orbital interactions  $\Delta E_{\text{orb}(1)} - \Delta E_{\text{orb}(3)}$  can be assigned to specific donations with the help of the associated deformation densities  $\Delta\rho$ . The shape of  $\Delta\rho_{(1)} - \Delta\rho_{(3)}$  of the pairwise interactions  $\Delta E_{\text{orb}(1)} - \Delta E_{\text{orb}(3)}$  in **4.14** is shown in the supporting information of the original paper.<sup>172</sup> The color of the charge flow is red→blue. It becomes obvious that besides the  $\sigma$ -donation and  $\pi$ -backdonation, there is also polarization within the fragments.

The bonding interactions in **4.12**–**4.18** were compared with that in carbene-stabilized bismuthenium **4.8**–**4.10** and bismuth CAAC-Bi(Ph)Cl<sub>2</sub> complexes.<sup>7</sup> The numerical results of the EDA-NOCV calculations shows that the intrinsic interaction in the CDC complexes is larger than that in the carbene adducts. The most important information comes from the breakdown of  $\Delta E_{\text{orb}}$  into the pairwise orbital interactions between the ligands and the metal fragments. There is only one dominating  $\sigma$  donation  $\Delta E_{\text{orb}(1)}$  in the carbene complexes [carbene]→[Bi] besides the  $\pi$  backdonation [carbene]←[Bi]  $\Delta E_{\text{orb}(2)}$ . In contrast, the CDC complexes exhibit two notable donor components from the ligand to the metal fragment. The remaining orbital interactions  $\Delta E_{\text{rest}}$  consist of a large number of weak polarization terms within the fragments. Thus, the EDA-NOCV calculations signal a clear difference in the donor-acceptor interactions between the carbene and carbene ligands. This is best exemplified by comparing the results of the carbene complex CDC-Bi(Ph)Cl<sub>2</sub> (**4.12**) with the analogous carbene adduct CAAC-Bi(Ph)Cl<sub>2</sub>. The total interaction energy  $\Delta E_{\text{int}}$  of **4.12** is only slightly higher (-81.5 kcal/mol) than that of the carbene complex (-

78.4 kcal/mol) but the orbital interactions  $\Delta E_{\text{orb}}$  of the former carbene complex are much larger (-108.0 kcal/mol) than for the latter carbene species (-98.0 kcal/mol), which is mainly due to the additional contribution of the  $\pi$  bond (-7.3 kcal/mol). The further strengthening of the orbital interactions is partly compensated by weaker electrostatic attraction in the carbene complex. It requires the analysis of the electronic structure in order to find that **4.12** and the other carbene complexes possess a double dative  $\text{C}\Rightarrow\text{Bi}$  bond, which consists of a strong  $\sigma$  and a significantly weaker  $\pi$  component, whereas the carbene complexes exhibit only a  $\sigma$  bond  $\text{C}\rightarrow\text{Bi}$ .

## 4.5 Summary of Carbodicarbene Bismaalkene Cations

In this study a series of carbene- and carbene-stabilized bismuthenium ions are reported. The  $\text{CDC-Bi(Ph)Cl}_2$  and  $[\text{CDC-BiBr}_3]_2$  complexes were used as starting materials to afford structurally diverse bismuth monocations, dications, and trication. The dication **4.14** and trication **4.18** possess short  $\text{Bi}=\text{C}$  bonds due to the low-coordinate, double dative-type interaction to Bi. Thus, compounds **4.14** and **4.18** may be viewed as bismaalkene cations, which are hitherto unprecedented. The enhanced stability of the  $\text{CDC-[Bi]}$  complexes, compared to  $\text{NHC-[Bi]}$  species, clearly highlights the superior donor ability of CDC and the importance of single atom  $\sigma$ - and  $\pi$ -donation in stabilization strategies employing neutral carbon-donor ligands. These interactions are also studied in detail with charge and energy decomposition analyses, which provide clear evidence that the carbene complexes  $\text{CDC-[Bi]}$  possess a double donor bond  $\text{C}\Rightarrow\text{Bi}$ , which consists of a strong  $\sigma$  and a significantly weaker  $\pi$  component, whereas the carbene complexes exhibit only a  $\sigma$  bond  $\text{C}\rightarrow\text{Bi}$ . Due to the highly electrophilic nature of the CDC-bismuth cations, they are expected to possess interesting reactivity toward energy-relevant small molecules ( $\text{CO}$ ,  $\text{CO}_2$ ,  $\text{H}_2$ , etc.), and these studies are currently under investigation in our laboratory.

## **Chapter 5: Indirect Access to Carbene Adducts of Bismuth and Antimony Substituted Phosphaketene and their Unusual Thermal Transformation to Dipnictines and [(NHC)<sub>2</sub>OCP][OCP]**

- Walley, J. E.; Warring, L. S.; Kertesz, E.; Wang, G.; Dickie, D. A.; Benko, Z.; Gilliard, R. J., Jr., *Inorg. Chem.* **2021**, *60*, 4733-4743.

## 5.1 Introduction to Phosphaketene Chemistry

### 5.1.1 The Diverse Reactivity of the 2-Phosphaethynolate Anion

Due to their unique electron distribution, heteroketenes show versatile and fascinating chemistry. Phosphorus-containing members of this family are phosphaketenes,  $R-P=C=O$ .<sup>174-175</sup> Although the first stable phosphaketene was reported nearly four decades ago,<sup>176</sup> the synthetic chemistry was experimentally challenging, and various products were thermally unstable. However, in the last decade, simple synthetic routes towards such compounds have emerged, which has resulted in the rapid development of the field. The utilization of the 2-phosphaethynolate anion,<sup>177-179</sup>  $[OCP]^-$ , as a synthon has proved to be an effective way to access phosphaketenes via nucleophilic substitution.<sup>180-184</sup> However, these synthetic processes are not always straightforward, and phosphaketene stability and reactivity may be hampered by a number of complications. The most important of these are summarized as follows: *i*) Dimer formation: the  $P=C$  bond of phosphaketenes is prone to cycloaddition, which results in 4-membered rings; however, this process can be minimized with the incorporation of bulky substituents, or with heteroatoms.<sup>185-186</sup> *ii*) Formation of constitutional isomers: due to its ambident reactivity, the  $[OCP]^-$  anion may bind through the P or the O center. Highly oxophilic elements, such as Mg,<sup>187</sup> B,<sup>128</sup> Al,<sup>182</sup> or U,<sup>188</sup> favor the oxyphosphaalkyne isomer, while soft Lewis acidic elements for example the heavy group 14 elements, (Ge, Sn, Pb),<sup>181, 189-193</sup> Ga,<sup>182, 194</sup> favor the phosphaketene isomer. *iii*) Redox chemistry: the OCP anion is prone to oxidation by many metals due to its reductive nature and the electrophilic character of the metals.<sup>177, 195-197</sup> While point *i*) can be circumvented by using sterically demanding substituents to stabilize the phosphaketene, points *ii*) and *iii*) are more challenging to avoid because the inherent electrophilic properties of the binding metal will differ widely across the periodic table. Nevertheless, phosphaketene isomers  $R-P=C=O$  are usually more stable than

their oxyphosphaalkyne  $R-O-C\equiv P$  analogues; thus *ii*) is a less common problem in synthetic routes. In this chapter, we aim to offer a solution to the problem described in point *iii*). Since the heavier pnictogens are easily reduced, neutral donor ligands such as *N*-heterocyclic carbenes (NHC) can be employed to stabilize the phosphaketene motif, thereby preventing reduction at the pnictogen center.

### 5.1.2 Select Examples in Main-Group Phosphaketene Chemistry

Phosphaketenes show rich and often unprecedented chemistry. In recent years, the phosphanyl and tetrel substituted phosphaketenes have attracted special interest. Bertrand, Su, and Grützmacher discovered a unique reaction where OCP rearranges to OPC when an *N*-heterocyclic phosphane (NHP)–phosphaketene adduct is reacted with NHC (Figure 5.1.1A).<sup>184</sup> Nucleophilic attack on the OCP carbon atom by the NHC results in a zwitterionic intermediate, which is followed by migration of the NHP unit to oxygen. Grützmacher *et. al.* showed that the CO unit of the phosphaketene can be substituted by a carbene, demonstrating similar phosphaketene reactivity with NHCs (Figure 5.1.1B).<sup>183</sup> Addition of NHC to a triphenylgermanium– or tin–phosphaketene led to the formation of NHC-phosphaketene adducts. When heated, the NHC transfers to phosphorus to release CO thereby forming NHC–phosphinidene germanium and tin complexes. Similarly, the  $C\equiv O$  unit of a phosphaketene can be exchanged by another donor. Bertrand and Hansmann *et al.* observed loss of CO from NHP-phosphaketenes when a Lewis-basic phosphine was introduced with moderate heating (Figure 5.1.1C).<sup>198</sup> The reaction proceeds via an associative mechanism, whereby the phosphine binds to the -PCO unit first, followed by loss of CO.

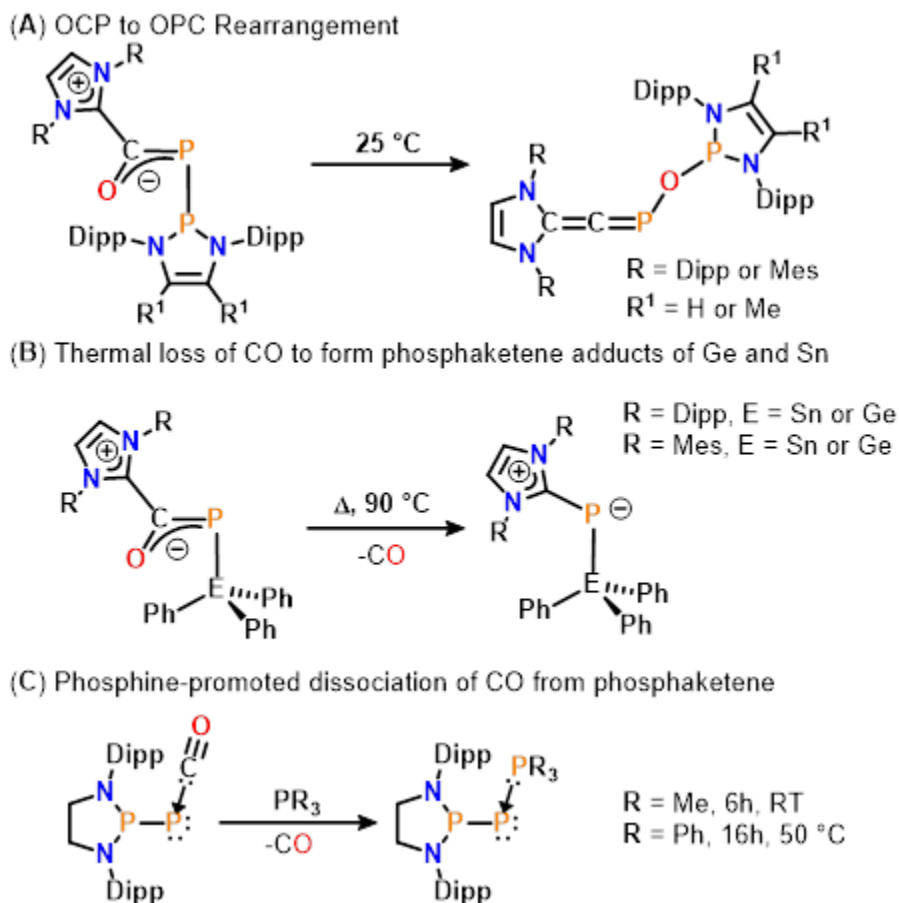


**Figure 5.1.1** (A) OCP to OPC rearrangement; (B) phosphine-promoted CO dissociation; (C) Thermal loss of CO from NHC-phosphaketene adducts of triphenyl-germanium or -tin to form NHC-phosphinidenes.

Within the realm of main-group elements, the reactivity of Na[OCP] has been established for group 2,<sup>187, 199</sup> group 13,<sup>128, 182</sup> group 14,<sup>5, 181, 184, 189-192, 200-201</sup> and group 15.<sup>184, 202-203</sup> For the lattermost, these examples are limited to phosphorous, with no current reports describing reactions of Na[OCP] with the heavier pnictogens (Sb and Bi). Nevertheless, the chemistry of the heavier two Pn elements (Sb, Bi) has seen a substantial increase in interest recently as novel bonding motifs and new applications in catalysis continue to be discovered.<sup>88-89, 92, 97-98, 102, 104, 107, 140, 204-213</sup>

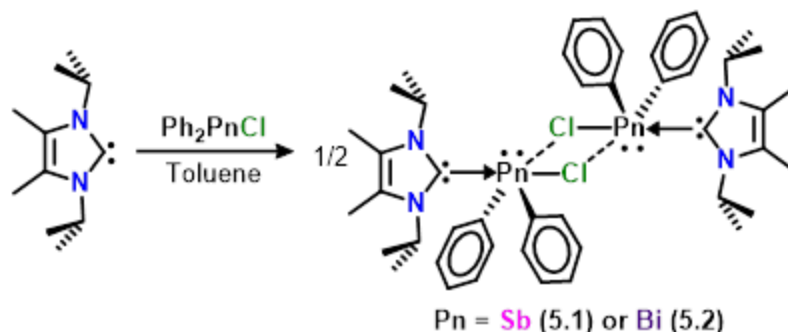
In this chapter, the first reactions of Na[OCP] with the antimony and bismuth compounds, [NHC–Sb(Ph)<sub>2</sub>Cl]<sub>2</sub> (**5.1**) and [NHC–Bi(Ph)<sub>2</sub>Cl]<sub>2</sub> (**5.2**) (compound **4.6** in previous chapter), are investigated. When the [NHC–PnPh<sub>2</sub>Cl]<sub>2</sub> is combined with [Na[OCP]•(dioxane)<sub>x</sub>], Sb and Bi–phosphaketene complexes can be isolated (**5.3** and **5.4**). Notably, compounds **5.3** and **5.4** undergo a thermal reduction process where the Pn<sup>III</sup> center is reduced to Pn<sup>II</sup> to form either tetraphenyldistibine or tetraphenyldibismuthine and the [(NHC)<sub>2</sub>OCP][OCP] salt (**5.5**). Compound **5.5** is the first example of a salt with 2-phosphaethynolate embodying both the cation and the anion. DFT calculations demonstrate that the formation of the cationic unit in **5.5** occurs in a mechanistic step where nucleophilic attack of a dissociated NHC on one unit of **5.4** leads to the loss of [Ph<sub>2</sub>Bi]<sup>–</sup>.

## 5.2 Synthesis of NHC Diphenylpnictogen Halide Complexes

### 5.2.1 Synthesis of NHC-Supported Diphenylpnictogen Chloride Dimers

Initially, the reaction of Na[OCP] with Ph<sub>2</sub>PnCl (Pn = Sb or Bi) was performed and the formation of either tetraphenyldistibine or tetraphenyldibismuthine species and an insoluble OCP-containing precipitate were observed. Extending the scope of this reaction, NHC ligand 4,5-dimethyl-1,3-diisopropylimidazolin-2-ylidene was reacted with diphenylantimony chloride (Ph<sub>2</sub>SbCl) or diphenylbismuth chloride (Ph<sub>2</sub>BiCl) in THF for 1 hour at room temperature (Scheme 5.2.1). Compounds **5.1** (Sb) and **5.2** (Bi) were obtained as white solids in 94% and 85% yield, respectively. The <sup>1</sup>H NMR spectrum of **5.1** in C<sub>6</sub>D<sub>6</sub> shows a broad heptet at 4.69 ppm, attributed to the NHC methine proton. This is shifted downfield from the methine of the NHC ligand (3.96 ppm). Due to poor solubility in C<sub>6</sub>D<sub>6</sub>, the <sup>1</sup>H NMR spectrum of compound **5.2** was recorded in

THF-*d*<sub>8</sub>, which showed a broadened heptet at 4.51 ppm attributed to the methine protons of coordinated NHC.



**Scheme 5.2.1** Synthesis of diphenylpnictogen halide *N*-heterocyclic carbene complexes.

### 5.2.2 Crystallographic Analysis of NHC-Supported Diphenylpnictogen Chloride Dimers

Colorless crystals suitable for X-ray diffraction of both **5.1** and **5.2** were obtained from toluene/hexanes (10:1) mixtures at  $-37$  °C. The molecular structures of both compounds **5.1** and **5.2** reveal dimers with distorted square pyramidal geometry around the metal center (**Figure 5.2.1**). The C1–Sb1 bond distance in compound **5.1** [2.356(3) Å] is outside the range of other <sup>NHC</sup>C–Sb bonds (2.144–2.268 Å);<sup>113, 140, 210, 212, 214-215</sup> likewise, the C1–Bi1 bond in compound **5.2** [2.489(6)] is slightly longer than the range for known <sup>NHC</sup>C–Bi bonds (2.339–2.428 Å).<sup>109-110, 113</sup> The Pn–Cl bond lengths are 2.8006(8) Å (**5.1**) and 2.8696(16) Å for (**5.2**), which are also significantly longer than those reported for other known NHC supported Sb–Cl (2.332–2.402 Å)<sup>214-215</sup> and NHC supported Bi–Cl (2.437–2.705 Å)<sup>109-110</sup> complexes. The longer <sup>NHC</sup>C–Pn bonds results from the weak lewis acidity of Ph<sub>2</sub>PnCl compared to PhBiCl<sub>2</sub> and BiCl<sub>3</sub>. The Pn–Cl distances corresponding to the dimeric interaction in **5.1** [3.9544(10) Å] is longer than that in **5.2** [3.7211(17) Å], which is caused by greater electronic saturation at antimony compared to bismuth.

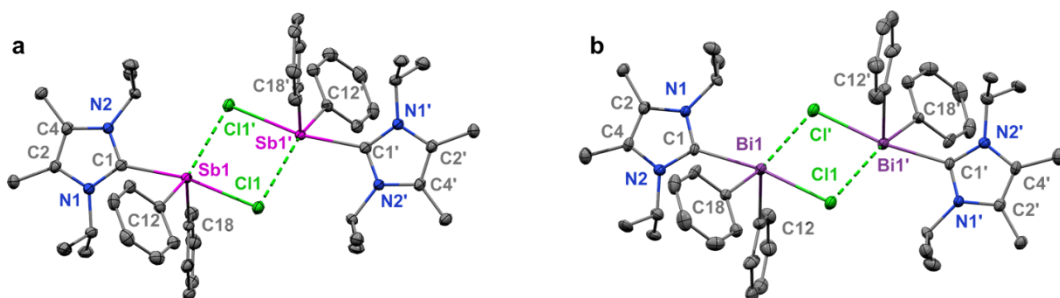


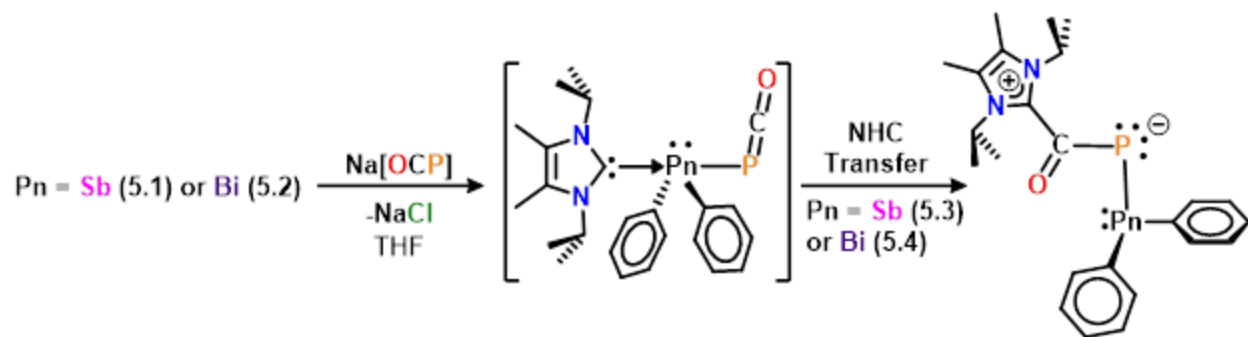
**Figure 5.2.1** Molecular structures – **5.1** (a): (thermal ellipsoids at 50% probability; H atoms omitted for clarity). Selected bond distances (Å) and angles (deg): Sb1–C1: 2.356(3); Sb1–C11: 2.8006(8); Sb1–C11': 3.9544(10); Sb1–C18: 2.168(3); Sb1–C12: 2.171(4). C18–Sb1–C12: 102.19(14); C18–Sb1–C1: 87.58(12); C12–Sb1–C1: 86.33(12); C18–Sb1–C11: 87.00(8); C12–Sb1–C11: 85.24(9); C1–Sb1–C11: 168.80(9). **5.2** (b): (thermal ellipsoids at 50% probability; H atoms were omitted for clarity). Selected bond distances (Å) and angles (deg): Bi1–C1: 2.489(6); Bi1–C11: 2.8696(16); Bi1–C11': 3.7211(17); Bi1–C18: 2.257(6); Bi1–C12: 2.267(6). C18–Bi1–C12: 99.0(2); C18–Bi1–C1: 86.3(2); C12–Bi1–C1: 88.1(2); C18–Bi1–C11: 86.26(16); C12–Bi1–C11: 88.26(16); C1–Bi1–C11: 171.05(15).

## 5.3 Isolation of NHC-Phosphaketene Adducts of Diphenylpnictogen

### 5.3.1 Reaction of Na[OCP] with NHC-Supported Diphenylpnictogen Chloride Dimers

For both compounds **5.1** and **5.2**, it was hypothesized that a combination of electronic stabilization from the coordinated NHC and steric protection from the two phenyl groups may suitably stabilize their OCP adducts. Based on the reactivity known for [OCP]<sup>−</sup> with other main group elements,<sup>177</sup> the formation of a pnictogen–phosphaketene adduct, Pn–PCO should be possible. Therefore, we reacted compounds **5.1** and **5.2** with Na[OCP] at −37 °C in THF (Scheme 5.3.1). The <sup>31</sup>P NMR spectra of the isolated complexes revealed shifts at 58.2 ppm (antimony) and 82.2 ppm (bismuth), which are downfield from other known main-group element Pn–PCO

compounds ( $-441$  to  $-225.8$  ppm).<sup>177</sup> Two doublets were observed in the  $^{13}\text{C}$  NMR for both the antimony [ $203.1$  ppm ( $J = 76.0$  Hz) and  $148.8$  ppm ( $J = 52.8$  Hz)] and bismuth [ $203.6$  ppm ( $J = 81.7$ ) and  $152.0$  ppm ( $J = 49.6$  Hz)] Pn–PCO complexes, which are assigned to two  $^{13}\text{C}$ – $^{31}\text{P}$  coupling environments.



**Scheme 5.3.1** Synthesis of bismuth and antimony phosphaketene adducts.

### 5.3.2 Crystallographic Analysis of NHC-Phosphaketene Adducts of Diphenylpnictogen

Crystals of both the antimony and bismuth compounds **5.3** and **5.4** were obtained from layering the filtrate of the original reaction mixture in THF with hexanes in a 1:1 ratio at  $-37$  °C. Interestingly, the crystal structure revealed that the NHC transferred from the pnicogen center to the phosphaketene (Figure 5.3.1). The formation of these products corroborates the two doublets observed by  $^{13}\text{C}$  NMR as  $^{13}\text{C}$ – $^{31}\text{P}$  coupling can be expected for both the carbonyl and carbene carbon atoms. We did not observe a stretching frequency for the carbonyl group in the IR spectrum. However, this is consistent with reported NHC-phosphaketenyl species.<sup>183</sup> The solid-state structures of **5.3** and **5.4** reveal pnicogen centers in a see-saw geometry with Pn–Pn interactions at  $3.9619(17)$  Å and  $3.8204(6)$  Å, respectively. Indeed, the Bi–Bi interaction in **5.4** is more substantial than the Sb–Sb interaction in **5.3**, this results from the lower energy of the interacting orbitals on Bi compared to Sb. The Pn–P bond lengths for both **5.3** ( $2.5042(16)$  Å) and **5.4**

(2.589(2)–2.594(2) Å) are close to the sum of covalent radii for antimony and phosphorous (2.50 Å), as well as bismuth and phosphorous (2.61 Å).<sup>216</sup>

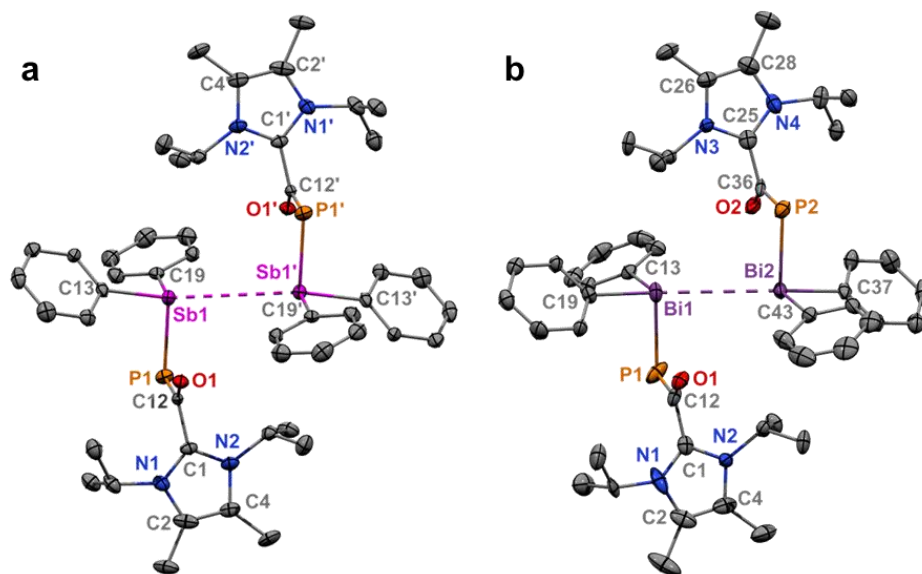


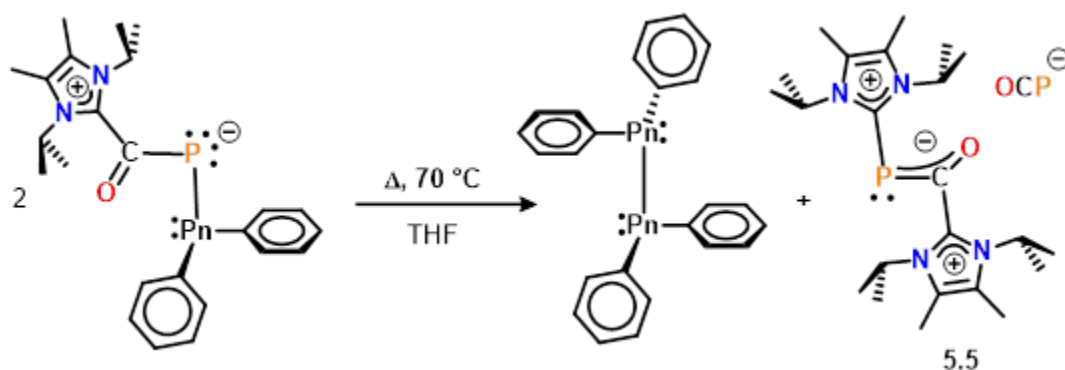
**Figure 5.3.1** Molecular structures – **5.3** (a): (thermal ellipsoids at 50% probability; H atoms omitted for clarity). Selected bond distances (Å) and angles (deg): Sb1–C13: 2.154(6); Sb1–C19: 2.155(6); Sb1–P1: 2.5042(16); Sb1–Sb1': 3.9619(17) P1–C12: 1.748(6); O1–C12: 1.264(7); C1–C12: 1.529(7). C13–Sb1–C19: 97.7(2); C13–Sb1–P1: 99.79(15); C19–Sb1–P1: 91.77(15); Sb1'–Sb1–P1: 94.602(40); Sb1'–Sb1–C19: 97.237(158); Sb1'–Sb1–C13: 158.899(168). **5.4** (b): (thermal ellipsoids at 50% probability; H atoms were omitted for clarity). Selected bond distances (Å) and angles (deg): Bi1–C19: 2.229(6); Bi1–C13: 2.272(7) Bi1–P1: 2.589(2); Bi1–Bi2: 3.8204(6); Bi2–C37: 2.251(7); Bi2–C43: 2.257(8); Bi2–P2: 2.594(2); P1–C12: 1.736(7); P2–C36: 1.746(8); O1–C12: 1.255(8); O2–C36: 1.258(8); C1–C12: 1.525(11); C25–C36: 1.515(11). C19–Bi1–C13: 94.2(2); C19–Bi1–P1: 97.38(19); C13–Bi1–P1: 87.26(19); C37–Bi2–C43: 94.8(3); C37–Bi2–P2: 98.56(19); C43–Bi2–P2: 90.99(19); Bi2–Bi1–P1: 86.913(49); Bi2–Bi1–C13:

101.940(176); Bi2–Bi1–C19: 163.528(178); Bi1–Bi2–P2: 89.365(43); Bi1–Bi2–C43: 104.176(179); Bi1–Bi2–C37: 159.346(177).

## 5.4 Thermal Reduction at Sb and Bi Centers

### 5.4.1 Thermal Reactivity of NHC-Phosphaketene Adducts of Diphenylpnictogen

Recently, Grützmacher and coworkers demonstrated that *N*-heterocyclic carbene (NHC)-phosphaketene adducts of  $\text{Ph}_3\text{Sn-P=C=O}$  and  $\text{Ph}_3\text{Ge-P=C=O}$  undergo a decarbonylation reaction when heated to form the phosphenidynyl complexes  $\text{NHC-P-SnPh}_3$  and  $\text{NHC-P-GePh}_3$ .<sup>183</sup> We were therefore interested in probing the thermal reactivity of compounds **5.3** and **5.4** (Scheme 5.4.1), which can be considered group 15 analogues of the aforementioned Sn and Ge phosphaketene complexes. Compound **5.3** was heated to 90 °C for 24 hours in a J. Young NMR tube. The peaks in this  $^1\text{H}$  NMR matched those reported in the literature for tetraphenyldistibine (Figure A2S105).<sup>213</sup> Compound **5.4**, being less stable than **5.3**, was heated at 70 °C for 3 hours in  $\text{C}_6\text{D}_6$  and observed the emergence of free NHC along with a 100% conversion to tetraphenyldibismuthine (Figure A2S106). Crystals suitable for X-ray diffraction were grown from  $\text{C}_6\text{D}_6$  inside the NMR tube. The solid-state structure revealed a new polymorph of tetraphenyldibismuthine (**5.6**) (Figure A3S32).



**Scheme 5.4.1** Thermal reduction at Sb or Bi center to tetraphenyldipnictogen compounds.

Along with the formation of either tetraphenyldibismuthine or tetraphenyldistibine, an orange solid formed from the C<sub>6</sub>D<sub>6</sub> solution. The orange solid is insoluble in most common organic solvents except for dichloromethane but decomposes within an hour after dissolution. The <sup>1</sup>H NMR spectrum of the orange solid revealed one broad and one well-defined heptet, suggesting two distinct NHC ligand environments. The <sup>31</sup>P NMR showed a broad singlet at 22.1 ppm and a sharp singlet at -395.1 ppm. This latter shift closely resembles the resonance of 2-phosphaethynolate in D<sub>2</sub>O (-396.4 ppm).<sup>178</sup> Four doublets ( $\delta = 200.7, 170.2, 150.2, 146.0$ ) were observed in the <sup>13</sup>C NMR spectrum. Further supporting our suspicions, the signal at 170.2 ppm ( $J = 63.4$  Hz) agrees well with other known <sup>13</sup>C NMR for 2-phosphaethynolate, while the others signals are attributed to three new <sup>13</sup>C-<sup>31</sup>P coupling environments. Similar to compounds **5.3** and **5.4**, no signals were observed in the IR spectrum for the CO stretch in the cationic unit of **5.5**. Two different signals were observed for the phosphaalkyne at 1788 cm<sup>-1</sup> and 1768 cm<sup>-1</sup>, which results from the different orientations of [OCP]<sup>-</sup> in the solid-state structure.

#### 5.4.2 Crystallographic Analysis of [(NHC)<sub>2</sub>OCP][OCP] Complex **5.5**

Orange single-crystals of compound **5.5** suitable for X-ray diffraction were obtained by heating an undisturbed THF solution of **5.3** at 55 °C overnight. The crystal structure shows two NHCs coordinated to a phosphaethynium [OCP]<sup>+</sup> cationic core with an [OCP]<sup>-</sup> counter-anion (Figure 5.4.1). A two-fold rotation axis perpendicular to the P1-C12 bond in the cation causes the two halves of the molecule to be disordered by symmetry in the solid state. This symmetry results in identical bond lengths and angles for both NHC ligands. A similar disorder exists in the anion. There are currently only eight other molecular structures containing uncoordinated [OCP]<sup>-</sup> counter-anions reported in the CSD database.<sup>182, 217-220</sup> The NHC-phosphorous bond (C1-P1) is

1.890(6) Å, which is longer than those known for neutral  $\text{NHC}_2\text{P}_2$  complexes (1.750–1.754 Å)<sup>221-</sup>  
<sup>223</sup> and those known for cationic  $[\text{NHC}_2\text{P}_2]^+$  complexes (1.795–1.841 Å).<sup>215, 221, 224-226</sup>

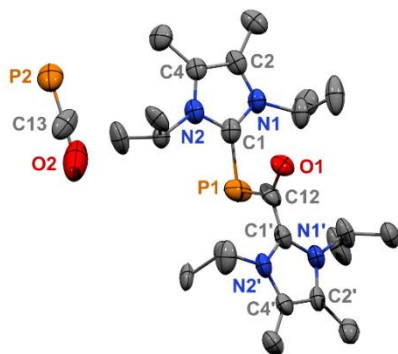


**Figure 5.4.1** Molecular structure of **5.5** (thermal ellipsoids at 50% probability; H atoms omitted for clarity, only one orientation of the symmetry disordered  $[\text{OCP}]^-$  anion is shown.). Selected bond distances (Å) and angles (deg): C1–P1: 1.890(6); P1–C12: 1.755(14); C12–O1: 1.268(12); C12–C1': 1.421(16). C1–P1–C12: 98.3(5); O1–C12–C1': 117.0(14).

## 5.5 Computational Analysis of Thermal Reduction at Sb and Bi

To gain insights into the formation mechanism leading to the new compounds and the bonding situation thereof, we carried out DFT calculations employing the  $\omega\text{B97XD}$  range separated functional with the def2-SVP and def2-TZVP basis sets, which is similar to the level of theory used previously to describe the bonding in carbene complexes of bismuth. Relevant energies and structural parameters are collected in Table 5.5.1.

Compound	1	2	NHC– SbPh <sub>2</sub> PCO	NHC– BiPh <sub>2</sub> PCO	3	4
$\Delta E$	-23.9	-26.2	-19.2	-21.5	-29.7	-29.2
$\Delta G$	-9.4	-11.7	-3.0	-7.1	-12.4	-12.0
$d(\text{Pn}-\text{C}_{\text{carbene}}/\text{C}-\text{C}_{\text{carbene}})$	2.572	2.715	2.638	2.801	1.513	1.513
$\text{WBI}(\text{Pn}-\text{C}_{\text{carbene}}/\text{C}-\text{C}_{\text{carbene}})$	0.37	0.31	0.32	0.26	0.93	0.93
$q(\text{Pn})$	1.182	1.246	1.058	1.121	0.899	0.936
$\Delta q$	0.235	0.202	0.226	0.186	0.755	0.751

**Table 5.5.1** Complex formation energies ( $\Delta E$ ) and Gibbs free energies ( $\Delta G$ ) in kcal/mol, geometrical parameters (bond length in Å/Wiberg Bond Indices), NPA partial charges of Pn ( $q$ ) in electrons and net charge transfer in electrons ( $\Delta q$ ) at the  $\omega$ B97XD/def2-TZVP level.

The complex formation energy leading to adduct **5.2** is  $-26.2$  kcal/mol (calculated with respect to the isolated carbene and diphenyl bismuth chloride). This value is greater than the values of  $-35.9$  to  $-44.6$  kcal/mol reported for NHC and CAAC complexes of  $\text{PhBiCl}_2$ ,<sup>110</sup> a stronger Lewis acid owing to the presence of two chlorine atoms instead of one in  $\text{Ph}_2\text{BiCl}$ . This agrees nicely with the observations above on the solid-state structures, which revealed rather long  $^{\text{NHC}}\text{C}-\text{Pn}$  bonds as a result of a weaker interaction. Compared to **5.2**, the antimony analogue **5.1** is slightly less stable ( $\Delta E = -23.9$  kcal/mol), explainable by the weaker electron pair accepting property of antimony than that of bismuth. The same phenomenon is observed for the NHC– $\text{Ph}_2\text{PnPCO}$

complexes, which are assumed as possible intermediates during the replacement of the chlorides of **5.1** and **5.2** by phosphoethynolate anion. However, the phosphaketene complexes are destabilized compared to their chloro analogues, due to the lower electronegativity of P compared to Cl. Indeed, the partial charge at the Bi center in the uncomplexed Ph<sub>2</sub>BiPCO and Ph<sub>2</sub>BiCl is +1.010 and +1.226 e, respectively, in line with the lower Lewis acidity of the former compared to the latter. The reduced stability of the phosphaketene complexes compared to analogous chloro-complexes is accompanied by the weakening of the <sup>NHC</sup>C–Pn bonds: these bonds are longer and their Wiberg Bond Indices (WBI) accounting for the covalent character are lower, thus the net charge transfer is smaller. The LUMO of Ph<sub>2</sub>BiPCO (Figure 5.5.1) shows main contributions both at the Bi center and the carbon atom of the PCO moiety, explaining why this species may be complexed either at Bi or on the phosphaketenylic carbon center. The rearranged phosphaketene carbene adducts **5.3** and **5.4**, in which the carbene is coordinated to the PCO carbon atom, are significantly more stable than the Pn-coordinated analogues. Thus, the driving force for the carbene migration is the formation of stronger a C–C bond instead of a dative C–Pn bond. These C–C bonds show a high covalent character (WBI: 0.93) and remarkable net charge transfer from the carbene to the PCO moiety of Δq = 0.751 and 0.755, meaning that the carbenic unit possesses a large partial positive charge. Furthermore, the WBIs of PC/CO bonds (1.41/1.48 and 1.42/1.47 for **5.3** and **5.4**, respectively) indicate delocalization in the PCO fragment. Hence, the structure of the C-coordinated Ph<sub>2</sub>PnPCO adducts **5.3** and **5.4** can be best described as a superposition of two zwitterionic resonance structures shown in Figure 5.5.2A. We also studied the electronic structure and bonding of the cationic fragment of compound **5.5**. Even though [OCP(NHC)<sub>2</sub>]<sup>+</sup> can be regarded formally as an adduct of a cationic OCP<sup>+</sup> unit and two carbenes, the NPA charges and WBI values suggest rather a description shown in Figure 5.5.2B. While the sum of charges in the

OCP core is  $-0.375e$ , both NHC fragments possess high partial charges of 0.804 and 0.571 e. The WBI of the P–C(carbene) and C–C(carbene) bonds of 0.93 indicate covalent character, and the PC/CO bonds show a delocalization in the OCP moiety. The bis-zwitterionic charge distribution of the  $[\text{OCP}(\text{NHC})_2]^+$  cation is also visible on the molecular electrostatic potential shown in Figure 5.5.3.

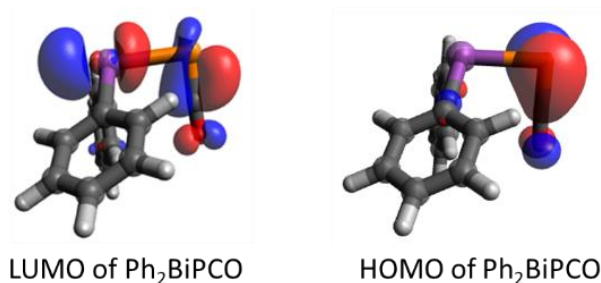


**Figure 5.5.1** LUMO and HOMO of  $\text{Ph}_2\text{BiPCO}$ .

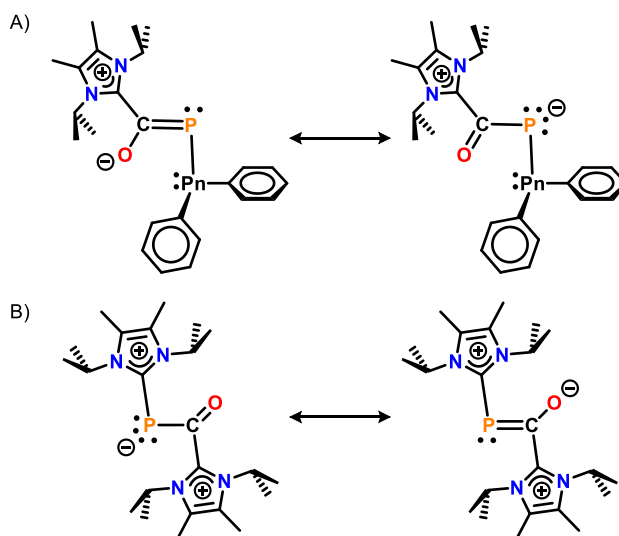


**Figure 5.5.2** Resonance structures for compounds **5.3 / 5.4** (A) and the cation of **5.5** (B).

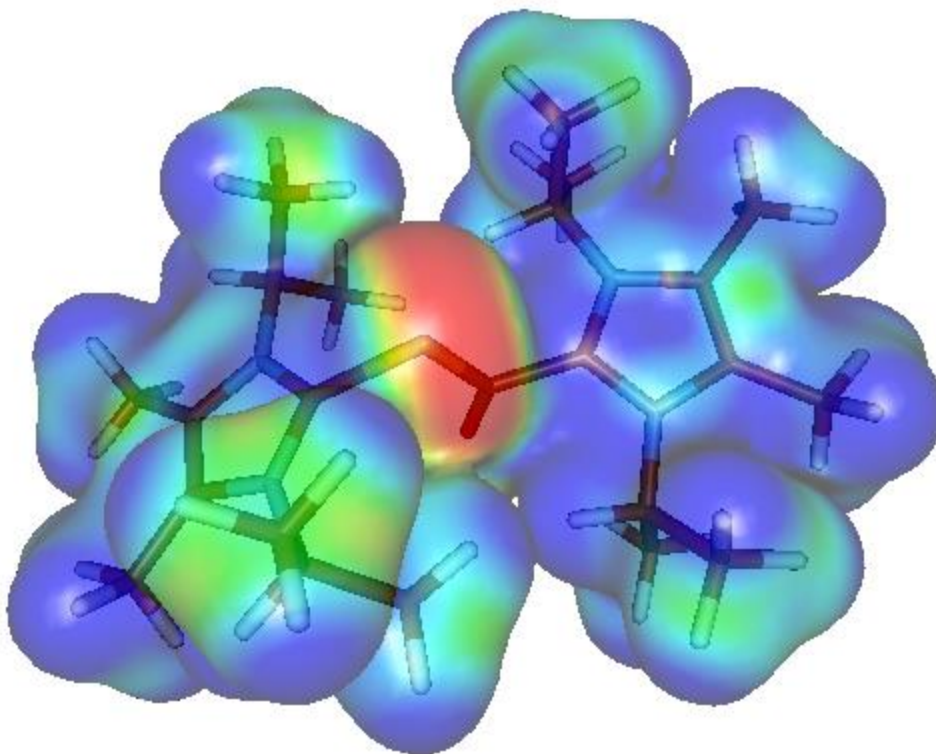


**Figure 5.5.3** Molecular electrostatic potential for the cationic moiety of **5.5**.

We also aimed to understand the formation of the  $\text{Ph}_2\text{PnPnPh}_2$  dimers and compound **5.5**; therefore, we investigated possible reaction mechanisms by means of DFT. As the reactivity of **5.3** and **5.4** are rather similar, we focused on the bismuth analogue. Because this reaction proceeds in  $\text{C}_6\text{D}_6$ , the gas phase approximation seems to be appropriate without solvent effects. In the following, we discuss the energies obtained at the  $\omega\text{B97XD/def2-SVP}$  level.

The formation of the tetraphenyldibismuthine may indicate a radical mechanism, in which the first step would be the homolytic dissociation at the P–Bi bond of adduct **5.4**, or alternatively, the free  $\text{Ph}_2\text{BiPCO}$ . However, both reactions are highly endothermic ( $\Delta H = 53.0$  and  $51.7$  kcal/mol, respectively); thus, they are unlikely to happen even at higher temperature. We considered further

alternative pathways, and a plausible mechanism is presented in Figure 5.5.4. The first step of the reaction is the partial dissociation of adduct **5.4**, resulting in the free carbene and  $\text{Ph}_2\text{BiPCO}$ . This reaction is rather endothermic and proceeds via an activation barrier of 27.9 kcal/mol, resulting in a weakly bound complex of NHC and  $\text{Ph}_2\text{BiPCO}$  at the energy of 27.2 kcal/mol. Even though this reaction is likely shifted towards the side of the starting adduct, the formation of small amounts of free carbene is expected, especially if the entropy factor is taken into account (dissociation Gibbs free energy: 12.0 kcal/mol). This is further supported by the experimental observation of uncoordinated NHC during the reaction. The second step of the reaction is an attack of the free carbene onto the P center of adduct **5.4**, delivering the contact ion pair of the  $[\text{OCP}(\text{NHC})_2]^+$  cation with a diphenyl bismuthide ( $[\text{BiPh}_2]^-$ ) counter anion. The nucleophilic substitution at the phosphaketene P center is known in the literature, and it has been shown that the attack of Lewis bases (LB) on the phosphorus center of phosphanyl phosphaketenes  $\text{R}-\text{P}=\text{C}=\text{O}$  results in the adduct  $\text{R}-\text{P}-\text{LB}$  and carbon monoxide. In our case, however, the C of the PCO unit is occupied by the carbene fragments; thus, the decarbonylation is hampered. Instead, the bismuthide anion is released in a practically thermoneutral reaction ( $\Delta E = 2.4$  kcal/mol). Since all of our attempts to locate the transition state of step 2 failed, we performed a relaxed optimization scan connecting the structures at the two sides of the equation and estimated a barrier of 12.6 kcal/mol via this approach. Thus, based on the low barrier and negligible reaction energy, step 2 is most likely reversible. The thermodynamic sink is obtained in reaction step 3, which is strongly exothermic with a reaction energy of  $\Delta E = -31.7$  kcal/mol (in a practically barrier-less process). In this final step, the attack of the  $[\text{BiPh}_2]^-$  anion at the Bi center of  $\text{Ph}_2\text{BiPCO}$  formed in step 1 delivers the dibismuthine  $\text{Ph}_2\text{BiBiPh}_2$  as well as the  $[\text{OCP}]^-$  anion for compound **5.5**.

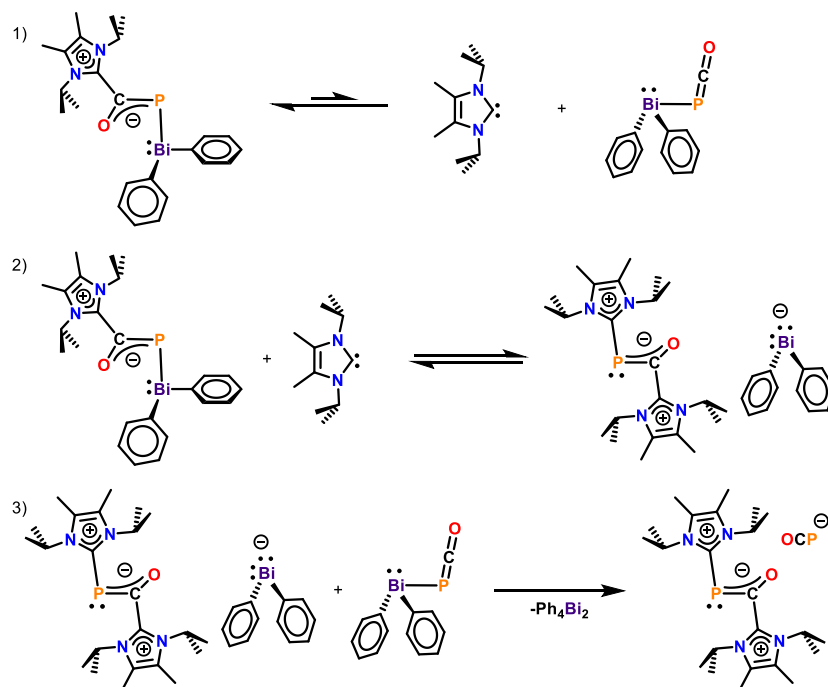


**Figure 5.5.4** Proposed mechanism for the formation of  $[\text{NHC}_2\text{OCP}]^+[\text{OCP}]^-$ .

## 5.6 Summary of Sb and Bi Thermal Reduction Chemistry

We initially found that the reaction of  $\text{Ph}_2\text{PnCl}$  with  $\text{Na}[\text{OCP}]$  results in the formation of tetraphenyldistibine or tetraphenyldibismuthine. We therefore prepared NHC supported antimony and bismuth complexes with  $\text{Pn}-\text{Cl}$  bonds and explored their reactivity with  $\text{Na}[\text{OCP}]$  in order to support the  $\text{Pn}-\text{P}=\text{C}=\text{O}$  moiety. In both cases, the NHC transfers from the pnictogen center to the phosphaketene carbon atom. The crystal structures of these two OCP complexes reveal significant metal-metal interactions. Heating the NHC-phosphaketene adducts **5.3** and **5.4** results in a formal reduction at the pnictogen center,  $\text{Pn}^{\text{III}}$  to  $\text{Pn}^{\text{II}}$ , resulting in the formation of either tetraphenyldistibine or tetraphenyldibismuthine and a bis-carbene supported phosphathynium salt (**5.5**). Notably, compound **5.5** represents the first example of an ionic compound where the cation and anion each possess an OCP unit. This result contrasts with the chemistry observed for the

group 14 (Sn and Ge) analogues, which undergo decarbonylation to yield phosphinidenyl species, and further demonstrates the utility of the 2-phosphaethynolate ion as a reductant.

## **Appendix 1: Experimental**

## Chapter 2 Synthetic Procedures

**Synthesis of Compound 2.5** To a 100 mL Schlenk flask bis(1-isopropyl-3-methyl-benzimidazol-2-ylidene)methane (1.00 grams, 2.77 mmol) was stirred in dry benzene (25 mL). A solution of  $(\text{Et}_2\text{O})_2\text{BeCl}_2$  (633 mg, 2.77 mmol) dissolved in benzene (10 mL) was added dropwise to the stirring solution, which formed a yellow precipitate immediately upon addition. After filtration and drying *in vacuo*, compound **2.5** was isolated as an air- and moisture-sensitive yellow solid (1.18 g, 97% yield). Yellow block-shaped crystals suitable for a single crystal X-Ray diffraction were obtained from a DCM/hexanes mixture (1:1) at  $-37\text{ }^\circ\text{C}$ .  $^1\text{H}$  NMR (500.13 MHz,  $\text{CD}_2\text{Cl}_2$ , 298K)  $\delta$  7.45-7.44 (m, 2H, *H*<sub>ortho</sub>-Ph-N-*i*pr), 7.24-7.15 (m, 6H, Aryl), 4.73-4.68 (m, 2H,  $\text{CH}(\text{CH}_3)_2$ ), 3.24 (s, 6H, N- $\text{CH}_3$ ), 1.64-1.56 (dd, 12H,  $\text{CH}(\text{CH}_3)_2$ );  $^{13}\text{C}$  NMR (800.13 MHz,  $\text{CD}_2\text{Cl}_2$ )  $\delta$  160.34 (Carbone), 134.59, 131.40, 122.98, 112.03, 109.56, 51.68, 32.82, 20.55, 20.21;  $^9\text{Be}$  NMR (600 MHz,  $\text{CD}_2\text{Cl}_2$ )  $\delta$  11.39. m.p.: decomposes at  $170\text{ }^\circ\text{C}$ .

**Synthesis of Compound 2.6** A suspension of compound **2.5** (200 mg, 0.454 mmol) was stirred in dry toluene (5 mL). A solution of potassium bis(trimethylsilyl)amide (75.4 mg, 0.378 mmol) in dry toluene (5 mL) was added dropwise to the stirring suspension. Upon addition, a yellow product went into solution. The reaction mixture was stirred for 15 minutes. After filtering and drying *in vacuo*, compound **6** was obtained as an air- and moisture-sensitive yellow solid (161 mg, 75.3 % yield). Yellow block-shaped crystals suitable for X-ray diffraction were obtained from a hexanes/toluene (3:1) mixture at room temperature.  $^1\text{H}$  NMR (500.13 MHz,  $\text{C}_6\text{D}_6$ , 298K)  $\delta$  6.97-6.95 (m, 2H, Aryl), 6.92-6.86 (m, 4H, Aryl), 6.53-6.52 (m, 2H, Aryl), 4.80 (m, 2H,  $\text{CH}(\text{CH}_3)_2$ ), 2.75 (s, 6H, N- $\text{CH}_3$ ), 1.40 (d, 6H,  $\text{C}(\text{CH}_3)_2$ ), 1.25 (d, 6H,  $\text{C}(\text{CH}_3)_2$ ), 0.57 (d, 18H,  $\text{N}[\text{Si}(\text{CH}_3)_3]_2$ );  $^{13}\text{C}$  NMR (800.13 MHz,  $\text{C}_6\text{D}_6$ )  $\delta$  160.81 (Carbone), 134.24, 131.09, 128.19, 122.15, 111.10, 108.66, 50.15, 32.23, 20.12, 19.60, 6.53;  $^9\text{Be}$  NMR (600 MHz,  $\text{C}_6\text{D}_6$ )  $\delta$  10.41. m.p.:  $65\text{-}69\text{ }^\circ\text{C}$ .

**Synthesis of Compound 2.7** (CDC)BeCl<sub>2</sub> (100 mg, 0.227 mmol) was suspended in dry toluene and stirred. LiBH<sub>4</sub> (9.9 mg, 0.454 mmol) was added to the stirring suspension. The reaction was stirred vigorously for 16 hours. After the filtration, the yellow solution was concentrated in vacuo. The concentrated solution was stored at -37 °C and yellow block-like crystals suitable for X-Ray diffraction formed after three days.

**Synthesis of Compound 2.8** (CDC)BeCl<sub>2</sub> (106 mg, 0.24 mmol) was suspended and stirred in dry toluene. An ether solution of 1.6M methyl lithium (0.3 mL, 0.48 mmol) was added slowly to the stirring suspension. As a result of ether competition, free CDC ligand was produced in during the reaction. Therefore, CDC ligand was removed by complexing with (Et<sub>2</sub>O)<sub>2</sub>BeCl<sub>2</sub> to form compound **2.8**, which is insoluble in toluene. After filtering to remove compound **2.8** and drying the filtrate *in vacuo*, compound **7** was produced as an air- and moisture-sensitive yellow solid. Crystals suitable for X-ray diffraction were obtained from a concentrated benzene solution. <sup>1</sup>H NMR (500.13 MHz, C<sub>6</sub>D<sub>6</sub>, 298K) δ 6.95-6.94 (m, 2H, Aryl), 6.92-6.86 (m, 4H, Aryl), 6.47-6.45 (m, 2H, Aryl), 4.91 (septet, 2H, CH(CH<sub>3</sub>)<sub>2</sub>), 2.47 (s, 6H, N-CH<sub>3</sub>), 1.48 (d, 6H, CH(CH<sub>3</sub>)<sub>2</sub>), 1.22 (d, 6H, CH(CH<sub>3</sub>)<sub>2</sub>), 0.08 (s, 6H, Be-CH<sub>3</sub>).

**Synthesis of Compound 2.9** Compound **2.5** (178 mg, 0.404 mmol) was suspended in dry toluene (5 mL) and stirred vigorously. A dry toluene (5 mL) solution of potassium bis(trimethylsilyl)amide (161 mg, 0.808 mmol) was added dropwise to the stirring suspension, a product was formed in solution upon addition. Free CDC ligand is produced during the reaction and cannot be removed by washing or extraction due to the solubility of compound **7**. Therefore, CDC ligand was removed by complexing with (Et<sub>2</sub>O)<sub>2</sub>BeCl<sub>2</sub> (19.4 mg, 0.085 mmol) to form compound **5**, which is insoluble in toluene. After filtering to remove compound **5** and drying the filtrate *in vacuo*, compound **7** was produced as an air- and moisture-sensitive yellow solid (109.8 mg, 51.4% yield). Yellow rod-

shaped crystals suitable for X-ray diffraction were obtained at  $-37\text{ }^{\circ}\text{C}$  from a hexanes/toluene mixture (10:1).  $^1\text{H}$  NMR (800.13 MHz,  $\text{C}_6\text{D}_6$ , 298K)  $\delta$  7.15-7.14 (m, 1H, Aryl), 7.08-7.06 (m, 2H, Aryl), 6.92-6.89 (m, 4H, Aryl), 6.58 (m, 1H, Aryl), 5.57 (m, 1H,  $\text{CH}(\text{CH}_3)_2$ ), 3.35 (m, 1H,  $\text{CH}(\text{CH}_3)_2$ ), 2.85 (s, 3H, N- $\text{CH}_3$ ), 2.76 (d, 1H, Be- $\text{CHH-N}$ ), 2.61 (d, 1H, Be- $\text{CHH-N}$ ), 2.95 (d, 3H,  $\text{CH}(\text{CH}_3)_2$ ), 1.18 (d, 3H,  $\text{CH}(\text{CH}_3)_2$ ), 1.03 (d, 3H,  $\text{CH}(\text{CH}_3)_2$ ), 0.68 (d, 3H,  $\text{CH}(\text{CH}_3)_2$ ), 0.33 (s, 18H,  $\text{N}[\text{Si}(\text{CH}_3)_3]_2$ );  $^{13}\text{C}$  NMR (800.13 MHz,  $\text{C}_6\text{D}_6$ )  $\delta$  164.38, 160.14, 138.58, 133.77, 133.47, 131.38, 122.78, 122.38, 122.22, 119.14, 111.41, 110.33, 108.96, 108.42, 49.69, 49.02, 33.71, 31.56, 21.42, 21.29, 20.20, 19.12, 5.31, 1.46;  $^9\text{Be}$  NMR (600 MHz,  $\text{C}_6\text{D}_6$ )  $\delta$  17.73. m.p.: 183-185  $^{\circ}\text{C}$ .

**Synthesis of Compound 2.10** To a 20 mL scintillation vial (carbodicarbene)-(hexamethyldisilazide)beryllacycle (**7**) (558 mg, 1.055 mmol) was stirred in dry toluene (5 mL). A solution of  $(\text{Et}_2\text{O})_2\text{BeCl}_2$  (132 mg, 0.633 mmol) in toluene was added to the stirring solution. After filtration and drying in vacuo, compound **2.10** was isolated as an air- and moisture-sensitive yellow solid (324 mg, 76% yield). Yellow block-shaped (crystals suitable for a single crystal X-Ray diffraction were obtained from a toluene/hexanes mixture (5:1) at  $-37\text{ }^{\circ}\text{C}$ .  $^1\text{H}$  NMR (500.13 MHz,  $\text{C}_6\text{D}_6$ , 298K)  $\delta$  7.07 (m, 1H, Aryl), 7.02 (m, 2H, Aryl), 6.90 (m, 4H, Aryl), 6.52 (m, 1H, Aryl), 5.58 (hept,  $J=7.1$  Hz, 1H, N- $\text{CH}(\text{CH}_3)_2$ ), 3.31 (hept,  $J=7.1$  Hz, 1H, N- $\text{CH}(\text{CH}_3)_2$ ), 2.85 (d,  $J=15$  Hz, 1H, N- $\text{CHH-Be}$ ), 2.78 (d,  $J=15$  Hz, 1H, N- $\text{CHH-Be}$ ), 2.59 (s, 3H, N- $\text{CH}_3$ ), 1.82 (d,  $J=7.1$  Hz, 3H,  $\text{CH}(\text{CH}_3)_2$ ), 1.09 (d,  $J=7.0$  Hz, 3H,  $\text{CH}(\text{CH}_3)_2$ ), 0.99 (d,  $J=7.1$  Hz, 3H,  $\text{CH}(\text{CH}_3)_2$ ), 0.74 (d,  $J=7.0$  Hz, 3H,  $\text{CH}(\text{CH}_3)_2$ ).  $^{13}\text{C}$  NMR (151 MHz,  $\text{C}_6\text{D}_6$ , 298K)  $\delta$  164.9 (Carbone), 159.1, 137.7, 133.5, 132.9, 130.9, 122.3, 122.1, 121.8, 118.9, 111.3, 110.1, 108.9, 108.1, 49.5, 48.9, 31.8, 31.2, 20.8, 20.5, 19.7, 18.9.  $^9\text{Be}$  NMR (84.28 MHz,  $\text{C}_6\text{D}_6$ , 298K)  $\delta$  18.2. m.p.: decomposed at 174  $^{\circ}\text{C}$ .

**Synthesis of Compound 2.11** A suspension of compound **2.10** (50 mg, 0.124 mmol) in dry toluene (5 mL). A solution of  $\text{Et}^2\text{CAAC}$  (39 mg, 0.124 mmol) in dry toluene (5 mL) was added to the stirring suspension. Upon addition, a yellow product went into solution. The reaction mixture was stirred for 15 minutes. After filtering, drying in vacuo and triturating with hexanes, compound **2.11** was obtained as an air- and moisture-sensitive yellow solid (75 mg, 84 % yield). Yellow block-shaped crystals suitable for X-ray diffraction were obtained from a saturated toluene solution at room temperature.  $^1\text{H}$  NMR (500.13 MHz,  $\text{C}_6\text{D}_6$ , 298K)  $\delta$  7.44 (m, 1H, Aryl), 7.29 (m, 4H, Aryl), 7.01 (m, 1H, Aryl), 6.90 (m, 2H, Aryl), 6.80 (m, 1H, Aryl), 6.72 (m, 1H, Aryl), 6.53 (m, 1H, Aryl), 5.73 (hept,  $J = 6.7$  Hz, 1H, N- $\text{CH}(\text{CH}_3)_2$ ), 4.96 (hept,  $J = 6.7$  Hz, 1H, Dipp- $\text{CH}(\text{CH}_3)_2$ ), 4.79 (hept,  $J = 6.4$  Hz, 1H, Dipp- $\text{CH}(\text{CH}_3)_2$ ), 4.55 (d,  $J = 12.6$  Hz, 1H, N- $\text{CHH}-\text{CR}_2\text{Be}$ ), 3.52 (d,  $J = 12.6$  Hz, 1H, N- $\text{CHH}-\text{CR}_2\text{Be}$ ), 3.10 (hept,  $J = 6.7$  Hz, 1H, N- $\text{CH}(\text{CH}_3)_2$ ), 2.98 (d,  $J = 13.1$  Hz, 1H,  $\text{Et}_2\text{RC}-\text{CHH}-\text{CNMe}_2$ ), 2.73 (m, 1H,  $\text{R}_2\text{C}(\text{CHH}-\text{CH}_3)_2$ ), 2.25 (d,  $J = 13.1$  Hz, 1H,  $\text{Et}_2\text{RC}-\text{CHH}-\text{CNMe}_2$ ), 2.19 (m, 1H,  $\text{R}_2\text{C}(\text{CHH}-\text{CH}_3)_2$ ), 2.07 (m, 1H,  $\text{R}_2\text{C}(\text{CHH}-\text{CH}_3)_2$ ), 1.99 (m, 1H,  $\text{R}_2\text{C}(\text{CHH}-\text{CH}_3)_2$ ), 1.97 (d,  $J = 6.9$  Hz, 3H,  $\text{CH}(\text{CH}_3)_2$ ), 1.73 (s, 3H,  $\text{R}_2\text{C}(\text{CH}_3)_2$ ), 1.56 (d,  $J = 6.7$  Hz, 3H,  $\text{CH}(\text{CH}_3)_2$ ), 1.52 (d,  $J = 6.7$  Hz, 3H,  $\text{CH}(\text{CH}_3)_2$ ), 1.47 (d,  $J = 6.5$  Hz, 3H,  $\text{CH}(\text{CH}_3)_2$ ), 1.39 (s, 3H,  $\text{R}_2\text{C}(\text{CH}_3)_2$ ), 1.15 (t,  $J = 7.5$  Hz, 3H,  $\text{R}_2\text{C}(\text{CH}_2-\text{CH}_3)_2$ ), 1.10 (d,  $J = 6.9$  Hz, 3H,  $\text{CH}(\text{CH}_3)_2$ ), 0.98 (d,  $J = 7.0$  Hz, 3H,  $\text{CH}(\text{CH}_3)_2$ ), 0.87 (d,  $J = 6.8$  Hz, 3H,  $\text{CH}(\text{CH}_3)_2$ ), 0.74 (t,  $J = 7.5$  Hz, 3H,  $\text{R}_2\text{C}(\text{CH}_2-\text{CH}_3)_2$ ), 0.64 (d,  $J = 7.0$  Hz, 3H,  $\text{CH}(\text{CH}_3)_2$ ).  $^{13}\text{C}$  NMR (151 MHz,  $\text{C}_6\text{D}_6$ )  $\delta$  161.6 (carbonyl), 157.6, 154.8, 154.4, 141.0, 136.2, 133.1, 131.6, 130.7, 126.0, 124.6, 124.5, 123.1, 122.8, 122.0, 120.0, 112.5, 110.1, 109.4, 108.4, 74.3, 59.9, 52.0, 51.1, 51.0, 49.0, 48.6, 31.5, 31.1, 31.0, 30.4, 28.2, 27.7, 27.4, 27.0, 24.7, 23.7, 22.8, 22.7, 19.6, 19.5, 19.4, 10.2, 9.6.  $^9\text{Be}$  NMR (84.28 MHz,  $\text{C}_6\text{D}_6$ , 298K)  $\delta$  14.0. m.p.: 179-180 °C.

**Synthesis of Compound 2.12** Compound **2.10** (50 mg, 0.124 mmol) was suspended in dry toluene (5 mL) and stirred vigorously. A dry toluene (5 mL) solution of sIPr (22.3 mg, 0.124 mmol) was added to the stirring suspension. Upon addition, a yellow product went into solution. After drying the filtrate *in vacuo*, compound **2.12** was isolated as an air- and moisture-sensitive yellow solid (68 mg, 94% yield). Yellow crystals suitable for X-ray diffraction were obtained from a toluene mixture at  $-37\text{ }^{\circ}\text{C}$  prior to purification.  $^1\text{H}$  NMR (500.13 MHz,  $\text{CD}_2\text{Cl}_2$ , 298K)  $\delta$  7.36 (m, 1H, Aryl), 7.20 (m, 5H, Aryl), 7.04 (m, 2H, Aryl), 6.91 (m, 1H, Aryl), 5.37 (hept,  $J = 6.5$  Hz, 1H, N- $\text{CH}(\text{CH}_3)_2$ ), 5.22 (hept,  $J = 6.8$  Hz, 1H, N- $\text{CH}(\text{CH}_3)_2$ ), 3.78 (hept,  $J = 6.7$  Hz, 1H, N- $\text{CH}(\text{CH}_3)_2$ ), 3.42 (s, 3H, N- $\text{CH}_3$ ), 2.36 (s, 2H, N- $\text{CH}_2$ -Be), 2.18 (s, 6H, C(backbone)- $\text{CH}_3$ ), 1.64 (d,  $J = 7.0$  Hz, 2H, N- $\text{CH}(\text{CH}_3)_2$ ), 1.41 (d,  $J = 7.0$  Hz, 2H, N- $\text{CH}(\text{CH}_3)_2$ ), 1.28 (m, 12H, (sIPr-N- $\text{CH}(\text{CH}_3)_2$ ), 1.24 (d,  $J = 7.1$  Hz, 2H, N- $\text{CH}(\text{CH}_3)_2$ ), 1.20 (d,  $J = 6.4$  Hz, 2H, N- $\text{CH}(\text{CH}_3)_2$ ).  $^{13}\text{C}$  NMR (151 MHz,  $\text{C}_6\text{D}_6$ , 333K)  $\delta$  181.5(carbene), 162.8(carbone), 138.8, 135.3, 123.8, 121.5, 121.1, 120.4, 118.5, 109.6, 108.0, 49.1, 35.7, 22.0, 20.6, 20.3, 19.6, 19.2, 9.8.  $^9\text{Be}$  NMR (84.28 MHz,  $\text{C}_6\text{D}_6$ , 333K)  $\delta$  5.3. m.p.: decomposes at  $165\text{ }^{\circ}\text{C}$ , further melts at  $192\text{-}196\text{ }^{\circ}\text{C}$ .

### Chapter 3 Synthetic Procedures

**Synthesis of Compound 3.19** To a 100 mL round bottom flask,  $(\text{Et}_2\text{O})_2\text{BeCl}_2$  (63.2 mg, 0.277 mmol) was suspended dry THF. 1,3-diisopropyl-4,5-dimethylimidazol-2-ylidene (100 mg, 0.554 mmol) was dissolved in dry THF and added to the stirring suspension. The reaction was allowed to stir for 1 hour before filtration to obtain a crude solid. After subsequent filtration drying *in vacuo*, compound **3.19** was obtained white air- and moisture-sensitive solid (103 mg, 84% yield). Colorless block-like crystals suitable for X-Ray diffraction were obtained from a THF/Hexanes mixture at  $-37\text{ }^{\circ}\text{C}$ .  $^1\text{H}$  NMR (800.13 MHz,  $\text{C}_6\text{D}_6$ , 298K)  $\delta$  6.34 (br, 4H,  $\text{CH}(\text{CH}_3)_2$ ), 1.69 (s, 12H,

C-CH<sub>3</sub>), 1.20 (d, 24H, CH(CH<sub>3</sub>)<sub>2</sub>); <sup>13</sup>C NMR (800.13 MHz, C<sub>6</sub>D<sub>6</sub>, 298K) δ 177.75, 124.37, 50.33, 21.67, 10.16

**Synthesis of Compound 3.20** To a 20 mL scintillation vial, lithium diisopropylphenoxide (83.6 mg, 0.454 mmol) was added and stirred in dry THF. A slurry of compound 1 (100 mg, 0.227 mmol) in dry THF was added to the stirring suspension. The reaction was allowed to stir for 18 hours. After filtration, the crude solid was washed with hexanes to remove uncoordinated sIPr ligand. Compound 2 was obtained as a white solid after drying *in vacuo* for 1 hour (42 mg, 34% yield). Colorless rod-shaped crystals suitable for X-Ray diffraction were obtained from a toluene solution at -37 °C. <sup>1</sup>H NMR (800.13 MHz, C<sub>6</sub>D<sub>6</sub>, 298K) δ 7.20 (d, 4H, *H*<sub>meta</sub>-2,6-diisopropylphenyl), 6.98 (t, 2H, *H*<sub>para</sub>-2,6-diisopropylphenyl), 4.87 (br, 2H, N-CH(CH<sub>3</sub>)<sub>2</sub>), 3.55 (hept, *J* = 6.7 Hz), 4H, C-CH(CH<sub>3</sub>)<sub>2</sub>), 1.44 (s, 6H, C-CH<sub>3</sub>), 1.28 (d, *J* = 6.8 Hz, 24H, C-CH(CH<sub>3</sub>)<sub>2</sub>), 1.25 (d, *J* = 6.8 Hz, 12H, N-CH(CH<sub>3</sub>)<sub>2</sub>); <sup>13</sup>C NMR (201.19 MHz, C<sub>6</sub>D<sub>6</sub>, 298K) δ 156.16, 136.74, 128.35, 123.13, 117.94, 52.12, 27.85, 23.64, 22.12, 9.41; <sup>9</sup>Be NMR (84.28 MHz, C<sub>6</sub>D<sub>6</sub>) δ 3.14.

**Synthesis of Compound 3.21** To a 20 mL vial, a slurry of compound 3.19 (200 mg, 0.554 mmol) was added to a stirring suspension of sodium ethoxide (31 mg, 0.554 mmol) in dry THF. The reaction was allowed to stir for two days before drying *in vacuo*. The resulting white crude solid was washed with hexanes, then extracted with toluene. Colorless crystals of compound 3.21 were obtained from a toluene solution at -37 °C. <sup>1</sup>H NMR (500.13 MHz, C<sub>6</sub>D<sub>6</sub>, 298K) δ 6.46 (hept, *J* = 7.0 Hz, 4H, N-CH(CH<sub>3</sub>)<sub>2</sub>), 4.30 (m, 4H, OCH<sub>2</sub>CH<sub>3</sub>), 3.96 (m, 4H, OCH<sub>2</sub>CH<sub>3</sub>), 1.71 (s, 12H, C-CH<sub>3</sub>), 1.47 (t, *J* = 7.0 Hz, 6H, OCH<sub>2</sub>CH<sub>3</sub>), 1.44 (d, *J* = 7.0 Hz, 24H, C-CH(CH<sub>3</sub>)<sub>2</sub>).

**Synthesis of Compound 3.26** To a 20 mL scintillation vial, (Et<sub>2</sub>O)<sub>2</sub>BeCl<sub>2</sub> (292 mg, 1.28 mmol) was stirred in dry toluene (5 mL). A solution of SIPr (500 mg, 1.28 mmol) dissolved in toluene (5 mL) was added dropwise to the stirring solution, which formed a white precipitate immediately

upon addition. After filtration and drying *in vacuo*, compound **3.26** was isolated as an air- and moisture-sensitive yellow solid (505 mg, 84% yield). Colorless plate-like crystals suitable for X-Ray diffraction were obtained from a saturated toluene solution at  $-37\text{ }^{\circ}\text{C}$ .  $^1\text{H}$  NMR (500.13 MHz,  $\text{C}_6\text{D}_6$ , 298K)  $\delta$  7.13 (m, 2H,  $H_{ortho}$ -Dipp), 7.03 (m, 4H,  $H_{meta}$ -Dipp), 3.51 (s, 4H,  $\text{CH}_2$ -backbone), 3.26 (hept,  $J = 3.26\text{ Hz}$ , 4H,  $\text{CH}(\text{CH}_3)_2$ ), 1.51 (d, 12H,  $\text{CH}(\text{CH}_3)_2$ ), 1.11(d, 12H,  $\text{CH}(\text{CH}_3)_2$ );  $^{13}\text{C}$  NMR (150.9 MHz,  $\text{C}_6\text{D}_6$ )  $\delta$  188.1 ( $\text{C}_{\text{carbene}}$ ), 146.9, 133.3, 130.3, 124.8, 53.8, 28.9, 26.1, 23.7;  $^9\text{Be}$  NMR (84.28 MHz,  $\text{C}_6\text{D}_6$ )  $\delta$  9.97.

**Synthesis of Compound 3.27** ( $\text{Et}^2\text{CAAC}$ ) $\text{BeCl}_2$  (127.0 mg, 0.320 mmol) and Bpy (50.0 mg, 0.320 mmol) were combined in a scintillation vial and dissolved in toluene, yielding a blue solution.  $\text{KC}_8$  (95.2 mg, 0.704 mmol) was added while the solution was at r.t., and the vial was stirred at r.t. overnight. The resulting dark purple suspension was filtered, and the dark purple filtrate reduced to incipient recrystallization under vacuum and kept at  $-37\text{ }^{\circ}\text{C}$ . The resulting dark purple solid were collected and washed with *n*-hexanes (2 mL) to yield the product as a dark purple solid (110.0 mg, 72%). Single crystals suitable for X-ray diffraction were obtained from a saturated toluene/hexanes mixture at  $-37\text{ }^{\circ}\text{C}$ .  $^1\text{H}$  NMR (500.13 MHz,  $\text{C}_6\text{D}_6$ , 298K)  $\delta$  7.27 (m, 2H,  $H$ -Bpy), 7.22 (m, 1H,  $H_{para}$ -Dipp), 7.10 (m, 2H,  $H_{meta}$ -Dipp), 6.49 (m, 2H,  $H$ -Bpy), 6.14 (m, 2H,  $H$ -Bpy), 5.70 (m, 2H,  $H$ -Bpy) 2.89 (hept,  $J = 2.89\text{ Hz}$ , 2H,  $\text{CH}(\text{CH}_3)_2$ -Dipp), 2.02 (m, 4H,  $\text{CH}_2\text{CH}_3$ ), 1.54 (s, 2H,  $\text{CH}_2$ (CAAC backbone)), 1.08 (m, 12H,  $\text{CH}_3$ -Dipp(CAAC)), 0.92 (s, 6H,  $(\text{CH}_3)_2$ ), 0.87 (t,  $J = 0.87\text{ Hz}$ , 6H( $\text{CH}_3$ ) $_2$ );  $^{13}\text{C}$  NMR (150.9 MHz,  $\text{C}_6\text{D}_6$ )  $\delta$  246.0 ( $\text{C}_{\text{carbene}}$ ), 148.5, 140.1, 136.2, 129.6, 128.1, 126.5, 125.4, 120.4, 114.3, 105.8, 78.6, 62.0, 43.5, 29.7, 29.4, 29.2, 25.4, 23.3, 9.7;  $^9\text{Be}$  NMR (84.28 MHz,  $\text{C}_6\text{D}_6$ )  $\delta$  4.80.

**Synthesis of Compound 3.28** Compound **3.26** (151.0 mg, 0.320 mmol) and Bpy (50.0 mg, 0.320 mmol) were combined in a scintillation vial and dissolved in toluene, yielding a pink solution.  $\text{KC}_8$

(95.2 mg, 0.704 mmol) was added while the solution was at r.t., and the vial was stirred at r.t. overnight. The resulting dark red suspension was filtered, and the dark red filtrate reduced to incipient recrystallization under vacuum and kept at -37 °C. The resulting dark red solid were collected and washed with *n*-hexanes (2 mL) to yield the product as a dark red solid (124.5 mg, 70%). Single crystals suitable for X-ray diffraction were obtained from a saturated toluene/hexanes mixture at -37 °C. <sup>1</sup>H NMR (500.13 MHz, C<sub>6</sub>D<sub>6</sub>, 298K) δ 7.04 (m, 6H, Aryl), 5.88 (m, 4H, Aryl), 5.24 (m, 2H, Aryl), 3.36 (s, 4H, CH<sub>2</sub>-backbone), 3.11 (hept, *J* = 3.11 Hz, 4H, CH(CH<sub>3</sub>)<sub>2</sub>-Dipp), 1.17 (d, *J* = 1.17 Hz, 12H, CH(CH<sub>3</sub>)<sub>2</sub>), 1.10 (d, *J* = 1.17 Hz, 12H, CH(CH<sub>3</sub>)<sub>2</sub>); <sup>13</sup>C NMR (150.9 MHz, C<sub>6</sub>D<sub>6</sub>) δ 185.1(C<sub>carbene</sub>), 146.5, 138.3, 135.3, 129.9, 125.1, 122.6, 119.6, 112.1, 102.5, 54.4, 28.9, 25.0, 23.2; <sup>9</sup>Be NMR δ 4.50.

## Chapter 4 Synthetic Procedures

**Synthesis of Compound 4.7** In a scintillation vial, a mixture of [sIPrBiPh<sub>2</sub>Cl]<sub>2</sub> (30 mg, 25.8 μmol) and AgSbF<sub>6</sub> (18 mg, 51.6 μmol) were dissolved in CD<sub>2</sub>Cl<sub>2</sub> and shaken. A white solid was removed by filtration. Colorless block-like crystals of [(sIPr)<sub>2</sub>Ag][SbF<sub>6</sub>] were obtained from the solution (See Figure A3S15). Spectral data matched previous reports for [(sIPr)<sub>2</sub>Ag]<sup>+</sup>.<sup>227-228</sup>

**Synthesis of Compound 4.8** A solution of sIPr (50 mg, 0.277 mmol) in THF was added to a solution of [BiPh<sub>2</sub>Cl]<sub>2</sub> (221 mg, 0.277 mmol) in THF and stirred for 30 minutes at room temperature. Solvent was removed and under reduced pressure to afford a white solid. After washing with THF (3 x 2 mL) then drying *in vacuo*, compound **4.8** was obtained as a white solid (125 mg, 46% yield). Crystals suitable for X-ray diffraction were obtained from a THF/Hexanes (2:1) layered mixture. <sup>1</sup>H NMR (500.13 MHz, THF-*d*<sub>8</sub>) δ 8.33 (br, 6H, Aryl), 7.43 (t, *J* = 7.4 Hz, 8H, Aryl), 7.23 (t, *J* = 7.4 Hz, 4H), 4.60 (hept, *J* = 6.8 Hz, 2H, N-CH(CH<sub>3</sub>)<sub>2</sub>), 2.20 (s, 6H, C-CH<sub>3</sub>),

1.14 (d,  $J = 6.9$  Hz, 12H, N-CH(CH<sub>3</sub>)<sub>2</sub>). <sup>13</sup>C NMR (201.19 MHz, THF-*d*<sub>8</sub>)  $\delta$  139.12 (br, C<sub>Aryl</sub>), 131.70 (C<sub>Aryl</sub>), 128.17 (br, C<sub>Aryl</sub>), 55.72 (N-CH(CH<sub>3</sub>)<sub>2</sub>), 30.82 (N-CH(CH<sub>3</sub>)<sub>2</sub>), 22.14 (N-CH(CH<sub>3</sub>)<sub>2</sub>), 10.52 (C<sub>Aryl</sub>-CH<sub>3</sub>). Anal. Calcd for C<sub>35</sub>H<sub>40</sub>Bi<sub>2</sub>Cl<sub>2</sub>N<sub>2</sub>: C, 43.00; H, 4.12; N, 2.87%. Found: C, 43.37; H, 4.31; N, 2.89%.

**Synthesis of Compound 4.9** In a 20 mL scintillation vial, a mixture of SIPr (250 mg, 0.64 mmol) and Ph<sub>2</sub>BiCl (513 mg, 1.28 mmol) were dissolved in dry toluene and allowed to stir overnight. After filtration, SIPr[BiPh<sub>2</sub>Cl]<sub>2</sub> was collected as a white solid (725 mg, 95% yield). Crystals suitable for X-ray diffraction were obtained from a THF/Hexanes (2:1) layered mixture. <sup>1</sup>H NMR (800.13 MHz, CD<sub>2</sub>Cl<sub>2</sub>)  $\delta$  8.03 (br, 8H), 7.41 (br, 10H), 7.31 – 7.21 (m, 4H, Aryl), 7.18 (d,  $J = 7.7$  Hz, 4H, Aryl), 4.20 (s, 4H, CH<sub>2</sub>-backbone), 3.08 (hept,  $J = 6.4$  Hz, 4H, CH(CH<sub>3</sub>)<sub>2</sub>-Dipp), 1.29 (d,  $J = 6.8$  Hz, 12H, CH(CH<sub>3</sub>)<sub>2</sub>-Dipp), 1.09 (d,  $J = 6.8$  Hz, 12H, CH(CH<sub>3</sub>)<sub>2</sub>-Dipp). <sup>13</sup>C NMR (201.19 MHz, CD<sub>2</sub>Cl<sub>2</sub>)  $\delta$  199.31 (C<sub>carbene</sub>), 146.16 (C<sub>Aryl</sub>), 138.48 (C<sub>Aryl</sub>), 133.54 (C<sub>Aryl</sub>), 131.22 (C<sub>Aryl</sub>), 130.95 (C<sub>Aryl</sub>), 127.61 (C<sub>Aryl</sub>), 125.14 (C<sub>Aryl</sub>), 55.04 (CH<sub>2</sub>-backbone), 29.17 (CH(CH<sub>3</sub>)<sub>2</sub>-Dipp), 26.22 (CH(CH<sub>3</sub>)<sub>2</sub>-Dipp), 22.73 (CH(CH<sub>3</sub>)<sub>2</sub>-Dipp). Anal. Calcd for C<sub>51</sub>H<sub>58</sub>Bi<sub>2</sub>Cl<sub>2</sub>N<sub>2</sub>: C, 51.57; H, 4.92; N, 2.36%. Found: C, 51.62; H, 5.07; N, 2.39%.

**Synthesis of Compound 4.10** A suspension of [(Ph<sub>2</sub>)BiCl]<sub>2</sub> (254 mg, 0.317 mol) was stirred in toluene (5 mL) for 5 minutes in a 20 mL scintillation vial. A toluene solution of CAAC (100 mg, 0.317 mol) was added to the stirring solution. The reaction was allowed to stir for 1 hour. After filtration and drying in vacuo, compound 5 was obtained as a white solid (300 mg, 85% yield). Colorless block-like crystals of **26** were obtained from a toluene/hexanes mixture at –37 °C. <sup>1</sup>H NMR (800.13 MHz, CD<sub>2</sub>Cl<sub>2</sub>)  $\delta$  8.39 (br, 4H, Aryl), 7.87 (br, 3H, Aryl), 7.66 (t,  $J = 7.8$  Hz, 1H, Dipp-*H*<sub>para</sub>), 7.49 (br, 9H, Aryl), 7.43 (d,  $J = 7.8$  Hz, 2H, Dipp-*H*<sub>meta</sub>), 7.27 (br, 4H, Aryl), 2.75 (hept,  $J = 6.6$  Hz, 2H, Dipp-CH(CH<sub>3</sub>)<sub>2</sub>), 2.10 (s, 2H, C-CH<sub>2</sub>-C), 1.58-1.54 (m, 2H, (CH<sub>2</sub>CH<sub>3</sub>)<sub>2</sub>),

1.49-1.44 (m, 2H, (CH<sub>2</sub>CH<sub>3</sub>)<sub>2</sub>), 1.47 (s, 6H, C(CH<sub>3</sub>)<sub>2</sub>), 1.36 (d, *J* = 6.5 Hz, 6H, CH(CH<sub>3</sub>)<sub>2</sub>-Dipp), 1.12 (d, *J* = 6.7 Hz, 6H, CH(CH<sub>3</sub>)<sub>2</sub>-Dipp), 0.78 (t, *J* = 7.4 Hz, 6H, (CH<sub>2</sub>CH<sub>3</sub>)<sub>2</sub>). <sup>13</sup>C NMR (201.19 MHz, CD<sub>2</sub>Cl<sub>2</sub>) δ 244.99 (C<sub>carbene</sub>), 183.90 (C<sub>Aryl</sub>), 169.01 (C<sub>Aryl</sub>), 144.50 (C<sub>Aryl</sub>), 139.40 (C<sub>Aryl</sub>), 138.12 (C<sub>Aryl</sub>), 131.13 (C<sub>Aryl</sub>), 129.12 (C<sub>Aryl</sub>), 127.07 (C<sub>Aryl</sub>), 126.78 (C<sub>Aryl</sub>), 85.72 (C(CH<sub>3</sub>)<sub>2</sub>), 68.63 (C-CH<sub>2</sub>-C), 41.56 (C(CH<sub>2</sub>CH<sub>3</sub>)<sub>2</sub>), 31.40 (C(CH<sub>2</sub>CH<sub>3</sub>)<sub>2</sub>), 29.57 (CH(CH<sub>3</sub>)<sub>2</sub>-Dipp), 29.15 (CH(CH<sub>3</sub>)<sub>2</sub>-Dipp), 27.06 (C(CH<sub>3</sub>)<sub>2</sub>), 24.40 (CH(CH<sub>3</sub>)<sub>2</sub>-Dipp), 9.77 ((CH<sub>2</sub>CH<sub>3</sub>)<sub>2</sub>). Suitable elemental analysis could not be obtained due to decomposition of the sample during shipping; thus, purity was assessed by <sup>1</sup>H and <sup>13</sup>C NMR.

**Synthesis of Compound 4.11** (THF)Bi(Ph)Cl<sub>2</sub> (222 mg, 0.555 mmol) was suspended in dry toluene and stirred for 10 minutes. An aliquot of THF was added to help solubilize (THF)Bi(Ph)Cl<sub>2</sub>. A solution of sIPr (100 mg, 0.555 mmol) in toluene was added to the stirring suspension. After stirring for 16 hours, the suspended white solid was obtained *via* filtration and dried *in vacuo*. Compound **27** was obtained in good yield (212 mg, 75% yield). Colorless rod-shaped crystals suitable for X-ray diffraction were obtained from a supersaturated benzene solution at room temperature. <sup>1</sup>H NMR (500.13 MHz, CD<sub>2</sub>Cl<sub>2</sub>) δ 9.20 (d, *J* = 7.6 Hz, 2H, Aryl), 7.79 (t, *J* = 7.5 Hz, 2H, Aryl), 7.45 (t, *J* = 7.6 Hz, 1H, Aryl), 4.95 (hept, *J* = 7.0 Hz, 2H, N-CH(CH<sub>3</sub>)<sub>2</sub>), 2.24 (s, 6H, C-CH<sub>3</sub>), 1.36 (d, *J* = 7.0 Hz, 12H, N-CH(CH<sub>3</sub>)<sub>2</sub>). <sup>13</sup>C NMR (201.19 MHz, CD<sub>2</sub>Cl<sub>2</sub>) δ 185.64 (C<sub>carbene</sub>), 185.03 (C<sub>Aryl</sub>), 139.61 (C<sub>Aryl</sub>), 132.91 (C<sub>Aryl</sub>), 129.19 (C<sub>Aryl</sub>), 128.76 (C<sub>Aryl</sub>), 56.40 (N-CH(CH<sub>3</sub>)<sub>2</sub>), 21.80 (N-CH(CH<sub>3</sub>)<sub>2</sub>), 10.89 (C<sub>Aryl</sub>-CH<sub>3</sub>). Anal. Calcd for C<sub>17</sub>H<sub>25</sub>BiCl<sub>2</sub>N<sub>2</sub>: C, 38.00; H, 4.69; N, 5.21%. Found: C, 38.22; H, 4.96; N, 5.45%.

**Synthesis of Compound 4.12** To a 20 mL scintillation vial, CDC (318 mg, 881 μmol) and (THF)BiPhCl<sub>2</sub> (378 mg, 881 μmol) were added and stirred in THF. A yellow precipitate formed from solution. After stirring for 1 hour the reaction was filtered, then the yellow solid was dried *in*

*vacuo*. (CDC)BiPhCl<sub>2</sub> was obtained as a yellow (434 mg, 69% yield). Crystals suitable for X-ray diffraction were obtained from a THF/hexanes (1:2) layered mixture. <sup>1</sup>H NMR (500.13 MHz, CD<sub>2</sub>Cl<sub>2</sub>) δ 8.45 (d, *J* = 7.8 Hz, 2H, Aryl), 7.55 (d, *J* = 7.4 Hz, 2H, Aryl), 7.30 (m, 6H, Aryl), 7.21 (t, *J* = 7.7 Hz, 1H, Aryl), 7.01 (d, *J* = 8.6 Hz, 2H, Aryl), 5.22 (hept, 2H, N-CH(CH<sub>3</sub>)<sub>2</sub>), 3.16 (s, 6H, N-CH<sub>3</sub>), 1.61 (d, *J* = 6.1 Hz, 12H, N-CH(CH<sub>3</sub>)<sub>2</sub>). <sup>13</sup>C NMR (201.19 MHz, CD<sub>2</sub>Cl<sub>2</sub>) δ 189.31 (C<sub>carbonyl</sub>), 158.29 (C<sub>carbonyl</sub>), 139.82 (C<sub>Aryl</sub>), 133.95 (C<sub>Aryl</sub>), 131.00 (C<sub>Aryl</sub>), 130.54 (C<sub>Aryl</sub>), 128.19 (C<sub>Aryl</sub>), 124.04 (C<sub>Aryl</sub>), 113.39 (C<sub>Aryl</sub>), 110.65 (C<sub>Aryl</sub>), 93.79 (C<sub>Aryl</sub>), 51.54 (N-CH(CH<sub>3</sub>)<sub>2</sub>), 33.45 (N-CH<sub>3</sub>), 21.62 (N-CH(CH<sub>3</sub>)<sub>2</sub>). Anal. Calcd for C<sub>29</sub>H<sub>33</sub>N<sub>4</sub>BiCl<sub>2</sub>: C, 48.55; H, 4.64; N, 7.81%. Found: C, 48.18; H, 4.58; N, 7.52%.

**Synthesis of Compound 4.13** To a 20 mL scintillation vial, (CDC)BiPhCl<sub>2</sub> (100 mg, 139 μmol) was added and stirred in THF. A solution of AgSbF<sub>6</sub> (48 mg, 139 μmol) in THF was added to the stirring suspension, a white precipitate attributed to AgCl formed from solution. Crystals suitable for X-ray diffraction were obtained from a THF/hexanes (1:1) layered mixture (100 mg, 78% yield). <sup>1</sup>H NMR (800.13 MHz, THF-*d*<sub>8</sub>) δ 8.09 (d, *J* = 7.3 Hz, 0H), 7.76 (d, *J* = 7.7 Hz, 2H, Aryl), 7.43 (t, *J* = 7.4 Hz, 2H, Aryl), 7.36–7.30 (m, 4H, Aryl), 7.28 (d, *J* = 7.6 Hz, 2H, Aryl), 7.22 (t, *J* = 7.5 Hz, 1H, Aryl), 5.03 (br, 2H, N-CH(CH<sub>3</sub>)<sub>2</sub>), 3.26 (s, 6H, N-CH<sub>3</sub>), 1.60 (d, 12H, N-CH(CH<sub>3</sub>)<sub>2</sub>). <sup>13</sup>C NMR (201 MHz, THF-*d*<sub>8</sub>) δ 191.63 (C<sub>carbonyl</sub>), 159.52 (C<sub>carbonyl</sub>), 138.58 (C<sub>Aryl</sub>), 134.34 (C<sub>Aryl</sub>), 132.25 (C<sub>Aryl</sub>), 130.82 (C<sub>Aryl</sub>), 129.45 (C<sub>Aryl</sub>), 125.13 (C<sub>Aryl</sub>), 125.10 (C<sub>Aryl</sub>), 114.26 (C<sub>Aryl</sub>), 112.02 (C<sub>Aryl</sub>), 52.47 (N-CH(CH<sub>3</sub>)<sub>2</sub>), 33.32 (N-CH<sub>3</sub>), 21.44, 21.09 (N-CH(CH<sub>3</sub>)<sub>2</sub>). Anal. Calcd for C<sub>29</sub>H<sub>33</sub>N<sub>4</sub>ClF<sub>6</sub>BiSb: C, 37.95; H, 3.62; N, 6.10%. Found: C, 37.99; H, 3.86; N, 6.08%.

**Synthesis of Compound 4.14** To a 20 mL scintillation vial, (CDC)BiPhCl<sub>2</sub> (300 mg, 418 μmol) was added and stirred in DCM. A solution of AgSbF<sub>6</sub> (288 mg, 837 μmol) was added to the stirring solution, a white precipitate attributed to AgCl formed from solution. Crystals suitable for X-ray

diffraction were obtained from a DCM/hexanes (1:1) layered mixture at  $-37\text{ }^{\circ}\text{C}$  (200 mg, 43% yield).  $^1\text{H}$  NMR (500.13 MHz, THF- $d_8$ )  $\delta$  8.04 (d,  $J = 7.9$  Hz, 2H, Aryl), 7.94 (d,  $J = 7.8$  Hz, 2H, Aryl), 7.76 (t,  $J = 7.7$  Hz, 2H, Aryl), 7.56 (d,  $J = 5.8$  Hz, 2H, Aryl), 7.52 – 7.46 (m, 4H, Aryl), 7.44 (t,  $J = 8.1$  Hz, 2H, Aryl), 4.57 (br, 2H, N-CH(CH<sub>3</sub>)<sub>2</sub>), 3.60 (br, 6H, N-CH<sub>3</sub>), 1.53 (br, 12H, N-CH(CH<sub>3</sub>)<sub>2</sub>).  $^{13}\text{C}$  NMR (201.19 MHz, THF- $d_8$ )  $\delta$  209.74 (C<sub>carbene</sub>), 159.85 (C<sub>carbene</sub>), 147.96 (C<sub>Aryl</sub>), 137.99 (C<sub>Aryl</sub>), 134.44 (C<sub>Aryl</sub>), 133.89 (C<sub>Aryl</sub>), 131.18 (C<sub>Aryl</sub>), 130.33 (C<sub>Aryl</sub>), 126.62 (C<sub>Aryl</sub>), 126.50 (C<sub>Aryl</sub>), 115.06 (C<sub>Aryl</sub>), 113.37 (C<sub>Aryl</sub>), 53.03 (N-CH(CH<sub>3</sub>)<sub>2</sub>), 33.25 (N-CH<sub>3</sub>), 20.97 (N-CH(CH<sub>3</sub>)<sub>2</sub>). Anal. Calcd for C<sub>29</sub>H<sub>33</sub>N<sub>4</sub>F<sub>12</sub>BiSb<sub>2</sub>: C, 31.15; H, 2.98; N, 5.01%. Found: C, 31.04; H, 3.20; N, 4.93%.

**Synthesis of Compound 4.15** To a 20 mL scintillation vial, CDC (200 mg, 555  $\mu\text{mol}$ ) and BiBr<sub>3</sub> (250 mg, 555  $\mu\text{mol}$ ) were added and stirred in THF. The solution turned red and a red solid precipitated from solution. After filtration and drying *in vacuo*, [(CDC)BiBr<sub>3</sub>]<sub>2</sub> was obtained as a red solid (388 mg, 86% yield). Red single crystals suitable for Xray diffraction were obtained from a THF/hexanes layered mixture at  $-37\text{ }^{\circ}\text{C}$ .  $^1\text{H}$  NMR (500.13 MHz, CD<sub>2</sub>Cl<sub>2</sub>)  $\delta$  7.60 (d,  $J = 8.7$  Hz, 2H, Aryl), 7.38 (m,  $J = 7.4$  Hz, 6H, Aryl), 5.01 (hept,  $J = 6.7$  Hz, 2H, N-CH(CH<sub>3</sub>)<sub>2</sub>), 3.89 (s, 6H, N-CH<sub>3</sub>), 1.63 (d,  $J = 7.0$  Hz, 12H, N-CH(CH<sub>3</sub>)<sub>2</sub>).  $^{13}\text{C}$  NMR (201.19 MHz, CD<sub>2</sub>Cl<sub>2</sub>)  $\delta$  159.03 (C<sub>carbene</sub>), 133.76 (C<sub>Aryl</sub>), 130.35 (C<sub>Aryl</sub>), 124.73 (C<sub>Aryl</sub>), 113.71 (C<sub>Aryl</sub>), 111.08 (C<sub>Aryl</sub>), 51.63 (N-CH(CH<sub>3</sub>)<sub>2</sub>), 33.72 (N-CH<sub>3</sub>), 22.07 (N-CH(CH<sub>3</sub>)<sub>2</sub>). Anal. Calcd for C<sub>29</sub>H<sub>33</sub>N<sub>4</sub>F<sub>12</sub>BiSb: C, 34.14; H, 3.49; N, 6.92%. Found: C, 33.57; H, 3.50; N, 6.86%. Despite multiple EA trials with compound **4.15**, the C always deviated from the acceptable standard deviation.

**Synthesis of Compound 4.16** To a 20 mL scintillation vial, [CDCBiBr<sub>3</sub>]<sub>2</sub> (100 mg, 124  $\mu\text{mol}$ ) was stirred in THF (5 mL). A THF solution of AgSbF<sub>6</sub> (42 mg, 124  $\mu\text{mol}$ ) was added slowly to the stirring solution. Upon addition, the solution turned dark red and the reaction was allowed to

stir for 30 minutes. After filtration, the dark red solution was layered with hexanes and red needle-like crystals of compound **4.16** were obtained within 24 hours (80 mg, 67% yield).  $^1\text{H}$  NMR (800.13 MHz,  $\text{CD}_2\text{Cl}_2$ )  $\delta$  7.63 (d,  $J = 8.1$  Hz, 2H, Aryl), 7.45 (m, 2H, Aryl), 7.44–7.39 (m, 2H, Aryl), 4.68 (hept,  $J = 6.7$  Hz, 2H, N- $\text{CH}(\text{CH}_3)_2$ ), 3.89 (s, 6H, N- $\text{CH}_3$ ), 3.73–3.46 (m, 8H, THF), 1.90–1.69 (m, 8H, THF), 1.55 (d,  $J = 6.9$  Hz, 12H, N- $\text{CH}(\text{CH}_3)_2$ ).  $^{13}\text{C}$  NMR (201.19 MHz,  $\text{CD}_2\text{Cl}_2$ )  $\delta$  159.06 ( $\text{C}_{\text{carbene}}$ ), 133.39 ( $\text{C}_{\text{Aryl}}$ ), 129.97 ( $\text{C}_{\text{Aryl}}$ ), 125.62 ( $\text{C}_{\text{Aryl}}$ ), 125.58 ( $\text{C}_{\text{Aryl}}$ ), 114.05 ( $\text{C}_{\text{Aryl}}$ ), 111.81 ( $\text{C}_{\text{Aryl}}$ ), 68.34 (THF), 52.17 (N- $\text{CH}(\text{CH}_3)_2$ ), 33.68 (N- $\text{CH}_3$ ), 26.13 (THF), 21.74 (N- $\text{CH}(\text{CH}_3)_2$ ). Anal. Calcd for  $\text{C}_{31}\text{H}_{44}\text{BiSbBr}_2\text{F}_6\text{N}_4\text{O}_2$ : C, 33.57; H, 4.00; N, 5.05%. Found: C, 33.23; H, 3.90; N, 5.29%.

**Synthesis of Compound 4.17** To a 20 mL scintillation vial,  $[\text{CDCBiBr}_3]_2$  (500 mg, 61.8  $\mu\text{mol}$ ) was stirred in DCM (5 mL) with an aliquot of THF. A solution of Silver *bis*(trifluoromethylsulfonyl)imide  $\text{AgNTf}_2$  (480 mg, 124  $\mu\text{mol}$ ) in DCM was added slowly to the stirring suspension. Upon addition, the solution turned dark red and the reaction was allowed to stir for 5 minutes. The solvent was then removed under reduced pressure to give compound **4.17** as a dark red solid (550 mg, 56% yield). After filtration, the dark red solution was layered with Hexanes and cooled to  $-37$  °C. Red plate-like crystals were obtained in 24 hours.  $^1\text{H}$  NMR (500.13 MHz,  $\text{CD}_2\text{Cl}_2$ )  $\delta$  7.73 (d,  $J = 8.2$  Hz, 2H, Aryl), 7.63 (d,  $J = 8.1$  Hz, 2H, Aryl), 7.59 – 7.48 (m, 4H, Aryl), 4.54 (br, 2H, N- $\text{CH}(\text{CH}_3)_2$ ), 4.16 (s, 6H, N- $\text{CH}_3$ ), 3.77 – 3.68 (m, 12H, THF), 1.87 – 1.81 (m, 12H, THF), 1.50 (d,  $J = 6.1$  Hz, 12H, N- $\text{CH}(\text{CH}_3)_2$ ).  $^{13}\text{C}$  NMR (201.19 MHz,  $\text{CD}_2\text{Cl}_2$ )  $\delta$  202.99 ( $\text{C}_{\text{carbone}}$ ), 157.97 ( $\text{C}_{\text{carbene}}$ ), 132.87 ( $\text{C}_{\text{Aryl}}$ ), 129.60 ( $\text{C}_{\text{Aryl}}$ ), 127.02 ( $\text{C}_{\text{Aryl}}$ ), 126.88 ( $\text{C}_{\text{Aryl}}$ ), 121.01 (q,  $J = 320.7$  Hz,  $\text{CF}_3$ ), 114.64 ( $\text{C}_{\text{Aryl}}$ ), 112.84 ( $\text{C}_{\text{Aryl}}$ ), 68.62 (THF), 52.54 (N- $\text{CH}(\text{CH}_3)_2$ ), 33.37 (N- $\text{CH}_3$ ), 26.14 (THF), 21.64 (N- $\text{CH}(\text{CH}_3)_2$ ). Suitable elemental analysis could not be obtained due to decomposition of the sample during shipping; thus, purity was assessed by  $^1\text{H}$  and  $^{13}\text{C}$  NMR.

**Synthesis of Compound 4.18** To a 20 mL scintillation vial, [CDCBiBr<sub>3</sub>]<sub>2</sub> (50 mg, 30.9 μmol) and CDC (22 mg, 61.8 μmol) were added and stirred in 5 mL chlorobenzene. In the dark, solid AgNTf<sub>2</sub> (72 mg, 185 μmol) was added to the stirring solution, which resulted in an immediate color change of the solution from red to dark blue. After stirring for 1 hour the reaction mixture was filtered and dried *in vacuo* to give compound **4.18** as a dark blue solid (53 mg, 73% yield). Dark blue crystals of **4.18** suitable for X-ray diffraction were obtained from a chlorobenzene/hexanes (10:1) mixture at -37 °C. <sup>1</sup>H NMR (800.13 MHz, CD<sub>2</sub>Cl<sub>2</sub>) δ 7.92 (m, 2H, Aryl), 7.79 (d, *J* = 8.3 Hz, 2H, Aryl), 7.65 (t, *J* = 7.8 Hz, 2H, Aryl), 7.53 (m, 4H, Aryl), 7.44 (m, 2H, Aryl), 7.34 (m, 2H, Aryl), 6.55 (d, *J* = 8.3 Hz, 2H, Aryl), 5.58 (hept, *J* = 6.8 Hz, 2H, N-CH(CH<sub>3</sub>)<sub>2</sub>), 4.45 (hept, *J* = 6.4 Hz, 2H, N-CH(CH<sub>3</sub>)<sub>2</sub>), 3.39 (s, 6H, N-CH<sub>3</sub>), 3.18 (s, 6H, N-CH<sub>3</sub>), 2.10 (d, *J* = 7.0 Hz, 6H), 1.77 (d, *J* = 6.6 Hz, 6H), 1.77 (d, *J* = 6.9 Hz, 6H), 1.09 (d, *J* = 7.1 Hz, 6H). <sup>13</sup>C NMR (201.19 MHz, CD<sub>2</sub>Cl<sub>2</sub>) δ 160.67 (C<sub>carbene</sub>), 154.33 (C<sub>carbene</sub>), 133.24 (C<sub>Aryl</sub>), 132.25 (C<sub>Aryl</sub>), 130.63 (C<sub>Aryl</sub>), 130.36 (C<sub>Aryl</sub>), 129.08 (C<sub>Aryl</sub>), 128.62 (C<sub>Aryl</sub>), 128.04 (C<sub>Aryl</sub>), 127.30 (C<sub>Aryl</sub>), 127.11 (C<sub>Aryl</sub>), 126.72 (C<sub>Aryl</sub>), 126.51 (C<sub>Aryl</sub>), 119.84 (*q*, *J* = 321.0 Hz, CF<sub>3</sub>), 114.95 (C<sub>Aryl</sub>), 114.89 (C<sub>Aryl</sub>), 112.58 (C<sub>Aryl</sub>), 112.46 (C<sub>Aryl</sub>), 53.14 (N-CH(CH<sub>3</sub>)<sub>2</sub>), 52.17 (N-CH(CH<sub>3</sub>)<sub>2</sub>), 33.62 (N-CH<sub>3</sub>), 32.16 (N-CH<sub>3</sub>), 24.17 (N-CH(CH<sub>3</sub>)<sub>2</sub>), 21.21 (N-CH(CH<sub>3</sub>)<sub>2</sub>), 20.69 (N-CH(CH<sub>3</sub>)<sub>2</sub>), 20.56 (N-CH(CH<sub>3</sub>)<sub>2</sub>). Anal. Calcd for C<sub>52</sub>H<sub>56</sub>BiF<sub>18</sub>N<sub>11</sub>O<sub>12</sub>S<sub>6</sub>: C, 35.28; H, 3.19; N, 8.70%. Found: C, 35.65; H, 3.27; N, 8.40%.

## Chapter 5 Synthetic Procedures

**Synthesis of Compound 5.1** To a 20 mL scintillation vial, Ph<sub>2</sub>SbCl (690 mg, 2.22 mmol) was added and stirred in toluene (5 mL). A toluene solution (5 mL) of NHC (400 mg, 2.22 mmol) was added, then the reaction was allowed to stir for 1 hour. After the filtration, the crude solid was washed with hexanes, then dried *in vacuo*. Compound 1 was obtained as a white solid (925 mg, 85%). Crystals suitable for X-ray diffraction studies were obtained from a toluene/hexanes mixture

at  $-37\text{ }^{\circ}\text{C}$ .  $^1\text{H}$  NMR ( $\text{C}_6\text{D}_6$ , 500.13 MHz):  $\delta$  8.17 (t, 4H,  $\text{CH}_{ortho}$ ), 7.22 (t, 4H,  $\text{CH}_{meta}$ ), 7.12 (t, 2H,  $\text{CH}_{para}$ ), 4.69 (br, 2H,  $\text{CH}(\text{CH}_3)_2$ ), 1.56 (s, 6H, C(backbone)– $\text{CH}_3$ ), 0.81 (s, 12H,  $\text{CH}(\text{CH}_3)_2$ ).  $^{13}\text{C}^{175}$  NMR ( $\text{THF-}d_8$ , 201.193 MHz):  $\delta$  146.53, 136.50, 128.51, 128.23, 125.33, 52.34, 21.23, 9.74. Anal. Calcd for  $\text{C}_{23}\text{H}_{30}\text{N}_2\text{SbCl}$ : C, 56.18; H, 6.15; N, 5.70%. Found: C, 55.95; H, 6.22; N, 5.68%.

**Synthesis of Compound 5.2** (Also referred to as **4.6**) To a 20 mL scintillation vial,  $\text{Ph}_2\text{BiCl}$  (1.111 g, 2.77 mmol) was added and stirred in toluene (5 mL). A toluene solution (5 mL) of NHC (500 mg, 2.77 mmol) was added, then the reaction was allowed to stir for 1 hour. After the filtration, the crude solid was washed with hexanes, then dried *in vacuo*. Compound 2 was obtained as a white solid (1.51 g, 94%). Colorless crystals suitable for X-ray diffraction studies were obtained from a toluene/hexanes mixture at  $-37\text{ }^{\circ}\text{C}$ .  $^1\text{H}$  NMR ( $\text{THF-}d_8$ , 500.13 MHz):  $\delta$  8.35 (br, 4H,  $\text{CH}_{ortho}$ ), 7.41 (t,  $J = 7.6\text{ Hz}$ , 4H,  $\text{CH}_{meta}$ ), 7.21 (t,  $J = 7.3\text{ Hz}$ , 2H,  $\text{CH}_{para}$ ), 4.51 (hept,  $J = 6.7\text{ Hz}$ , 2H,  $\text{CH}(\text{CH}_3)_2$ ), 2.15 (s, 6H, C(backbone)– $\text{CH}_3$ ), 1.17 (d,  $J = 7\text{ Hz}$ , 12H,  $\text{CH}(\text{CH}_3)_2$ ).  $^{13}\text{C}\{^1\text{H}\}$  NMR ( $\text{THF-}d_8$ , 201.19 MHz):  $\delta$  139.35, 131.45, 128.08, 126.48, 54.12, 22.75, 10.28. Anal. Calcd for  $\text{C}_{23}\text{H}_{30}\text{N}_2\text{BiCl}$ : C, 47.72; H, 5.22; N, 4.84%. Found: C, 47.37; H, 5.41; N, 4.77%.

**Synthesis of Compound 5.3** To a 20 mL vial,  $(\text{NHC})\text{BiPh}_2\text{Cl}$  (97 mg, 0.197 mmol) was added and stirred in THF.  $\text{Na}[\text{OCP}]\cdot 2.5\text{Dioxane}$  (65 mg, 0.217 mmol) was added to the stirring solution. Immediately upon addition, the solution turned yellow. After stirring for 5 minutes at room temperature, insoluble NaCl was removed by filtration and the yellow THF solution was layered with hexanes in a 1:1 ratio and allowed to sit for one day at  $-37^{\circ}\text{C}$ . After removal of the solvent and drying *in vacuo*, the product was obtained as a yellow crystalline solid (50 mg, 49% yield).  $^1\text{H}$  NMR ( $\text{C}_6\text{D}_6$ , 500.13 MHz)  $\delta$  8.18 (d,  $J = 7.9\text{ Hz}$ , 4H,  $\text{CH}_{ortho}$ ), 7.21 – 7.15 (m, 4H,  $\text{CH}_{meta}$ ), 7.12 (t,  $J = 7.3\text{ Hz}$ , 2H  $\text{CH}_{para}$ ), 5.10 (hept,  $J = 6.9\text{ Hz}$ , 2H,  $\text{CH}(\text{CH}_3)_2$ ), 1.34 (s, 6H, C(backbone)– $\text{CH}_3$ ),

1.06 (d,  $J = 7.1$  Hz, 12H,  $\text{CH}(\text{CH}_3)_2$ ).  $^{13}\text{C}$  NMR (201.19 MHz,  $\text{C}_6\text{D}_6$ )  $\delta$  203.13 (d,  $J = 76.0$  Hz), 148.84 (d,  $J = 52.8$  Hz), 141.01, 137.73, 128.28, 127.28, 123.30, 51.16, 21.08, 9.25.  $^{31}\text{P}\{^1\text{H}\}$  NMR (202.46 MHz,  $\text{C}_6\text{D}_6$ )  $\delta$  58.18 (s, 1P).

**Synthesis of Compound 5.4** To a 20 mL vial,  $(\text{NHC})\text{BiPh}_2\text{Cl}$  (200 mg, 0.344 mmol) was added and stirred in THF.  $\text{Na}[\text{OCP}] \cdot 2.5\text{Dioxane}$  (302 mg, 0.344 mmol) was added to the stirring solution. Immediately upon addition, the solution turned yellow. After stirring for 5 minutes at room temperature, insoluble NaCl was removed by filtration and the yellow THF solution was layered with hexanes in a 1:1 ratio and allowed to sit for one day at  $-37^\circ\text{C}$ . After removal of the solvent and drying in vacuo, the product was obtained as a yellow crystalline solid (92 mg, 48% yield).  $^1\text{H}$  NMR ( $\text{C}_6\text{D}_6$ , 500.13 MHz):  $\delta$  8.51 (d,  $J = 7.6$  Hz, 4H,  $\text{CH}_{ortho}$ ), 7.25 (t,  $J = 7.5$  Hz, 4H,  $\text{CH}_{meta}$ ), 7.20 – 7.13 (m, 2H,  $\text{CH}_{para}$ ), 5.13 (hept,  $J = 6.9$  Hz, 2H,  $\text{CH}(\text{CH}_3)_2$ ), 1.33 (s, 6H, C(backbone)– $\text{CH}_3$ ), 1.06 (d,  $J = 7.1$  Hz, 12H,  $\text{CH}(\text{CH}_3)_2$ ).  $^{13}\text{C}$  NMR (201.19 MHz,  $\text{C}_6\text{D}_6$ )  $\delta$  203.58 (d,  $J = 81.7$  Hz), 152.03 (d,  $J = 49.6$  Hz), 151.04, 140.05, 130.15, 126.75, 123.45, 51.36, 21.37, 9.46.  $^{31}\text{P}\{^1\text{H}\}$  NMR (202.46 MHz,  $\text{C}_6\text{D}_6$ )  $\delta$  82.17 (s, 1P).

**Synthesis of Compound 5.5** To a 20 mL scintillation vial,  $(\text{NHC})\text{BiPh}_2\text{Cl}$  (505 mg, 869  $\mu\text{mol}$ ) was added and suspended in 10 mL dry THF.  $\text{Na}[\text{OCP}] \cdot 2.5\text{Dioxane}$  (262 mg, 869  $\mu\text{mol}$ ) was added to the suspension and the suspension was shaken vigorously for 1 minute. The reaction mixture was then extracted into a 100 mL Schlenk tube. Orange crystals of  $[(\text{NHC})_2\text{OCP}][\text{OCP}]$  formed from the solution after sitting undisturbed overnight at  $55^\circ\text{C}$  (106 mg, 51%).  $^1\text{H}$  NMR (500.13 MHz,  $\text{CD}_2\text{Cl}_2$ )  $\delta$  5.35 (br, 4.99, 2H,  $\text{CH}(\text{CH}_3)_2$ ) (hept,  $J = 7.0$  Hz, 2H,  $\text{CH}(\text{CH}_3)_2$ ), 2.38 (s, 6H, C(backbone)– $\text{CH}_3$ ), 2.35 (s, 6H, C(backbone)– $\text{CH}_3$ ), 1.62 (d,  $J = 7.1$  Hz, 12H,  $\text{CH}(\text{CH}_3)_2$ ), 1.58 (d,  $J = 7.1$  Hz, 12H,  $\text{CH}(\text{CH}_3)_2$ ).  $^{13}\text{C}$  NMR (201.19 MHz,  $\text{CD}_2\text{Cl}_2$ )  $\delta$  200.71 (d,  $J = 64.2$  Hz), 170.20 (d,  $J = 63.0$  Hz), 150.24 (d,  $J = 86.9$  Hz), 146.04 (d,  $J = 67.5$  Hz), 128.8, 126.5, 53.9, 52.5,

21.9, 21.8, 11.0, 10.7.  $^{31}\text{P}\{^1\text{H}\}$  NMR (242.94 MHz,  $\text{CD}_2\text{Cl}_2$ )  $\delta$  22.72 (br, 1P,  $[\text{OCP}]^+$ ), -395.09 (s, 1P,  $[\text{OCP}]^-$ ). Anal. Calcd for  $\text{C}_{24}\text{H}_{40}\text{N}_4\text{O}_2\text{P}_2$ : C, 60.24; H, 8.43; N, 11.71%. Found: C, 60.09; H, 8.52; N, 11.70%.

## **Appendix 2: Spectral Data**

## Chapter 2 Spectral Data

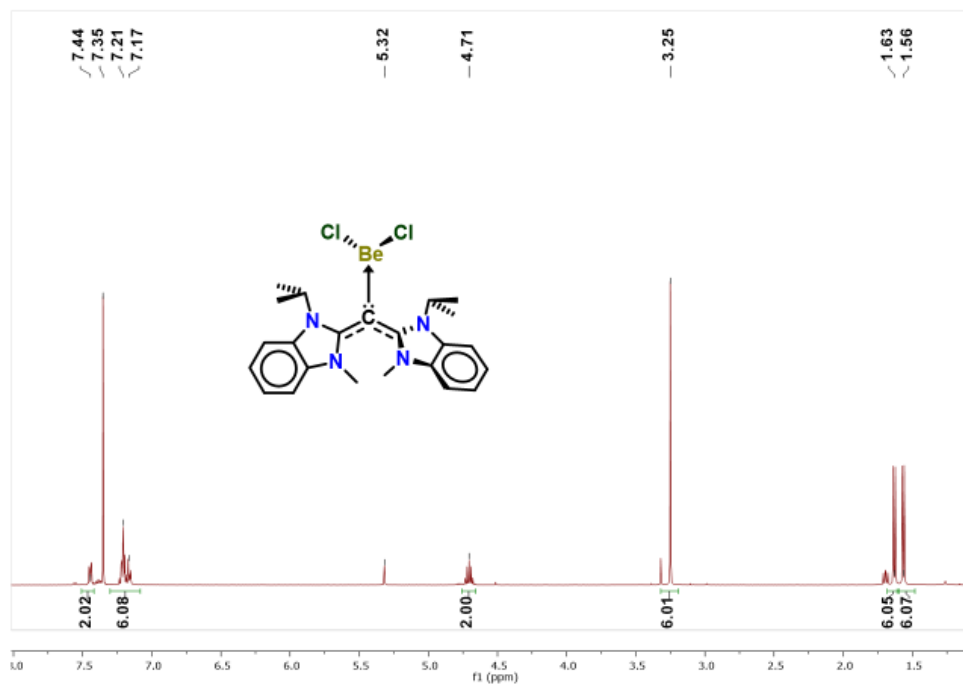


Figure A2S1. <sup>1</sup>H NMR of compound 2.5.

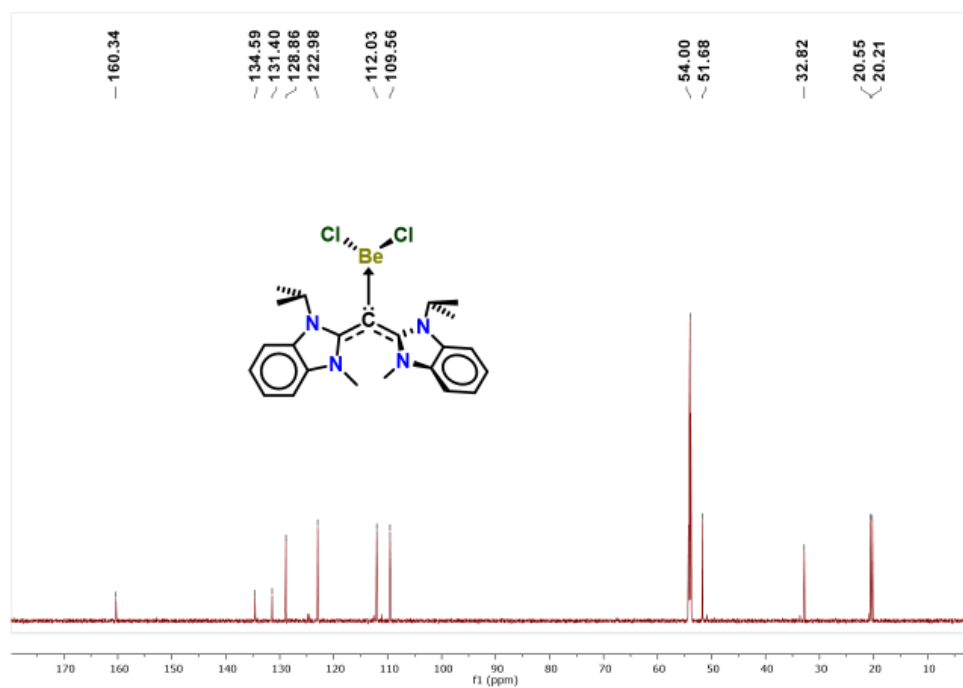


Figure A2S2. <sup>13</sup>C NMR of compound 2.5.

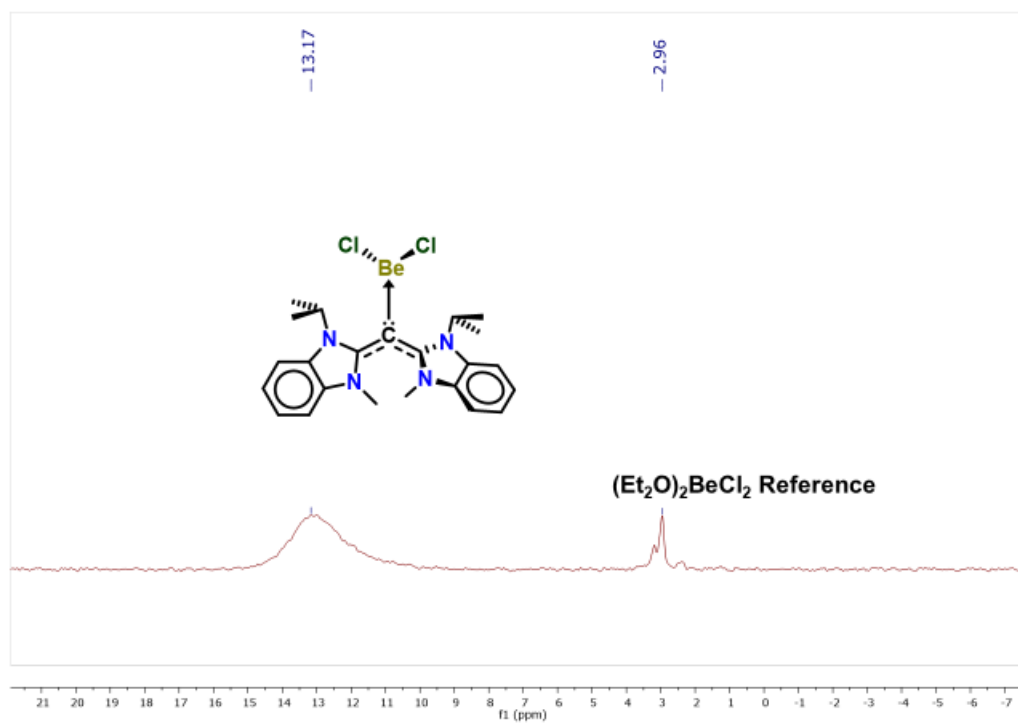


Figure A2S3.  $^9\text{Be}$  NMR of compound 2.5.

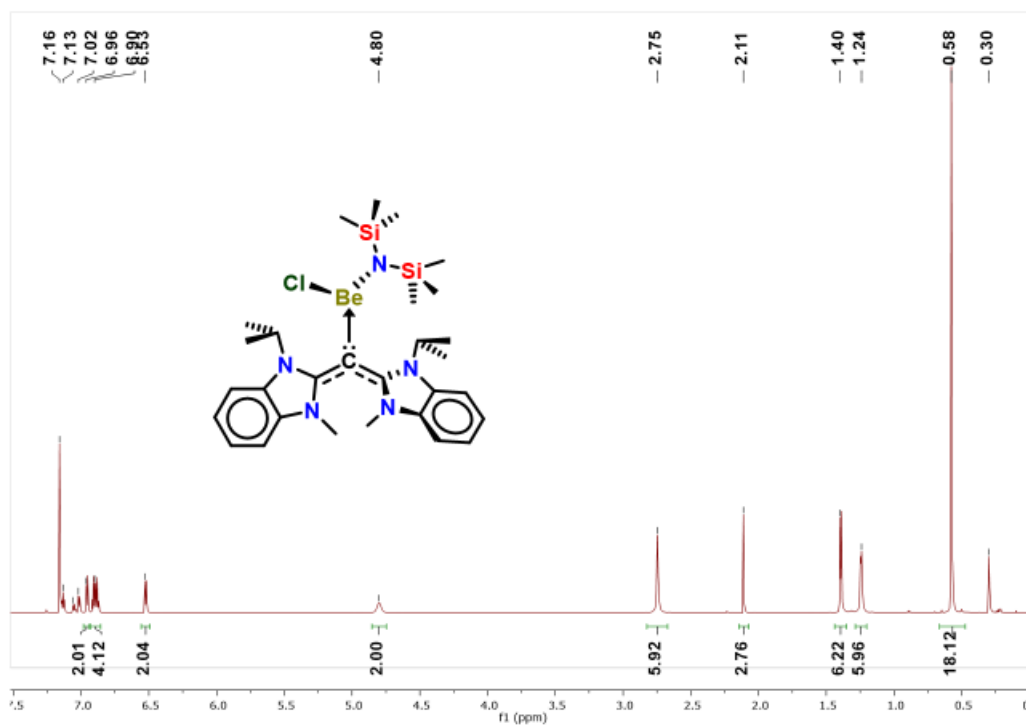


Figure A2S4.  $^1\text{H}$  NMR of compound 2.6.

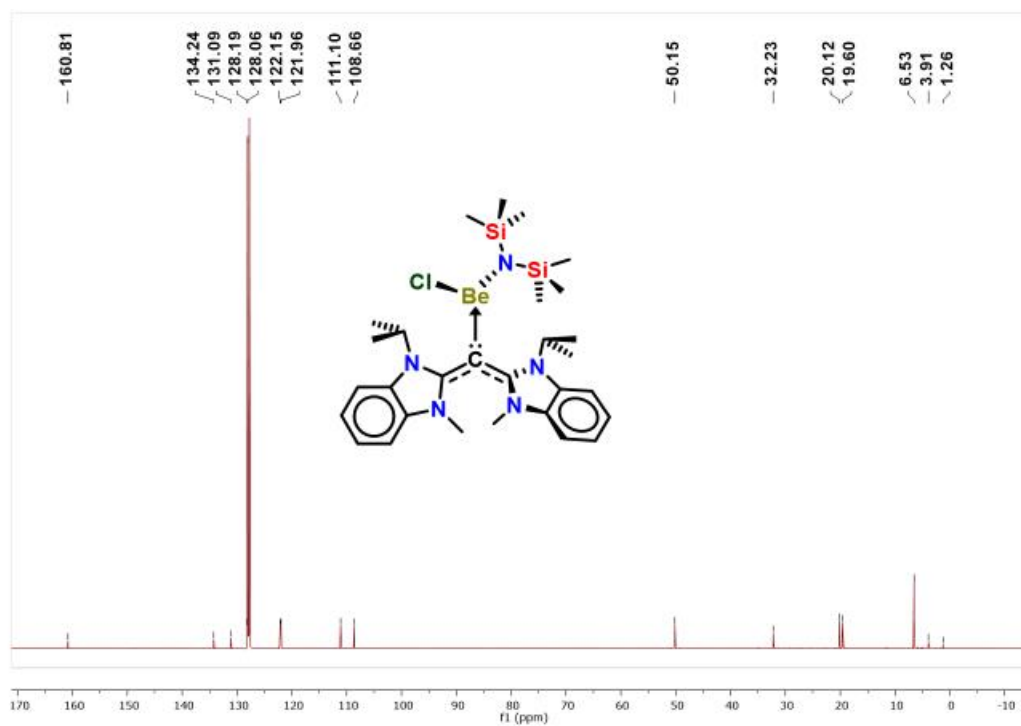


Figure A2S5.  $^{13}\text{C}$  NMR of compound 2.6.

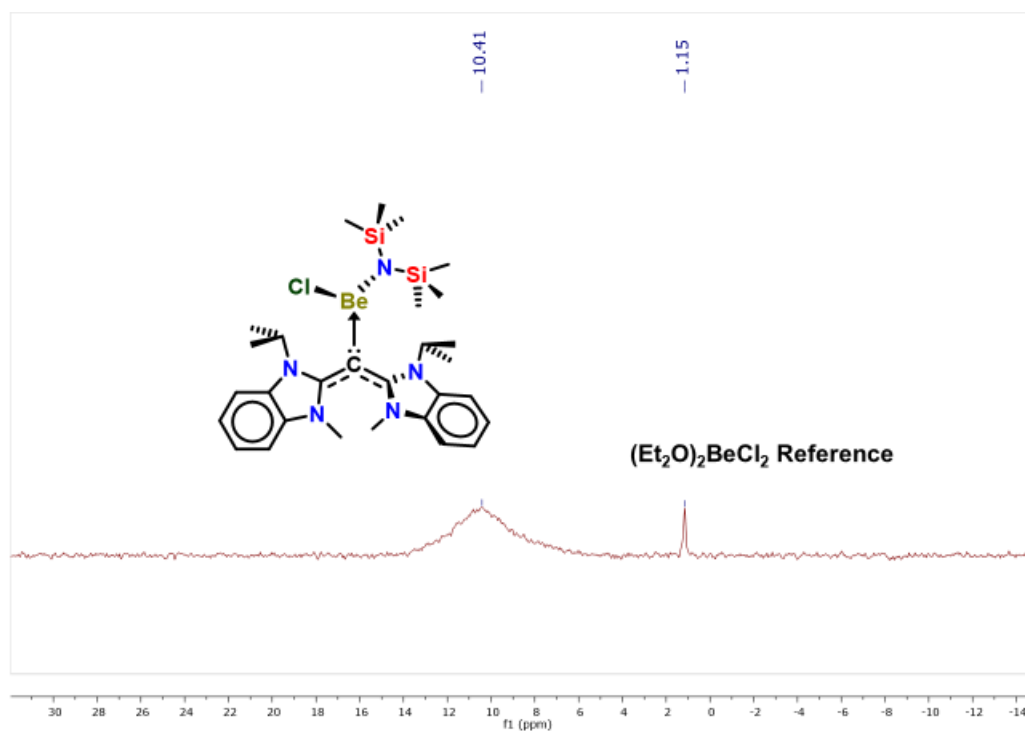


Figure A2S6.  $^9\text{Be}$  NMR of compound 2.6.

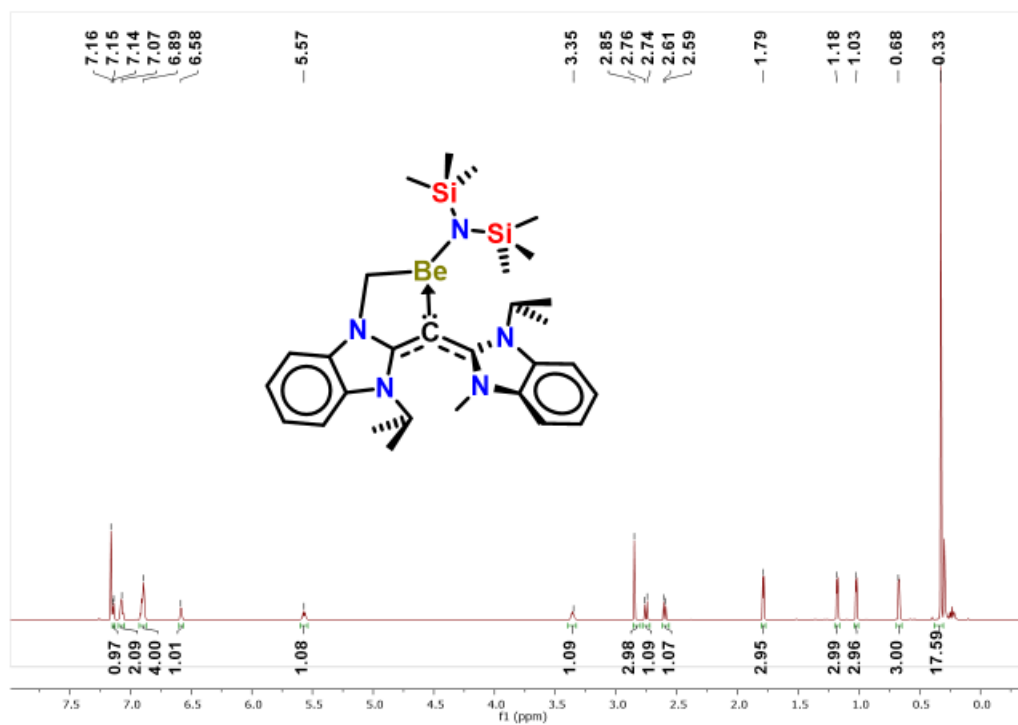


Figure A2S7.  $^1\text{H}$  NMR of compound 2.9.

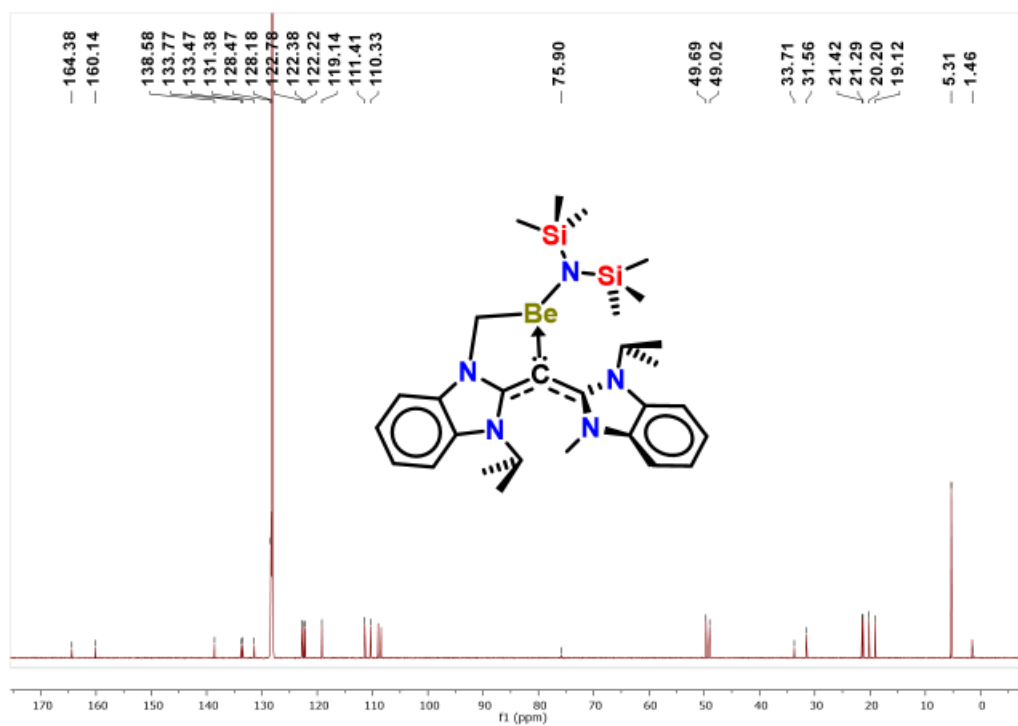
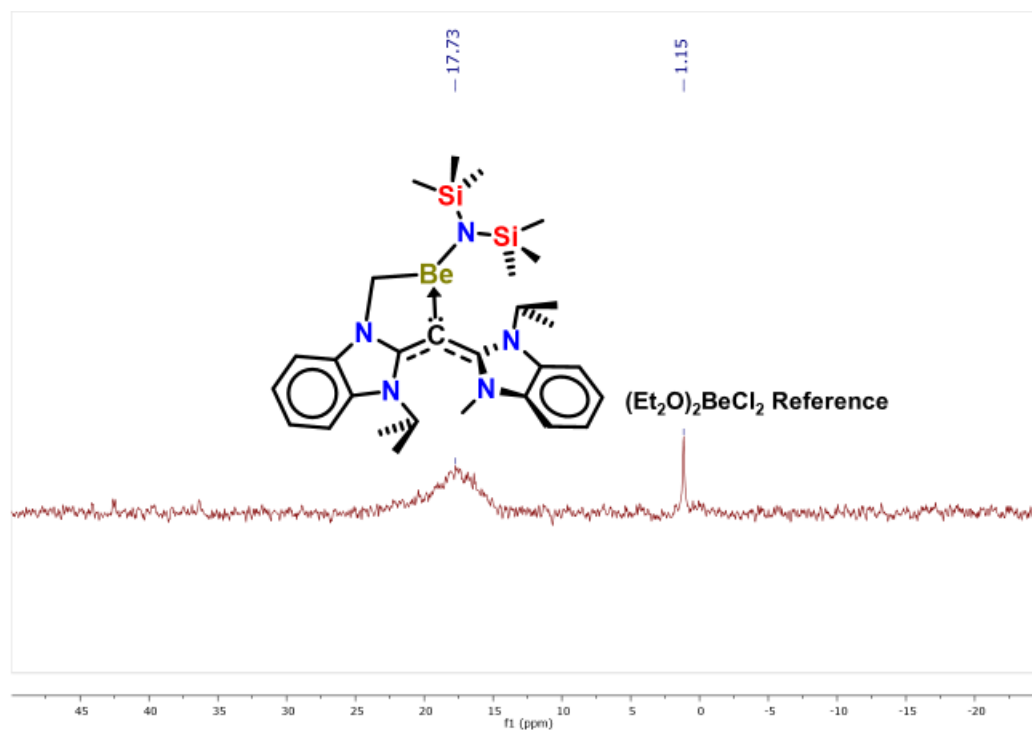
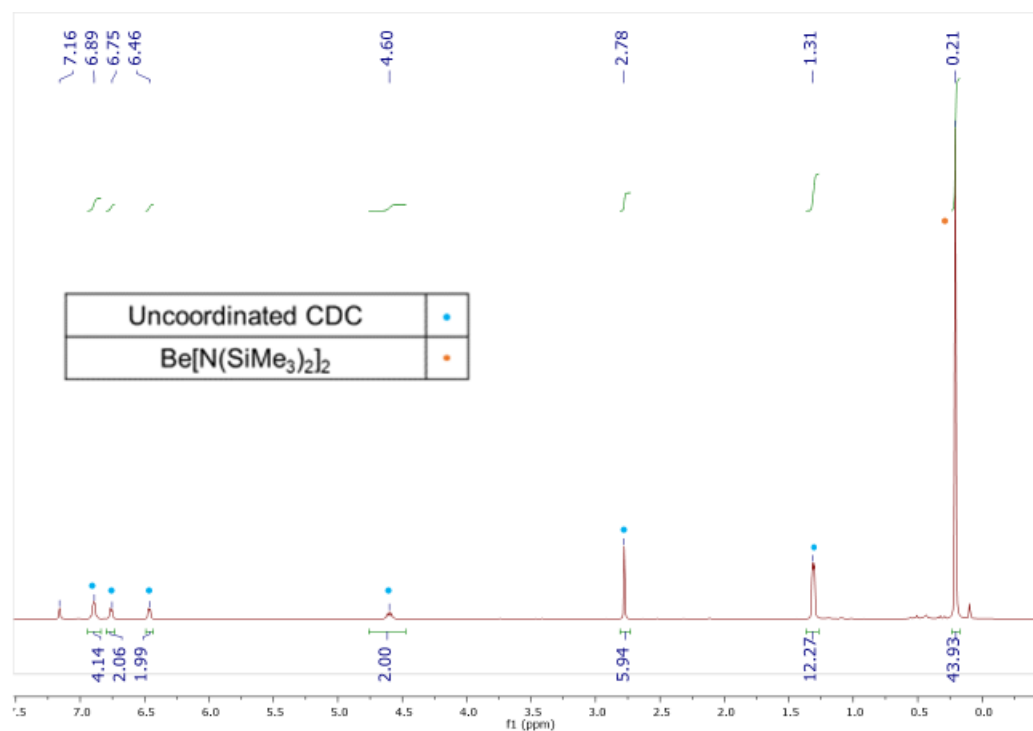


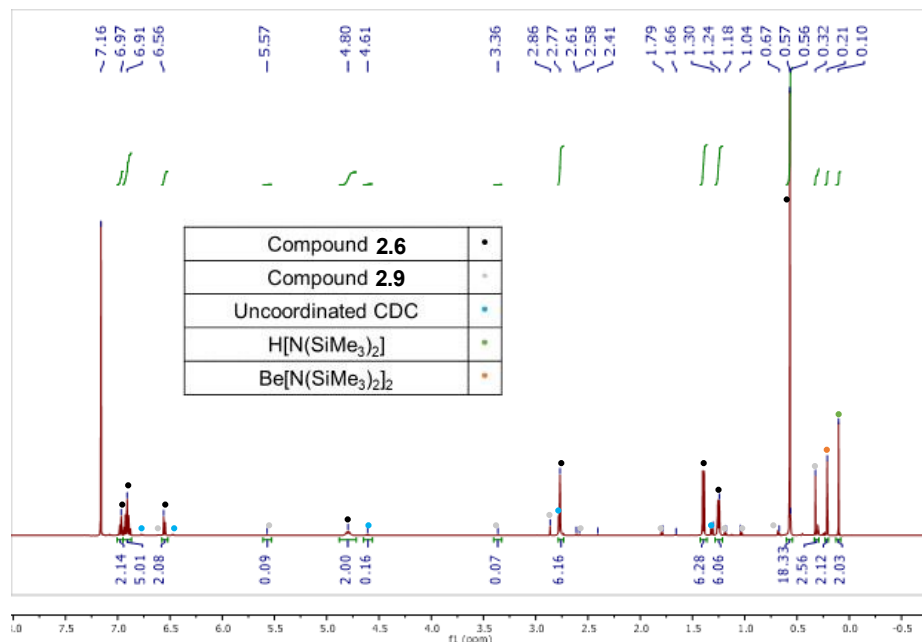
Figure A2S8.  $^{13}\text{C}$  NMR of compound 2.9.



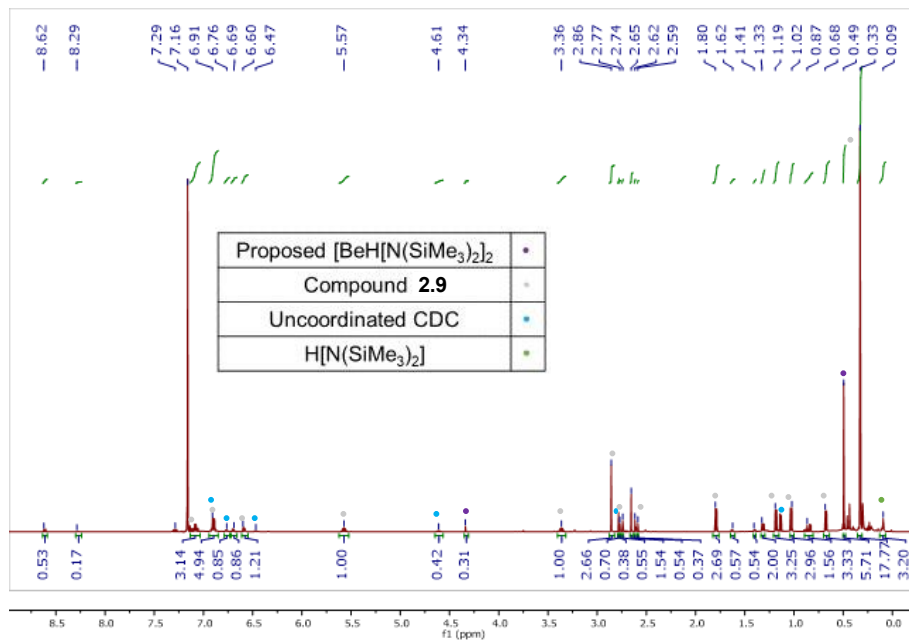
**Figure A2S9.**  $^9\text{Be}$  NMR of compound **2.9**.



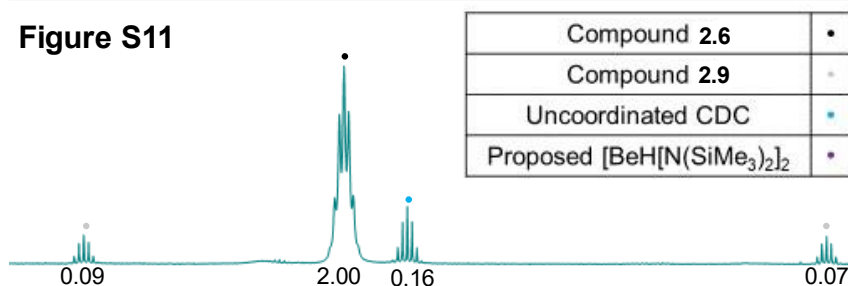
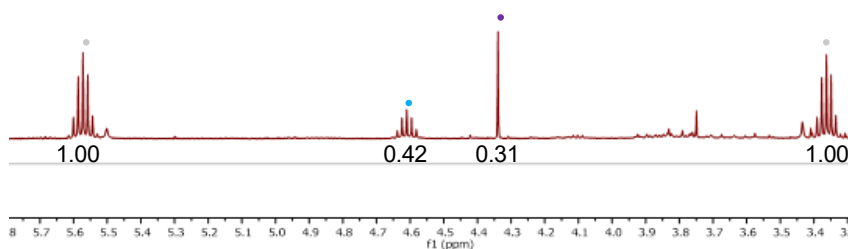
**Figure A2S10.** Reaction of CDC with  $\text{Be}[\text{N}(\text{SiMe}_3)_2]_2$ . In the reaction of **2.6** with  $\text{K}[\text{N}(\text{SiMe}_3)_2]$ ,  $\text{Be}[\text{N}(\text{SiMe}_3)_2]_2$  is a side product. Therefore, we synthesized  $\text{Be}[\text{N}(\text{SiMe}_3)_2]_2$  independently and confirmed that it does not react with CDC, there was no reaction even at elevated temperatures.



**Figure A2S11.** Reaction of compound **2.5** with 1.1 equivalents of  $\text{K}[\text{N}(\text{SiMe}_3)_2]$ . 1.1 equivalents of  $\text{K}[\text{N}(\text{SiMe}_3)_2]$  was added to compound **2.5**. This generated approximately 8% of compound **2.9** with respect to compound **2.6** (major product). The uncoordinated CDC was approximately 8%.



**Figure A2S12.** Reaction from Figure A2S11 with 1 equivalent of  $\text{KC}_8$ . The reaction mixture from **Figure A2S11** was combined with  $\text{KC}_8$  and stirred overnight. The ratio of metallocycle to free CDC increased.

**Figure S11****Figure S12**

**Figure A2S13.** Stacked spectra, comparison of the methine region from **Figure A2S11** and **A2S12**. With the reaction from **Figure A2S11**, we added a slight excess (1.1 eq) of  $\text{K}[\text{N}(\text{SiMe}_3)_2]$ , which partially converted to compound **2.9**. We then want to see if  $\text{KC}_8$  could make the same compound (Reaction 3). Relative to free ligand, compound **2.9** increased substantially in the reaction from **Figure A2S12**, confirming that  $\text{KC}_8$  results in the formation of the same compounds.

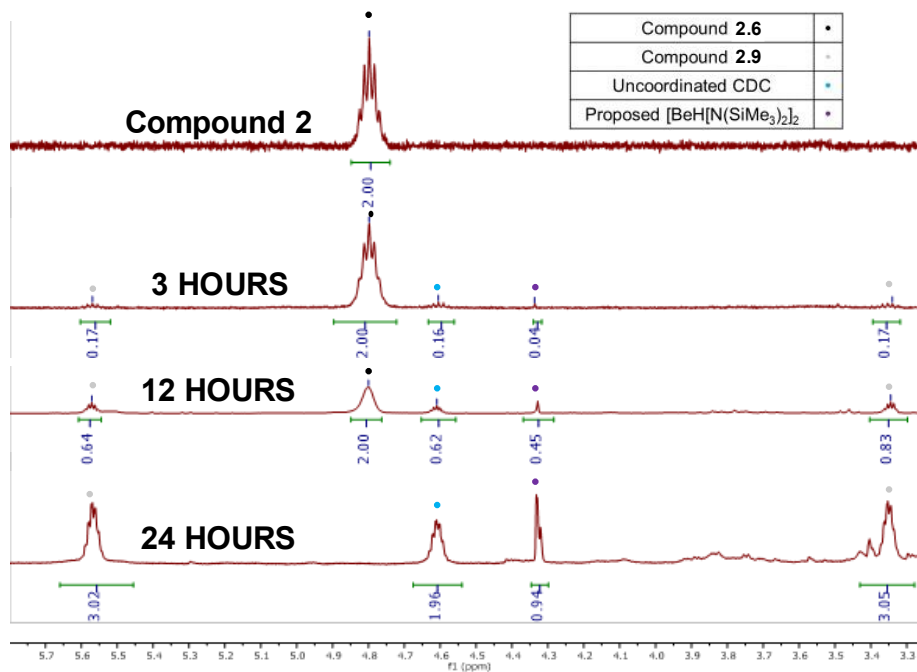


**Figure A2S14.** Reaction of pure compound **2.6** reaction with 1 equivalent of  $\text{KC}_8$  at different time intervals.

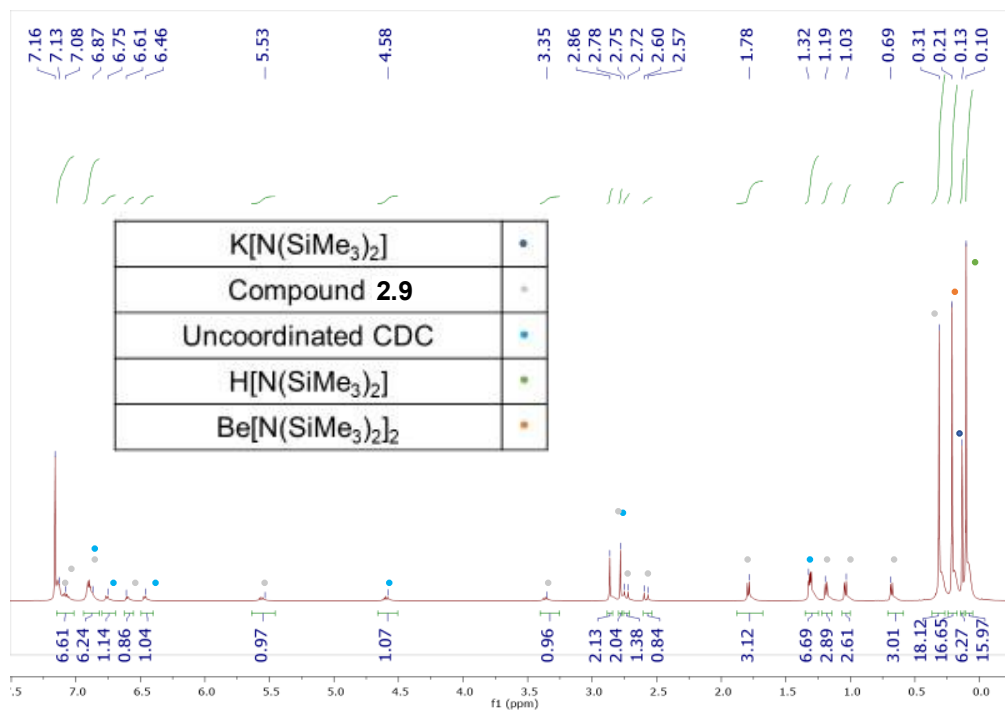


**Figure A2S15.** Reaction of compound **2.6** with 1 equivalents of K[N(SiMe<sub>3</sub>)<sub>2</sub>]. The reaction of **2.6** with 1 equivalent of K[N(SiMe<sub>3</sub>)<sub>2</sub>] shows a smaller ratio of **2.9** to free CDC (2:1) than with the reaction of **2.6** with KC<sub>8</sub> (3:1). The crystal structure for **2.9** was obtained from a similar reaction mixture with toluene as the solvent. Therefore, **2.9** co-crystallized as a 1:1 mixture with a toluene adduct of K[N(SiMe<sub>3</sub>)<sub>2</sub>].

## IR Spectra (Compounds 2.5, 2.6, and 2.9)

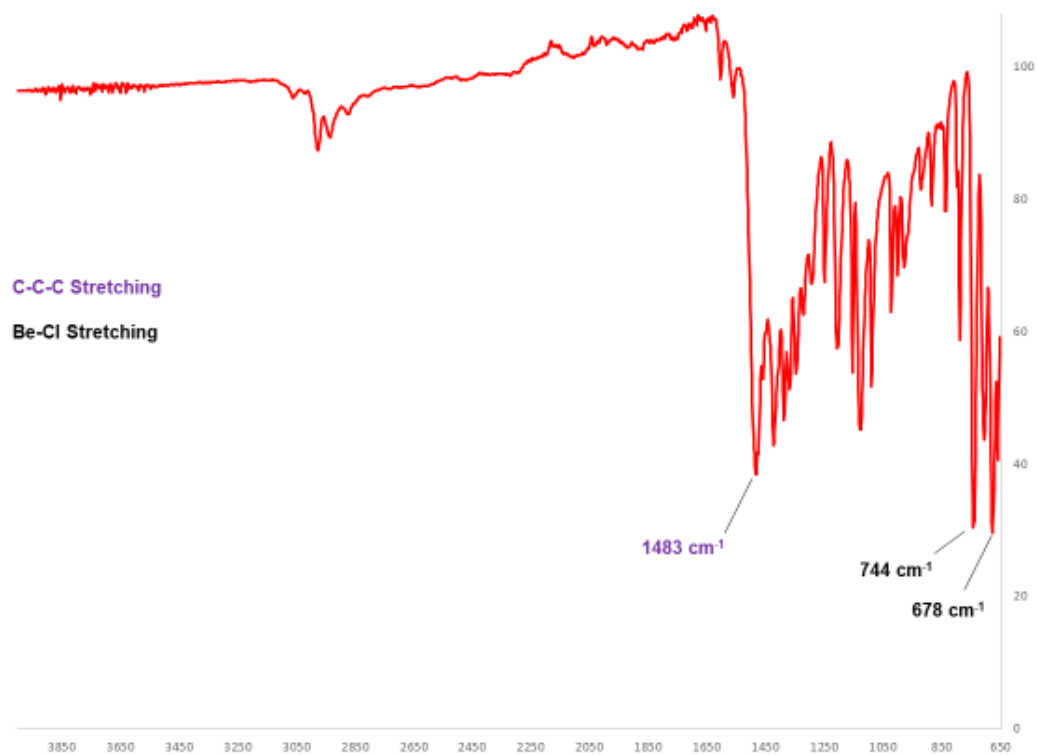


**Figure A2S16.** IR spectra of (CDC)BeCl<sub>2</sub> (Compound 2.5).

**Table A2S1:** Computed B3LYP-D3(BJ)/def2-TZVP vibrational frequencies of (CDC)BeCl<sub>2</sub>.

Scaled Freq	Intensity	Vib.
17.142	198.572	Cl-Be-Cl Rock
119.044	135.798	Cl-Be-Cl Scissoring
259.009	44.623	Cl-Be-Cl Scissoring
360.747	8.411	Cl-Be-Cl Wag

414.980	116.761	Cl-Be-Cl Wag
423.330	58.261	Cl-Be-Cl Wag
517.331	111.678	Cl-Be-Cl Symm. Stretch
653.308	227.178	Cl-Be-Cl Symm. Stretch
720.740	165.501	Cl-Be-Cl Symm. Stretch
653.308	227.178	Cl-Be-Cl Symm. Stretch
720.740	165.501	Cl-Be-Cl Symm. Stretch
1480.226	401.498	C-C-C Symm. Stretch
1507.253	6186.954	C-C-C Asymm. Stretch

---

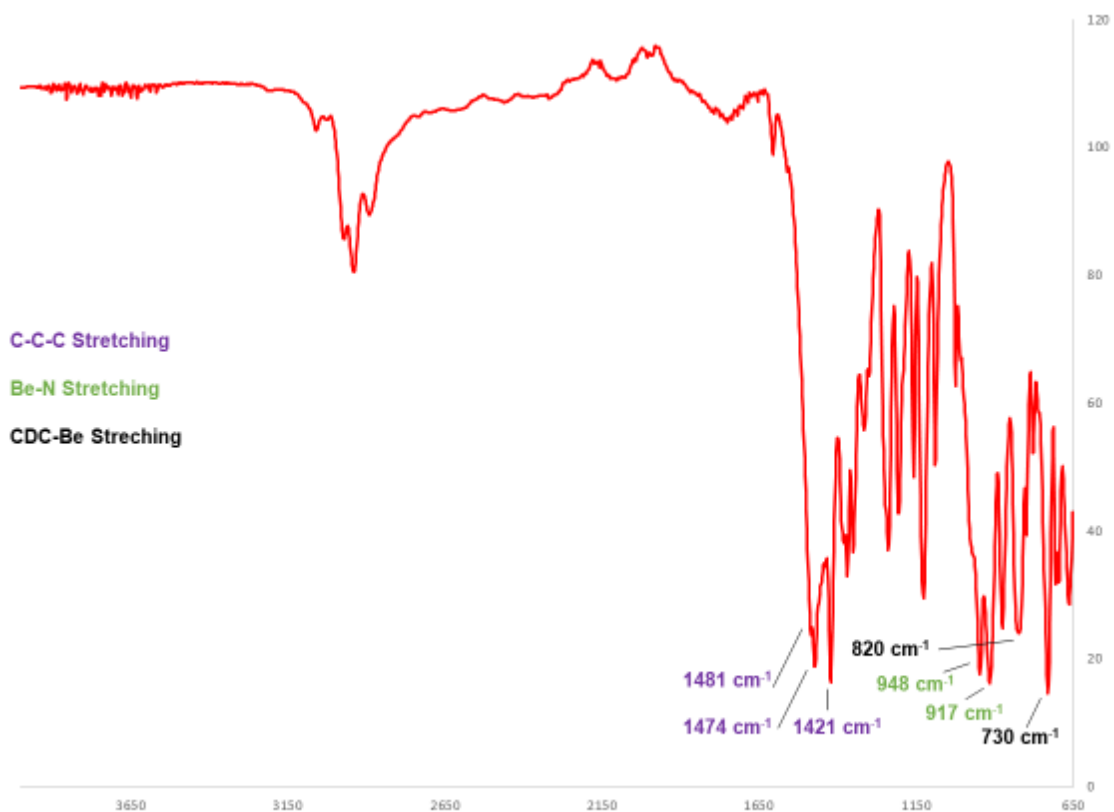


**Figure A2S17.** IR spectra of (CDC)BeCl[N(SiMe<sub>3</sub>)<sub>2</sub>] (Compound **2.6**).

**Table A2S2:** Computed B3LYP-D3(BJ)/def2-TZVP vibrational frequencies of (CDC)BeCl[N(SiMe<sub>3</sub>)<sub>2</sub>].

Scaled Freq	Intensity	Vib.
336.452	95.634	Si-N-Si Scissoring
357.526	47.096	Si-N-Si Scissoring
447.280	13.560	CDC-Be Wag
452.749	22.654	CDC-Be Wag

476.508	270.573	CDC-Be Wag
509.633	37.481	CDC-Be Symm. Stretch
525.891	15.104	CDC-Be Symm. Stretch
566.745	87.099	CDC-Be Asymm. Stretch
570.847	72.355	CDC-Be Asymm. Stretch
635.501	199.827	CDC-Be Symm. Stretch
684.955	43.350	CDC-Be Symm. Stretch
767.718	53.978	CDC-Be Symm. Stretch
906.936	1104.208	N-Be Asymm. Stretch
939.083	1261.513	N-Be Asymm. Stretch
996.322	1830.127	N-Be Asymm. Stretch
1365.075	388.692	C-C-C Symm. Stretch
1479.911	619.670	C-C-C Symm. Stretch
1509.380	5469.159	C-C-C Asymm. Stretch

---

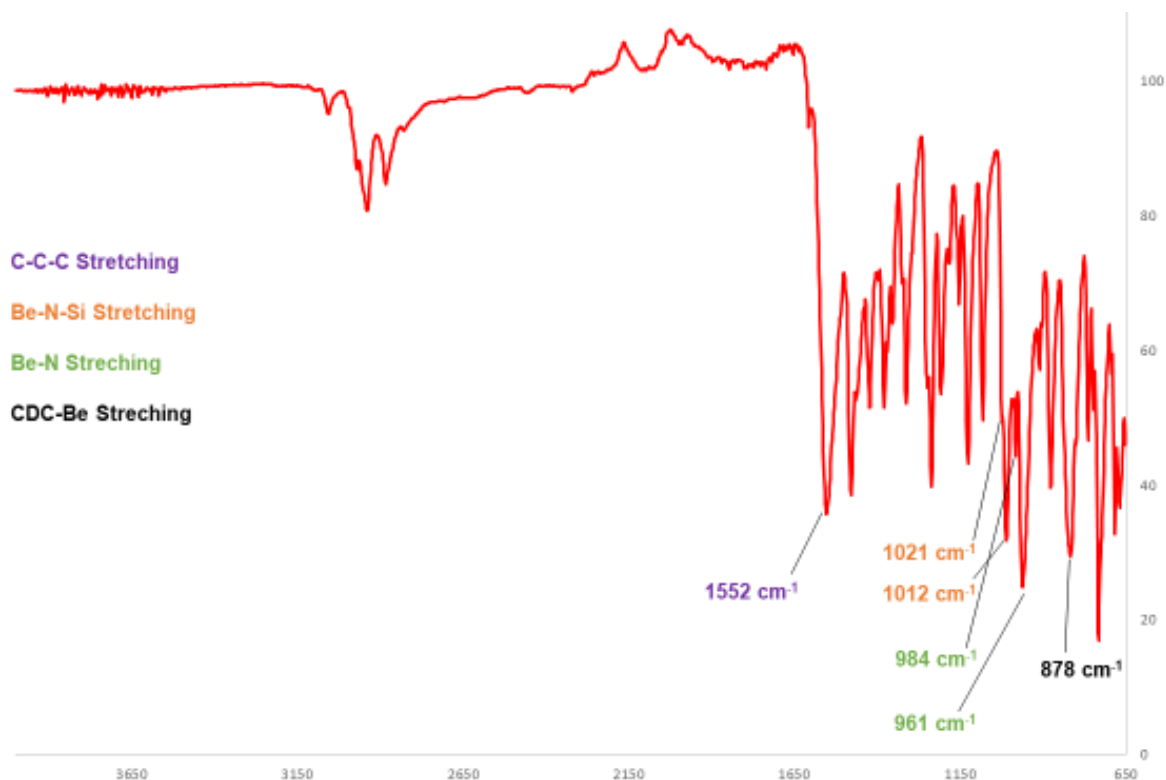


**Figure A2S18.** IR spectra of (CDC)Be[N(SiMe<sub>3</sub>)<sub>2</sub>] (Compound **2.9**).

**Table A2S3:** Computed B3LYP-D3(BJ)/def2-TZVP vibrational frequencies of (CDC)Be[N(SiMe<sub>3</sub>)<sub>2</sub>].

Scaled Freq	Intensity	Vib.
342.226	7.204	Si-N-Si Symm. Stretch
352.362	37.572	Si-N-Si Scissoring
497.421	17.125	CDC-Be Wag
544.246	46.720	CDC-Be Wag
577.181	15.376	CDC-Be Wag

586.575	25.151	CH <sup>2</sup> -Be-C Twist
593.636	35.019	CH <sup>2</sup> -Be-C Symm. Stretch
646.027	66.287	CH <sup>2</sup> -Be-C Asymm. Stretch
664.223	71.288	C-Be-N Scissoring
685.161	27.049	C-Be-N Scissoring
709.169	232.907	CH <sup>2</sup> -Be-N Scissoring
756.578	243.886	CH <sup>2</sup> -Be-CDC Asymm. Stretch
900.849	68.548	Be-CDC Stretch
968.822	715.072	Be-N Stretch
972.870	218.745	Be-N Stretch
978.599	1491.082	Be-N-Si Symm. Stretch
993.115	1254.196	Be-N-Si Symm. Stretch
1363.470	355.180	C-C-C Symm. Stretch
1559.873	5685.994	C-C-C Asymm. Stretch

---

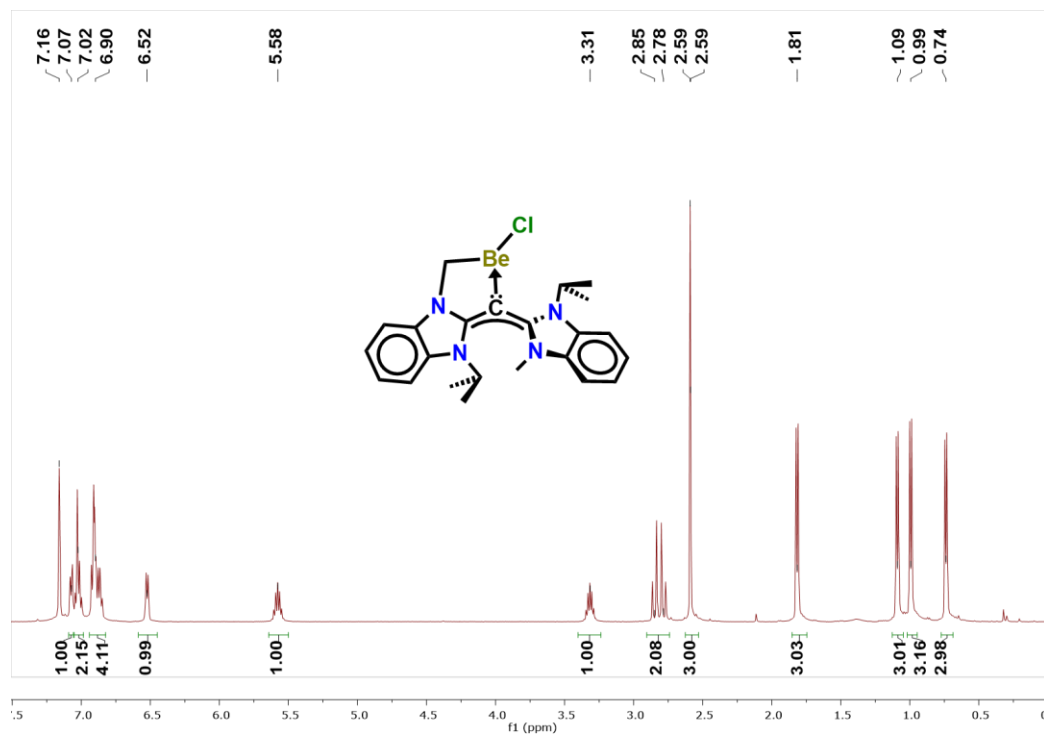


**Figure A2S19.**  $^1\text{H}$  NMR spectrum (500.13 MHz,  $\text{C}_6\text{D}_6$ , 298 K) of compound **2.10**.

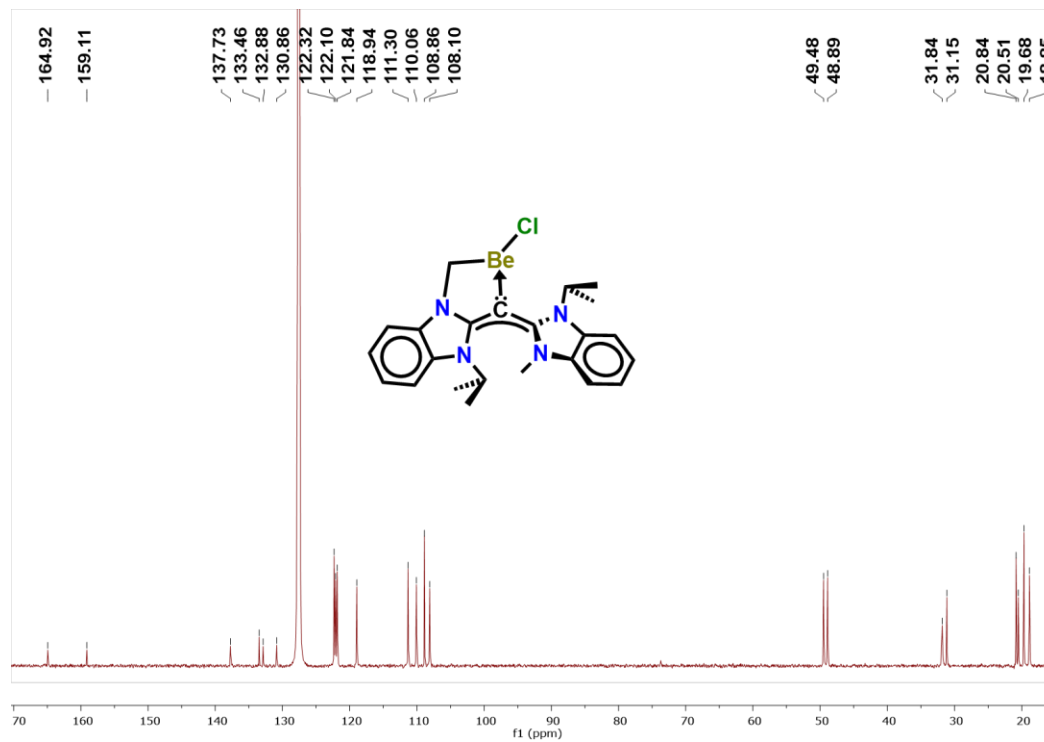


**Figure A2S20.**  $^{13}\text{C}\{^1\text{H}\}$  NMR (150.9 MHz,  $\text{C}_6\text{D}_6$ , 298 K) of compound **2.10**.

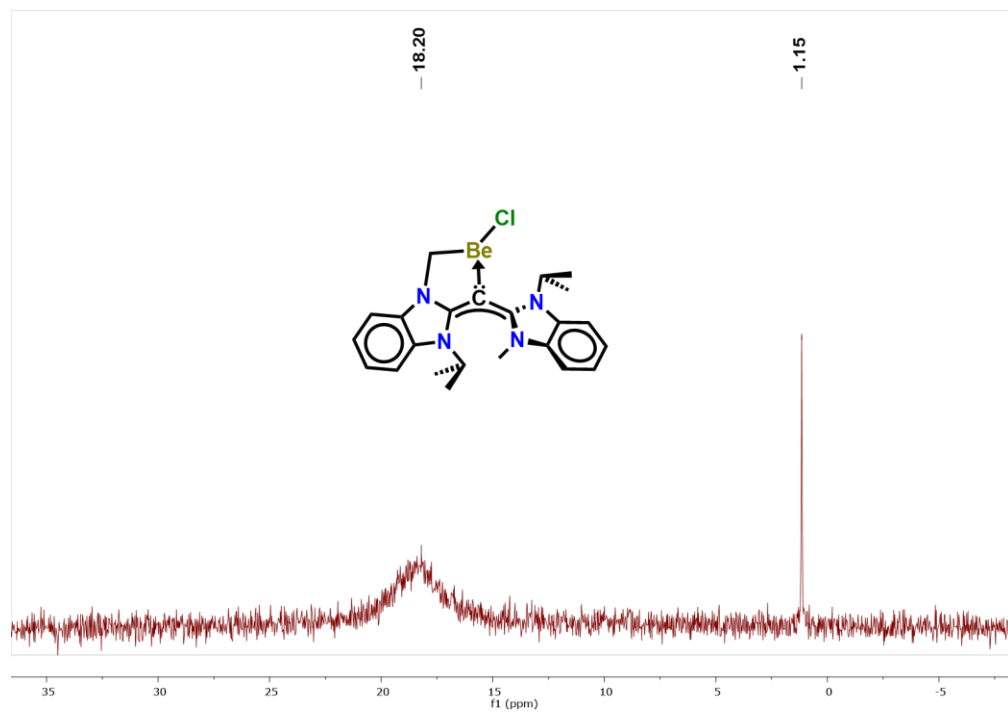


**Figure A2S21.**  $^9\text{Be}\{^1\text{H}\}$  NMR (84.28 MHz,  $\text{C}_6\text{D}_6$ , 298 K) of compound **2.10**.

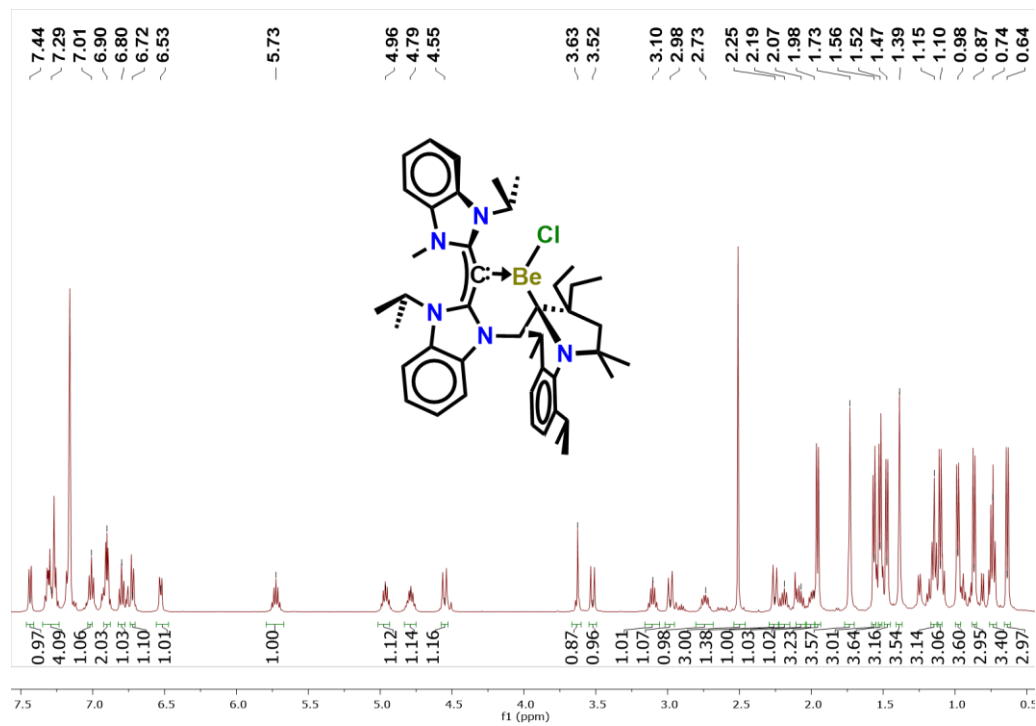


**Figure A2S22.**  $^1\text{H}$  NMR spectrum (500.13 MHz,  $\text{C}_6\text{D}_6$ , 298 K) of compound **2.11**.

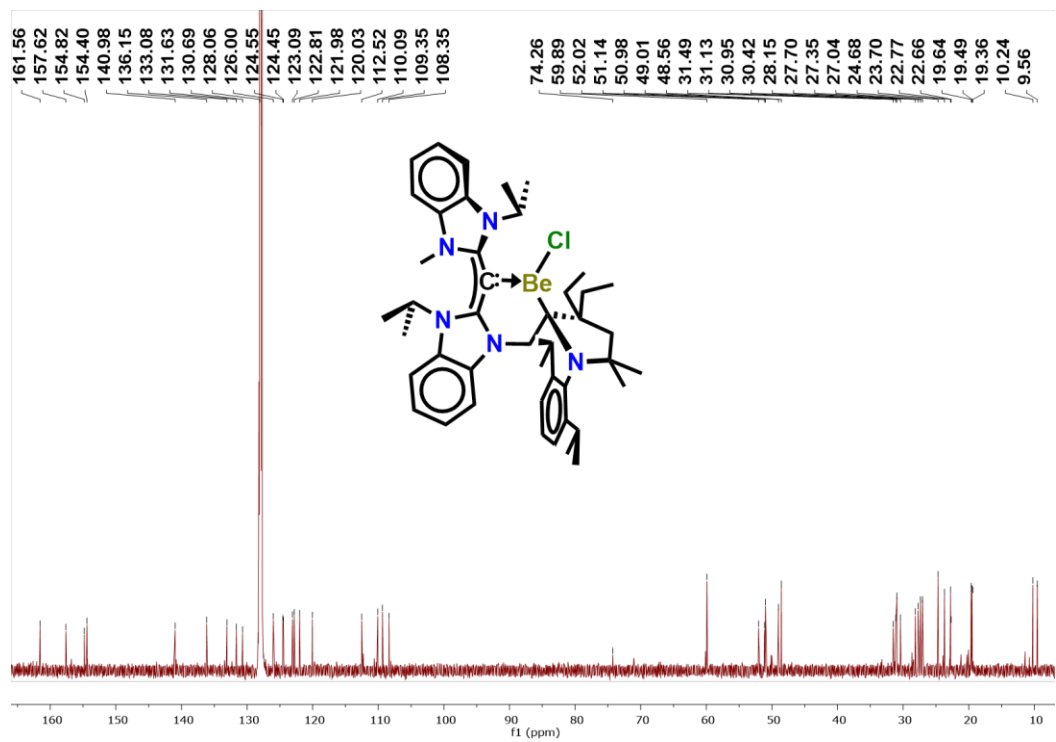


**Figure A2S23.**  $^{13}\text{C}\{^1\text{H}\}$  NMR (150.9 MHz,  $\text{C}_6\text{D}_6$ , 298 K) of compound 2.11.

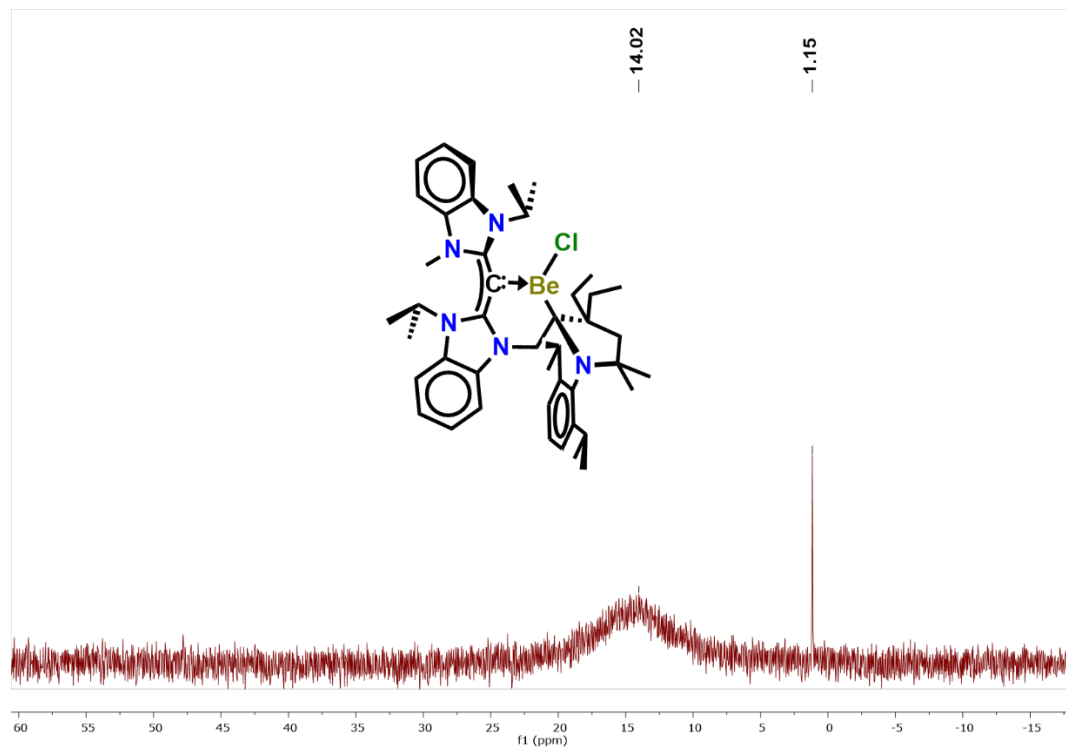


**Figure A2S24.**  $^9\text{Be}\{^1\text{H}\}$  NMR (84.28 MHz,  $\text{C}_6\text{D}_6$ , 298 K) of compound 2.11.

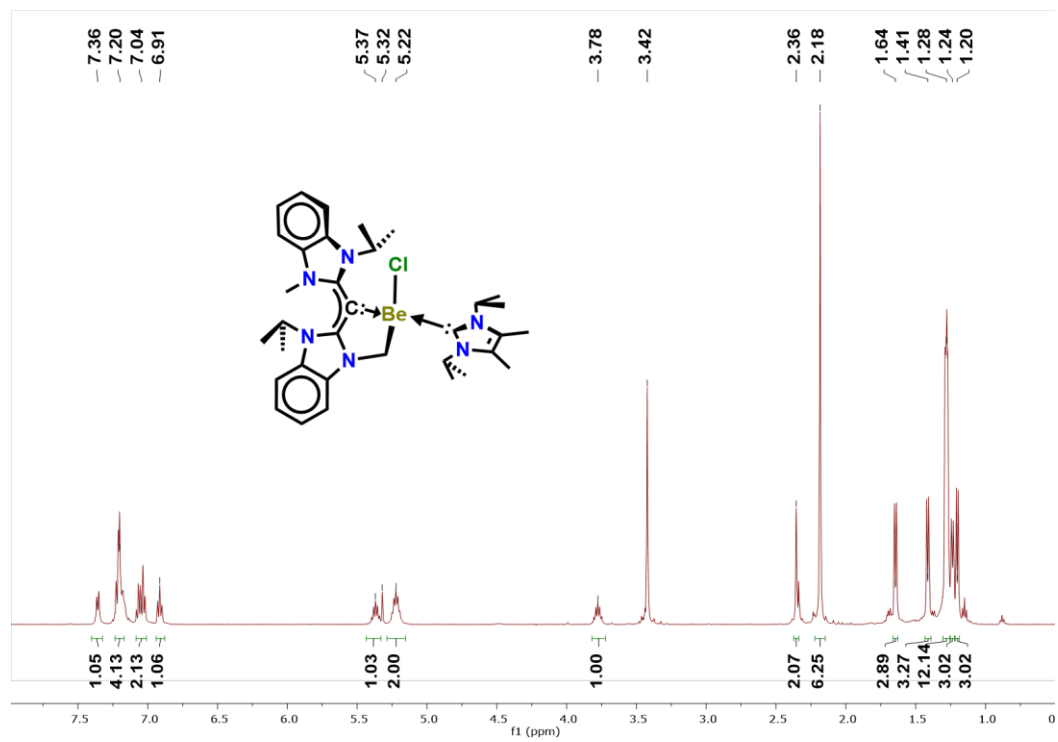


Figure A2S25.  $^1\text{H}$  NMR spectrum (500.13 MHz,  $\text{CD}_2\text{Cl}_2$ , 298 K) of compound 2.12.

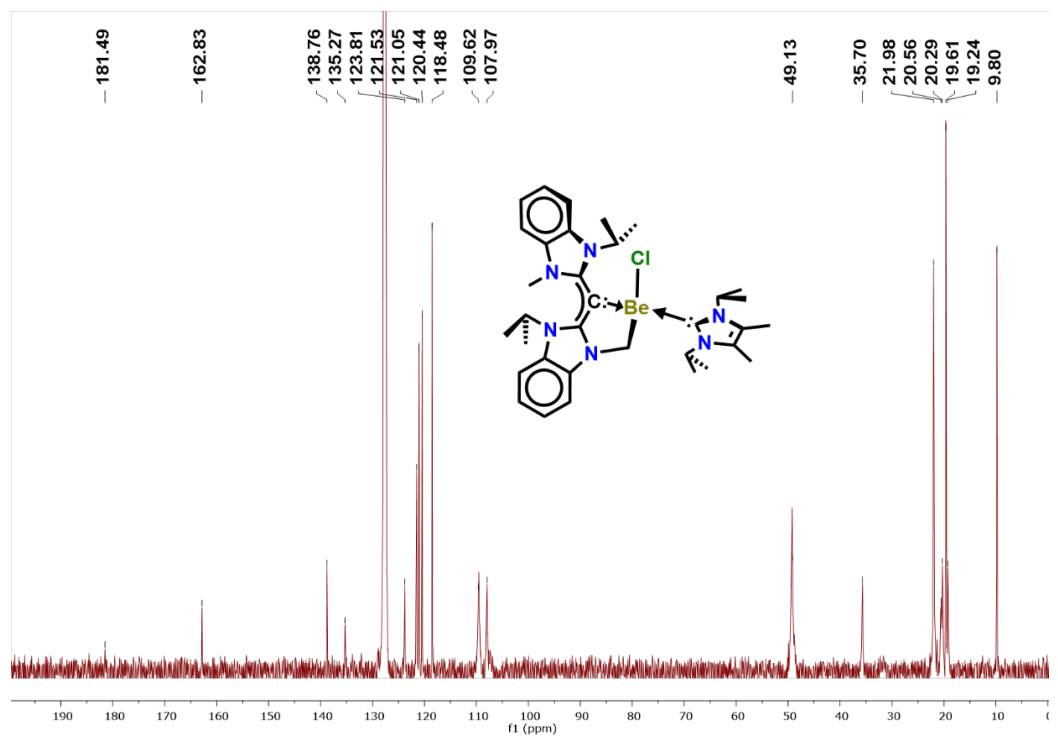
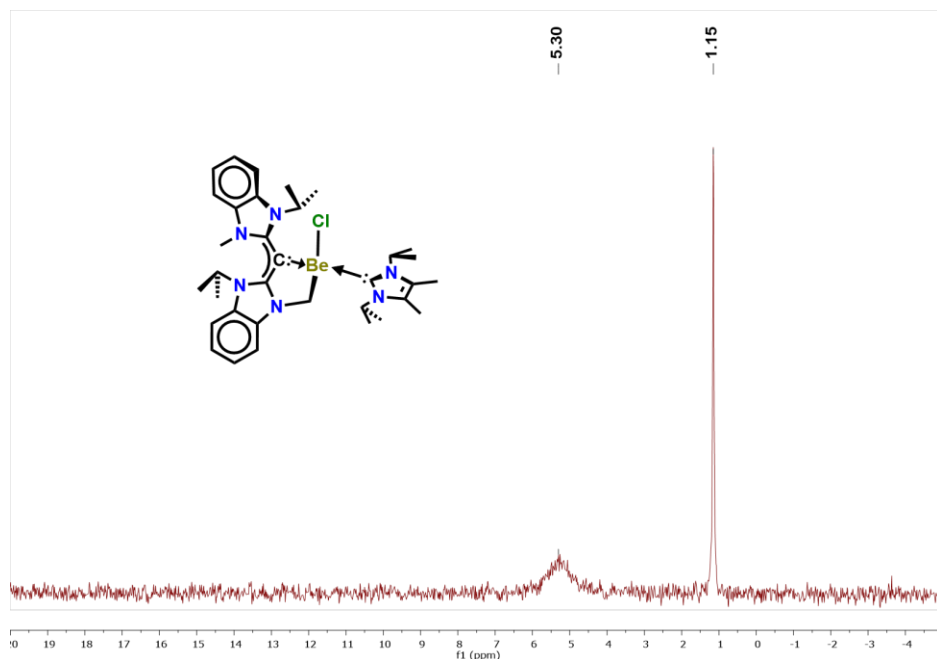
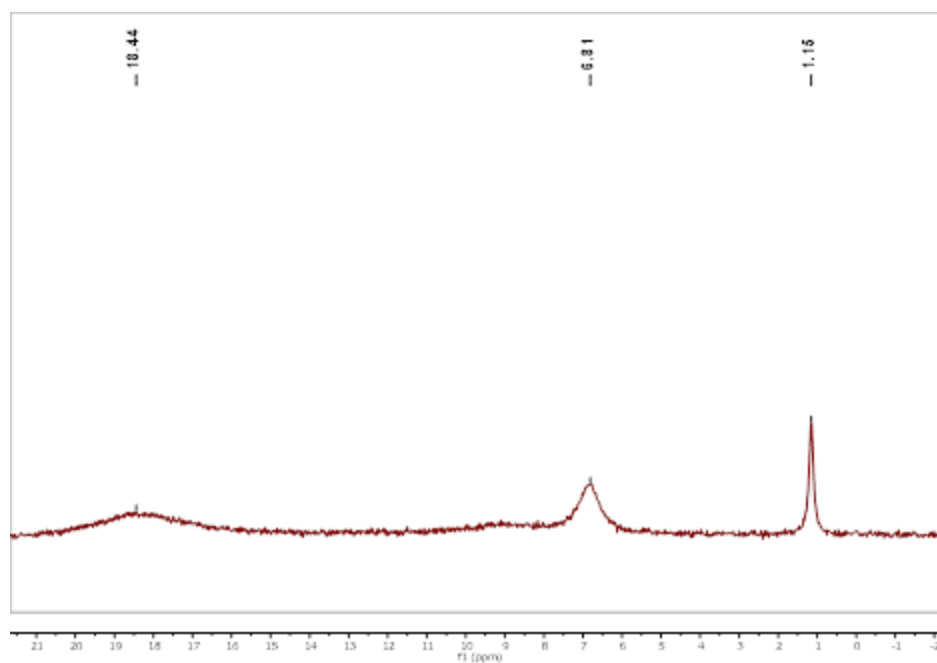


Figure A2S26.  $^{13}\text{C}\{^1\text{H}\}$  NMR (150.9 MHz,  $\text{C}_6\text{D}_6$ , 298 K) of compound 2.12.



**Figure A2S27.**  $^9\text{Be}\{^1\text{H}\}$  NMR (84.28 MHz,  $\text{C}_6\text{D}_6$ , 298 K) of compound **2.12**.



**Figure A2S28.**  $^9\text{Be}\{^1\text{H}\}$  NMR (84.28 MHz,  $\text{C}_6\text{D}_6$ , 298 K) of compound **2.9** +  $(\text{Et}_2\text{O})_2\text{BeCl}_2$  reaction mixture. The shift  $\delta$  6.81 is in agreement with  $(\text{Cl})\text{Be}[\text{N}(\text{SiMe}_3)_2]$ .<sup>1</sup> The broad shift at  $\delta$  18.44 is a mixture of **2.9** and **2.10**.

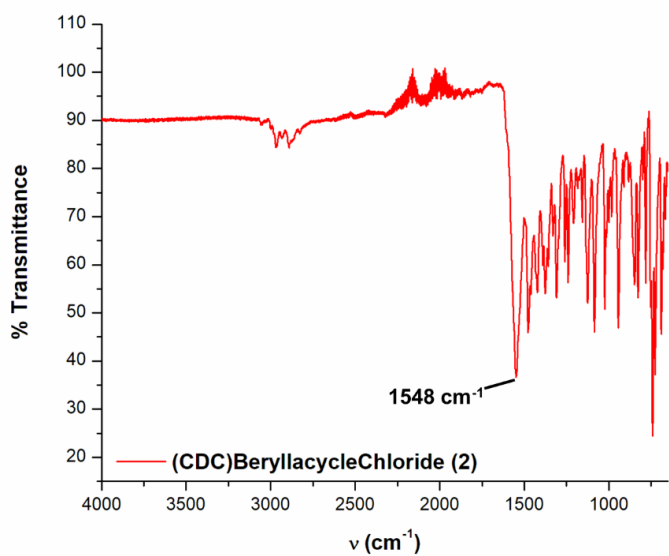


**Figure A2S29.** FTIR spectrum of compound **2.10**

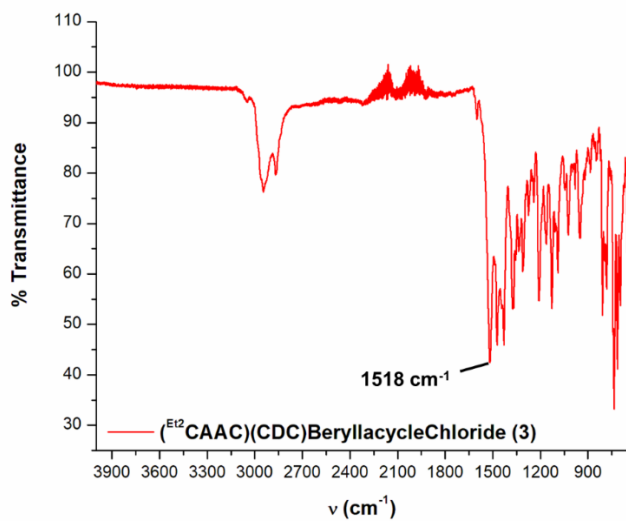


**Figure A2S30.** FTIR spectrum of compound **2.11**

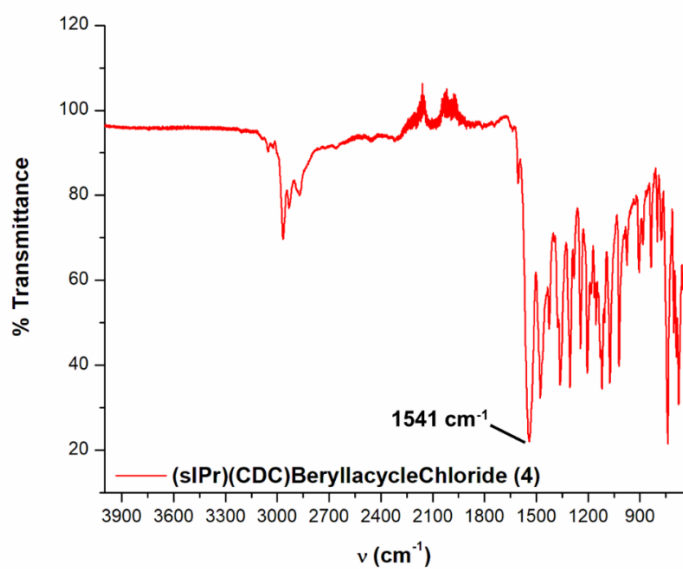


**Figure A2S31.** FTIR spectrum of compound **2.12**

## Chapter 3 Spectral Data

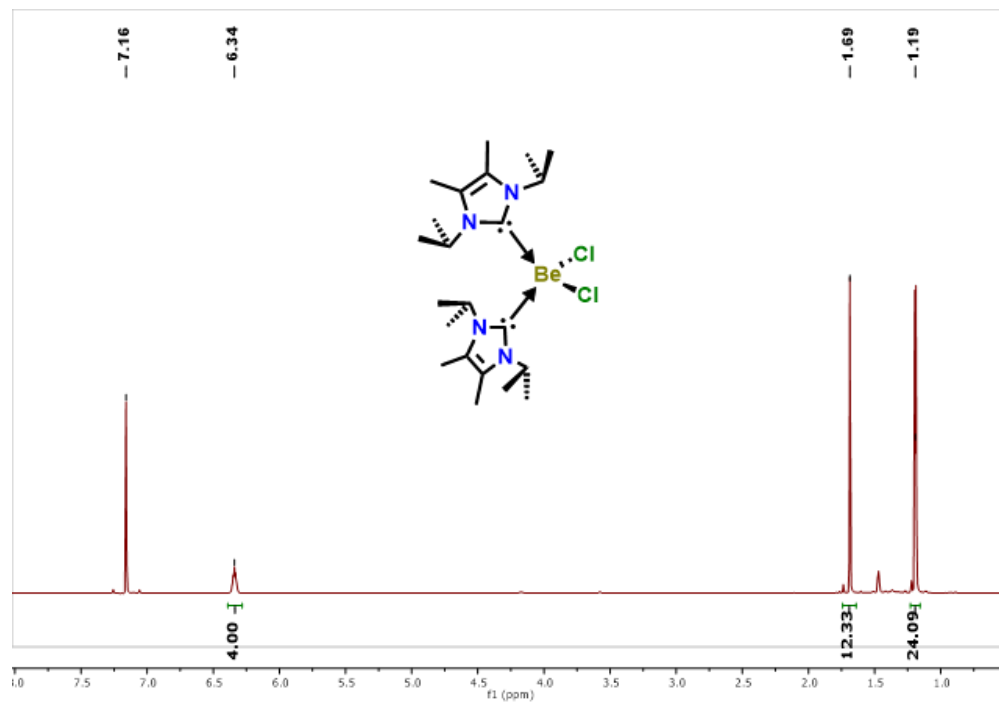


Figure A2S32.  $^1\text{H}$  NMR spectrum (800.13 MHz,  $\text{C}_6\text{D}_6$ , 298 K) of compound 3.19.

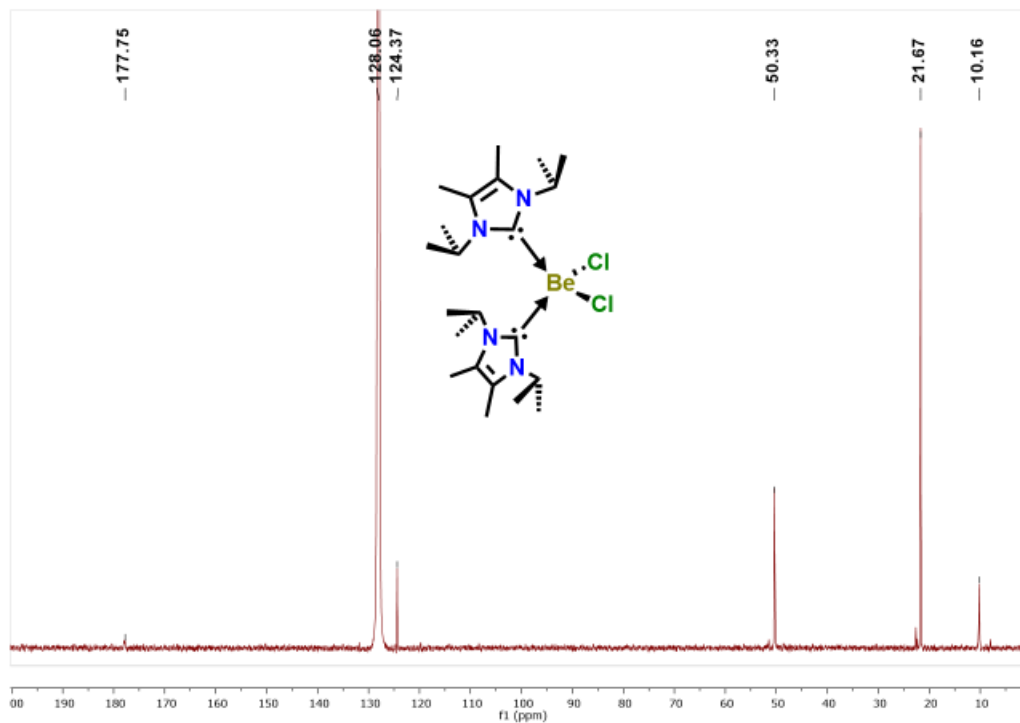
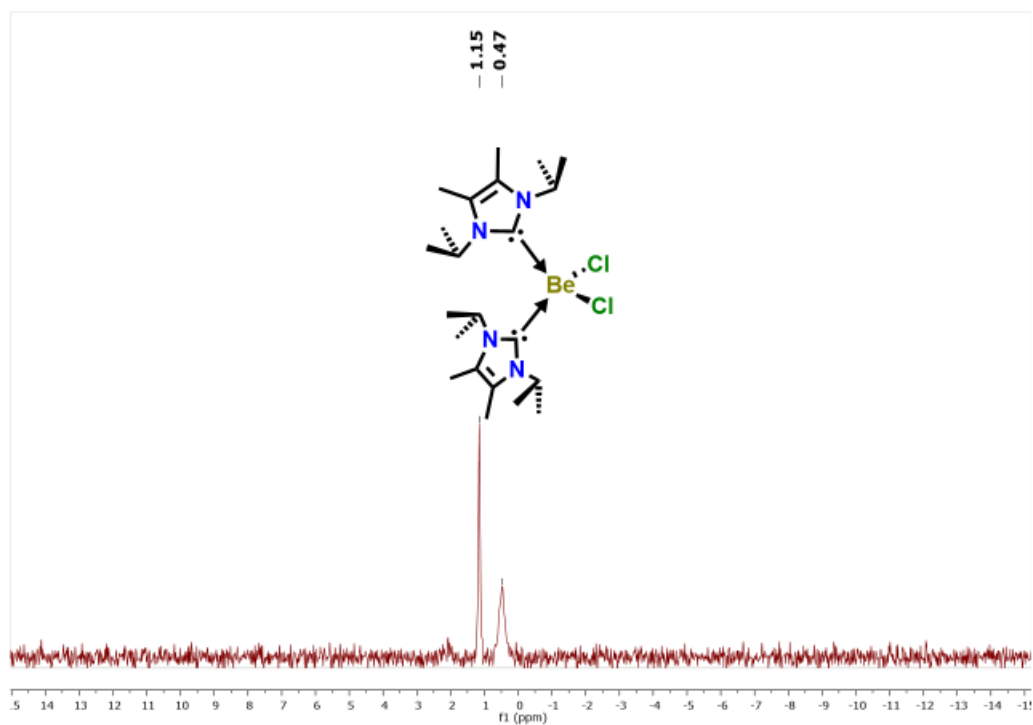
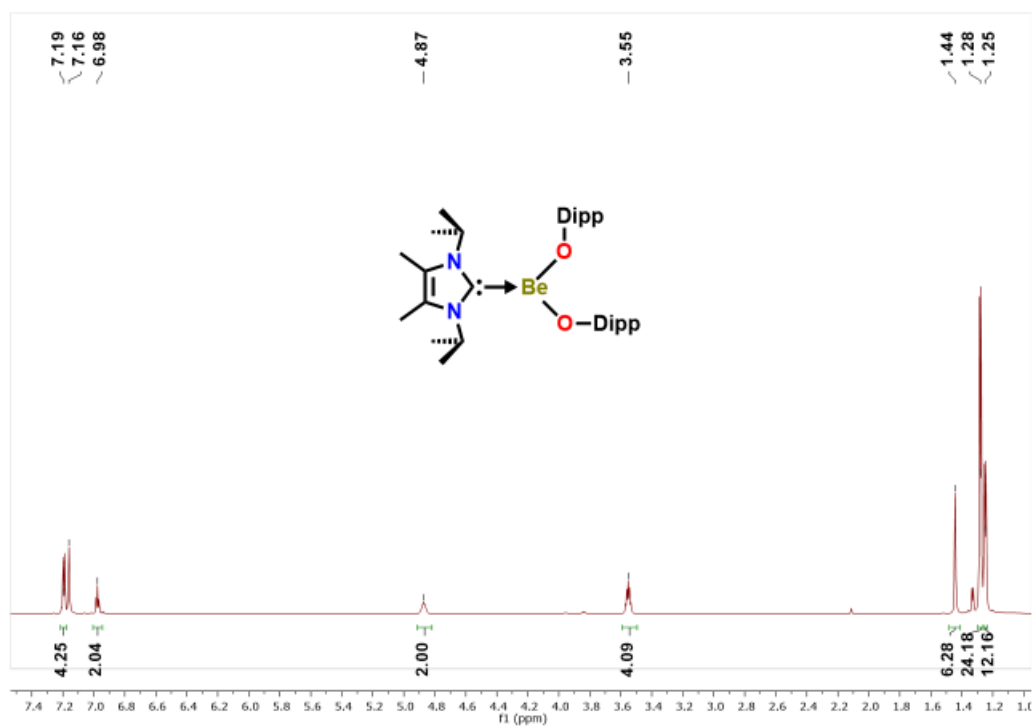


Figure A2S33.  $^{13}\text{C}\{^1\text{H}\}$  NMR (201.19 MHz,  $\text{C}_6\text{D}_6$ , 298 K) of compound 3.19.



**Figure A2S34.**  $^9\text{Be}$  NMR (84.28 MHz,  $\text{C}_6\text{D}_6$ , 298 K) of compound **3.19**.



**Figure A2S35.**  $^1\text{H}$  NMR spectrum (800.13 MHz,  $\text{C}_6\text{D}_6$ , 298 K) of compound **3.20**.

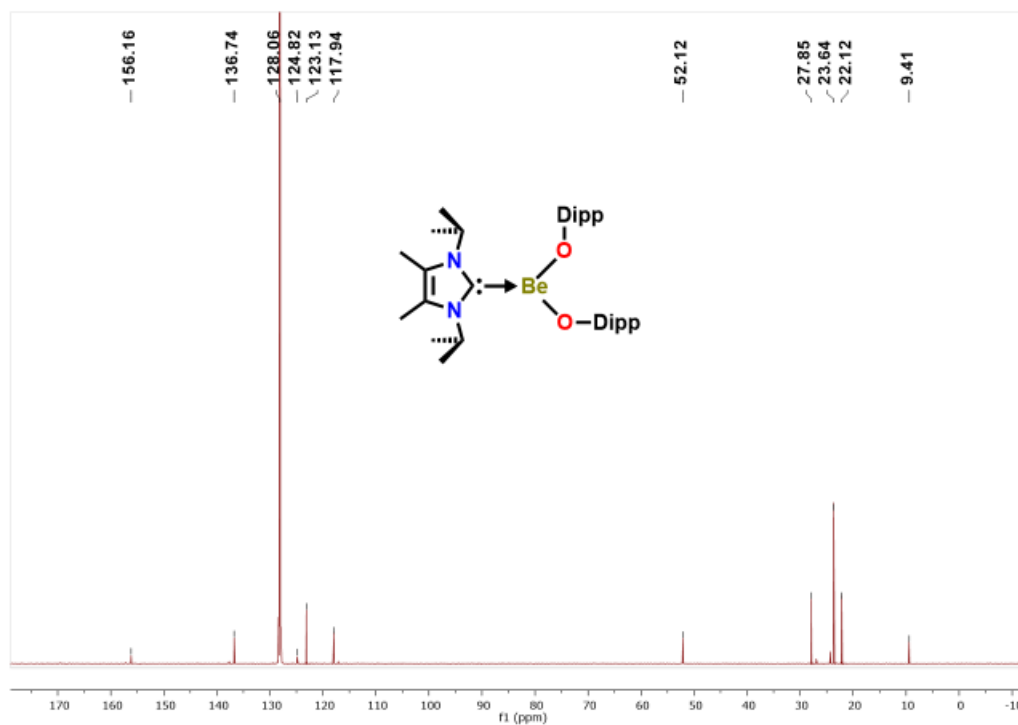


**Figure A2S36.**  $^{13}\text{C}\{^1\text{H}\}$ NMR (201.19 MHz,  $\text{C}_6\text{D}_6$ , 298 K) of compound **3.20**.

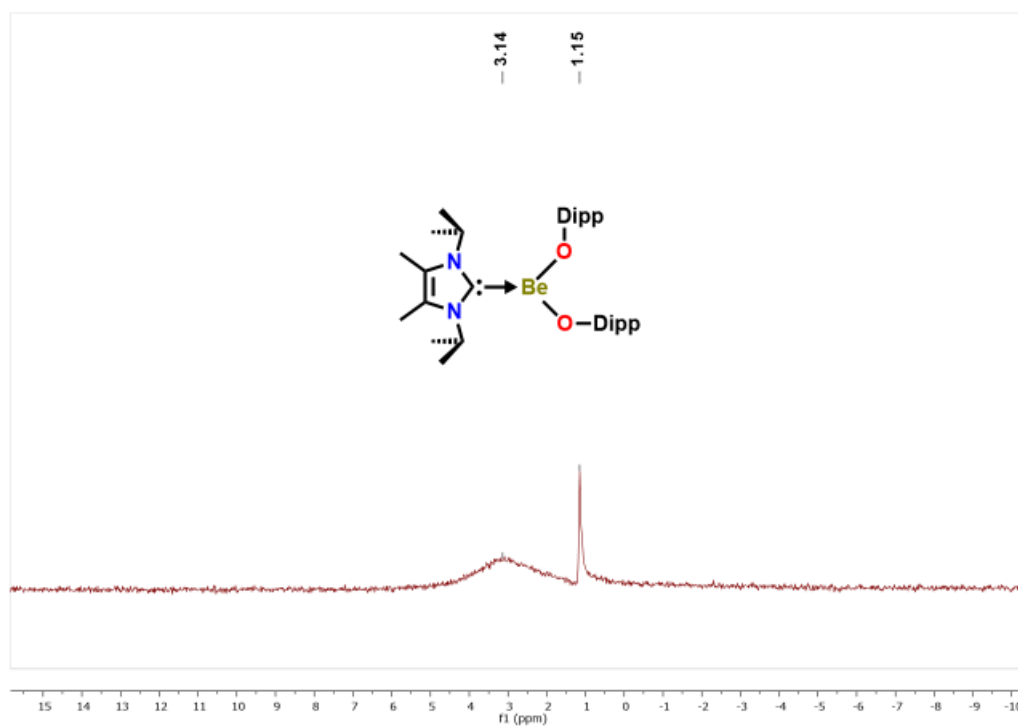


**Figure A2S37.**  $^9\text{Be}$  NMR (84.28 MHz,  $\text{C}_6\text{D}_6$ , 298 K) of compound **3.20**.

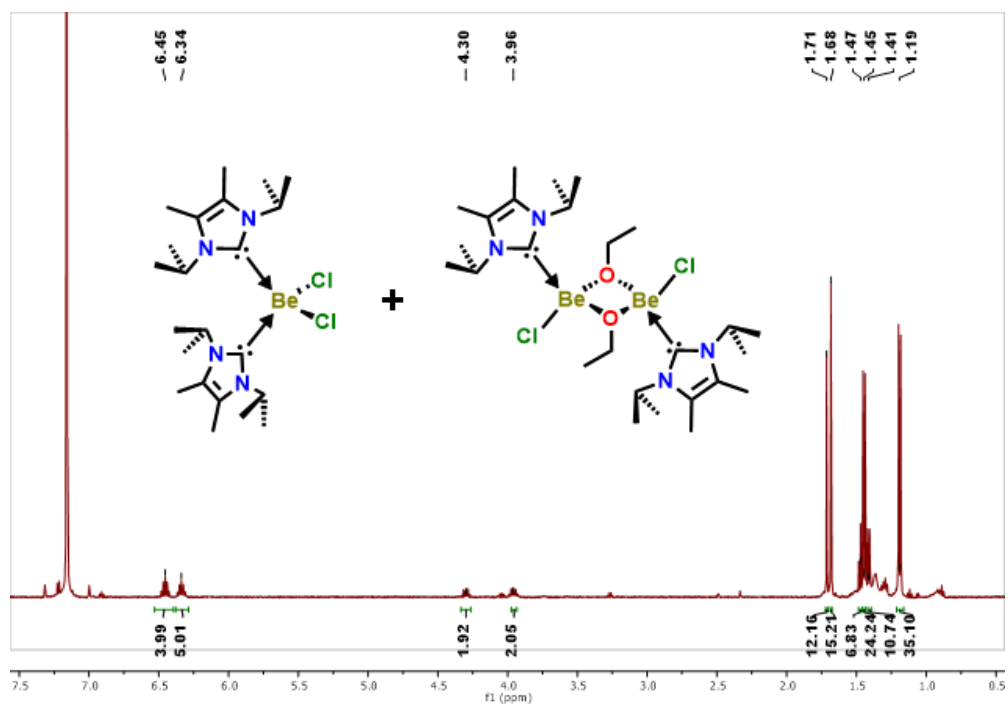


**Figure A2S38.**  $^1\text{H}$  NMR spectrum (500.13 MHz,  $\text{C}_6\text{D}_6$ , 298 K) of compound **3.21** mixed with compound **3.19**.

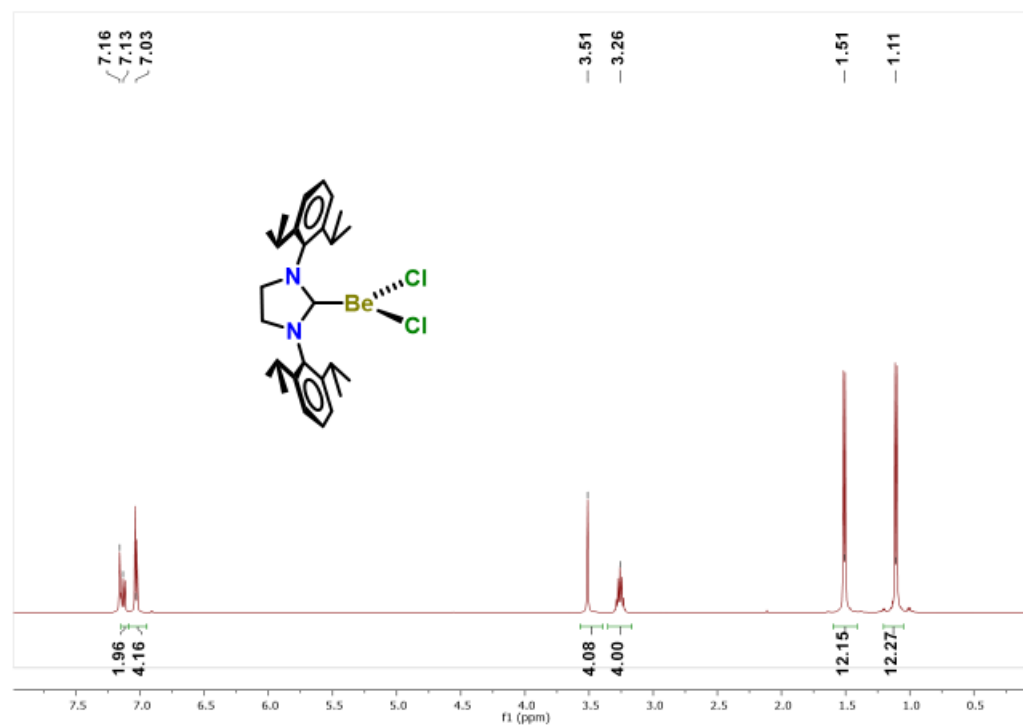


**Figure A2S39.**  $^1\text{H}$  NMR spectrum (600 MHz,  $\text{C}_6\text{D}_6$ , 298 K) of compound **3.26**.

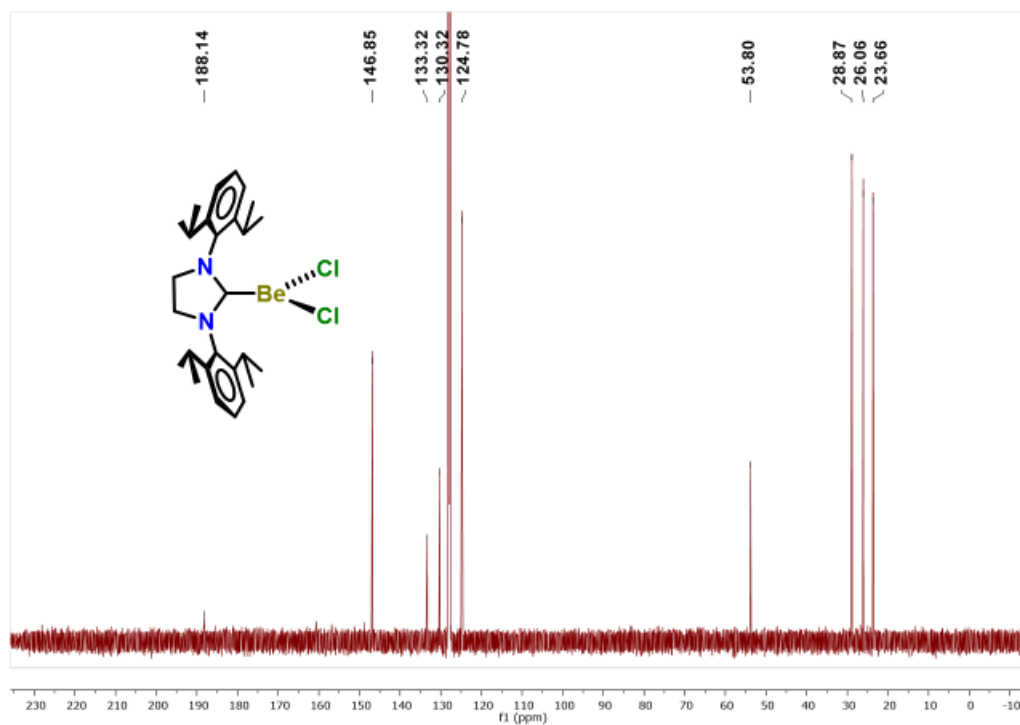


**Figure A2S40.**  $^{13}\text{C}\{^1\text{H}\}$  NMR (150.9 MHz,  $\text{C}_6\text{D}_6$ , 298 K) of compound **3.26**.

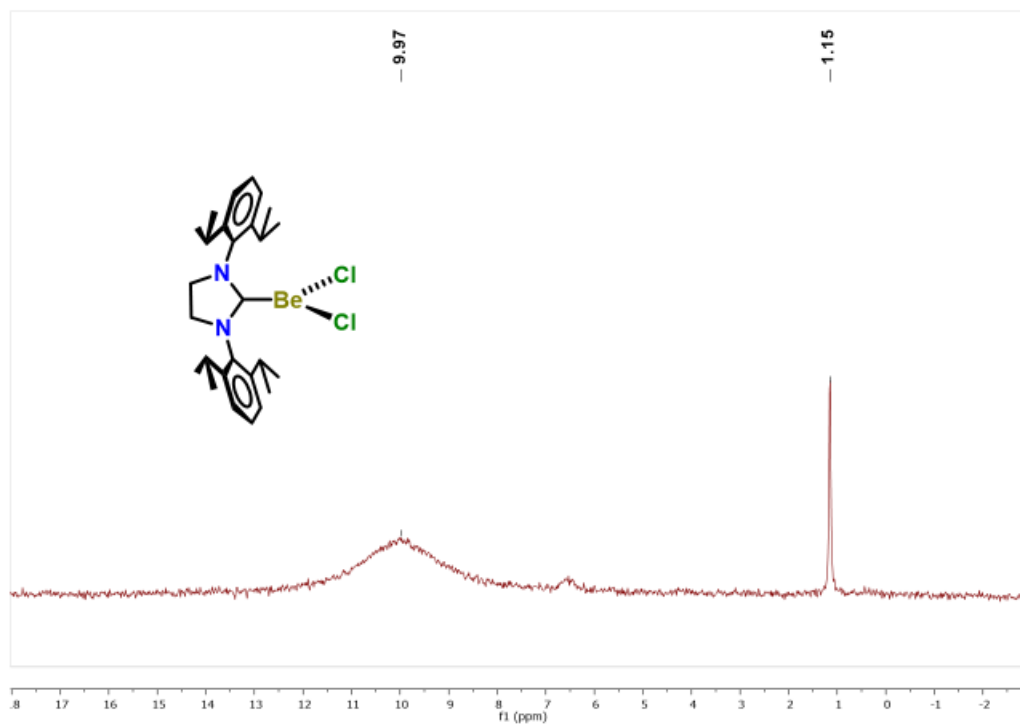


**Figure A2S41.**  $^9\text{Be}\{^1\text{H}\}$  NMR (84.28 MHz,  $\text{C}_6\text{D}_6$ , 298 K) of compound **3.26**.

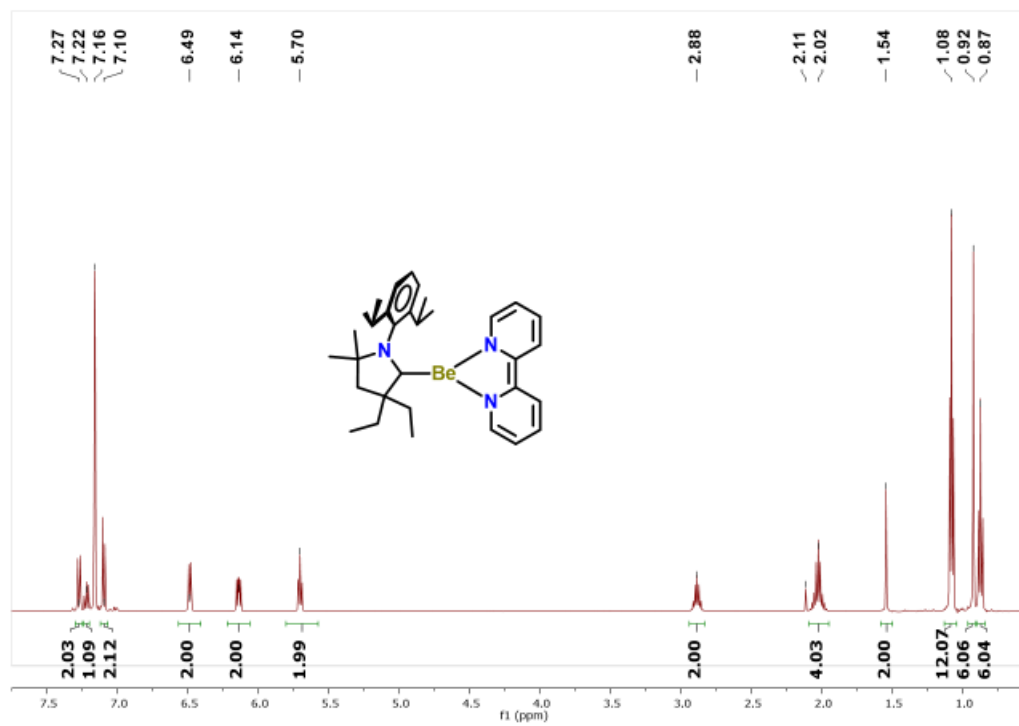


**Figure A2S42.**  $^1\text{H}$  NMR spectrum (600 MHz,  $\text{C}_6\text{D}_6$ , 298 K) of compound **3.27**.

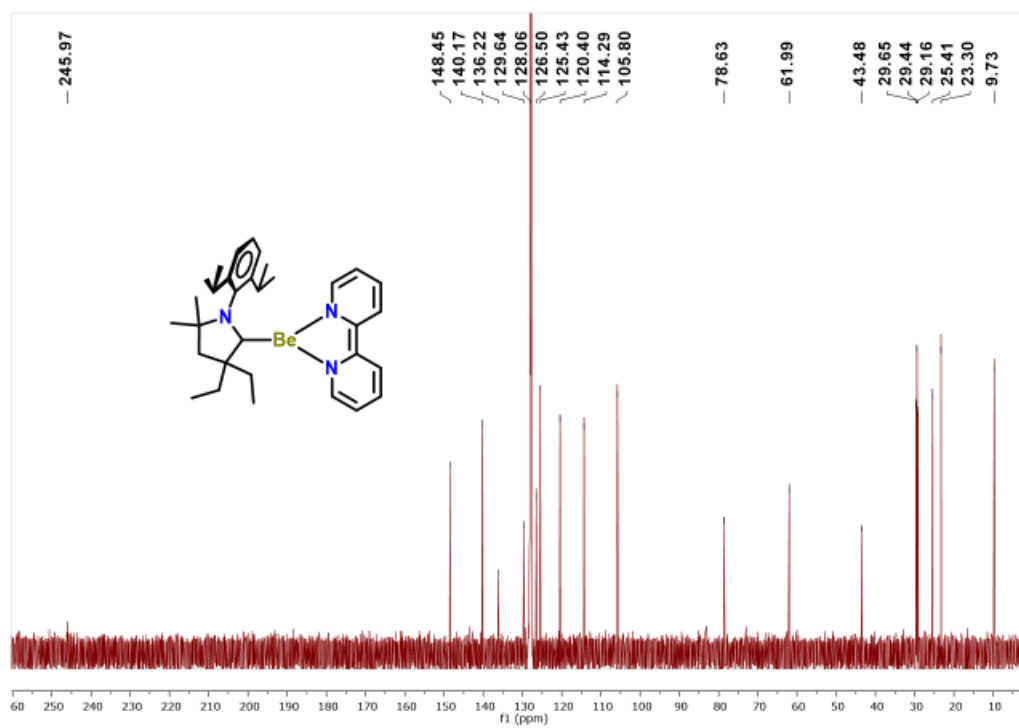


**Figure A2S43.**  $^{13}\text{C}^{229}$  NMR (150.9 MHz,  $\text{C}_6\text{D}_6$ , 298 K) of compound **3.27**.



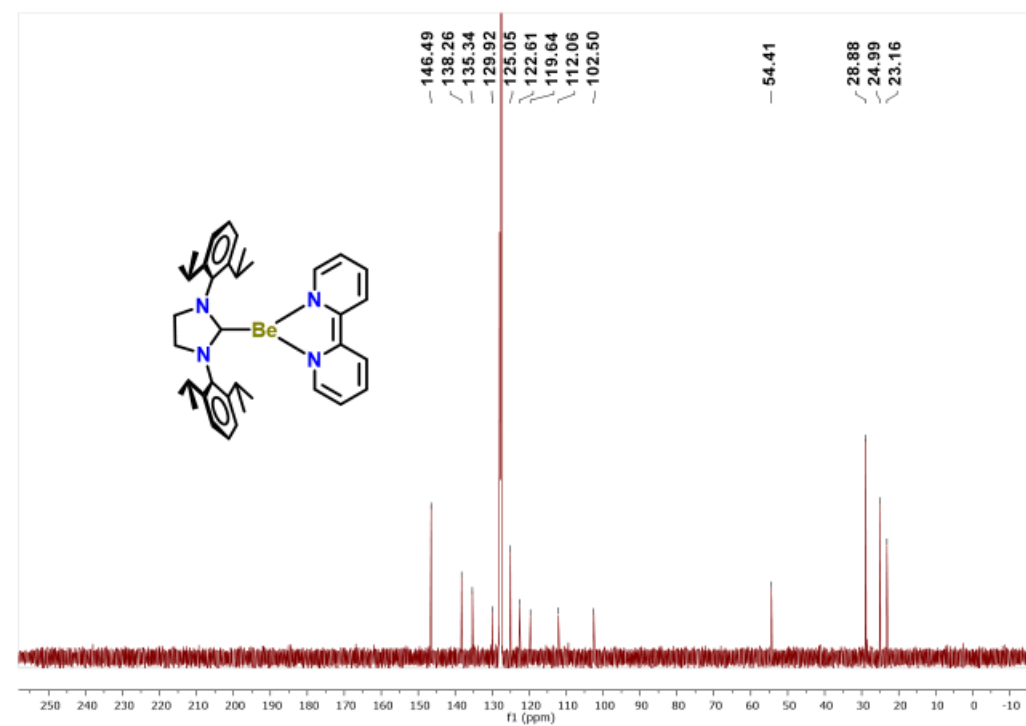


**Figure A2S46.**  $^{13}\text{C}\{^1\text{H}\}$  NMR (150.9 MHz,  $\text{C}_6\text{D}_6$ , 298 K) of compound **3.28**.

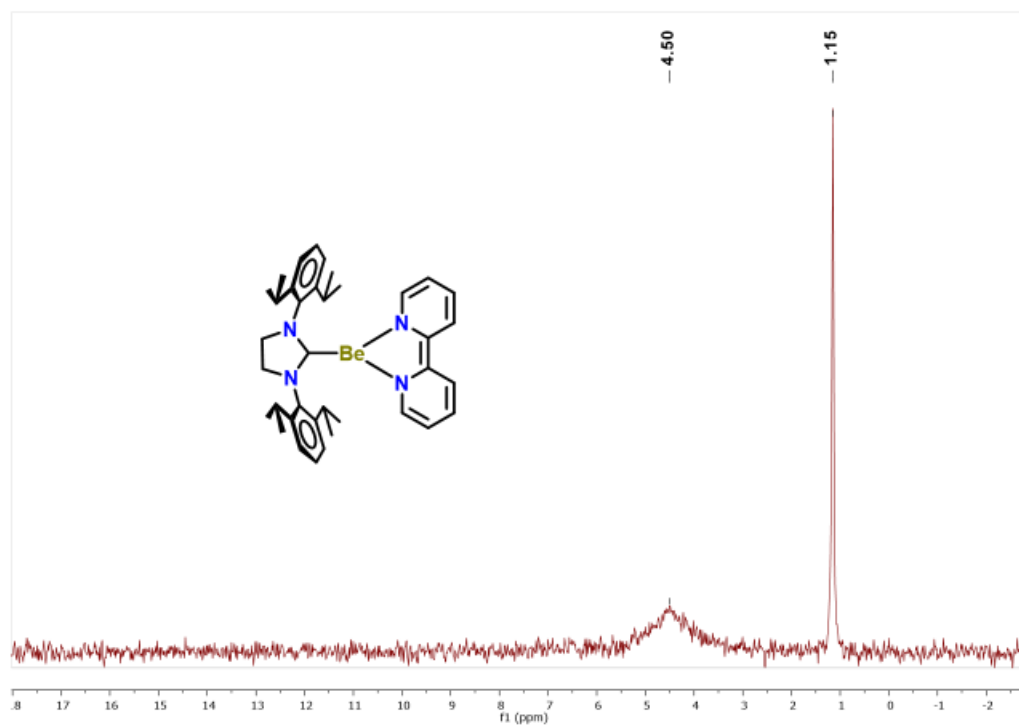


**Figure A2S47.**  $^9\text{Be}\{^1\text{H}\}$  NMR (84.28 MHz,  $\text{C}_6\text{D}_6$ , 298 K) of compound **3.28**.

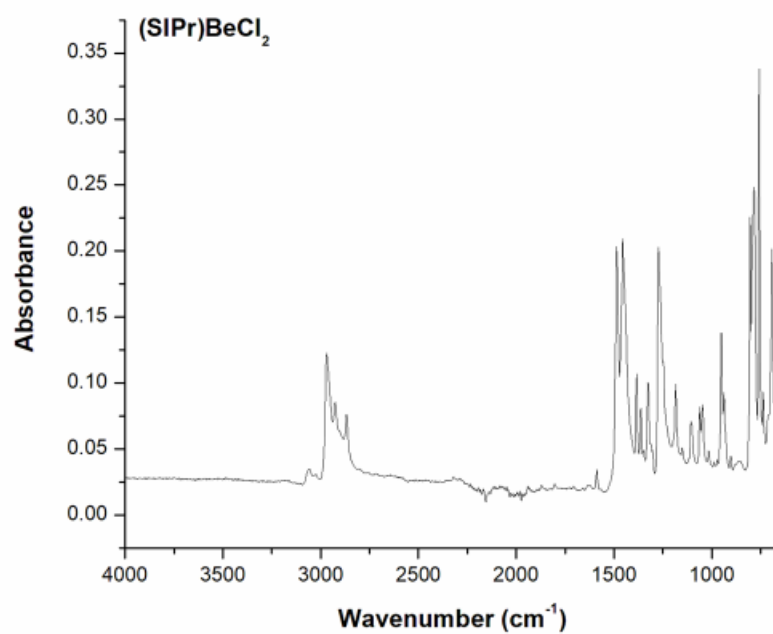


**Figure A2S48.** FT-IR spectrum of compound **3.26**.

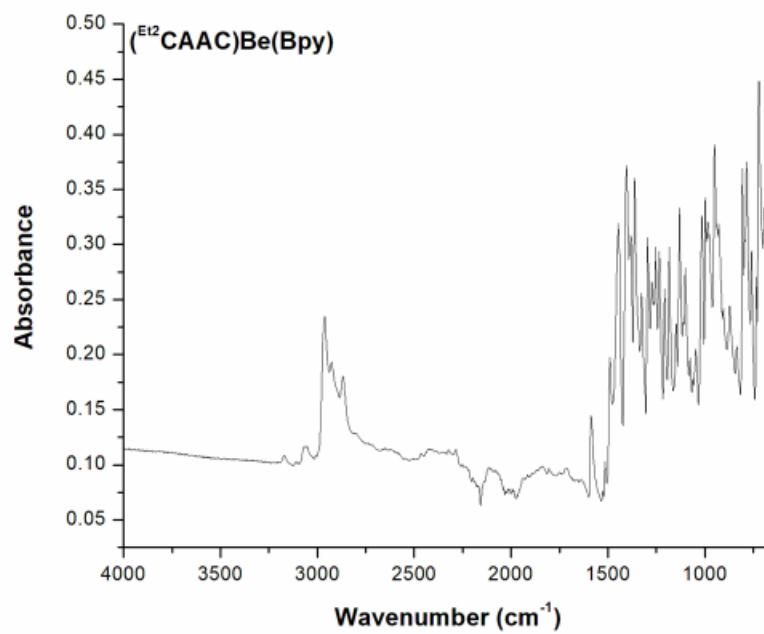


**Figure A2S49.** FT-IR spectrum of compound **3.27**.

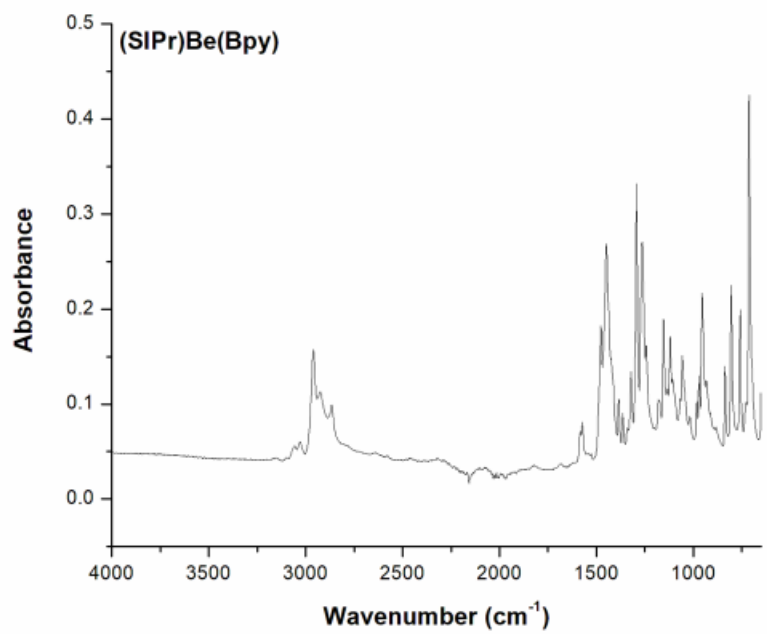


Figure A2S50. FT-IR spectrum of compound 3.28.

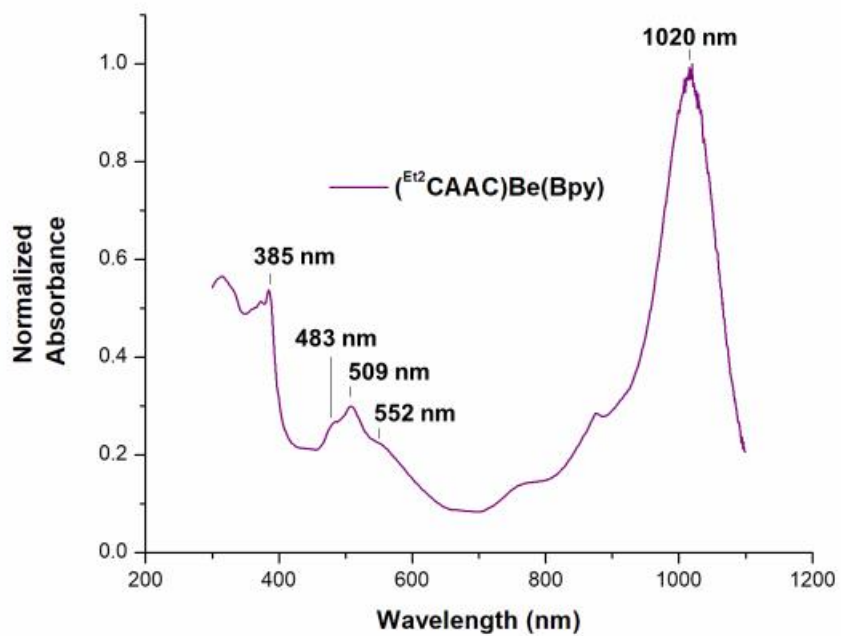
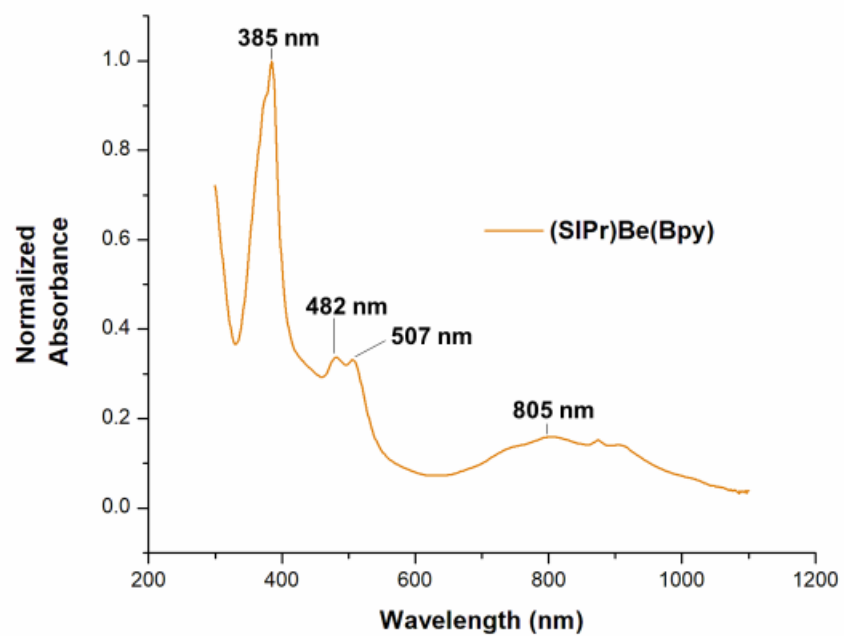
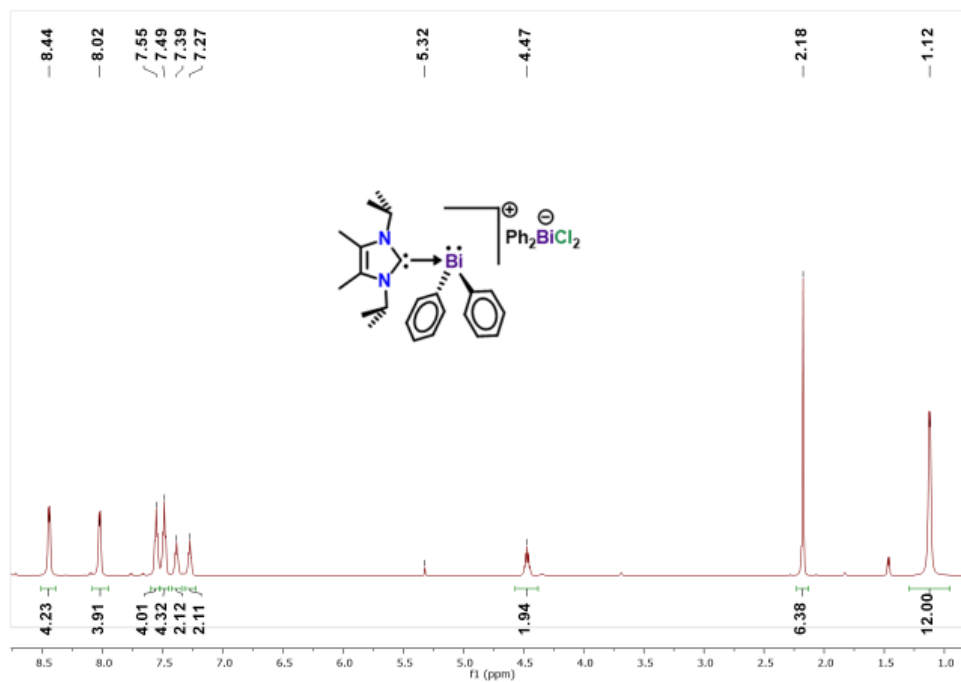


Figure A2S51. UV-Vis spectrum of compound 3.27 in toluene (0.1 mg mL<sup>-1</sup>)



**Figure A2S52.** UV-Vis spectrum of compound **3.28** in toluene ( $0.05 \text{ mg mL}^{-1}$ )

## Chapter 4 Spectral Data



**Figure A2S53.** <sup>1</sup>H NMR spectrum (600.13 MHz, CD<sub>2</sub>Cl<sub>2</sub>, 298 K) of compound **4.8**.

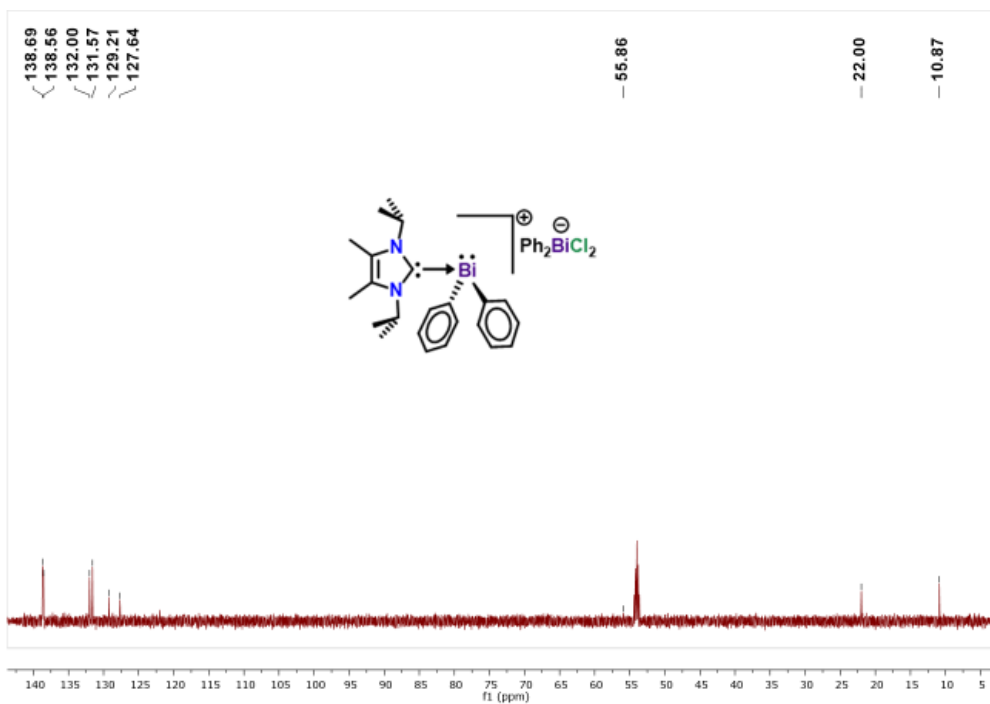


**Figure A2S54.** <sup>13</sup>C NMR spectrum (150.903 MHz, CD<sub>2</sub>Cl<sub>2</sub>, 298 K) of compound **4.8**.

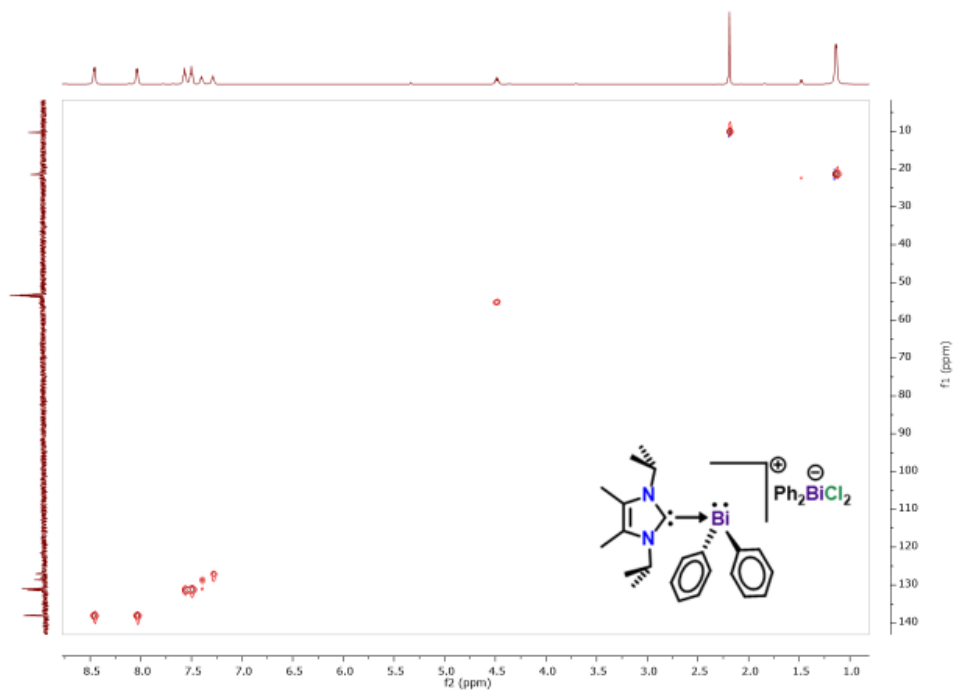


Figure A2S55.  $^1\text{H}$ - $^{13}\text{C}$  HSQC 2D NMR spectrum of compound **4.8**.

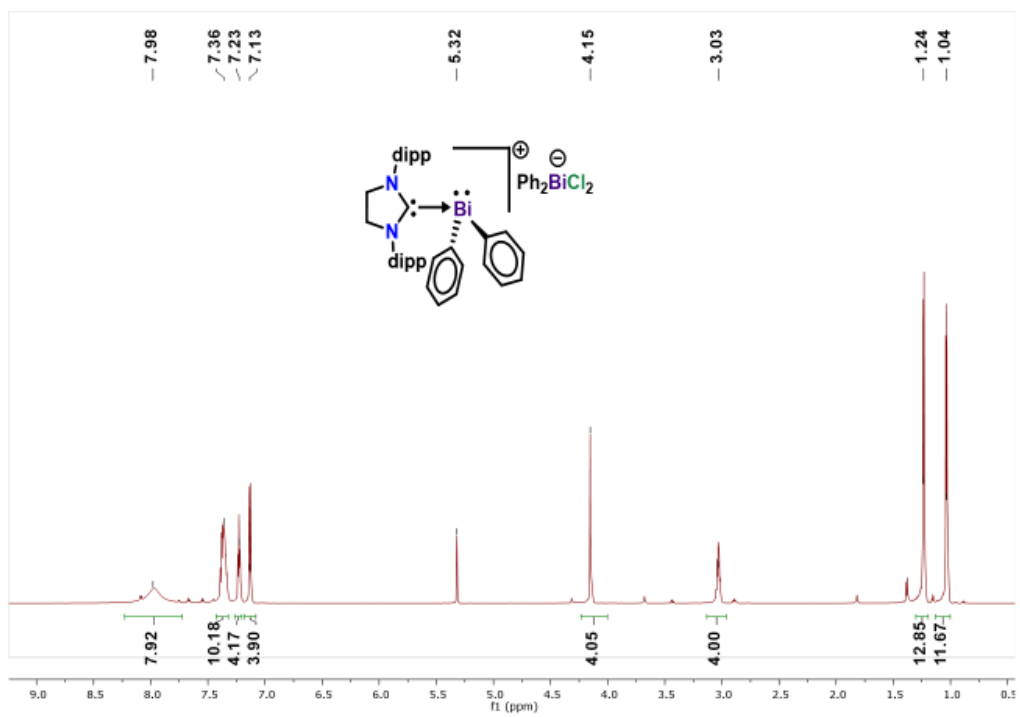
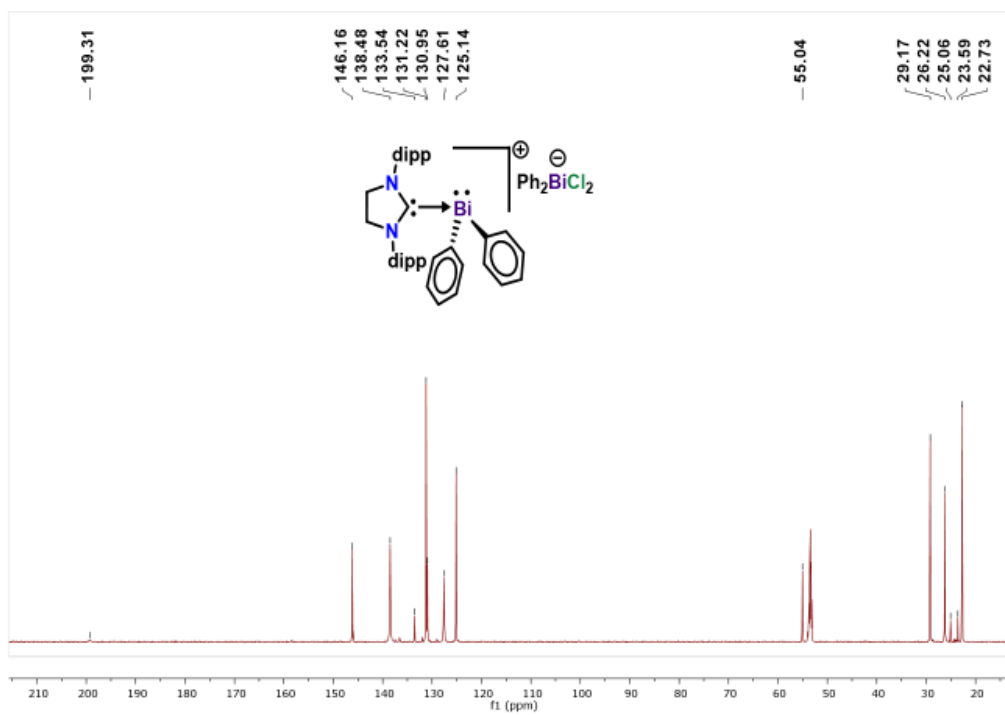
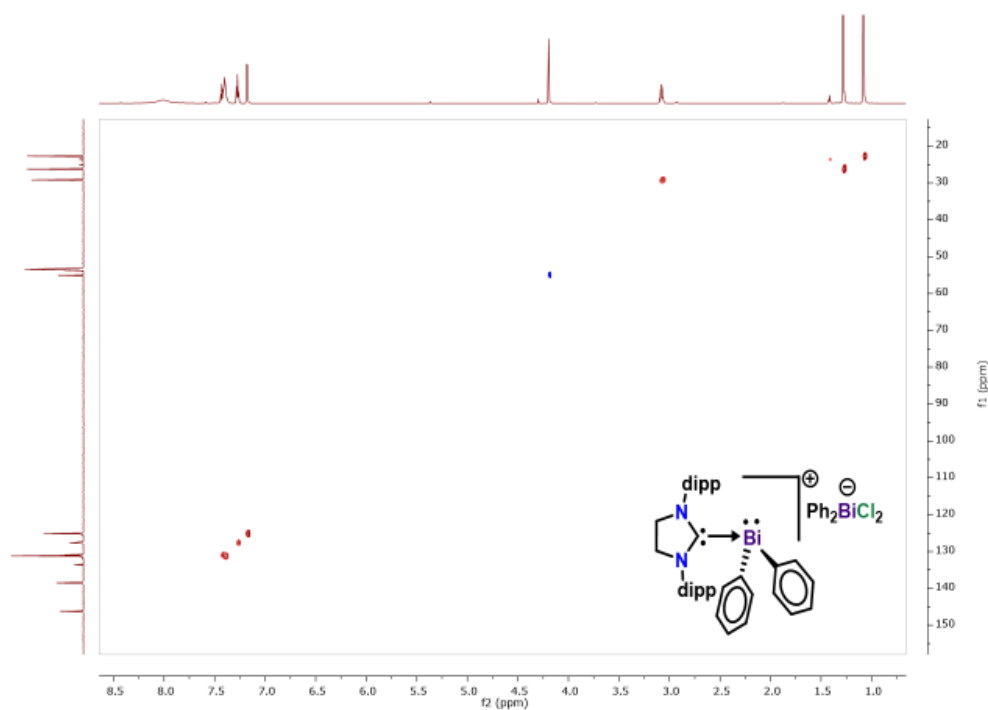


Figure A2S56.  $^1\text{H}$  NMR spectrum (800.13 MHz,  $\text{CD}_2\text{Cl}_2$ , 298 K) of compound **4.9**.



**Figure A2S57.**  $^{13}\text{C}$  NMR spectrum (201.19 MHz,  $\text{CD}_2\text{Cl}_2$ , 298 K) of compound **4.9**.



**Figure A2S58.**  $^1\text{H}$ - $^{13}\text{C}$  HSQC 2D NMR spectrum of compound **4.9**.

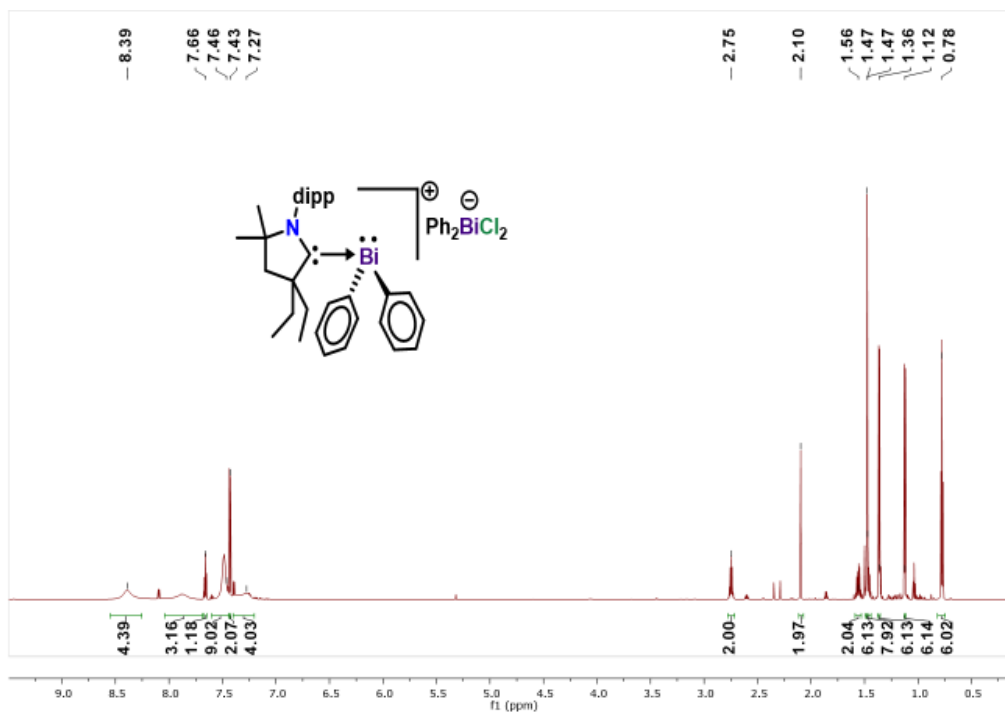


Figure A2S59.  $^1\text{H}$  NMR spectrum (800.13 MHz,  $\text{CD}_2\text{Cl}_2$ , 298 K) of compound 4.10.

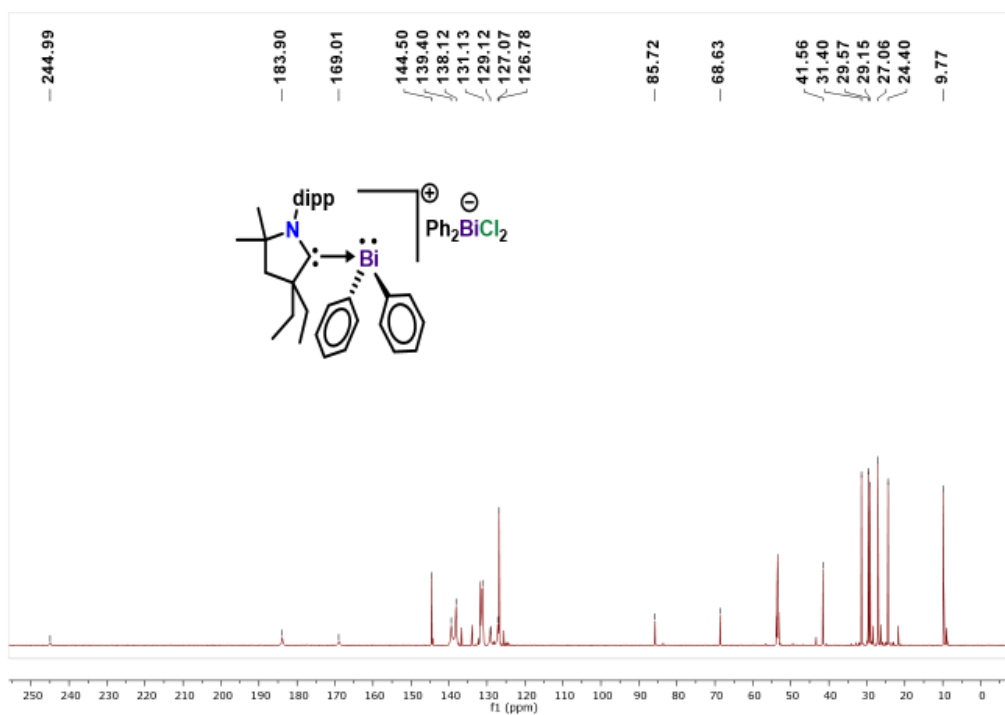
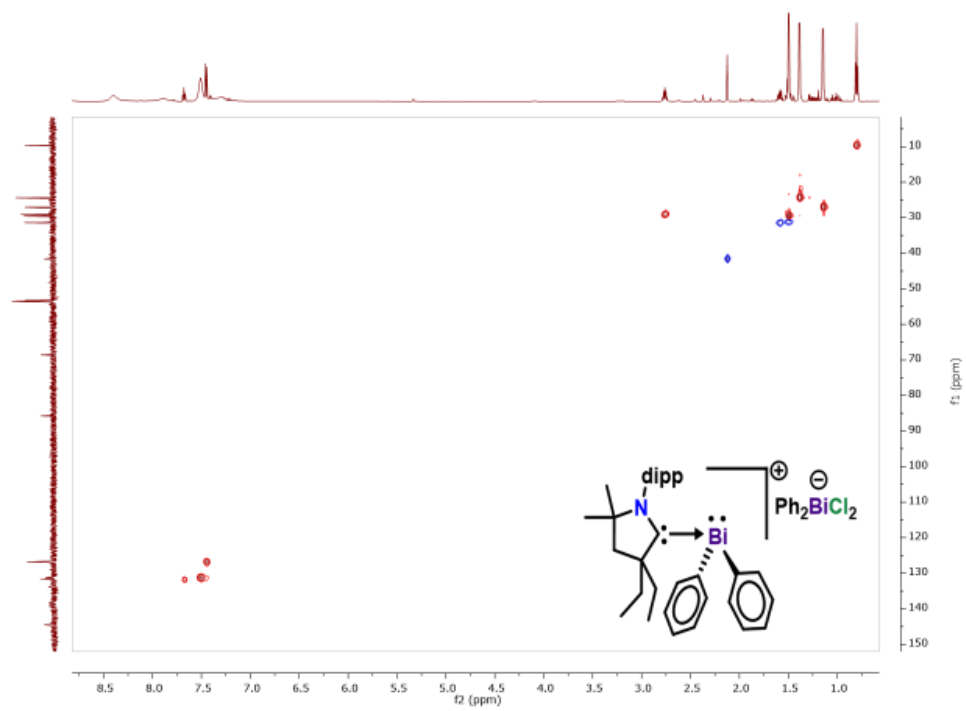
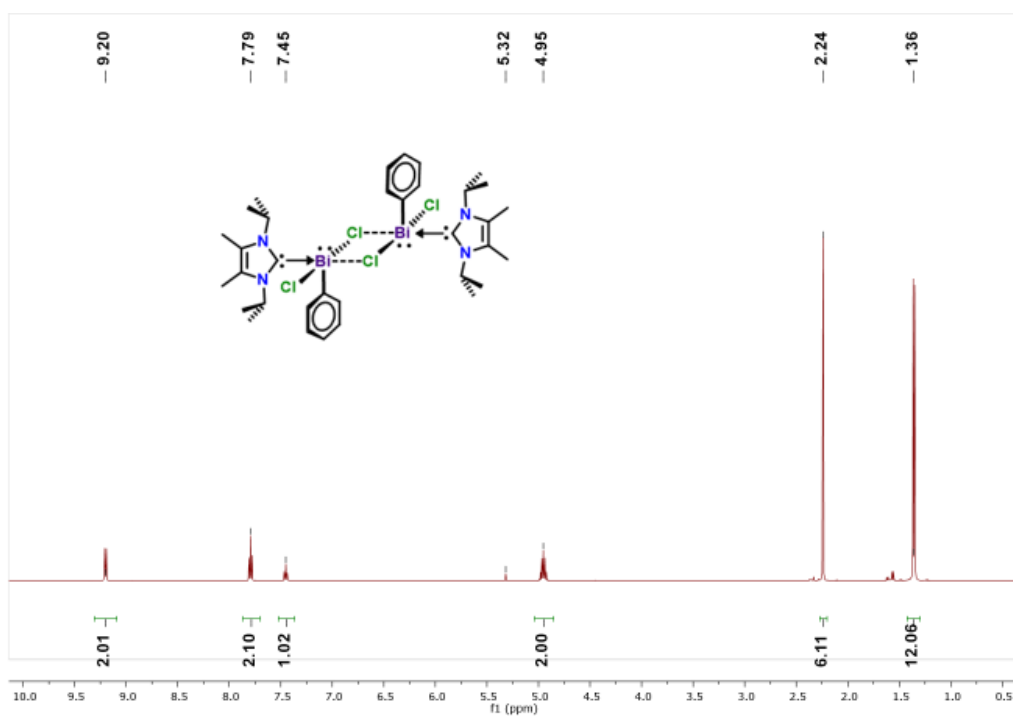


Figure A2S60.  $^{13}\text{C}$  NMR spectrum (201.19 MHz,  $\text{CD}_2\text{Cl}_2$ , 298 K) of compound 4.10.



**Figure A2S61.**  $^1\text{H}$ - $^{13}\text{C}$  HSQC 2D NMR spectrum of compound **4.10**.



**Figure A2S62.**  $^1\text{H}$  NMR spectrum (500.13 MHz,  $\text{CD}_2\text{Cl}_2$ , 298 K) of compound **4.11**.

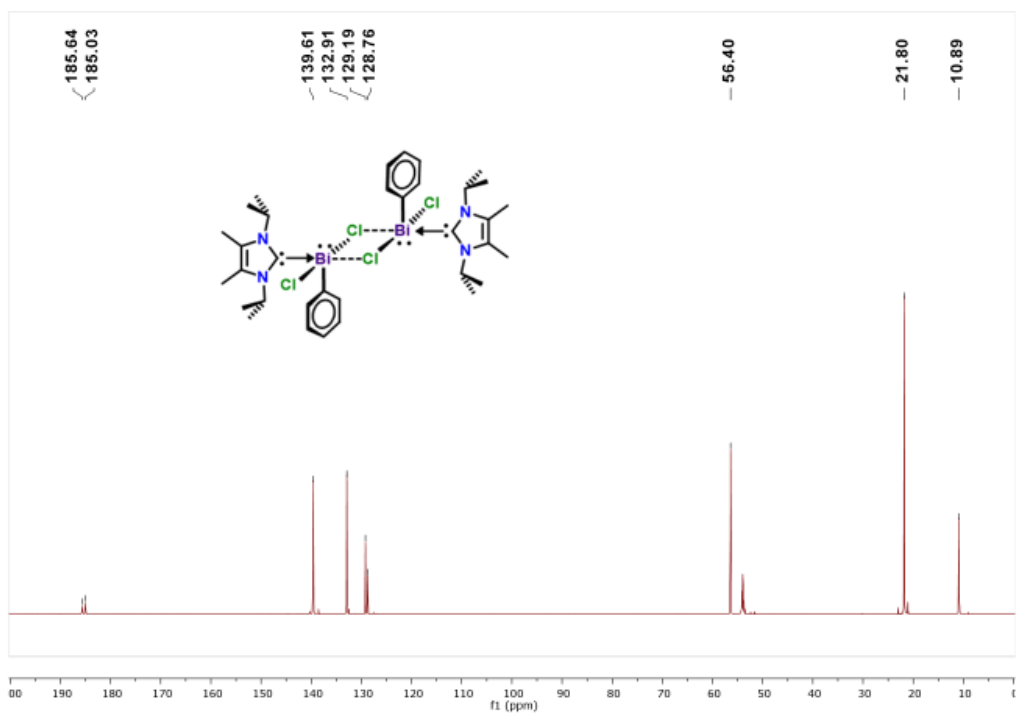


**Figure A2S63.**  $^{13}\text{C}$  NMR spectrum (201.19 MHz,  $\text{CD}_2\text{Cl}_2$ , 298 K) of compound **4.11**.

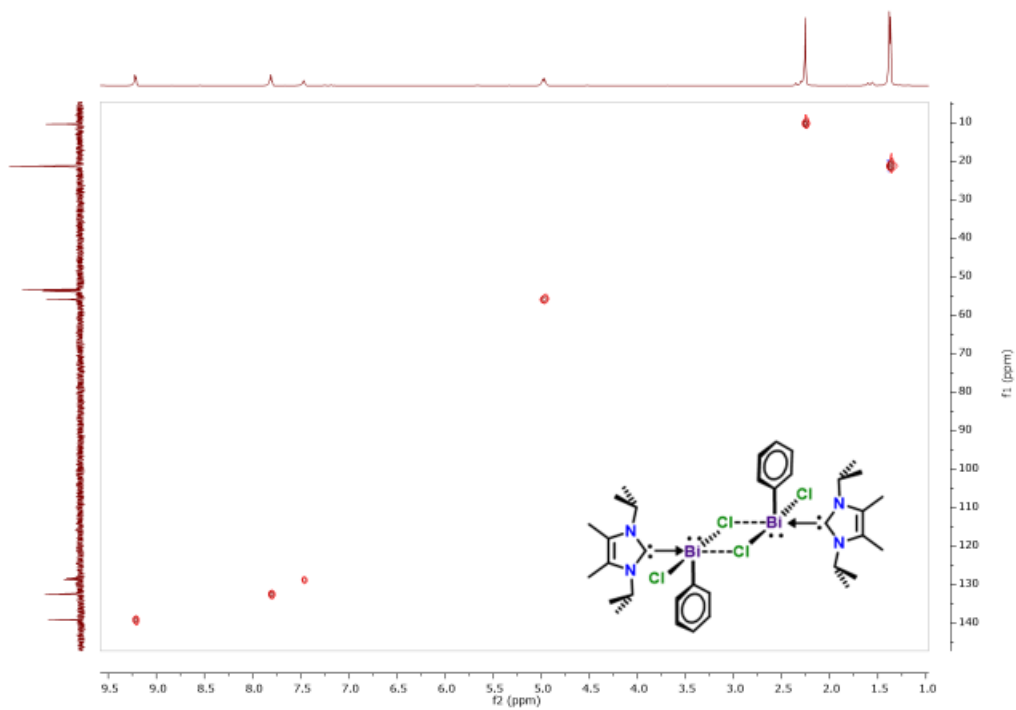


**Figure A2S64.**  $^1\text{H}$ - $^{13}\text{C}$  HSQC 2D NMR spectrum of compound **4.11**.

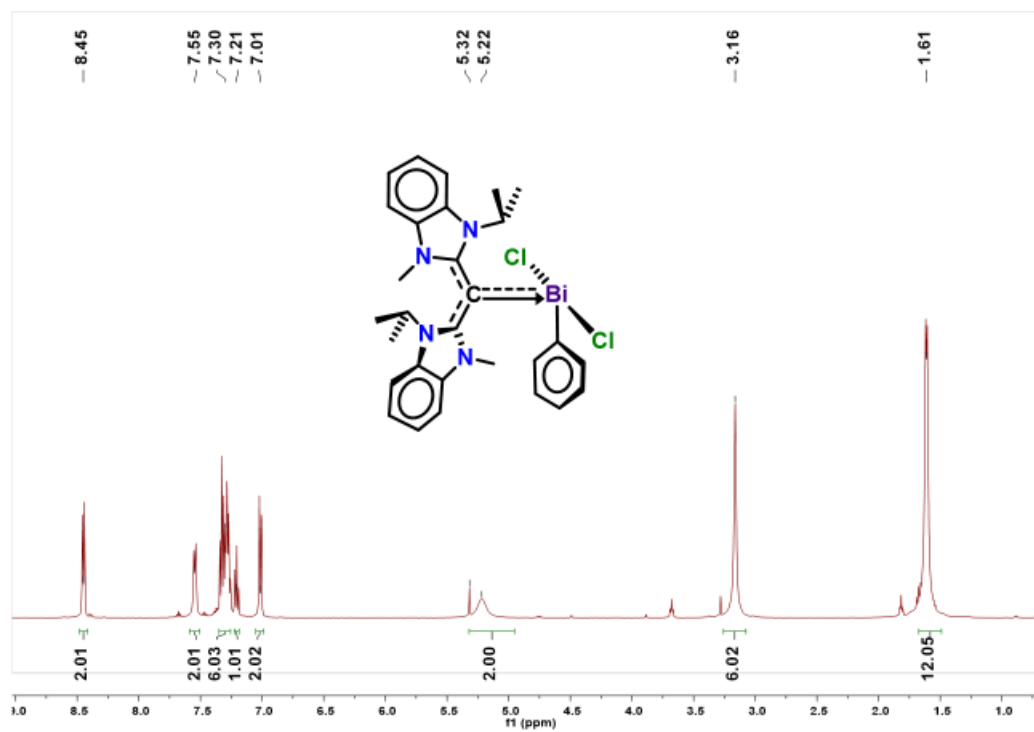


**Figure A2S65.**  $^1\text{H}$  NMR spectrum (500.13 MHz,  $\text{CD}_2\text{Cl}_2$ , 298 K) of compound **4.12**.

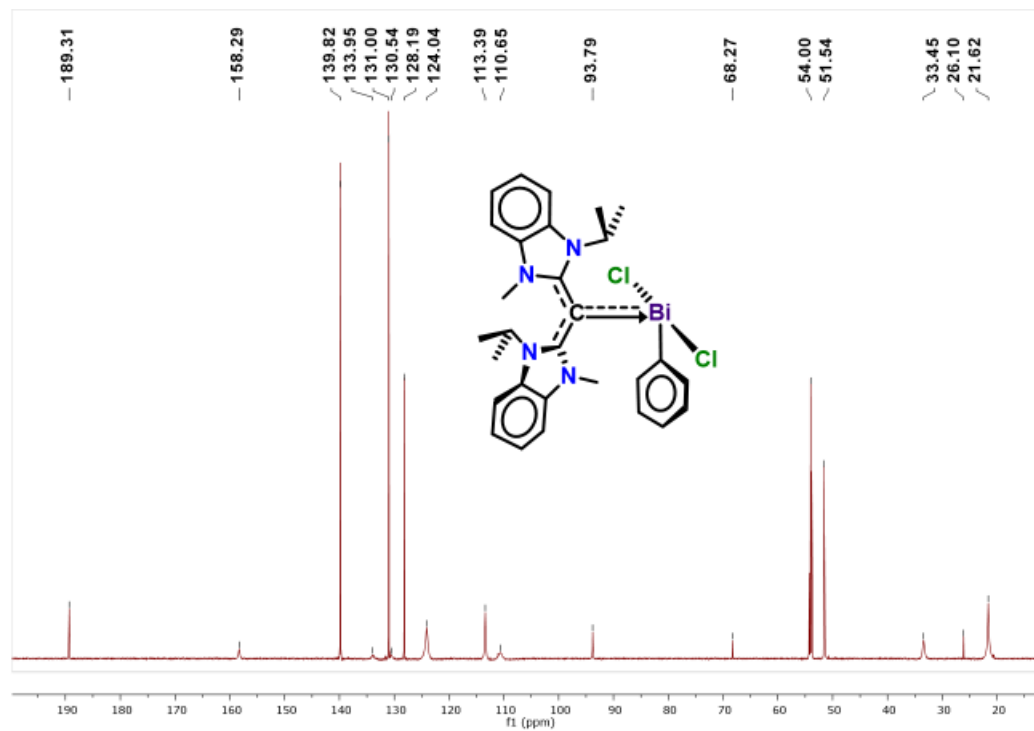


**Figure A2S66.**  $^{13}\text{C}$  NMR spectrum (201.19 MHz,  $\text{CD}_2\text{Cl}_2$ , 298 K) of compound **4.12**.

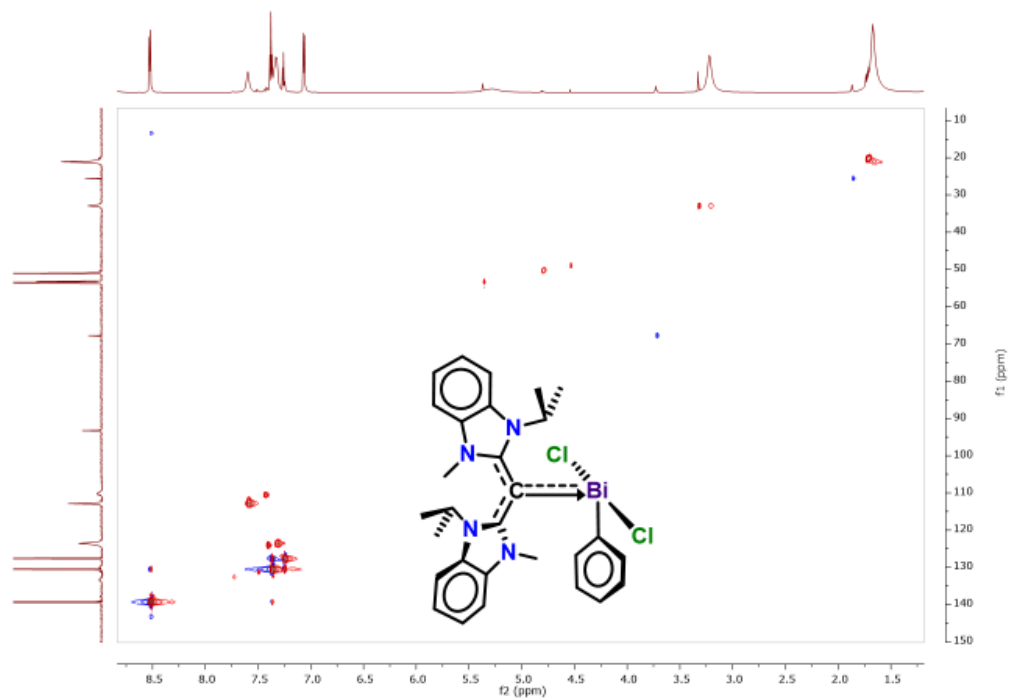


**Figure A2S67.**  $^1\text{H}$ - $^{13}\text{C}$  HSQC 2D NMR spectrum of compound **4.12**.

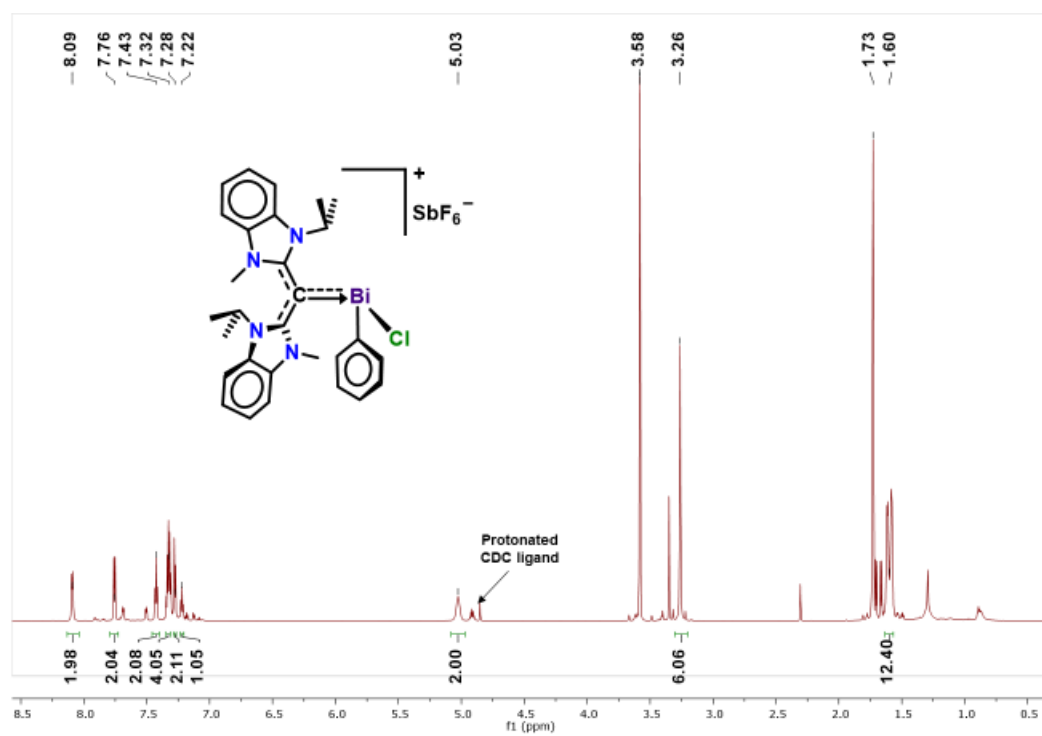


**Figure A2S68.**  $^1\text{H}$  NMR spectrum (800.13 MHz,  $\text{THF-}d_8$ , 298 K) of compound **4.13**.

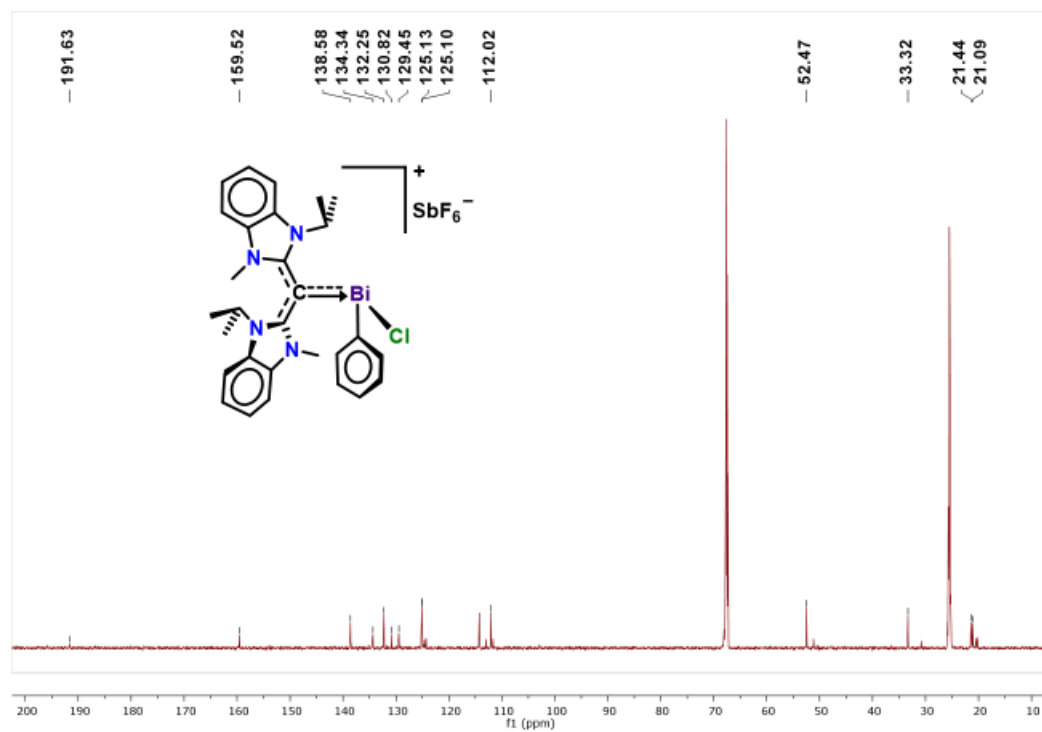


**Figure A2S69.**  $^{13}\text{C}$  NMR spectrum (201 MHz,  $\text{THF-}d_8$ , 298 K) of compound **4.13**.

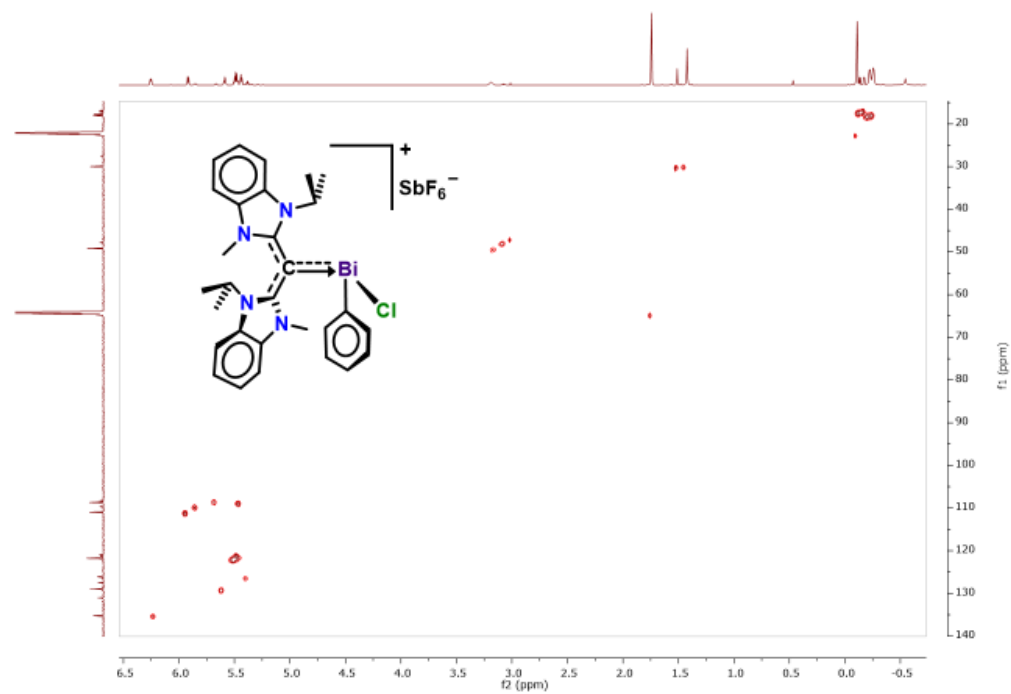


**Figure A2S70.**  $^1\text{H-}^{13}\text{C}$  HSQC 2D NMR spectrum of compound **4.13**.



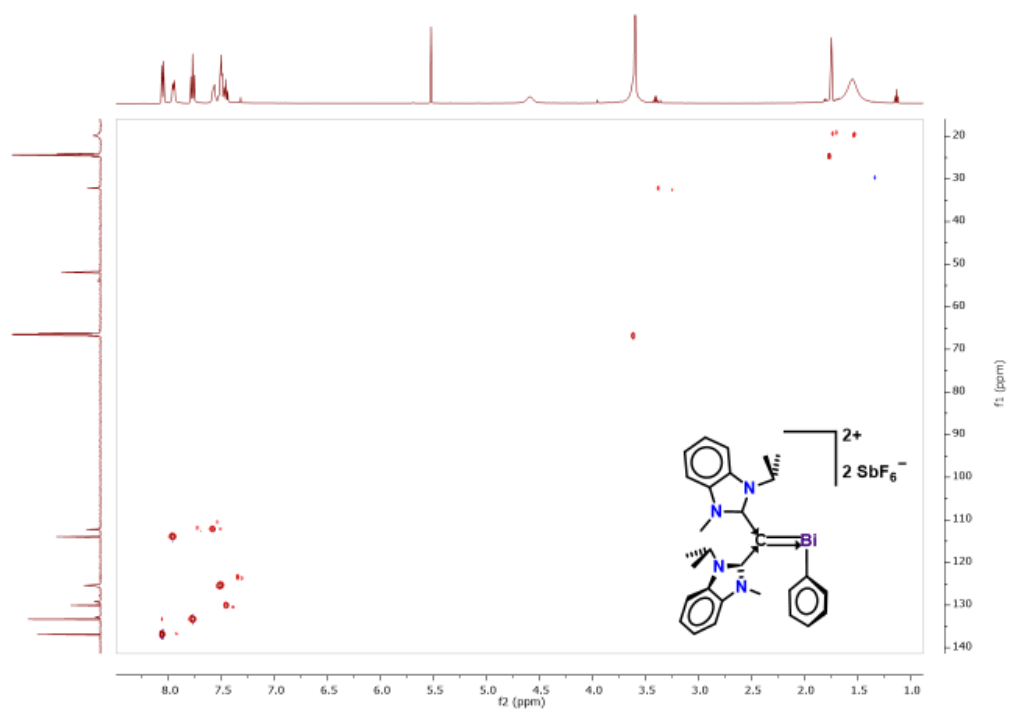


**Figure A2S73.**  $^1\text{H}$ - $^{13}\text{C}$  HSQC 2D NMR spectrum of compound **4.14**.

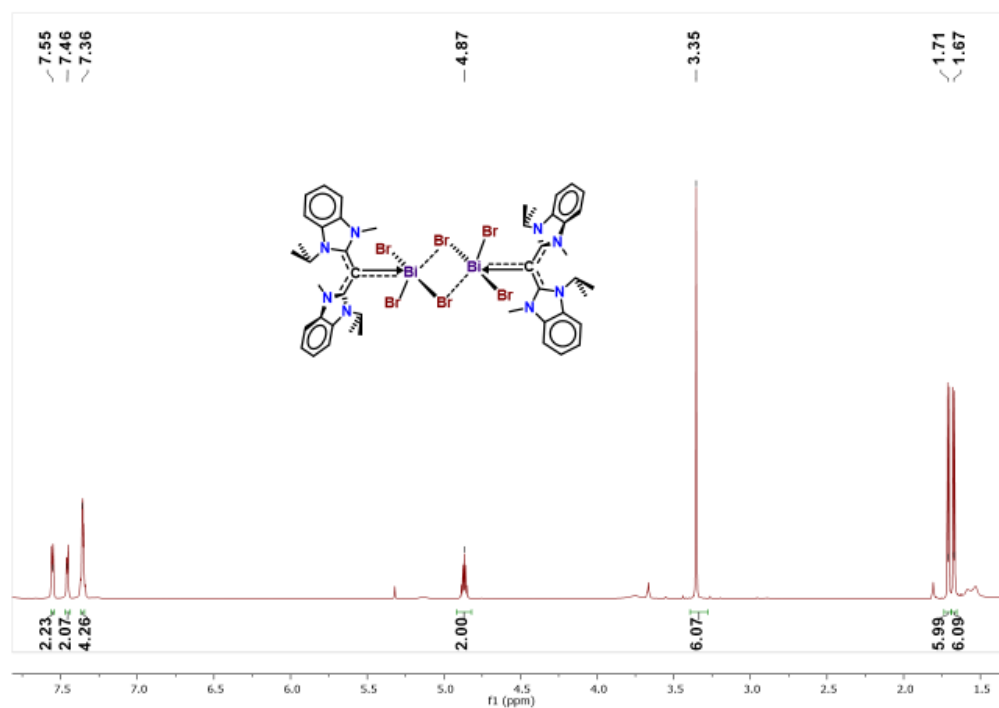


**Figure A2S74.**  $^1\text{H}$  NMR spectrum (800.13 MHz,  $\text{CD}_2\text{Cl}_2$ , 298 K) of compound **4.15**.

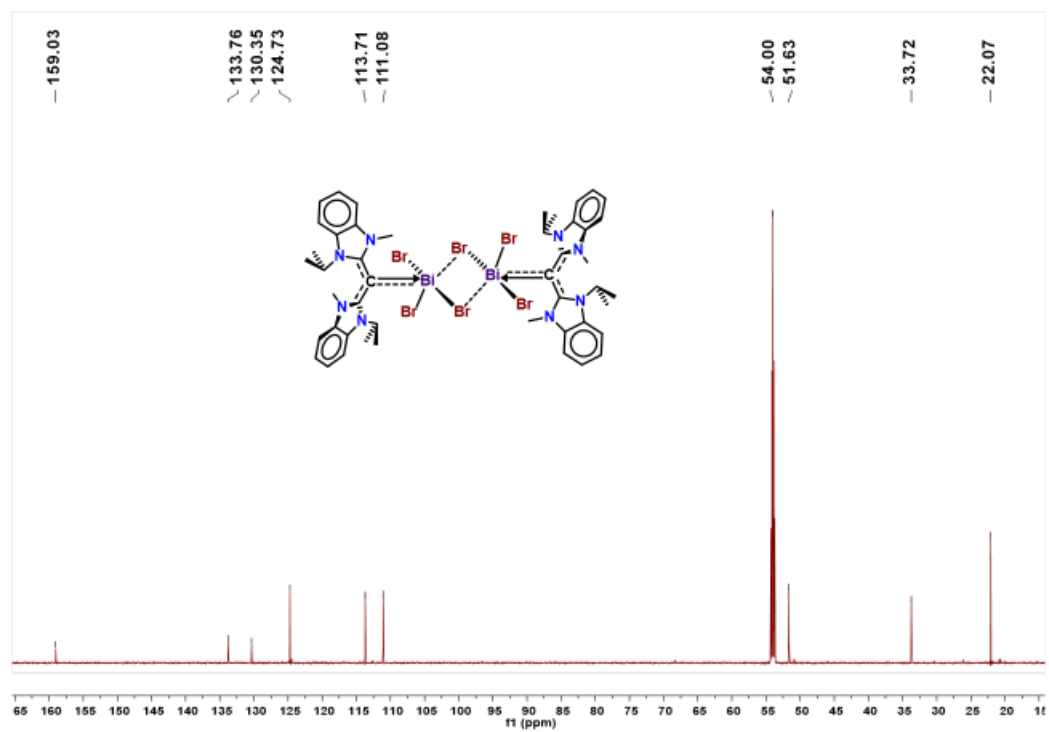


**Figure A2S75.**  $^{13}\text{C}$  NMR spectrum (201.19 MHz,  $\text{CD}_2\text{Cl}_2$ , 298 K) of compound **4.15**.

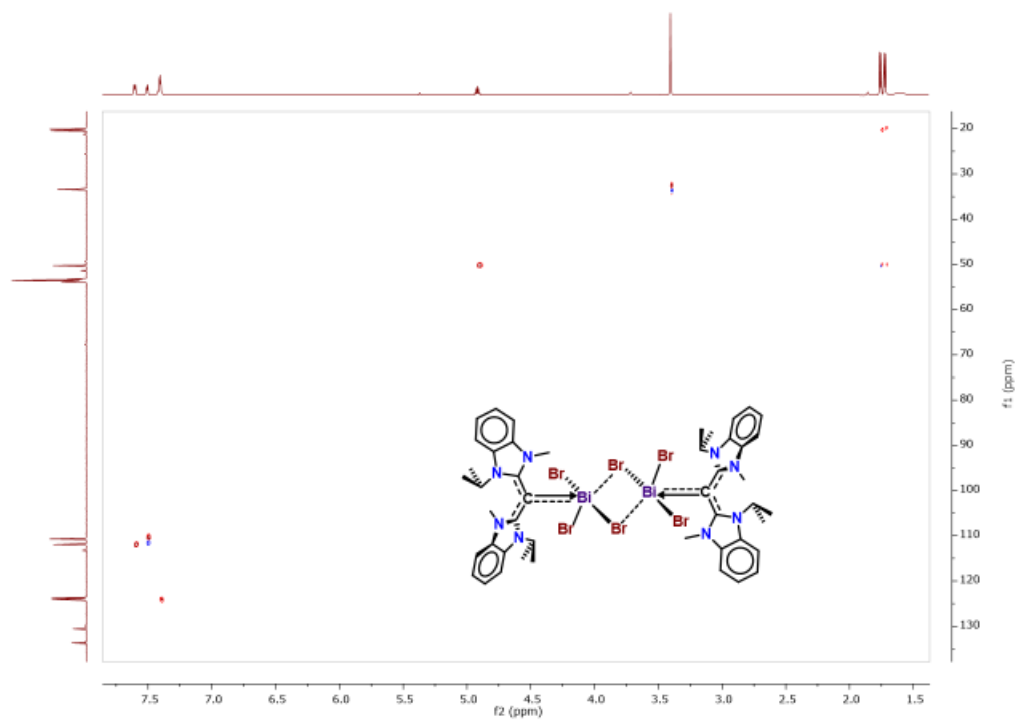


**Figure A2S76.**  $^1\text{H}$ - $^{13}\text{C}$  HSQC 2D NMR spectrum of compound **4.15**.

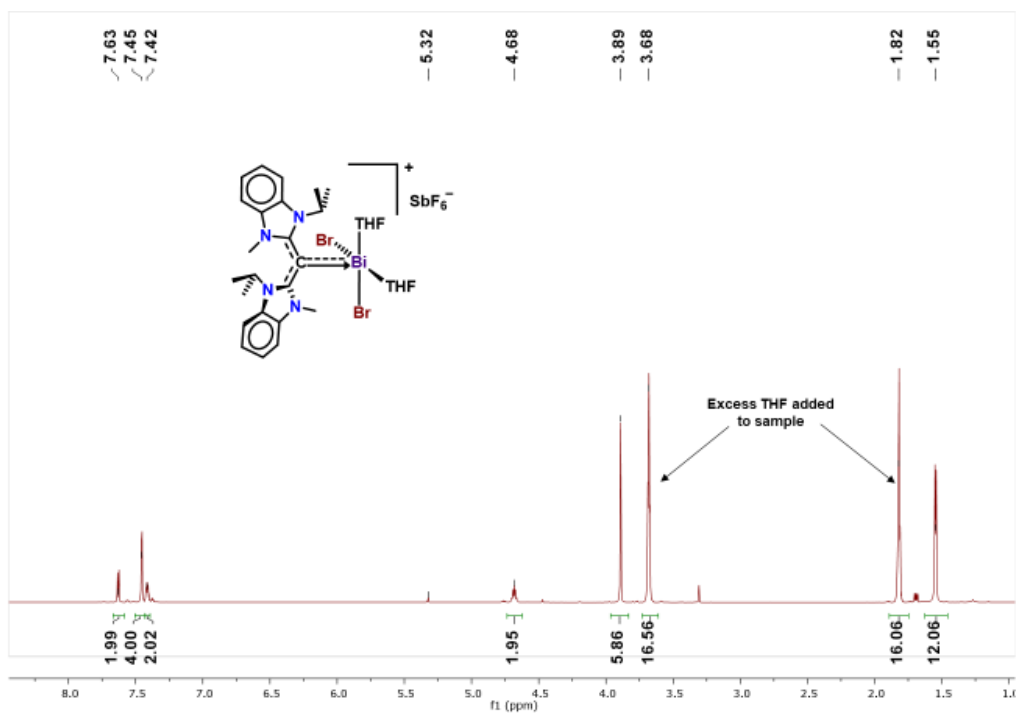


**Figure A2S77.** <sup>1</sup>H NMR spectrum (800.13 MHz, CD<sub>2</sub>Cl<sub>2</sub>, 298 K) of compound **4.16**. Note: Attempts to dissolve the single X-ray quality crystals in CD<sub>2</sub>Cl<sub>2</sub> resulted in substantial ligand protonation. Suitable NMR spectra were obtained from generating compound **4.16** in CD<sub>2</sub>Cl<sub>2</sub> and taking the NMR spectrum directly.

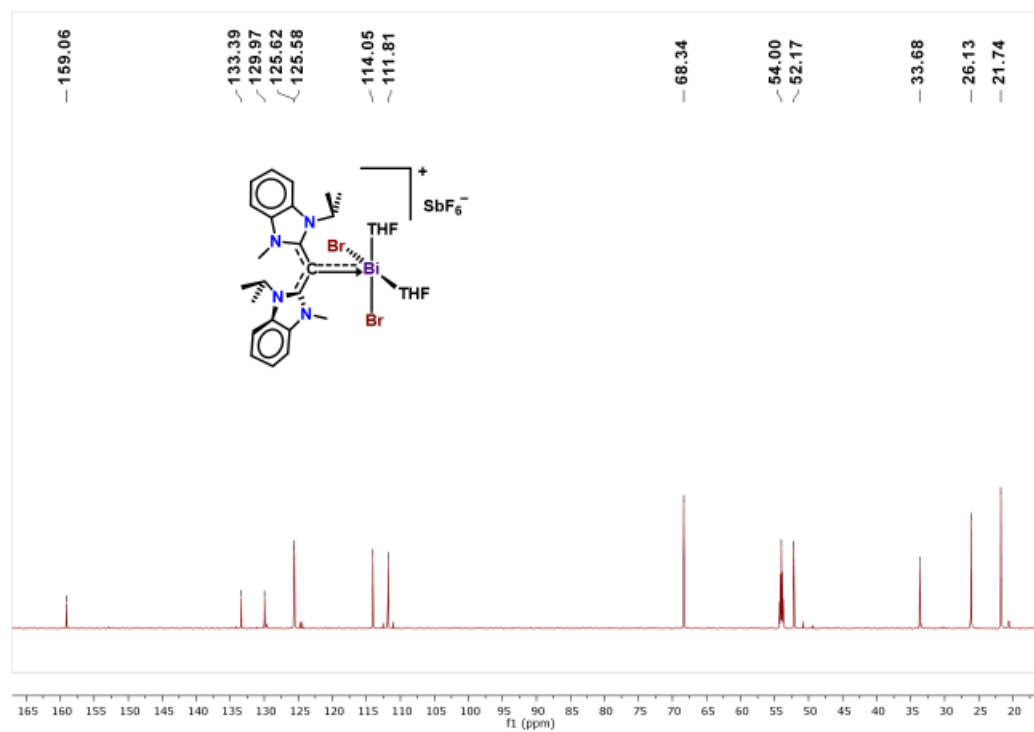


**Figure A2S78.**  $^{13}\text{C}$  NMR spectrum (201.19 MHz,  $\text{CD}_2\text{Cl}_2$ , 298 K) of compound **4.16**. Note: Attempts to dissolve the single X-ray quality crystals in  $\text{CD}_2\text{Cl}_2$  resulted in substantial ligand protonation. Suitable NMR spectra were obtained from generating compound **4.16** in  $\text{CD}_2\text{Cl}_2$  and taking the NMR spectrum directly.

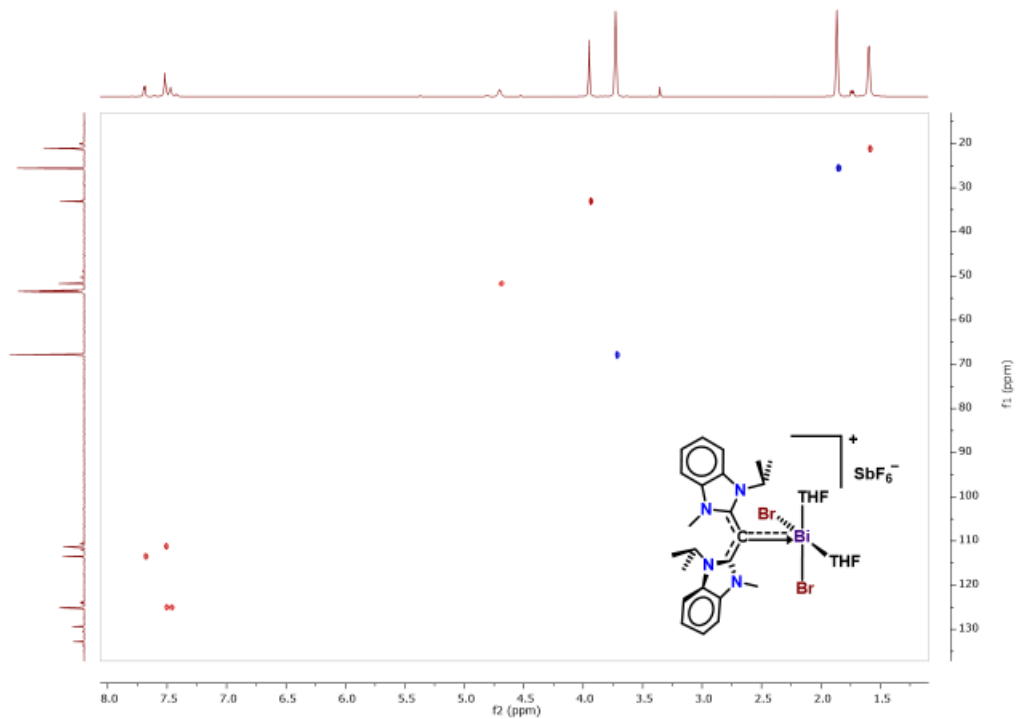


**Figure A2S79.**  $^1\text{H}$ - $^{13}\text{C}$  HSQC 2D NMR spectrum of compound **4.16**.

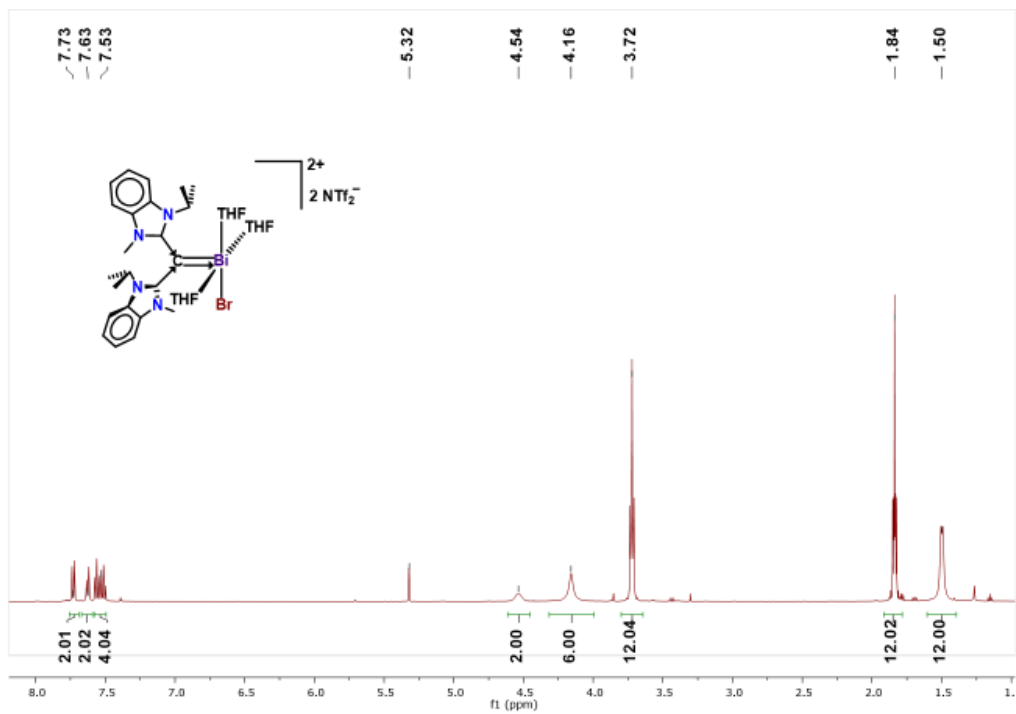


**Figure A2S80.**  $^1\text{H}$  NMR spectrum (800.13 MHz,  $\text{CD}_2\text{Cl}_2$ , 298 K) of compound **4.17**.

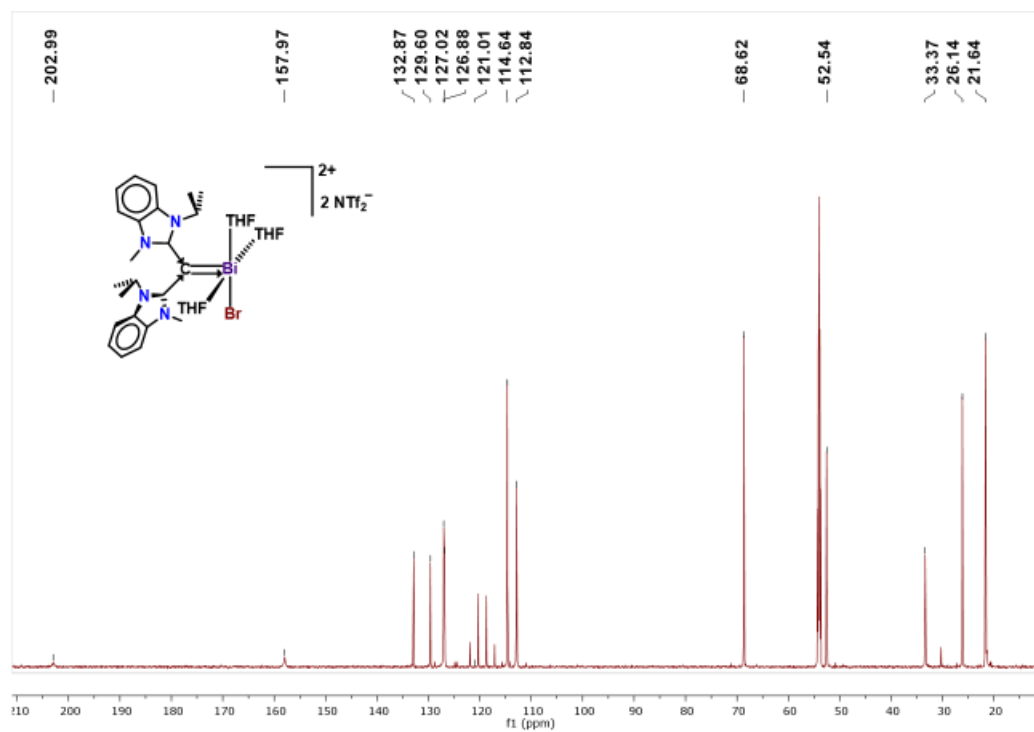


**Figure A2S81.**  $^{13}\text{C}$  NMR spectrum (201.19 MHz,  $\text{CD}_2\text{Cl}_2$ , 298 K) of compound **4.17**.

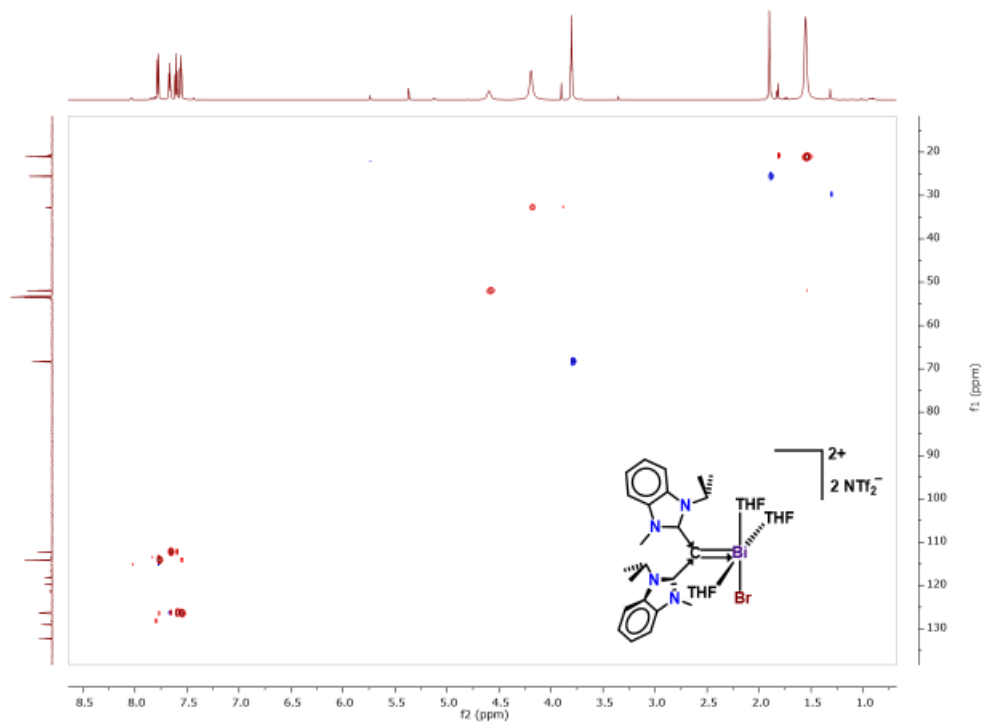


**Figure A2S82.**  $^1\text{H}$ - $^{13}\text{C}$  HSQC 2D NMR spectrum of compound **4.17**.

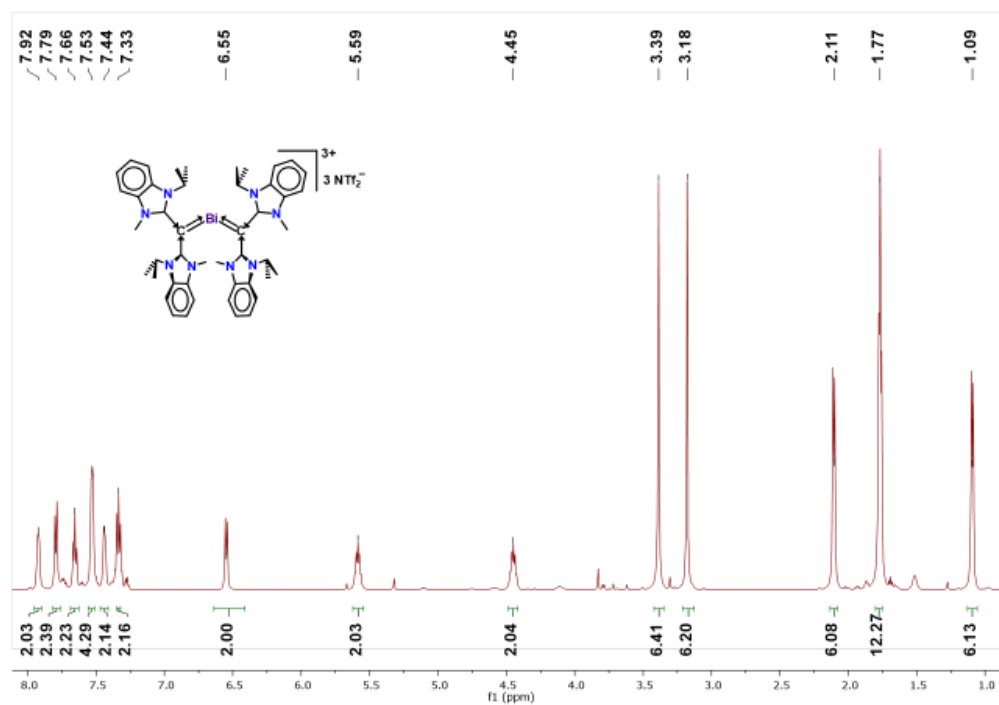


Figure A2S83.  $^1\text{H}$  NMR spectrum (800.13 MHz,  $\text{CD}_2\text{Cl}_2$ , 298 K) of compound 4.18.

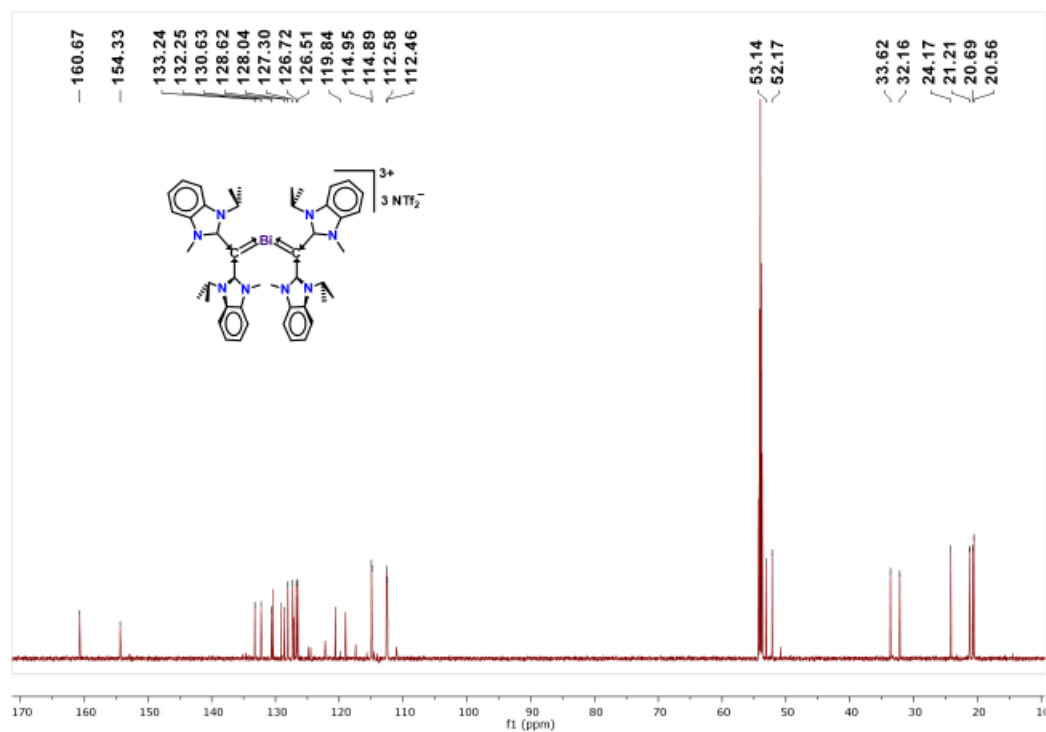
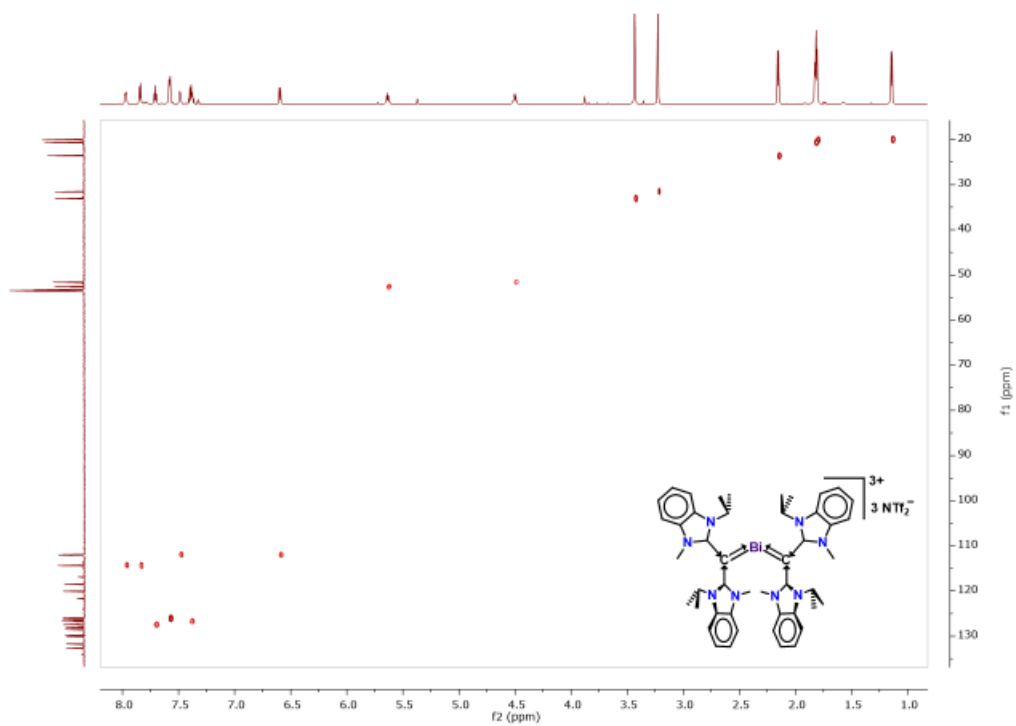
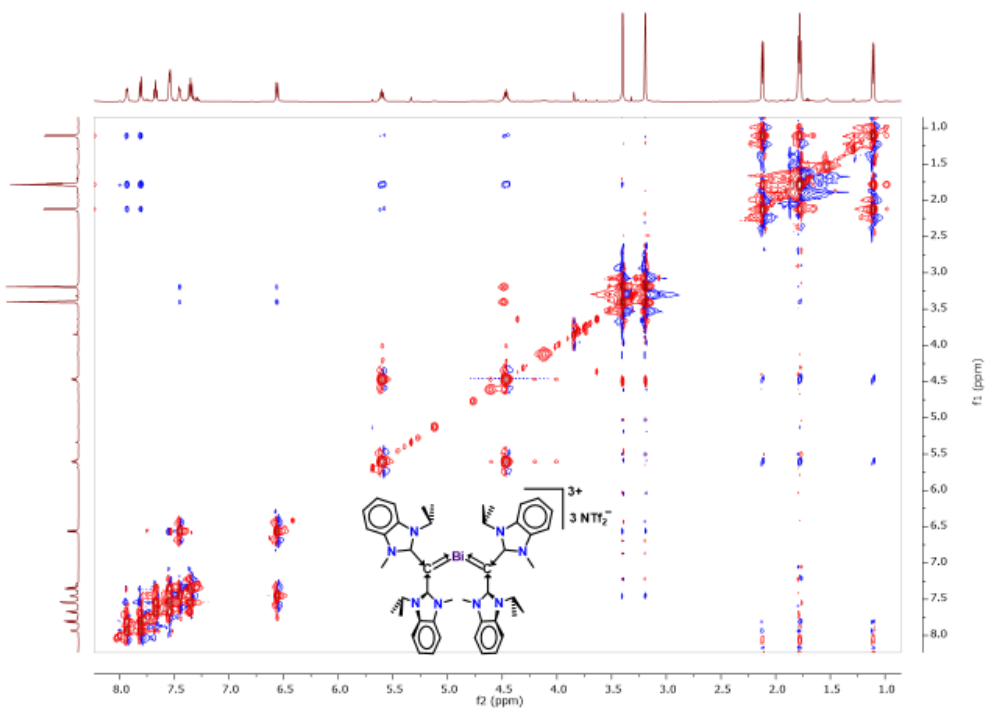


Figure A2S84.  $^{13}\text{C}$  NMR spectrum (201.19 MHz,  $\text{CD}_2\text{Cl}_2$ , 298 K) of compound 4.18.



**Figure A2S85.**  $^1\text{H}$ - $^{13}\text{C}$  HSQC 2D NMR spectrum of compound **4.18**.



**Figure A2S86.**  $^1\text{H}$ - $^1\text{H}$  NOESY 2D NMR spectrum of compound **4.18**.

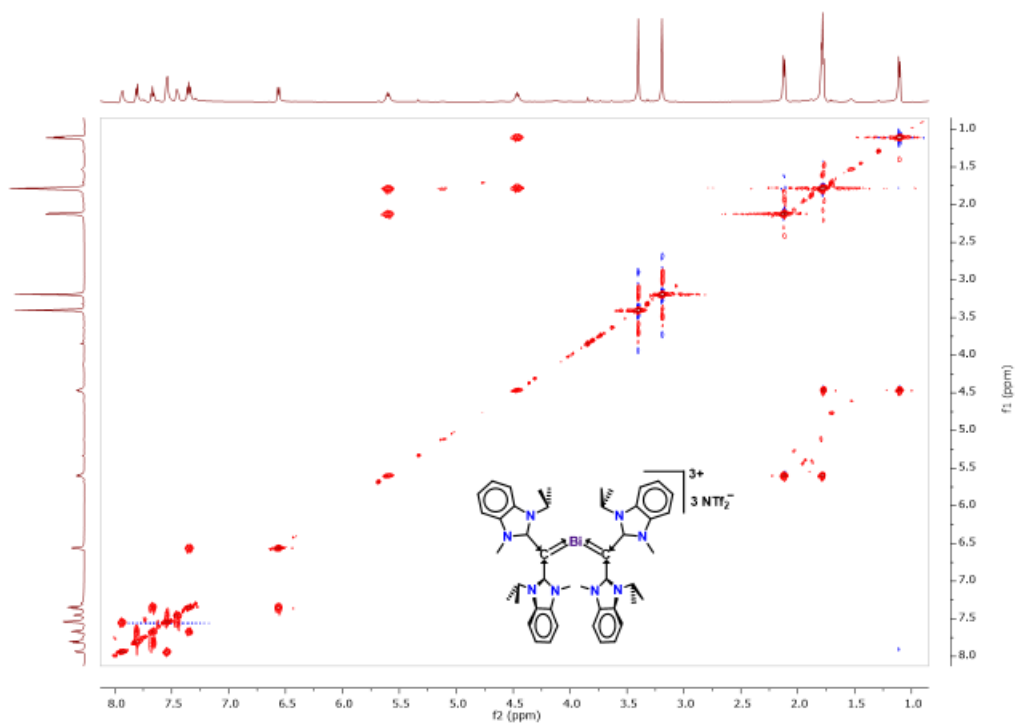


**Figure A2S87.**  $^1\text{H}$ - $^1\text{H}$  COSY 2D NMR spectrum of compound **4.18**.

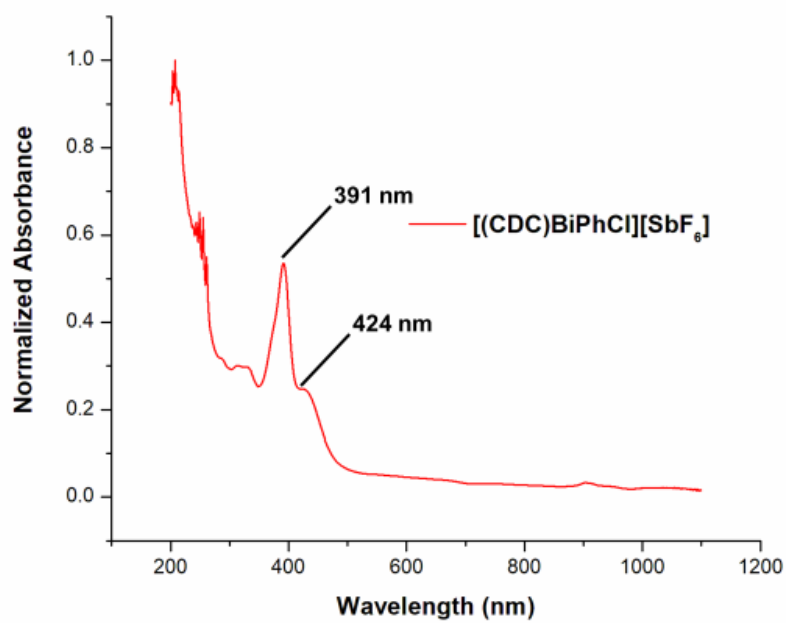


**Figure A2S88.** UV-Vis spectrum of compound **4.13**.

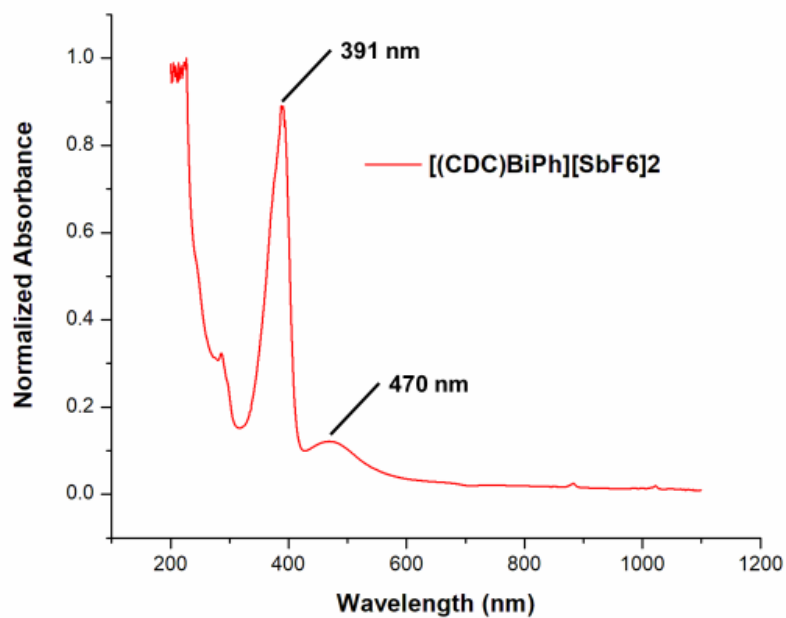


Figure A2S89. UV-Vis spectrum of compound 4.14.

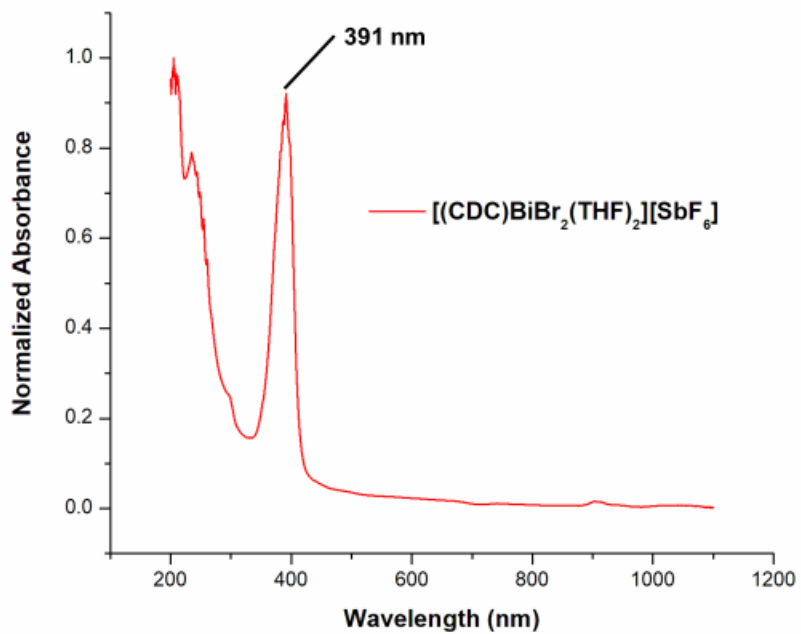
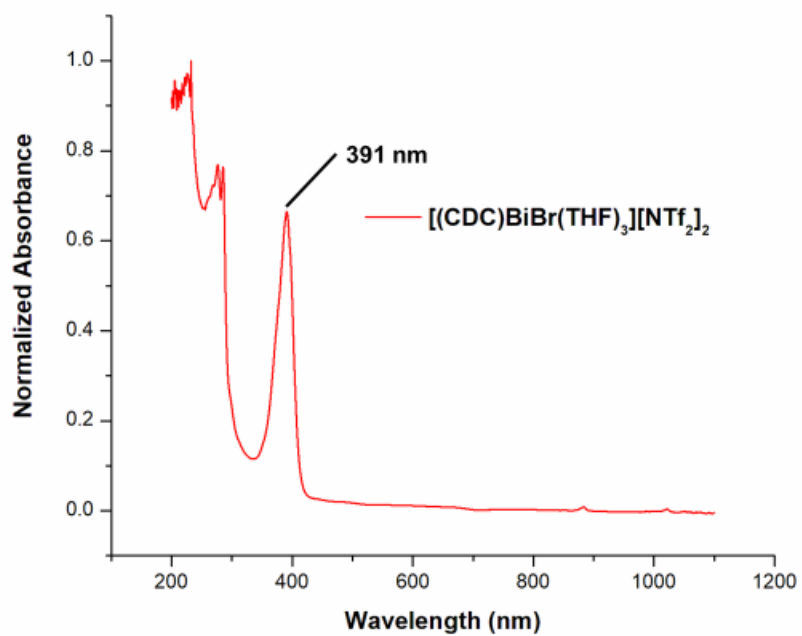
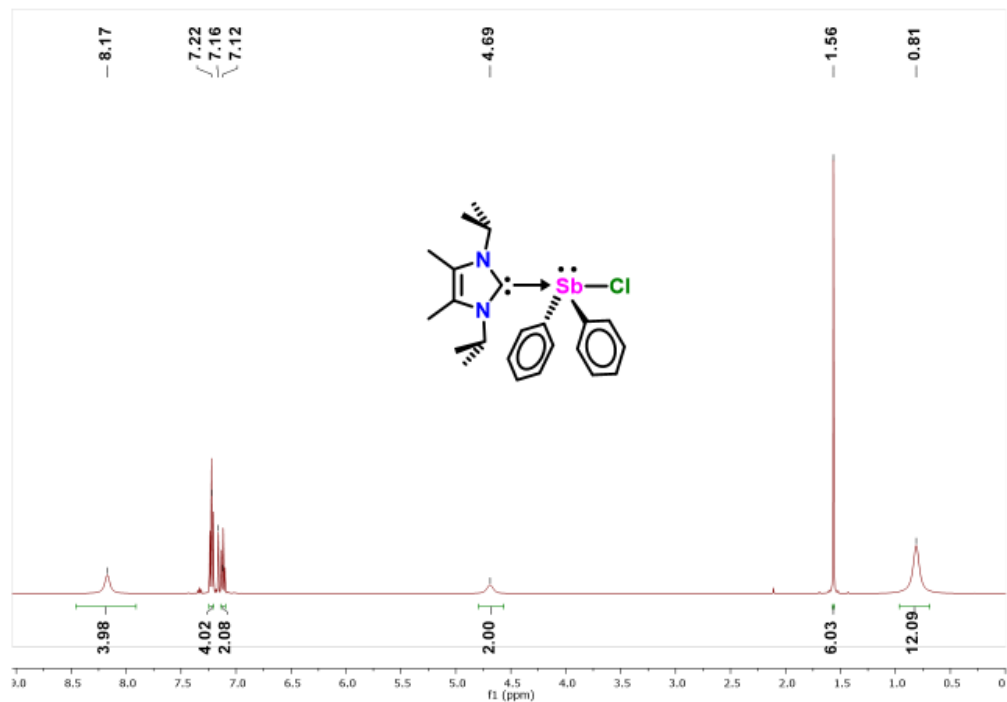


Figure A2S90. UV-Vis spectrum of compound 4.16.



**Figure A2S91.** UV-Vis spectrum of compound **4.17**.

## Chapter 5 Spectral Data



**Figure A2S92:**  $^1\text{H}$  NMR spectrum (500.13 MHz,  $\text{C}_6\text{D}_6$ , 298 K) of complex **5.1**.

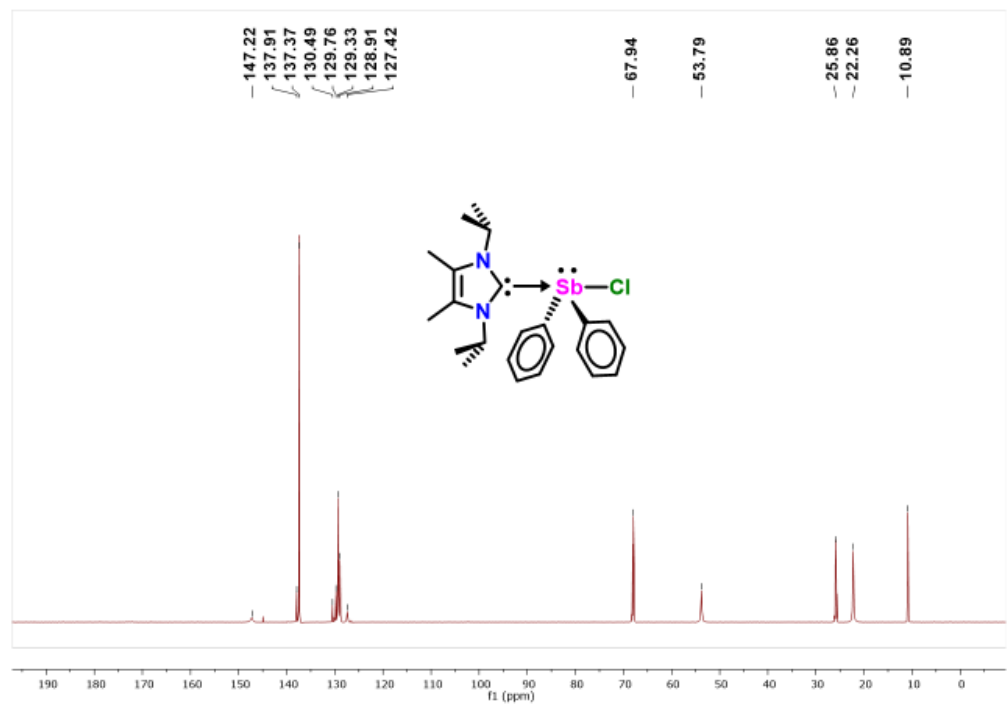


**Figure A2S93:**  $^{13}\text{C}\{^1\text{H}\}$  NMR spectrum (201.19 MHz,  $\text{C}_6\text{D}_6$ , 298 K) of complex **5.1**.

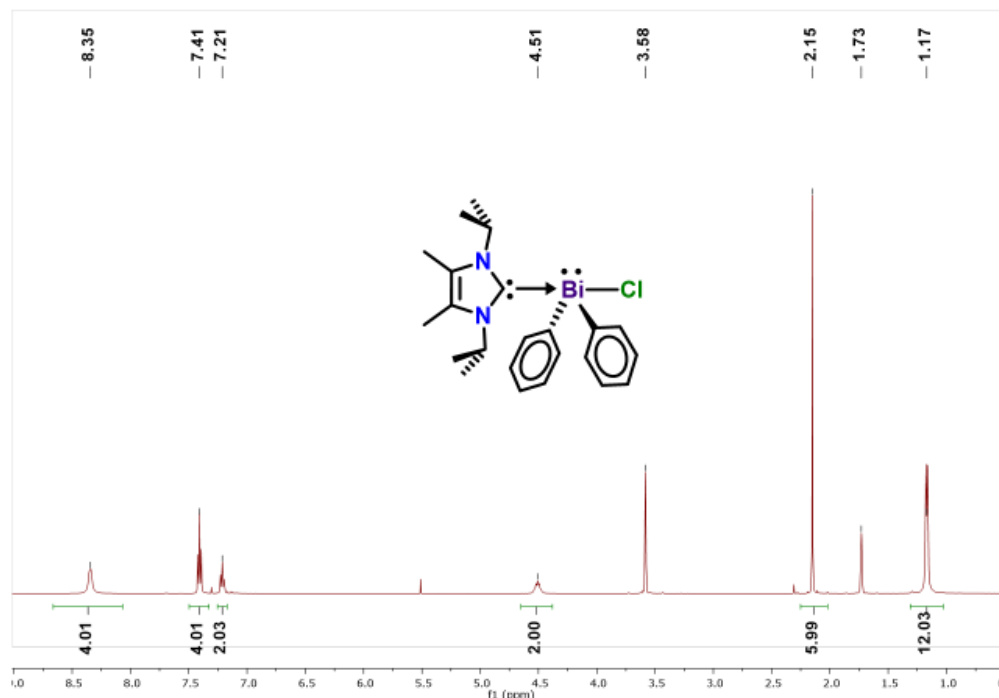


**Figure A2S94:**  $^1\text{H}$  NMR spectrum (500.13 MHz,  $\text{C}_6\text{D}_6$ , 298 K) of complex **5.2** (also identified as **4.6**).

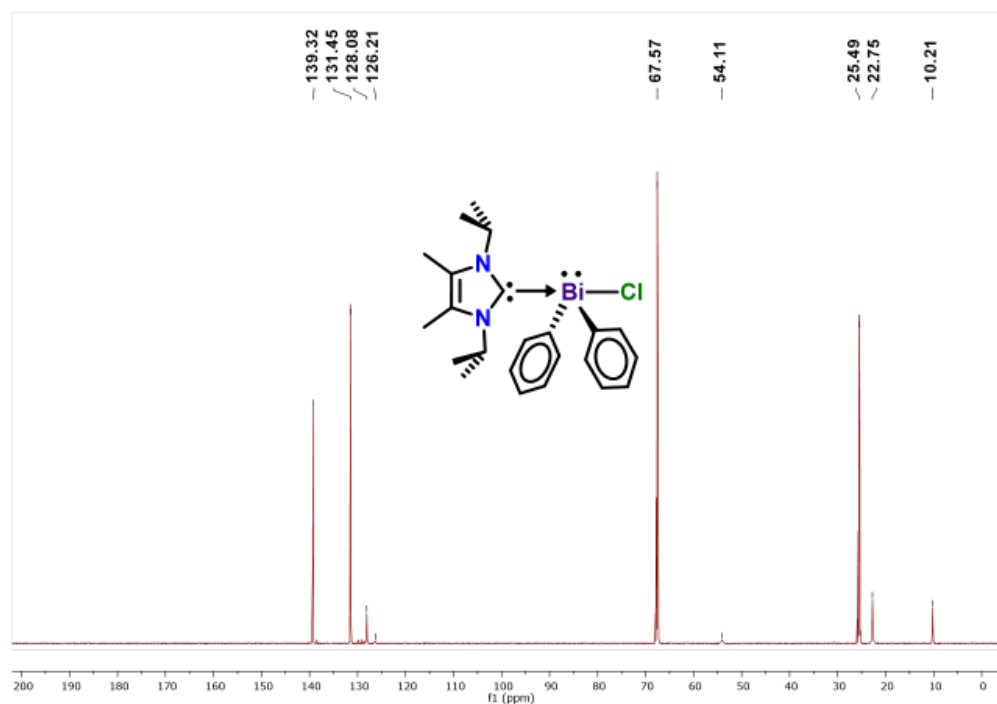


**Figure A2S95:**  $^{13}\text{C}\{^1\text{H}\}$  NMR spectrum (201.19 MHz,  $\text{C}_6\text{D}_6$ , 298 K) of complex **5.2** (also identified as **4.6**).

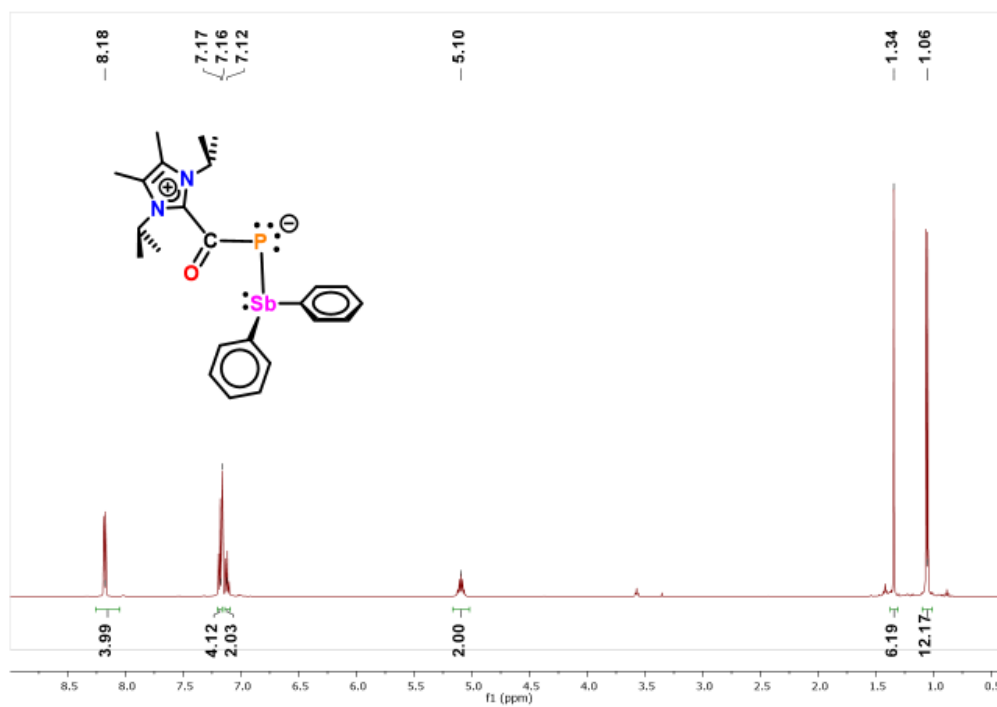


**Figure A2S96:**  $^1\text{H}$  NMR spectrum (500.13 MHz,  $\text{C}_6\text{D}_6$ , 298 K) of complex **5.3**.

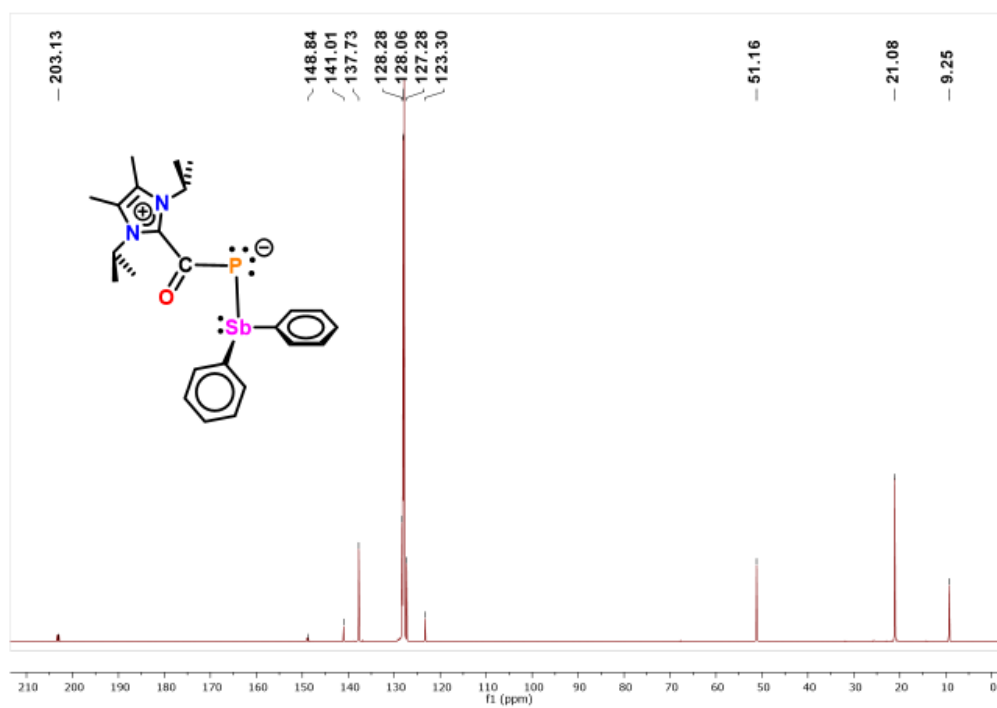


**Figure A2S97:**  $^{13}\text{C}\{^1\text{H}\}$  NMR spectrum (201.193 MHz,  $\text{C}_6\text{D}_6$ , 298 K) of complex **5.3**.

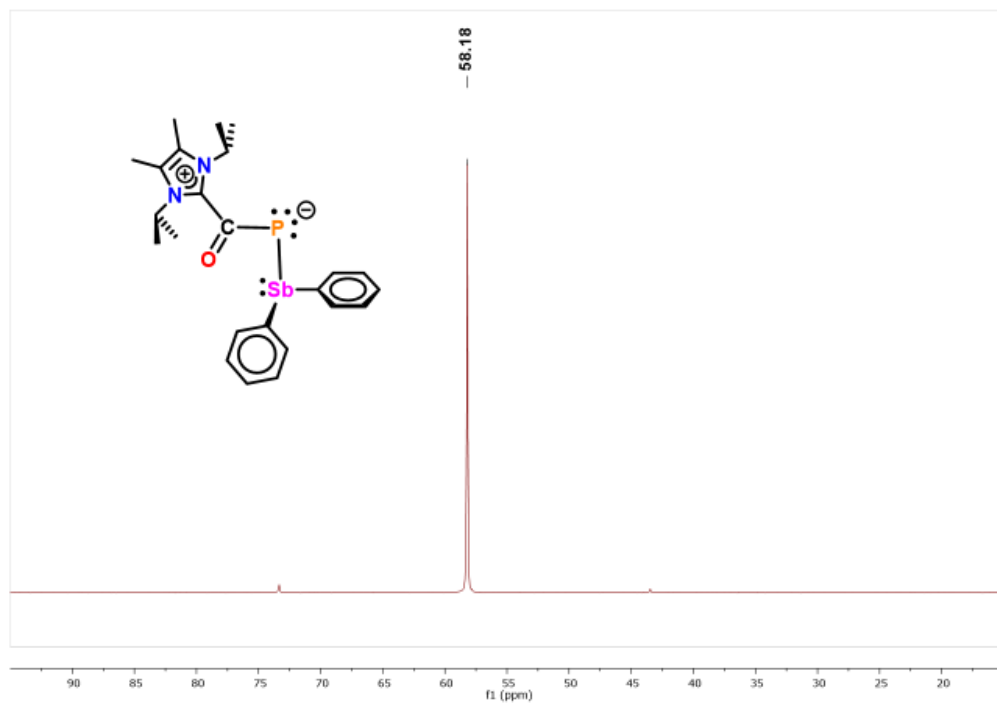


**Figure A2S98:**  $^{31}\text{P}\{^1\text{H}\}$  NMR spectrum (202.46 MHz, 298 K) of complex 5.3.

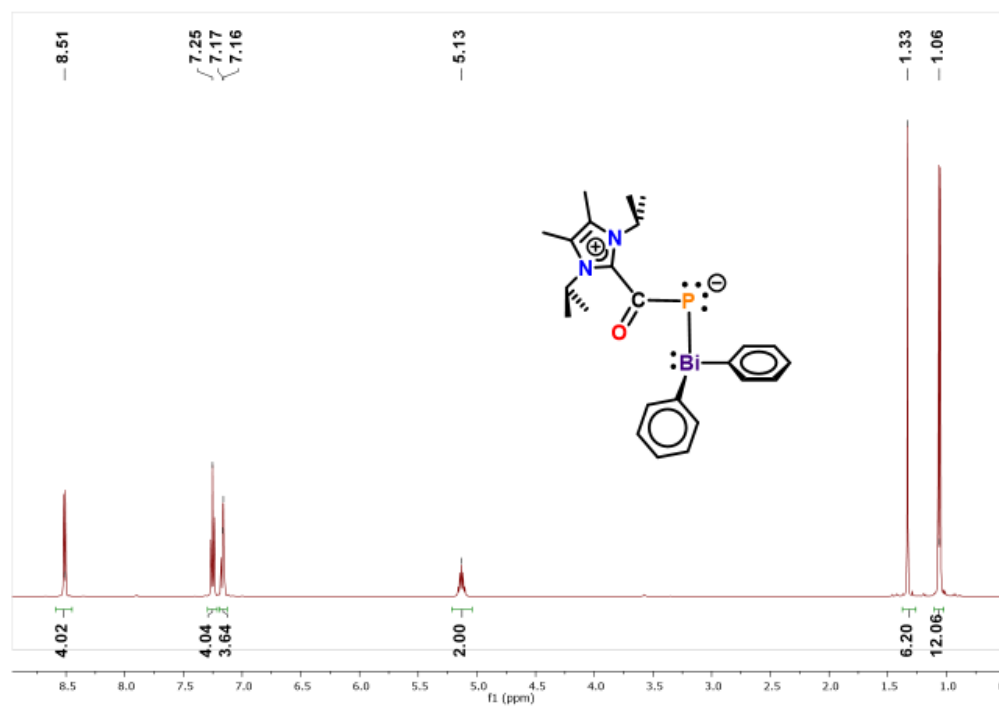


**Figure A2S99:**  $^1\text{H}$  NMR spectrum (500.13 MHz,  $\text{C}_6\text{D}_6$ , 298 K) of complex 5.4.

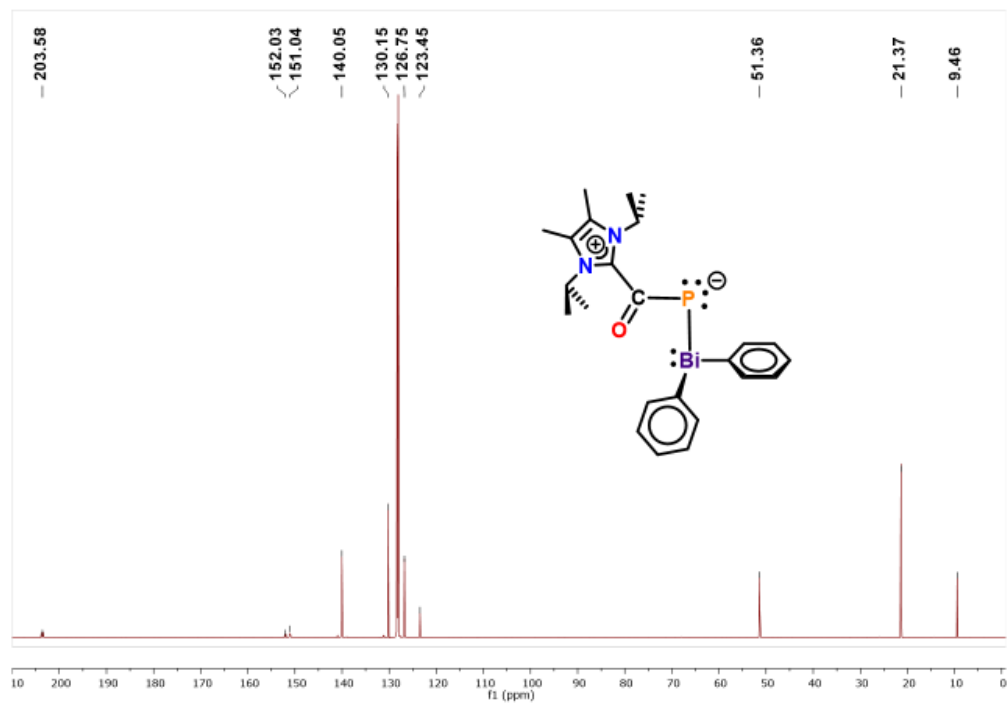


**Figure A2S100:**  $^{13}\text{C}\{^1\text{H}\}$  NMR spectrum (201.193 MHz,  $\text{C}_6\text{D}_6$ , 298 K) of complex **5.4**.

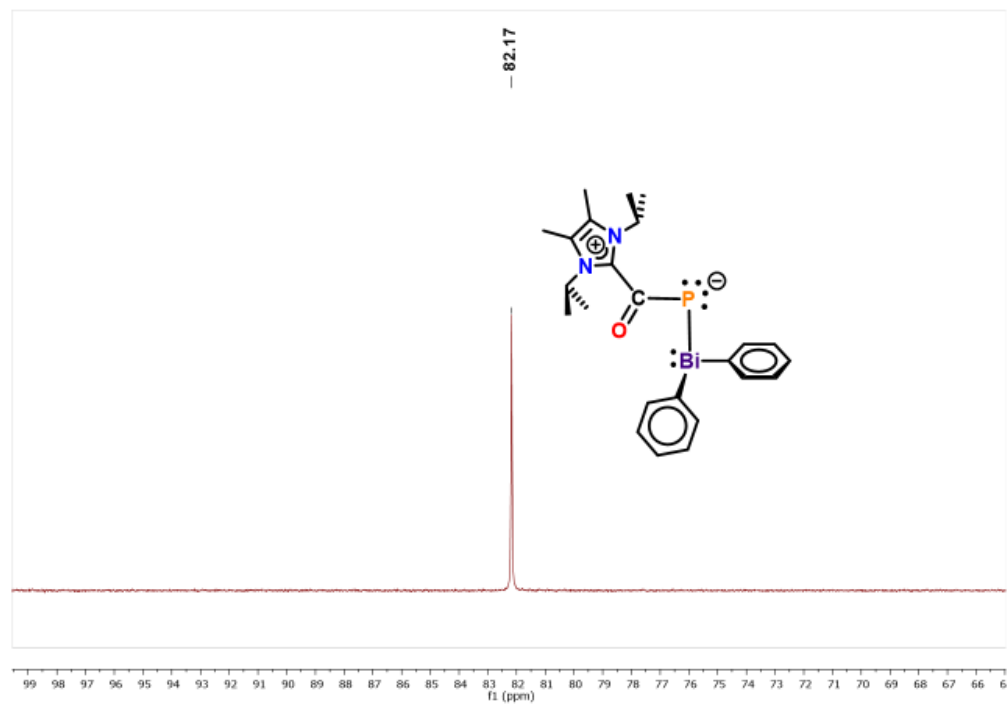


**Figure A2S101:**  $^{31}\text{P}\{^1\text{H}\}$  NMR spectrum (202.46 MHz, 298 K) of complex **5.4**.

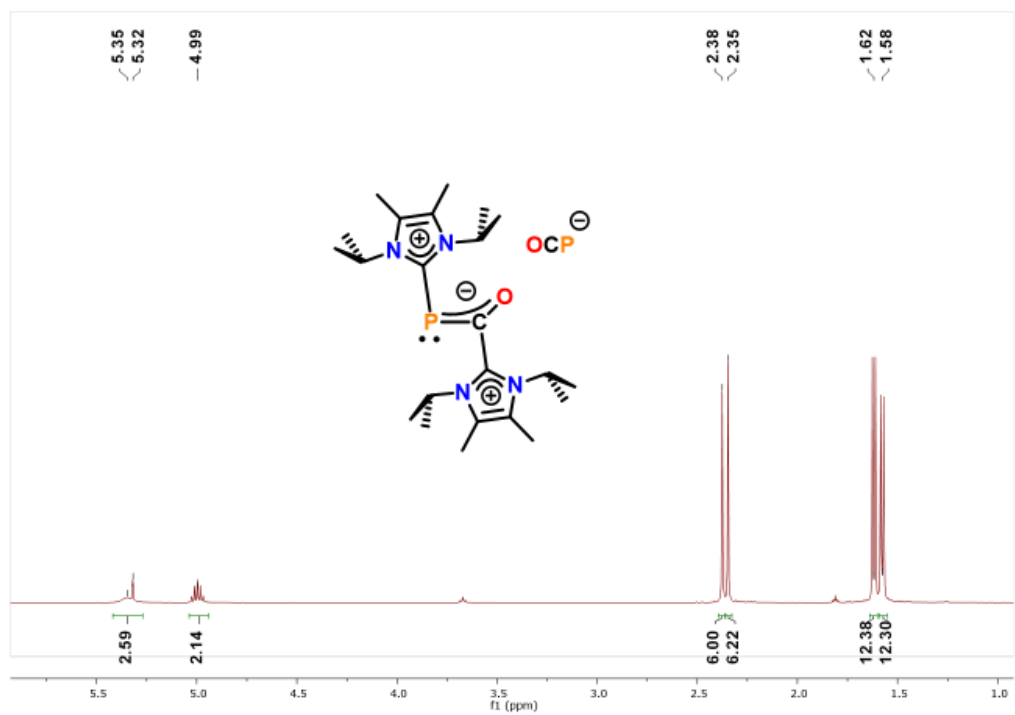


**Figure A2S102:**  $^1\text{H}$  NMR spectrum (500.13 MHz,  $\text{C}_6\text{D}_6$ , 298 K) of complex **5.5**.

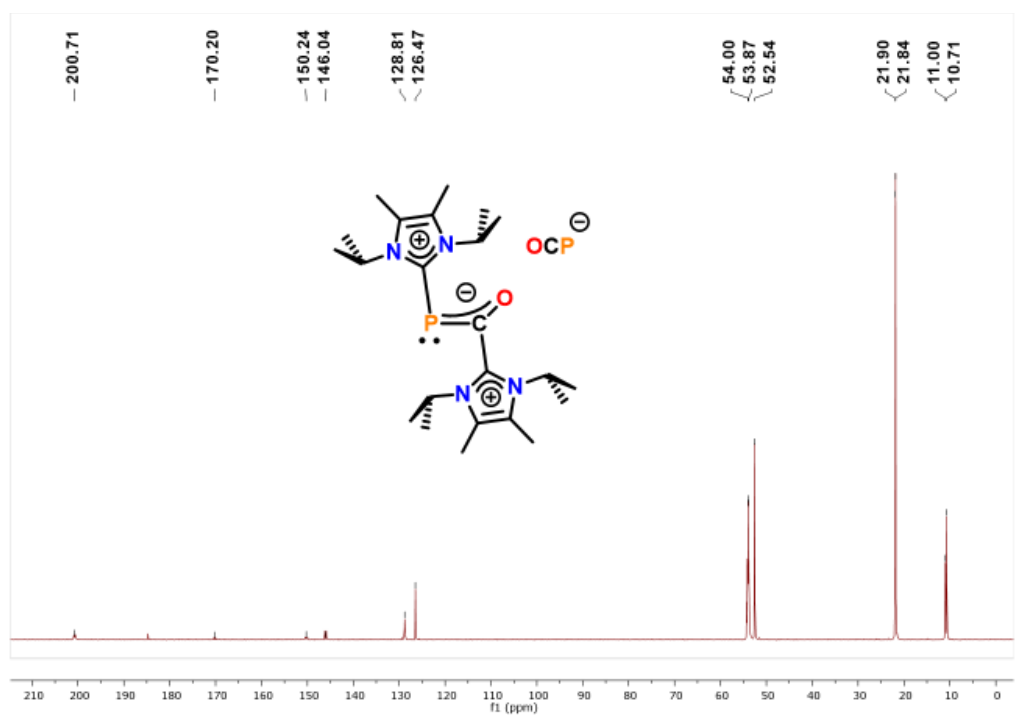


**Figure A2S103:**  $^{13}\text{C}\{^1\text{H}\}$  NMR spectrum (201.193 MHz,  $\text{C}_6\text{D}_6$ , 298 K) of complex **5.5**.

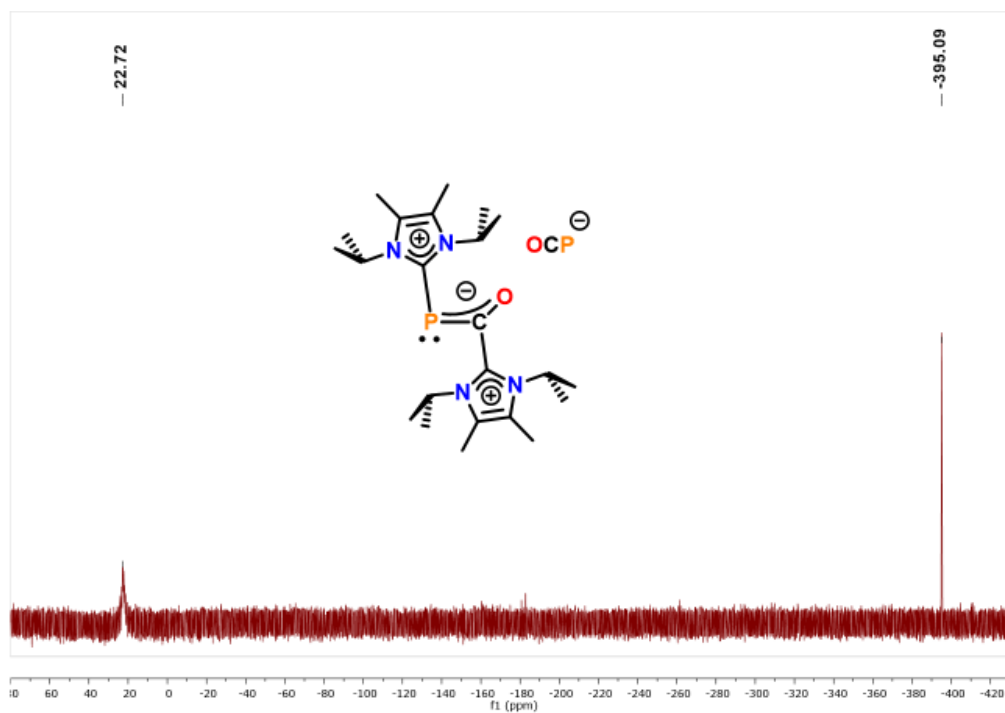


**Figure A2S104:** <sup>31</sup>P{<sup>1</sup>H} NMR spectrum (242.94 MHz, 298 K) of complex **5.5**.

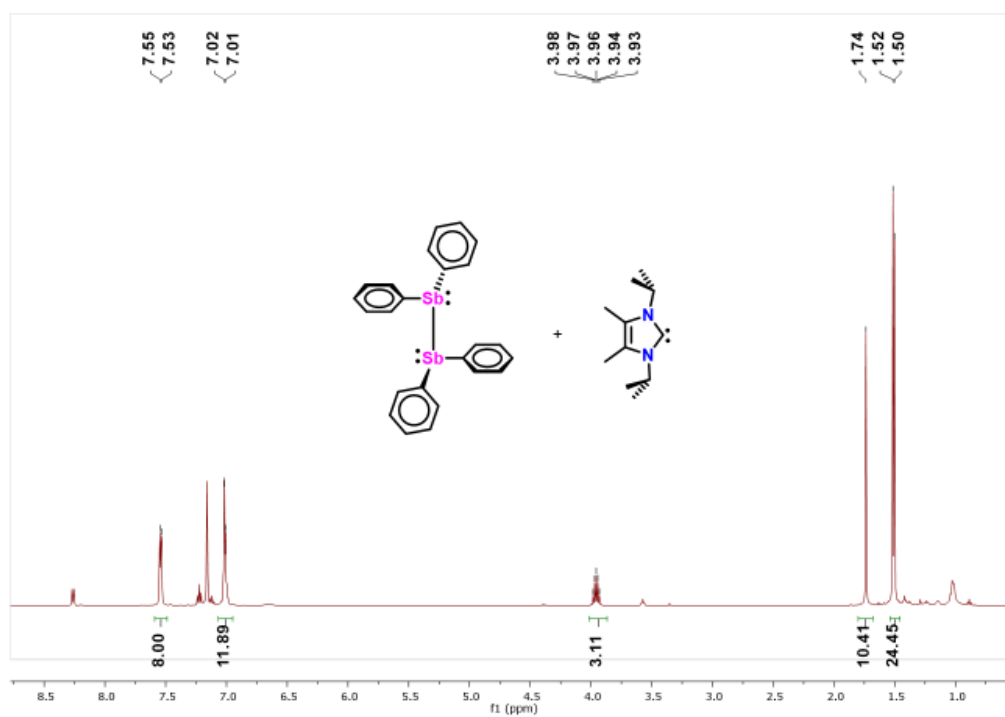


**Figure A2S105:** <sup>1</sup>H NMR spectrum (500.13 MHz, C<sub>6</sub>D<sub>6</sub>, 298 K) of the reaction mixture after heating compound **5.3** at 90 °C for 24 hours.

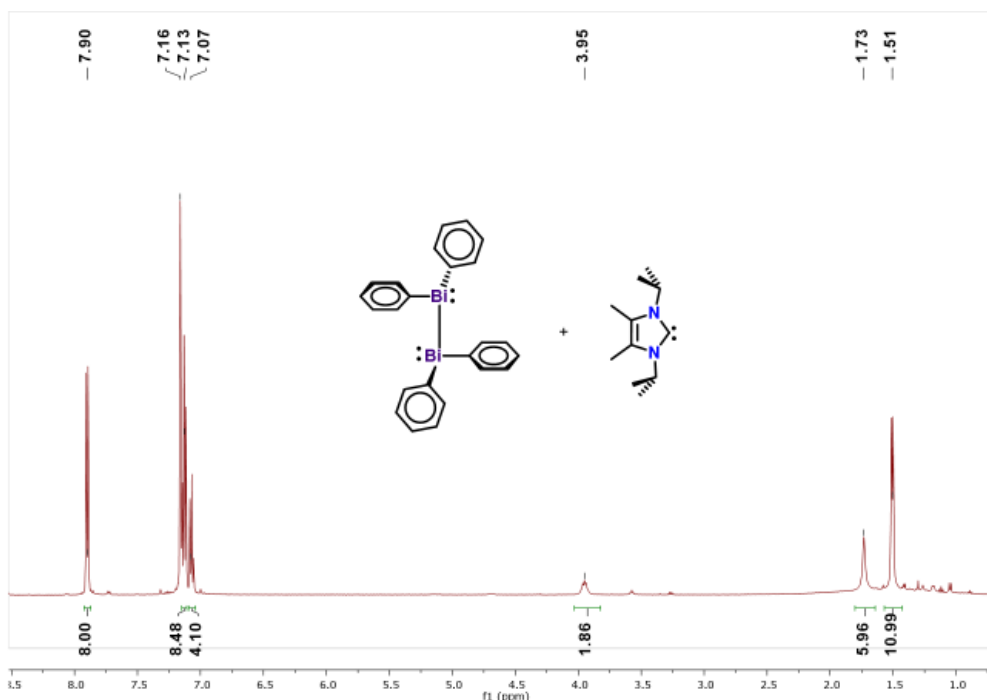


**Figure A2S106:**  $^1\text{H}$  NMR spectrum (500.13 MHz,  $\text{C}_6\text{D}_6$ , 298 K) of the reaction mixture after heating compound **5.4** at 70 °C for 3 hours.

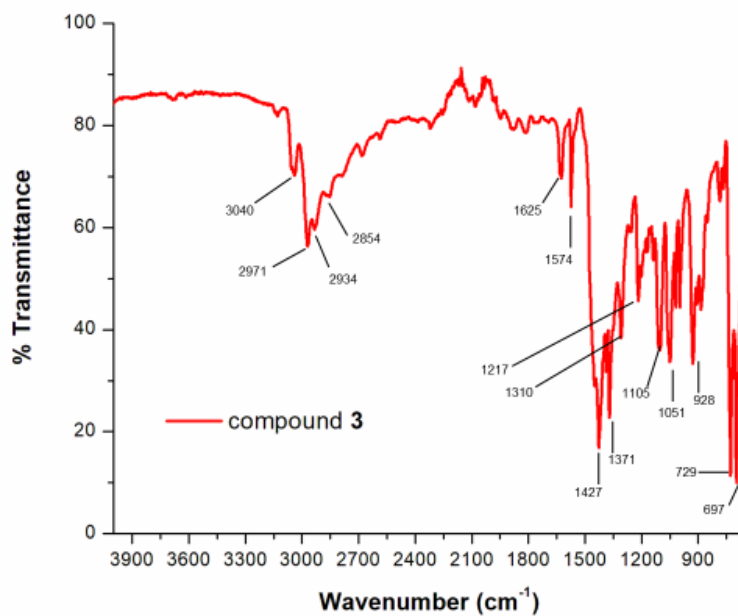


**Figure A2S107:** FT-IR Spectrum of compound **5.3**.

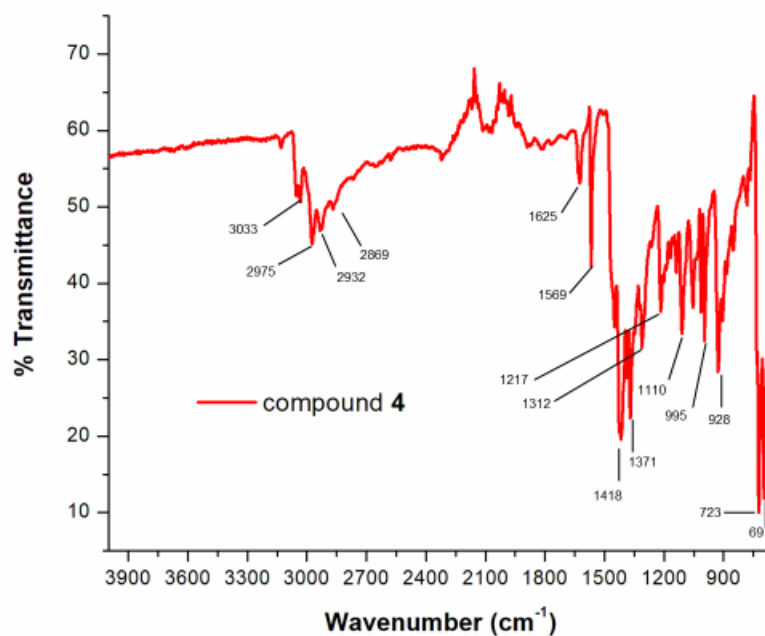


Figure A2S108: FT-IR Spectrum of compound 5.4.

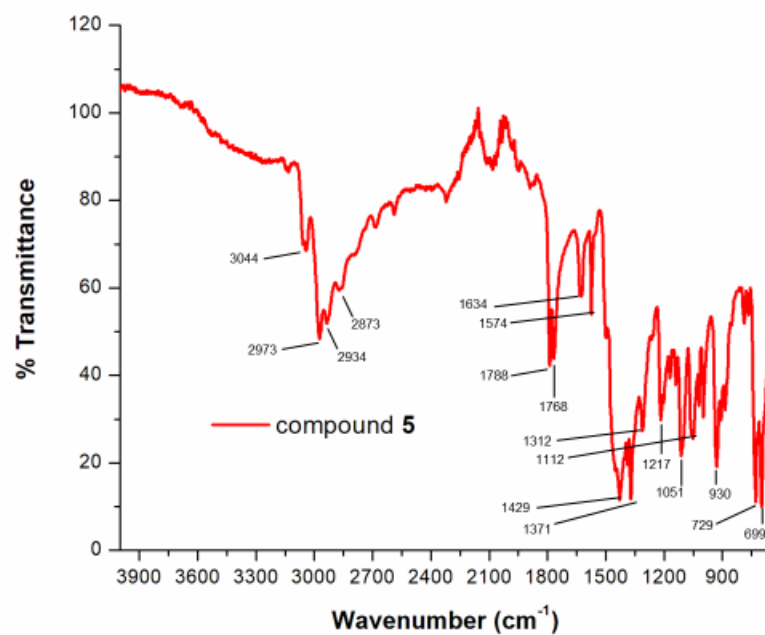
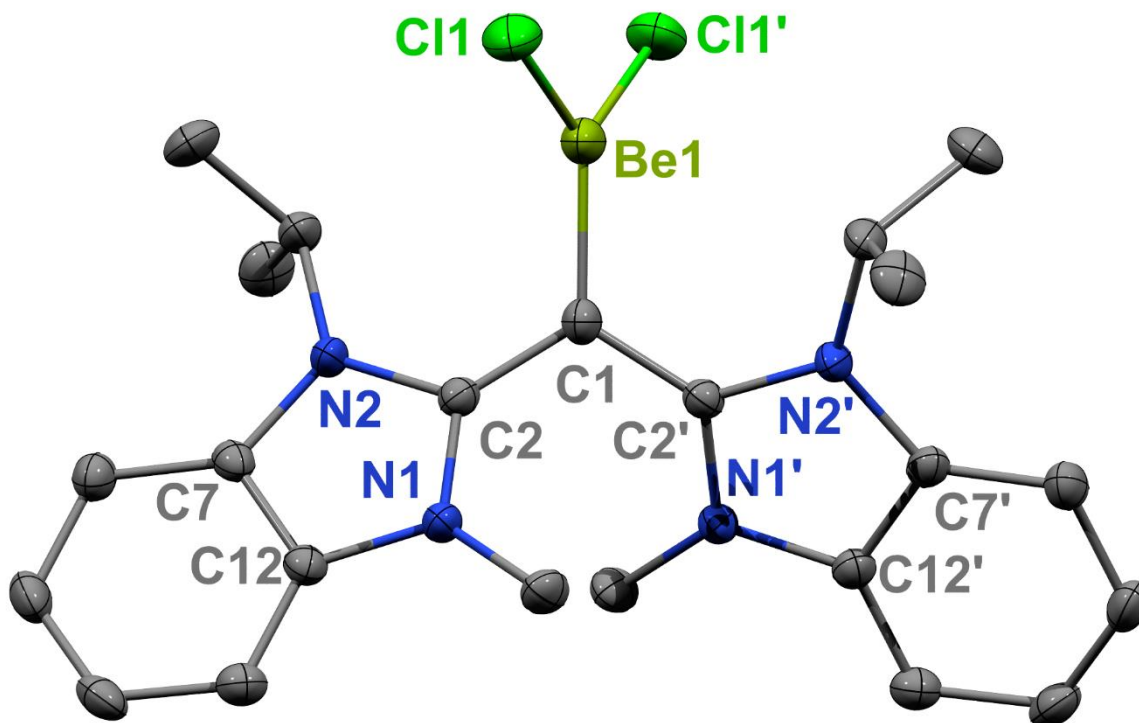


Figure A2S109: FT-IR Spectrum of compound 5.5.

## **Appendix 3: Crystallographic Data**

## Chapter 2 Crystal Structures



**Figure A3S1:** Molecular structure of **2.5** (thermal ellipsoids at 50% probability; H atoms omitted for clarity). Selected bond distances (Å) and angles (deg): Be1–C1: 1.748(6); Be1–Cl1: 1.941(3); N1–C2: 1.375(3); N2–C2: 1.383(3); C1–C2: 1.405(3). C1–Be1–Cl1': 121.39(13); Cl1–Be1–Cl1: 117.2(3). C2–C1–C2': 116.6(3); C2–C1–Be1: 121.72(16).

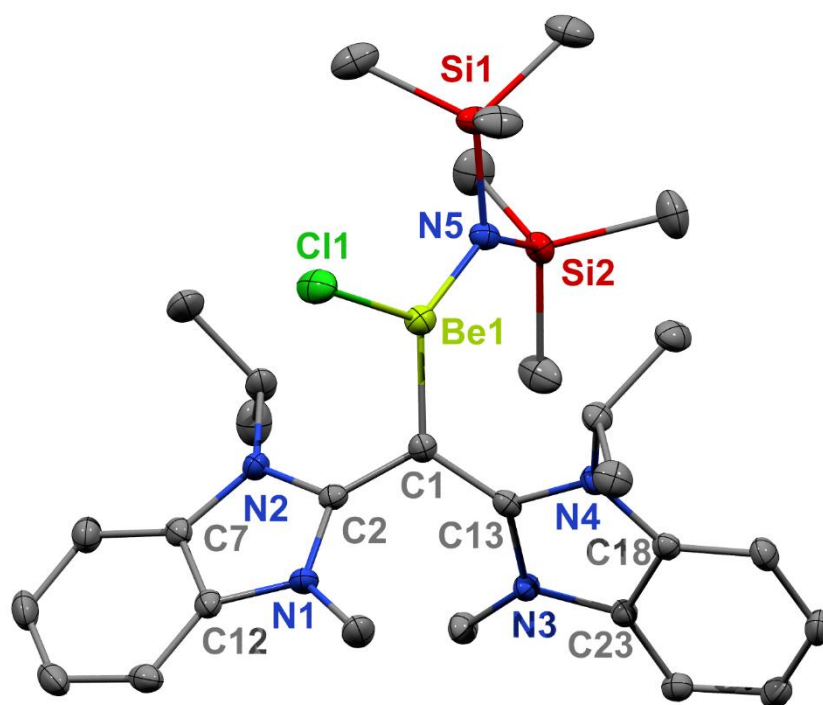


**Figure A3S2:** Molecular structure of **2.6** (thermal ellipsoids at 50% probability; H atoms and a non-coordinated toluene solvent omitted for clarity). Selected bond distances (Å) and angles (deg): N5–Be1: 1.605(2); Cl1–Be1: 1.996(2); C1–Be1: 1.766(3); C1–C2: 1.409(2); C1–C13: 1.385(2); N2–C2: 1.372(2); N1–C2: 1.372(2); N4–C13: 1.391(2); N3–C13: 1.3867(19). C13–C1–C2: 117.60(14); C13–C1–Be1: 124.09(14); C2–C1–Be1: 118.29(13); N5–Be1–C1: 129.51(14); N5–Be1–Cl1: 120.77(13); C1–Be1–Cl1: 109.71(12).

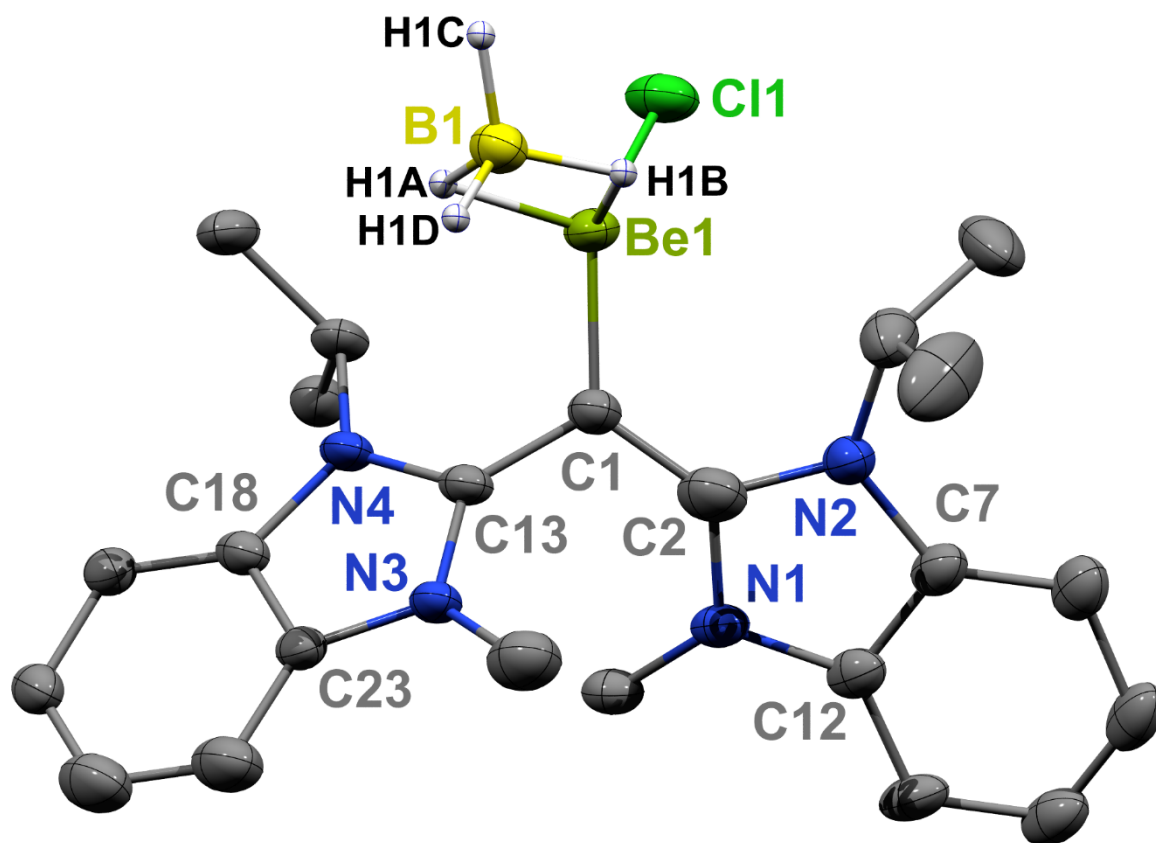


**Figure A3S3:** Molecular structure of **2.7**. Displacement ellipsoids at 30% probability; H atoms (except B–H) and non-coordinating solvent omitted for clarity. Selected bond distances (Å) and angles (deg): Be1–Cl1: 1.933(5); Be1–C1: 1.750(6); C1–C2: 1.388(5); C2–N1: 1.386(5); N1–C3: 1.443(5); C1–C13: 1.414(5). C1–Be1–H1A: 109.7(12); C1–Be1–H1B: 118.0(15); C1–Be1–Cl1: 123.6(3); C2–C1–C13: 115.0(3).

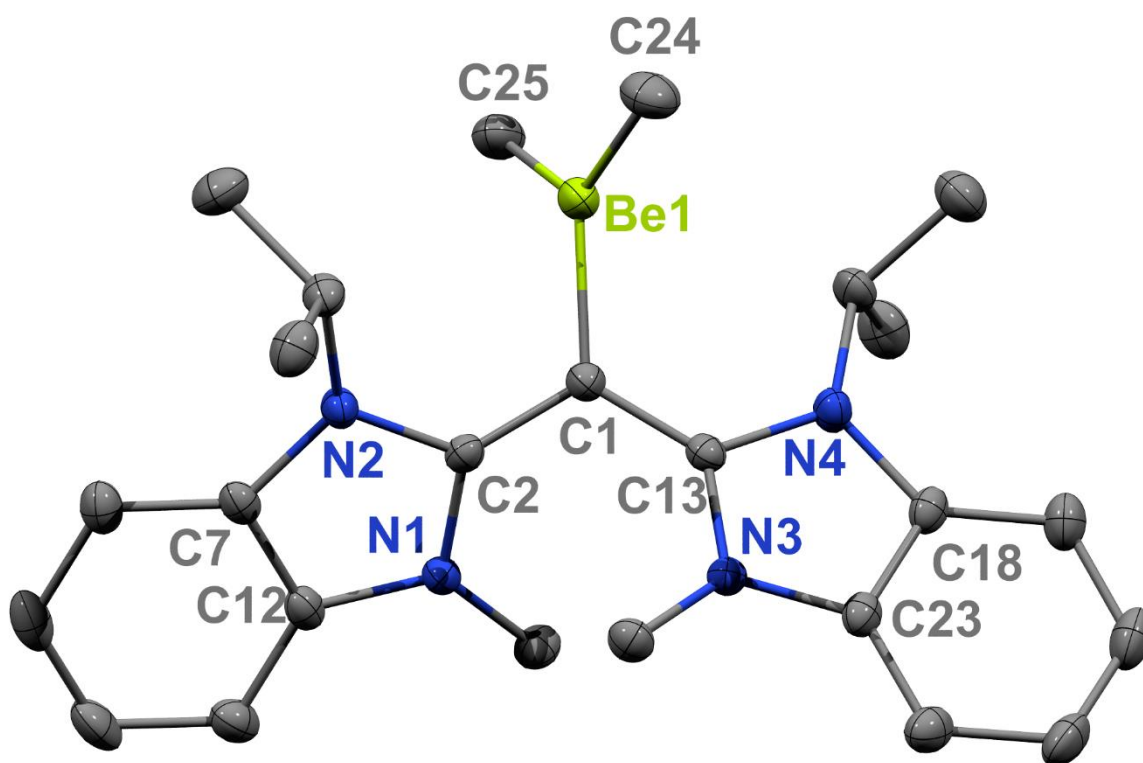


**Figure A3S4:** Molecular structure of **2.8** (thermal ellipsoids at 50% probability; H atoms and a non-coordinated toluene solvent were omitted for clarity). Selected bond distances (Å) and angles (deg): Be1–C25: 1.756(3); Be1–C24: 1.758(3); Be1–C1: 1.817(2); C1–C2: 1.3949(19); C1–C13: 1.386(2); N1–C2: 1.3801(18); N2–C2: 1.3842(18); N3–C13: 1.3834(18); N4–C13: 1.3949(19). C25–Be1–C24: 124.18(14); C25–Be1–C1: 116.04(13); C24–Be1–C1: 119.78(14).

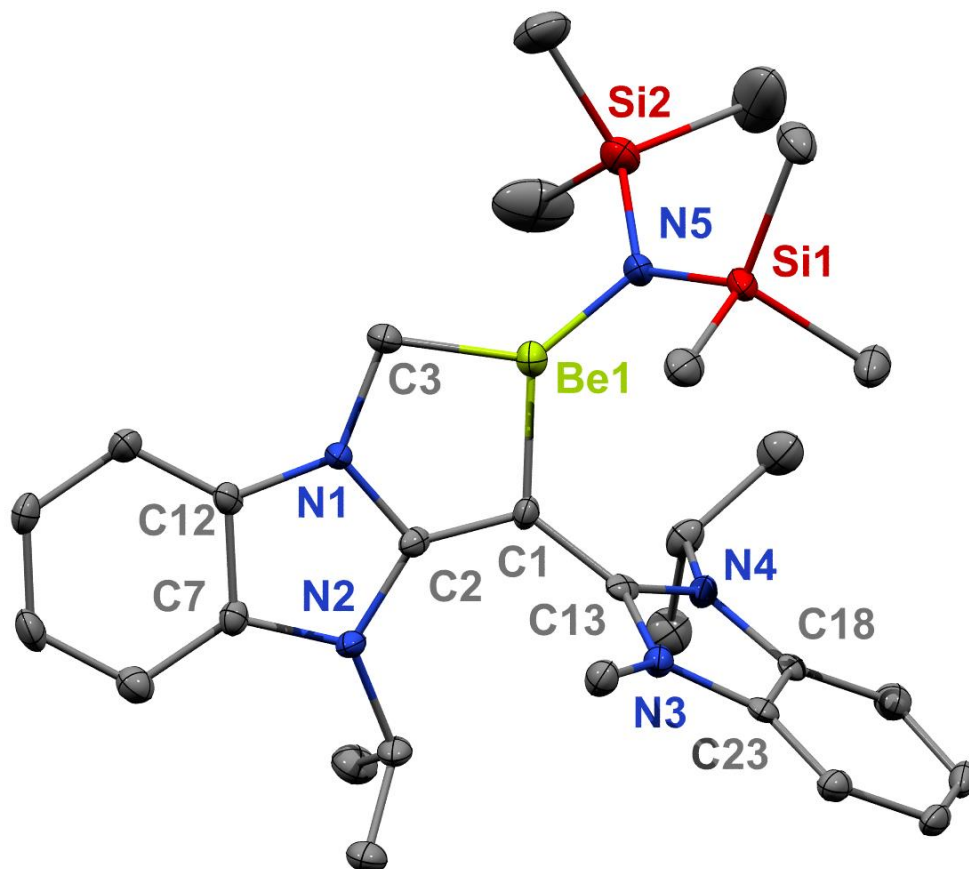


**Figure A3S5:** Molecular structure of **2.9** (thermal ellipsoids at 50% probability; H atoms and co-crystallized  $\text{K}[\text{N}(\text{SiMe}_3)_2] \cdot 0.5\text{toluene}$  omitted for clarity). Selected bond distances ( $\text{\AA}$ ) and angles (deg): N5–Be1: 1.615(5); C1–C2: 1.373(4); C1–C13: 1.412(4); C1–Be1: 1.796(5); C3–Be1: 1.790(5); N1–C2: 1.374(4); N1–C3: 1.462(4); N2–C2: 1.395(4); N3–C14: 1.460(4); N4–C13: 1.366(4). N5–Be1–C3: 131.3(3); N5–Be1–C1: 131.0(3); C3–Be1–C1: 97.4(3); C2–C1–C13: 126.7(3); C2–C1–Be1: 104.7(3).

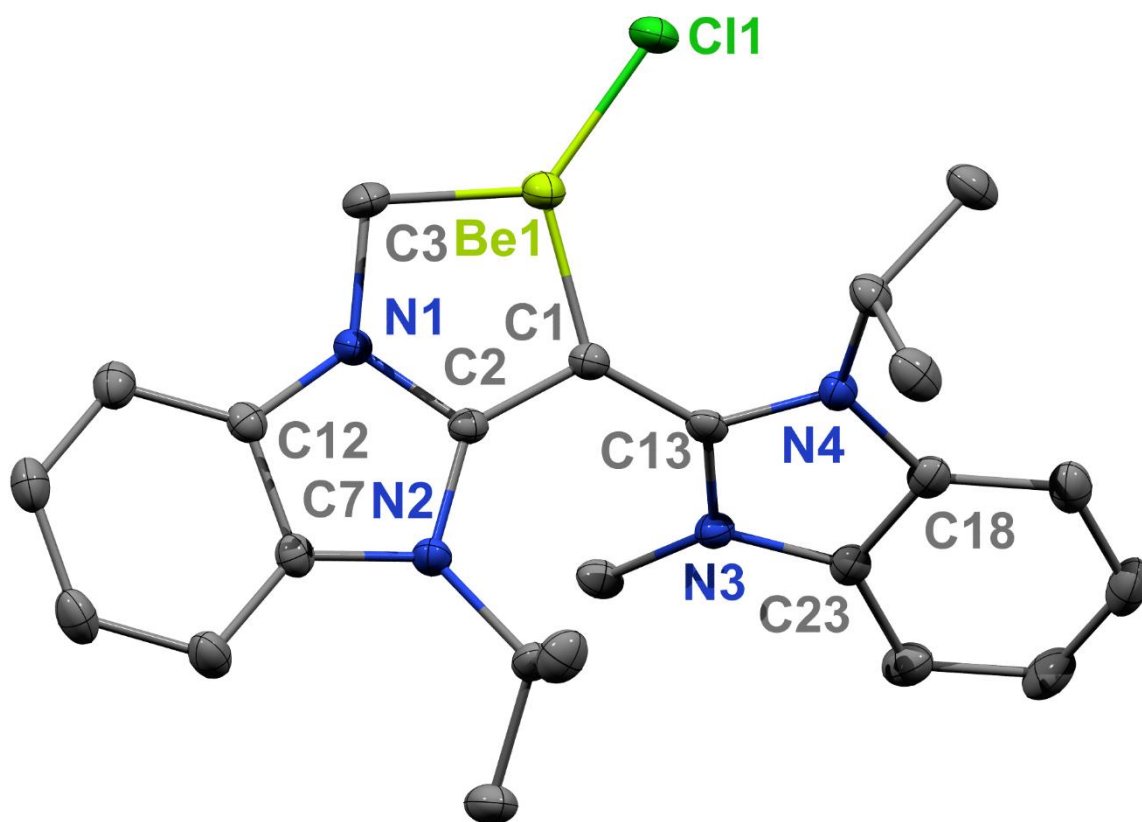


**Figure A3S6:** Molecular structure of **2.10** (thermal ellipsoids at 50% probability; H atoms and noncoordinating solvent omitted for clarity). Selected bond distances (Å) and angles (deg): Be1–Cl1: 1.916(2); Be1–C1: 1.743(3); C1–C2: 1.391(2); C2–N1: 1.378(2); N1–C3: 1.471(2); Be1–C3: 1.769(3); C1–C13: 1.403(2). C1–Be1–C3: 101.01(14); C1–Be1–Cl1: 129.41(14); C3–Be1–Cl1: 129.56(14); C2–C1–C13: 125.28(15) C2–C1–Be1: 103.55(14).

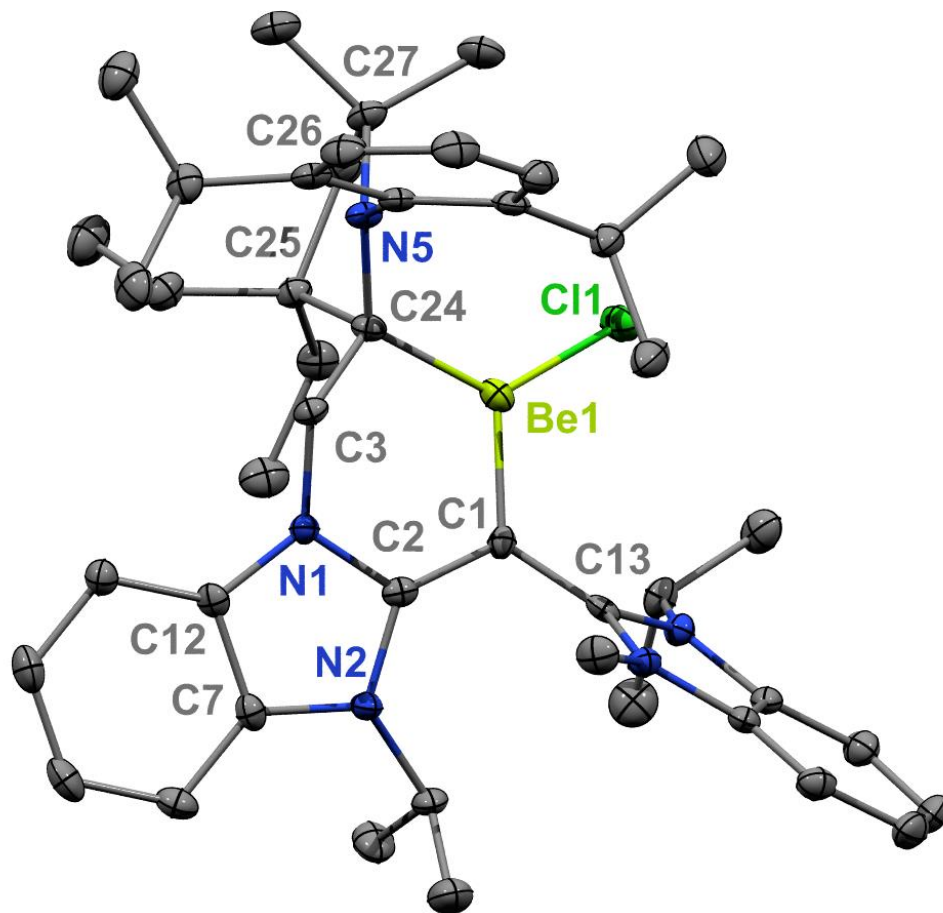


**Figure A3S7:** Molecular structure of **2.11** (thermal ellipsoids at 50% probability; H atoms omitted for clarity). Selected bond distances (Å) and angles (deg): Be1–Cl1: 1.973(3); Be1–C1: 1.754(3); C1–C2: 1.387(3); C2–N1: 1.392(2); N1–C3: 1.467(2); C3–C24: 1.531(3); Be1–C24: 1.791(3); C1–C13: 1.428(3). C1–Be1–C24: 114.46(17); C1–Be1–Cl1: 119.13(16); C24–Be1–Cl1: 126.13(16); C2–C1–C13: 118.63(17); C2–C1–Be1: 115.70(18).

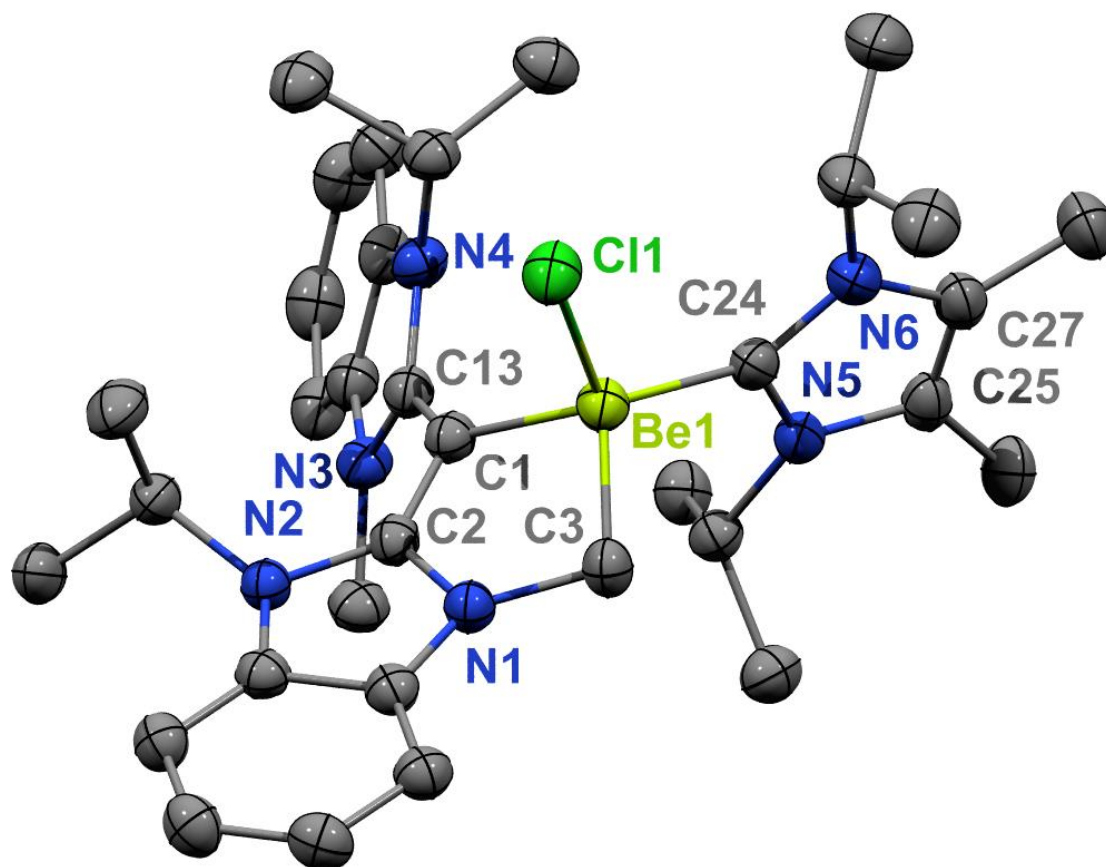


**Figure A3S8:** Molecular structure of **2.12** (thermal ellipsoids at 50% probability; H atoms omitted for clarity). Selected bond distances (Å) and angles (deg): Be1–Cl1: 2.084(3); Be1–C24: 1.856(4); Be1–C1: 1.862(4); C1–C2: 1.387(3); C2–N1: 1.361(3); N1–C3: 1.474(3); Be1–C3: 1.833(4); C1–C13: 1.373(3). C1–Be1–C3: 94.65(17); C1–Be1–Cl1: 106.38(15); C3–Be1–Cl1: 106.89(16); C3–Be1–C24: 113.08(18); C24–Be1–C1: 118.46(19); C24–Be1–Cl1: 115.07(16); C2–C1–C13: 125.3(2).

## Chapter 3 Crystal Structures

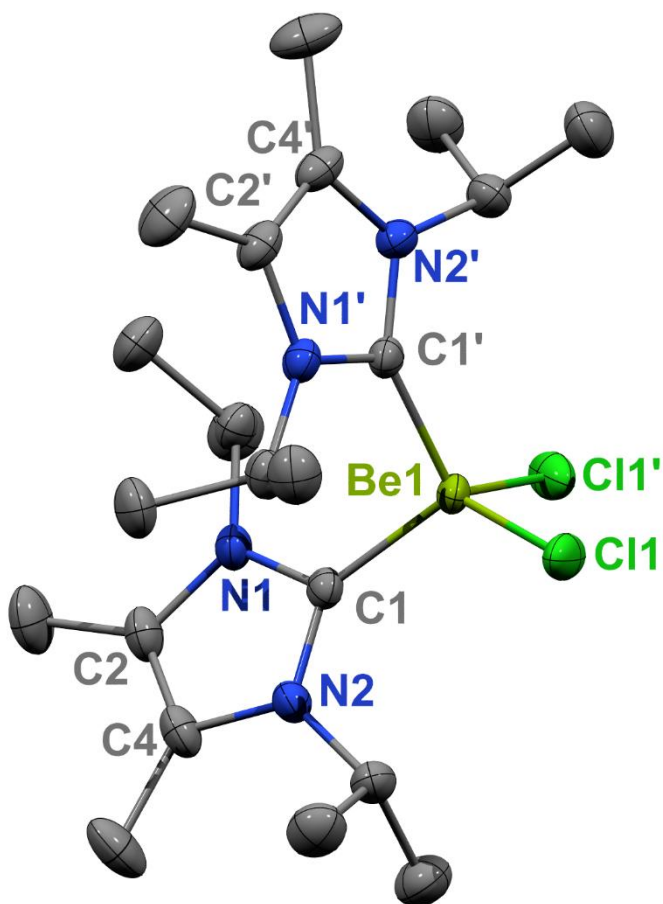


**Figure A3S9:** Molecular structure of **3.19** (thermal ellipsoids at 50% probability; H atoms and toluene solvent molecules omitted for clarity). Selected bond distances (Å) and angles (deg): Cl1–Be1: 2.0445(19); C1–Be1: 1.849(3); N1–C1: 1.367(2); N1–C2: 1.397(2); C2–C4: 1.354(3); N2–C4: 1.397(2); N2–C1: 1.357(2). N2–C1–Be1: 132.29(14); N1–C1–Be1: 123.10(14); C1–Be1–Cl1: 105.37(19); C1–Be1–Cl1': 118.13(6); Cl1–Be1–Cl1': 103.79(6).

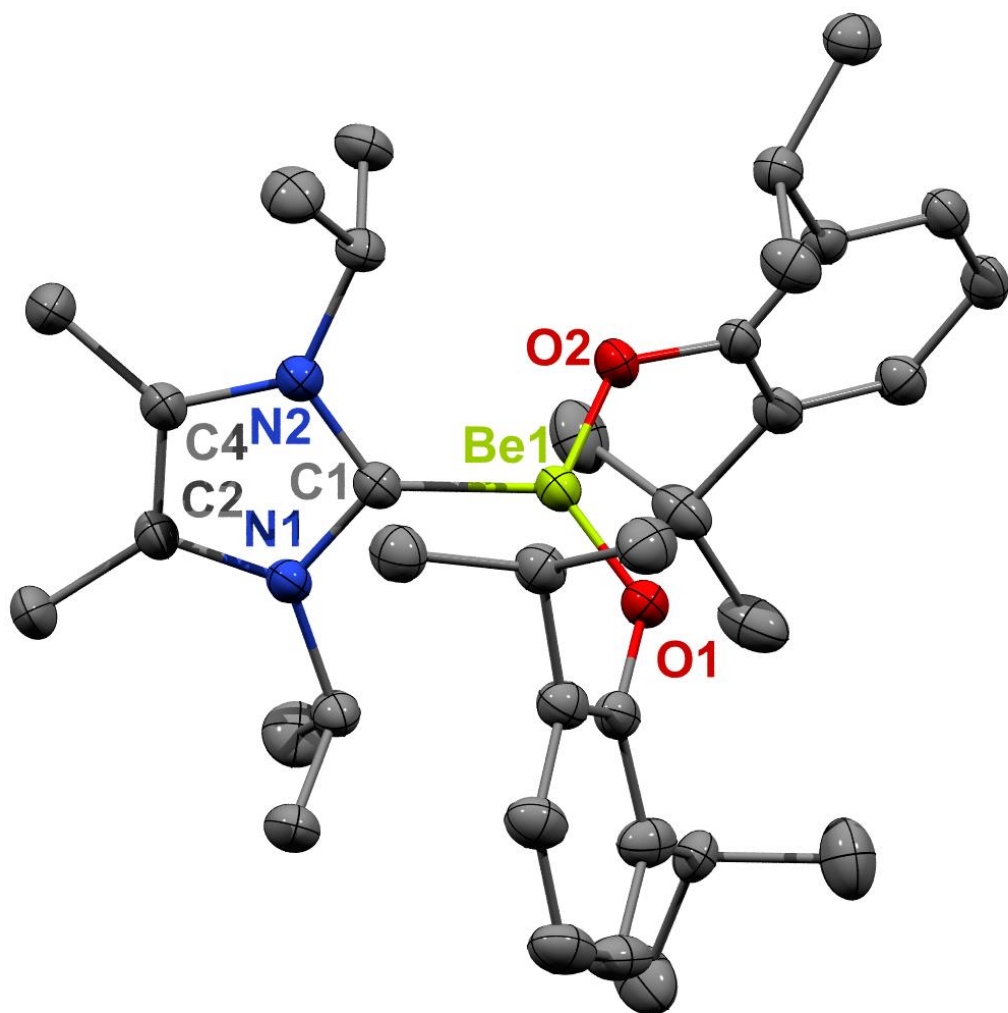


**Figure A3S10:** Molecular structure of **3.20** (thermal ellipsoids at 50% probability; H atoms omitted for clarity). Selected bond distances (Å) and angles (deg): Be1–O2: 1.497(3); Be1–O1: 1.507(3); Be1–C1: 1.797(3); N1–C2: 1.393(2); N1–C1: 1.353(2); N1–C2: 1.359(2); N2–C4: 1.391(2); C2–C4: 1.362(3). O2–Be1–O1: 122.34(17); O2–Be1–C1: 112.66(15); O1–Be1–C1: 124.99(17).

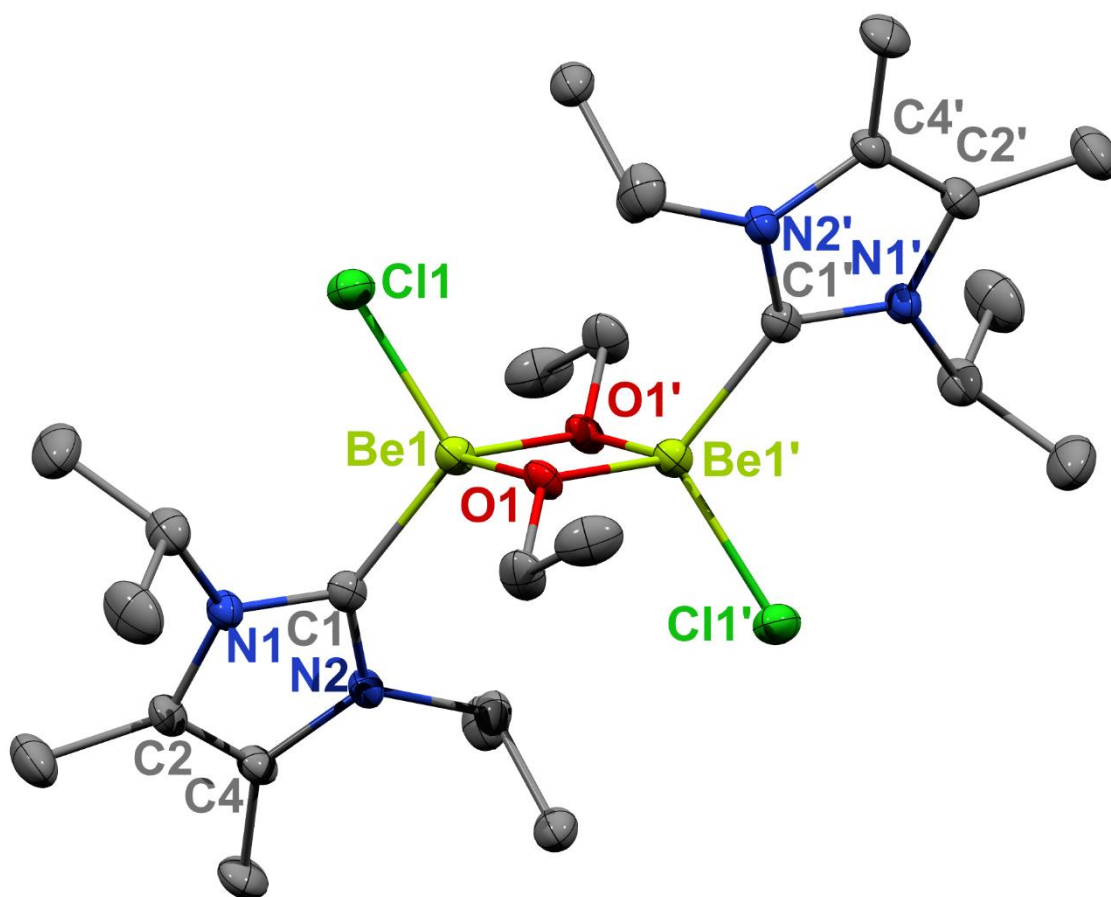


**Figure A3S11:** Molecular structure of **3.21** (thermal ellipsoids at 50% probability; H atoms omitted for clarity). Selected bond distances (Å) and angles (deg): Be1–O1: 1.621(4); Be1–O1: 1.641(4); Be1–C1: 1.855(4); Be1–Cl1: 2.044(3); N1–C1: 1.362(3); N1–C2: 1.391(3); 1.362(3); N2–C4: 1.393(3); C2–C4: 1.355(4). O1–Be1–O1: 89.99(18); O1–Be1–C1: 113.9(2); O1–Be1–C1: 119.0(2); C1–Be1–Cl1: 109.11(18).

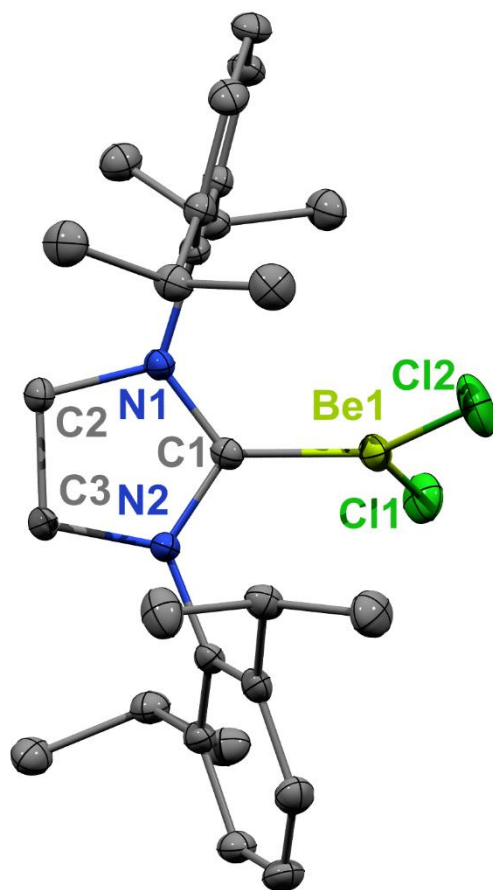


**Figure A3S12:** A) Molecular structures of **3.26** (with H atoms omitted for clarity). Selected bond distances (Å) and angles (°): C1–Be1: 1.786(3); C1–N1: 1.330(2); Be1–Cl1: 1.904(2); Be1–Cl2: 1.888(2); C1–Be1–Cl1: 115.30(13); C1–Be1–Cl2: 121.85(14); Cl1–Be1–Cl2: 122.82(11);

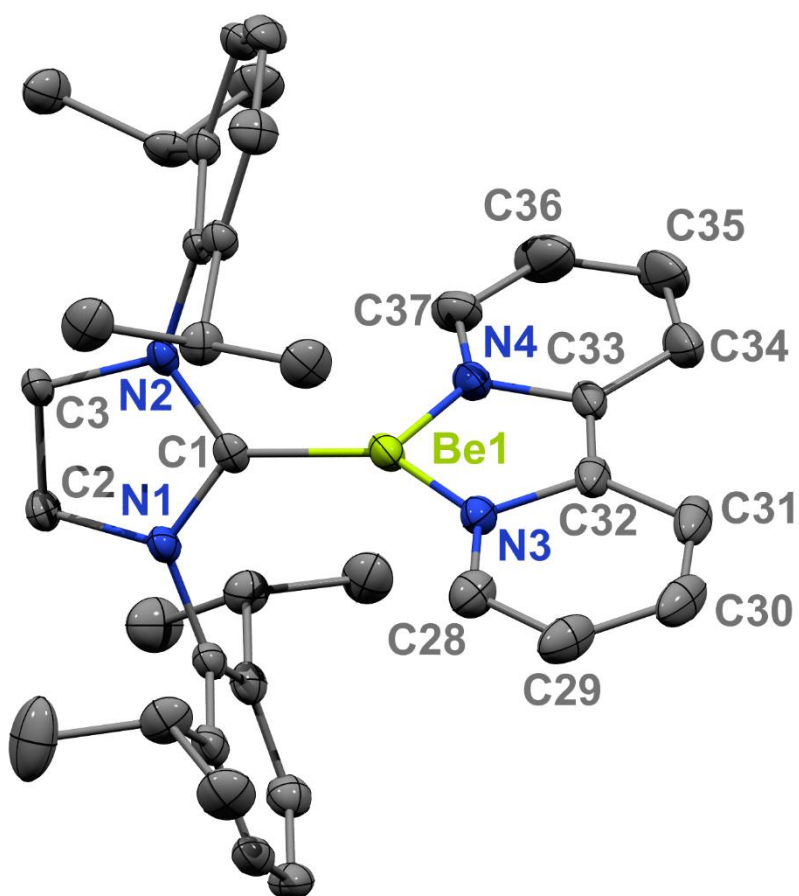


**Figure A3S13:** Molecular structures of **3.27** with H atoms omitted for clarity. Selected bond distances (Å) and angles (°): Be1–C1: 1.799(6); Be1–N2: 1.631(6); N2–C27: 1.430(5); C27–C28: 1.382(5); N3–C28: 1.430(5); Be1–N3: 1.621(5); N1–C1: 1.321(5); N2–C23: 1.358(5); N3–C32: 1.383(5). N2–Be1–N3: 99.2(3); N3–Be1–C1: 128.6(3); N2–Be1–C1: 132.2(3); N1–C1–Be1: 128.8(3); C4–C1–Be1: 122.2(3). N1–C1–Be1–N2: 18.7(7); Be1–N3–C28–C27: 1.1(4).

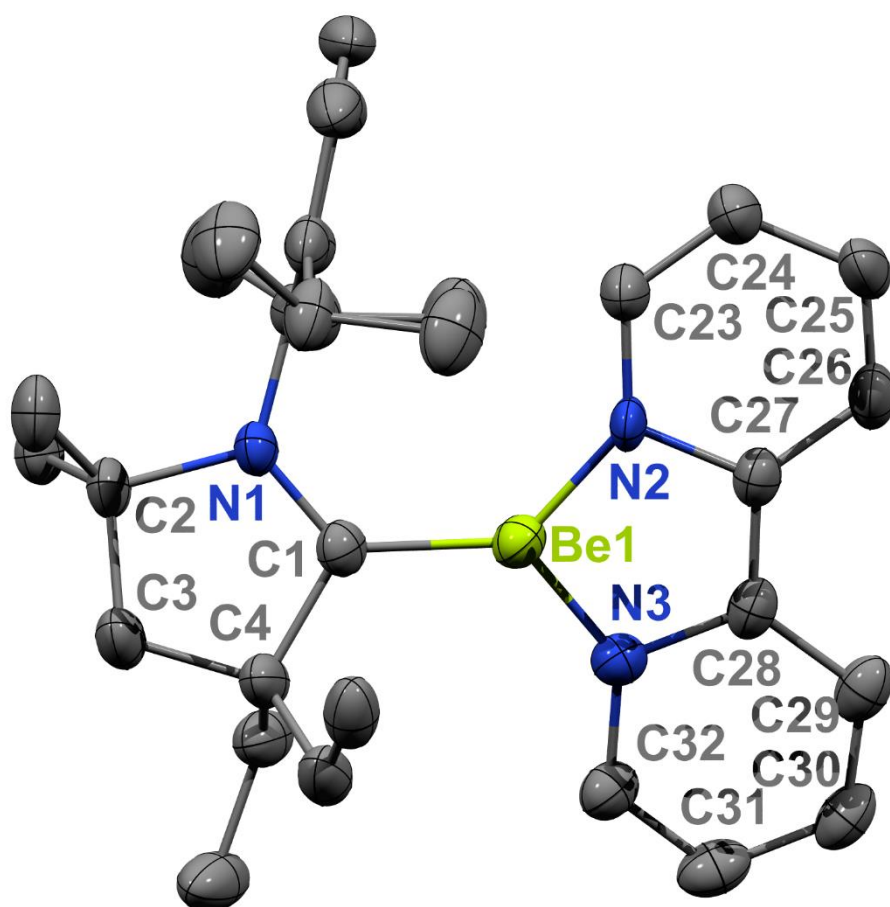


**Figure A3S14:** Molecular structures of **3.28** with H atoms omitted for clarity. Selected bond distances (Å) and angles (°): Be1–C1: 1.781(5); Be1–N3: 1.592(5); N3–C32: 1.429(4); C32–C33: 1.384(6); N4–C33: 1.429(4); Be1–N4: 1.581(5); N1–C1: 1.327(4); N2–C1: 1.346(4); N4–C37: 1.372(5); N3–C28: 1.374(5). N4–Be1–N3: 100.8(3); N3–Be1–C1: 135.0(3); N4–Be1–C1: 124.1(3); N2–C1–Be1: 124.8(3); N1–C1–Be1: 126.8(3). N2–C1–Be1–N4: 57.5(5); Be1–N3–C32–C33: 1.0(4).

## Chapter 4 Crystal Structures

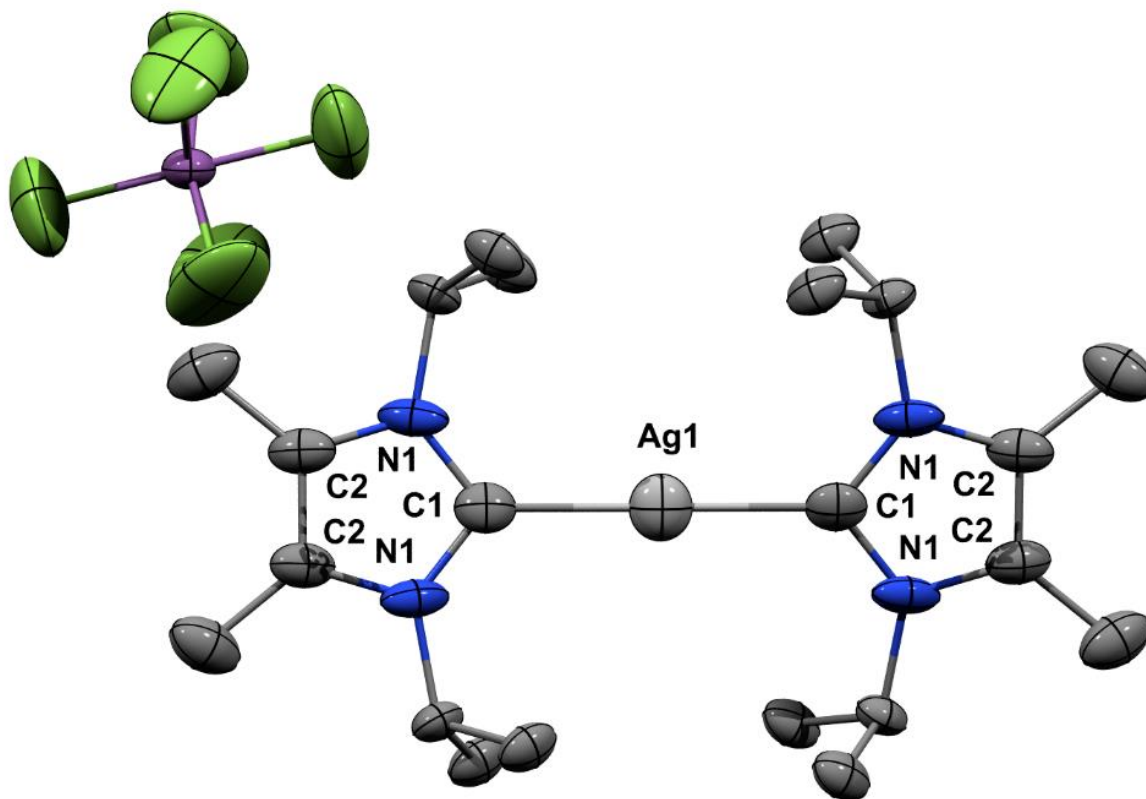


**Figure A3S15:** Molecular structure of compound **4.7** (thermal ellipsoids at 50% probability; H atoms and minor position of disordered anion omitted for clarity). Selected bond distances (Å) and angles (deg): C1–Ag1: 2.086(6); N1–C1: 1.365(5); N1–C2: 1.384(5); C2–C2: 1.350(7).

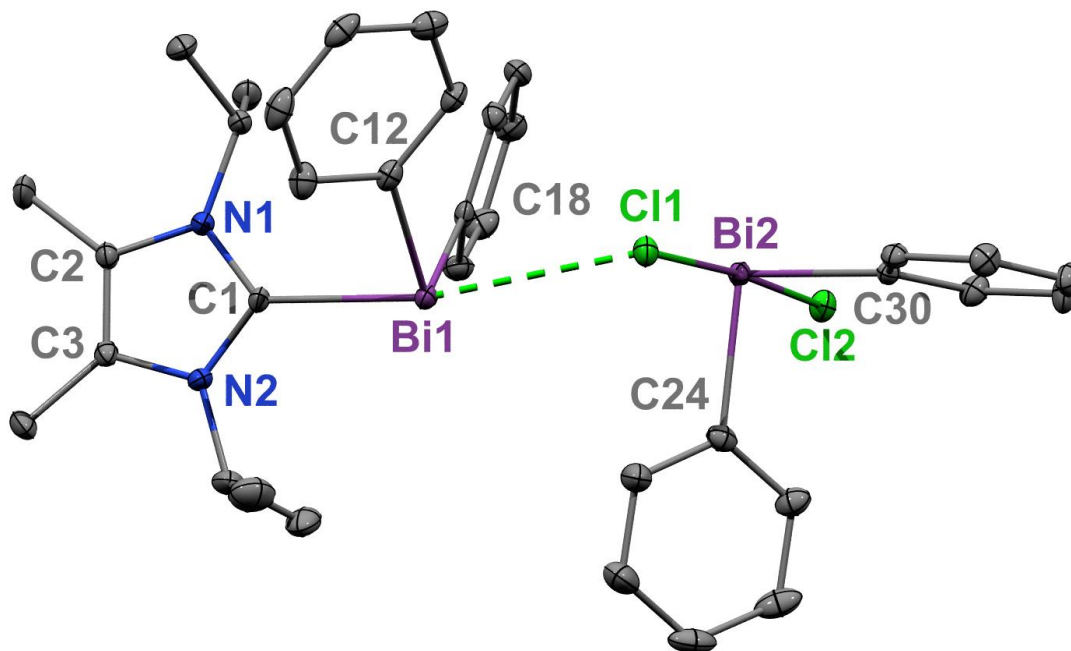


**Figure A3S16:** Molecular structures of **4.8** (thermal ellipsoids at 50% probability; H atoms omitted for clarity). Selected bond distances (Å) and angles (deg): C1–Bi1: 2.383(2); Bi1---C11: 3.1092(8); C11–Bi2: 2.8039(7); Bi2–C12: 2.6832(7). C1–Bi1–C11: 175.45(11); C12–Bi2–C11: 178.24(4).

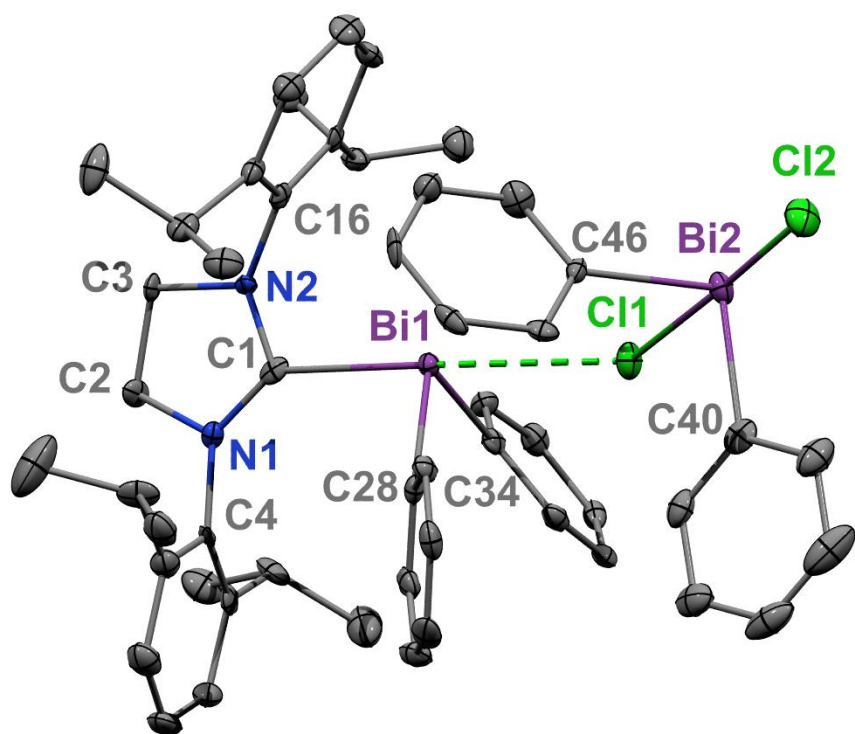


**Figure A3S17:** Molecular structures of **4.9** (thermal ellipsoids at 50% probability; H atoms omitted for clarity). Selected bond distances (Å) and angles (deg): C1–Bi1: 2.431(5); Bi1---Cl1: 3.0405(13); Cl1–Bi2: 2.8347(13); Bi2–Cl2: 2.6392(14). C1–Bi1–Cl1: 167.194(66); Cl2–Bi2–Cl1: 176.258(18).

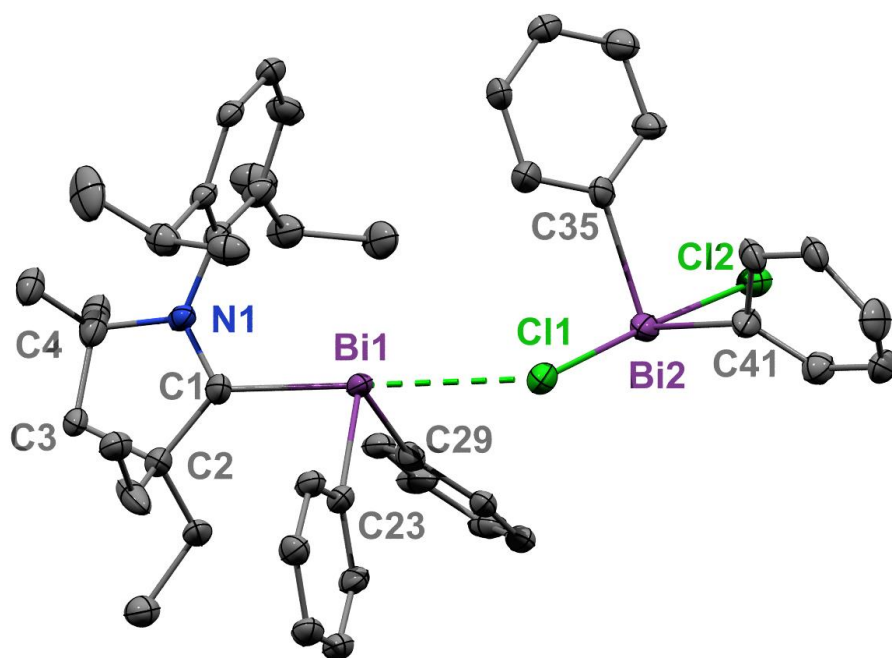


**Figure A3S18:** Molecular structures of **4.10** (thermal ellipsoids at 50% probability; H atoms and minor position of disordered atoms omitted for clarity): C1–Bi1: 2.393(9); Bi1---Cl1: 3.090(2); Cl1–Bi2: 2.818(3); Bi2–Cl2: 2.649(3). C1–Bi1–Cl1: 179.2(2); Cl2–Bi2–Cl1: 174.12(8).

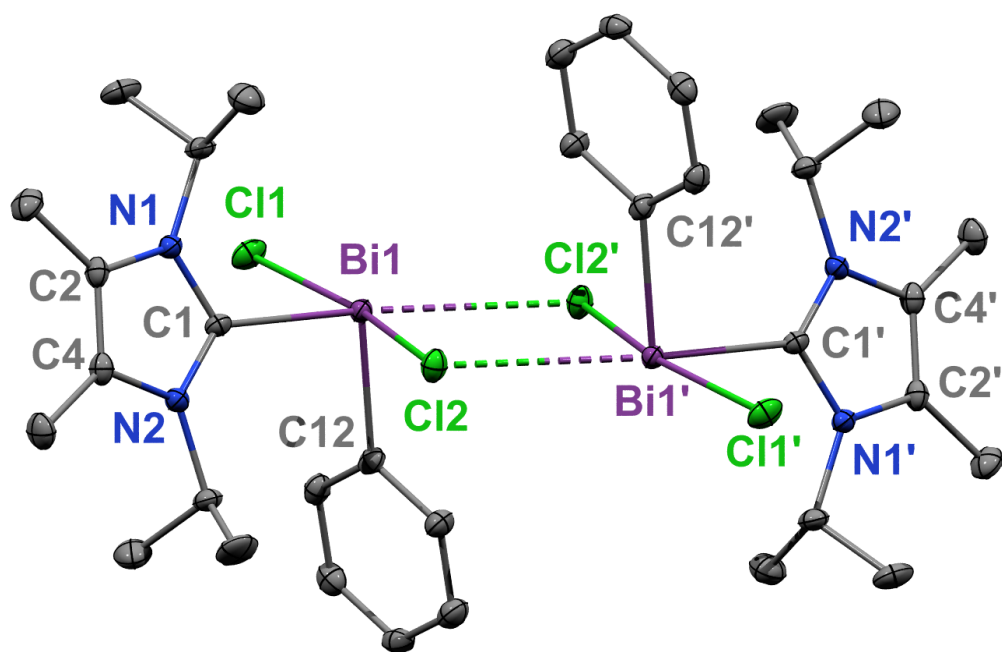


**Figure A3S19:** Molecular structures of **4.11** (thermal ellipsoids at 50% probability; H atoms omitted for clarity): C1–Bi1: 2.346(2); Bi1---Cl2': 3.2473(7); Bi1–Cl1: 2.6857(6); Bi1–Cl2: 2.7031(6). Cl1–Bi1–Cl2: 166.081(18); Cl2–Bi1–C1: 99.21(8); Cl1–Bi1–C1: 84.96(5); Cl2–Bi1–Cl1: 92.21(6); Cl2–Bi1–Cl2: 91.65(6); Cl2–Bi1–C1: 99.21(8).

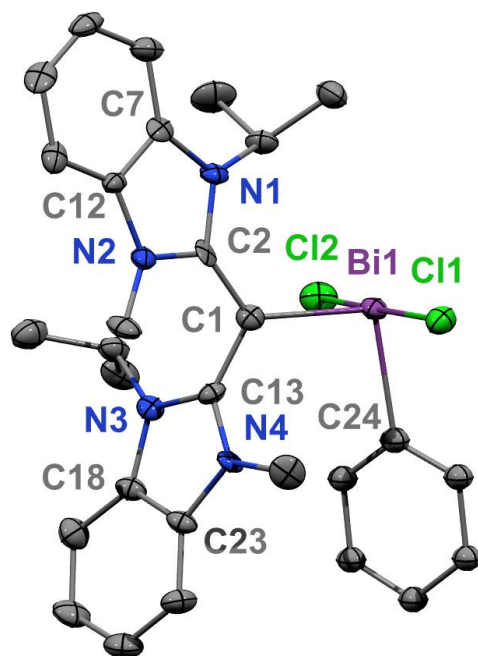


**Figure A3S20:** Molecular structures of **4.12** (thermal ellipsoids at 50% probability; H atoms omitted for clarity): C1–Bi1: 2.249(6); Bi1–Cl1: 2.7693(14); Bi1–Cl2: 2.6989(15); Bi1–C24: 2.275(12); C1–C2: 1.393(8); C1–C13: 1.445(8). Cl1–Bi1–Cl2: 176.21(5); Cl2–Bi1–C1: 90.52(15); Cl1–Bi1–C1: 93.23(15); C24–Bi1–Cl1: 89.8(5); C24–Bi1–Cl2: 89.2(5); C24–Bi1–C1: 97.2(6).

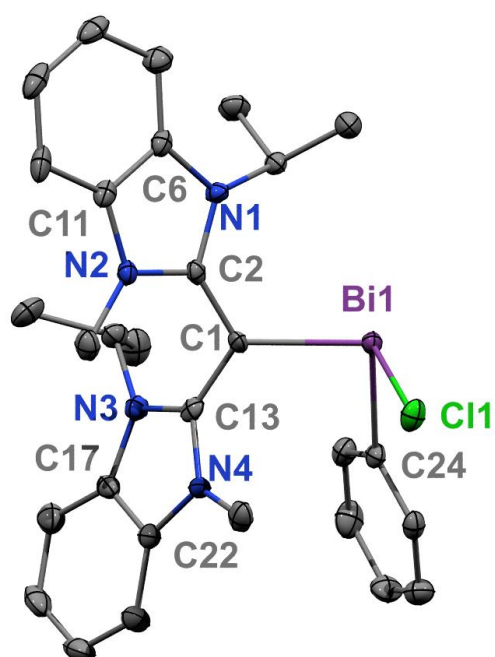


**Figure A3S21:** Molecular structures of **4.13** (thermal ellipsoids at 50% probability; H atoms and coordinating  $[\text{SbF}_6]^-$  anions were omitted for clarity): C1–Bi1: 2.226(3); Bi1–Cl1: 2.5573(9); C24–Bi1: 2.242(3); C1–C2: 1.417(5); C1–C13: 1.427(5). C1–Bi1–Cl1: 102.82(9); C1–Bi1–C24: 93.60(13); C24–Bi1–Cl1: 93.86(10).

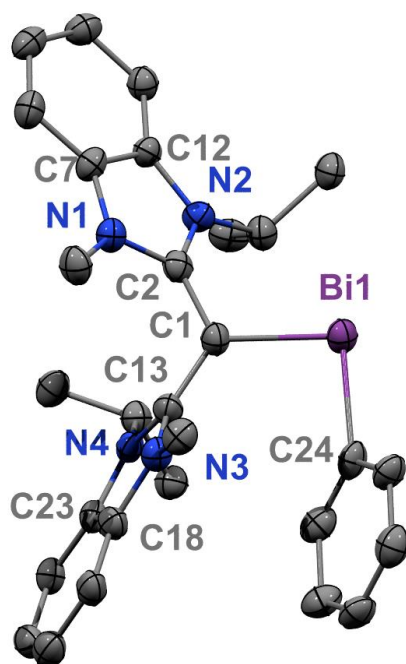


**Figure A3S22:** Molecular structures of **4.14** (thermal ellipsoids at 50% probability; H atoms and coordinating  $[\text{SbF}_6]^-$  anions were omitted for clarity): C1–Bi1: 2.157(11); Bi1–C24: 2.223(12); C1–C2: 1.444(15); C1–C13: 1.426(15). C1–Bi1–C24: 96.7(4).

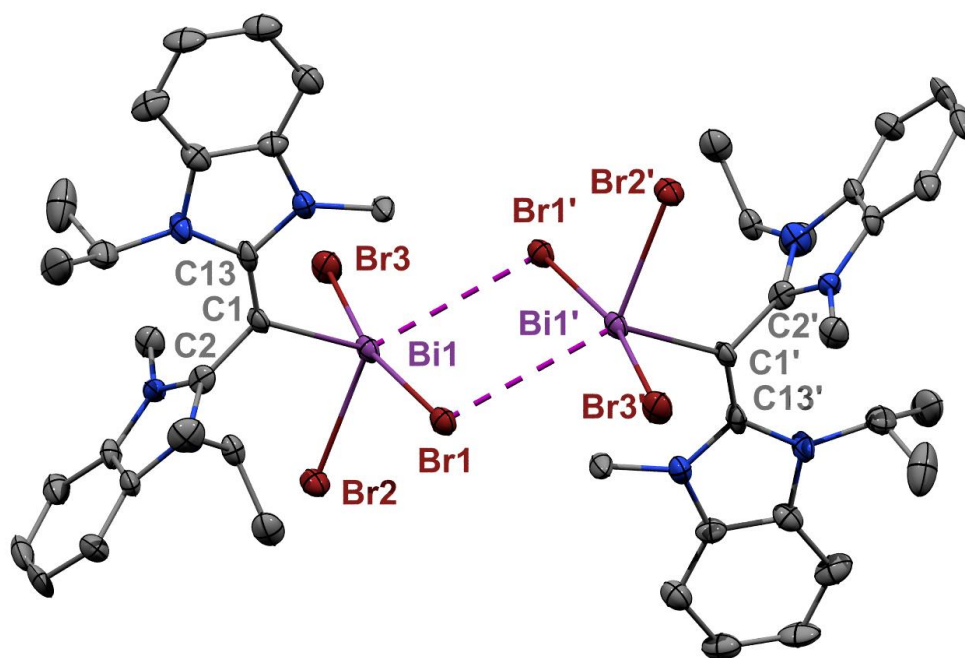


**Figure A3S23:** Molecular structures of **4.15** (thermal ellipsoids at 50% probability; H atoms, counteranions and non-coordinating solvent omitted for clarity): Bi1–C1: 2.292(9); Bi1–Br1: 2.9196(12); Bi1–Br2: 2.6483(11); Bi1–Br3: 2.8390(12); Bi1---Br1': 3.4829(15); C1–C13: 1.367(13); C1–C2: 1.438(12).

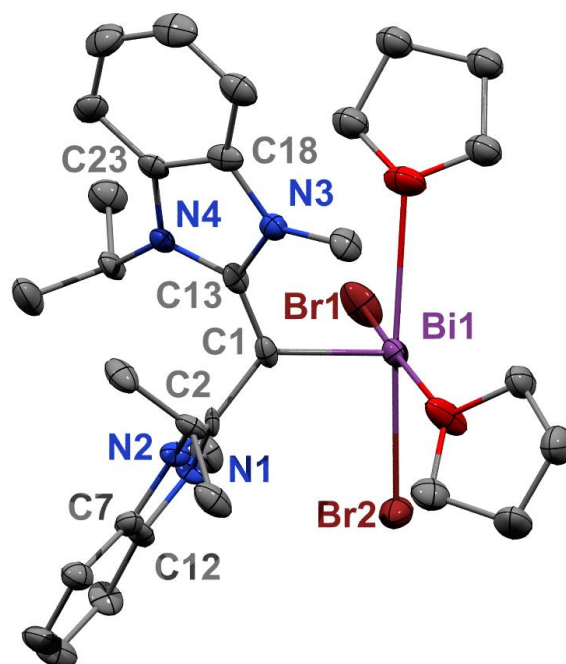


**Figure A3S24:** Molecular structures of **4.16** (thermal ellipsoids at 50% probability; H atoms, counter-anions and non-coordinating solvent omitted for clarity): Bi1–C1: 2.226(12); Bi1–Br2: 2.6629(16); Bi1–Br1: 2.7052(18); C1–C13: 1.395(17); C1–C2: 1.447(15).

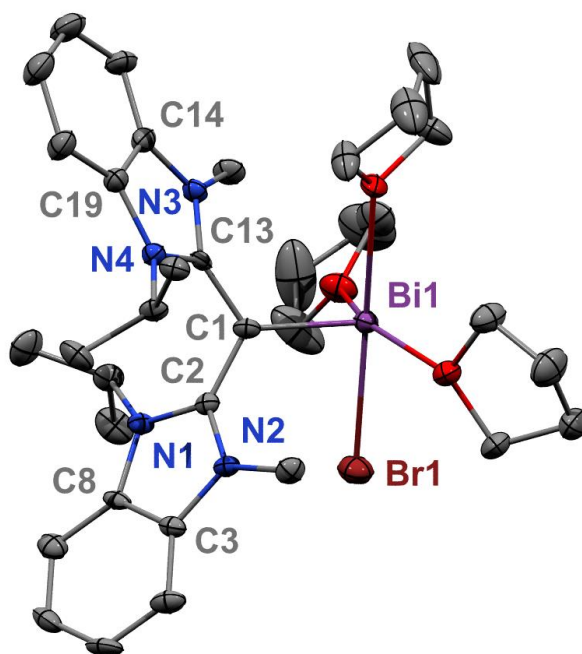


**Figure A3S25:** Molecular structures of **4.17** (thermal ellipsoids at 50% probability; H atoms, counteranions and non-coordinating solvent omitted for clarity): Bi1–Br1: 2.6439(6); Bi1–C1: 2.199(5); C1–C2: 1.441(6); C1–C13: 1.433(6).

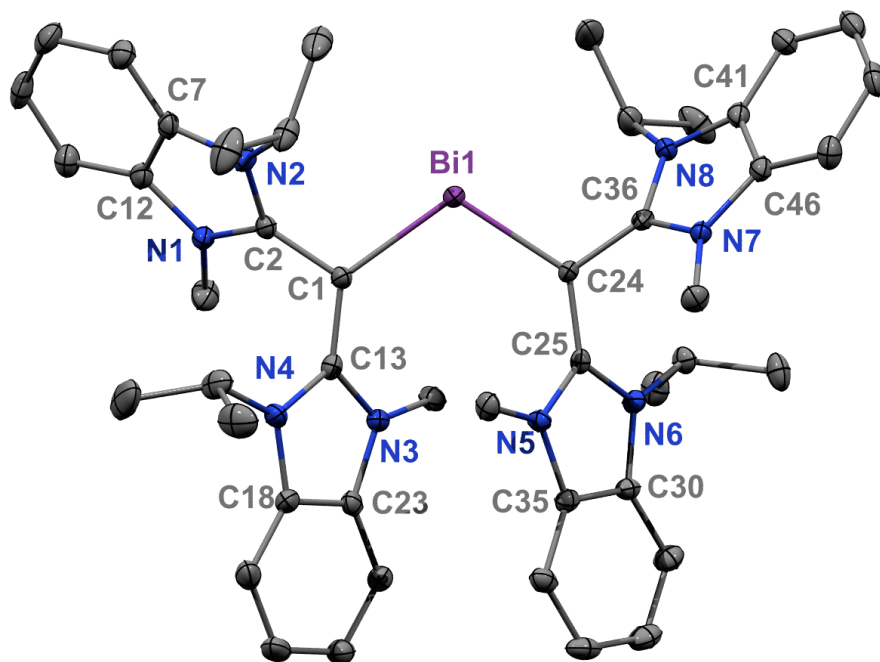


**Figure A3S26:** Molecular structures of **4.18** (thermal ellipsoids at 50% probability; H atoms, counteranions and non-coordinating solvent omitted for clarity): Bi1–C24: 2.166(2); Bi1–C1: 2.197(2); C1–C13: 1.424(3); C1–C2: 1.443(3); C24–C25: 1.436(3); C24–C36: 1.444(3). C24–Bi1–C1: 111.23(9).

## Chapter 5 Crystal Structures

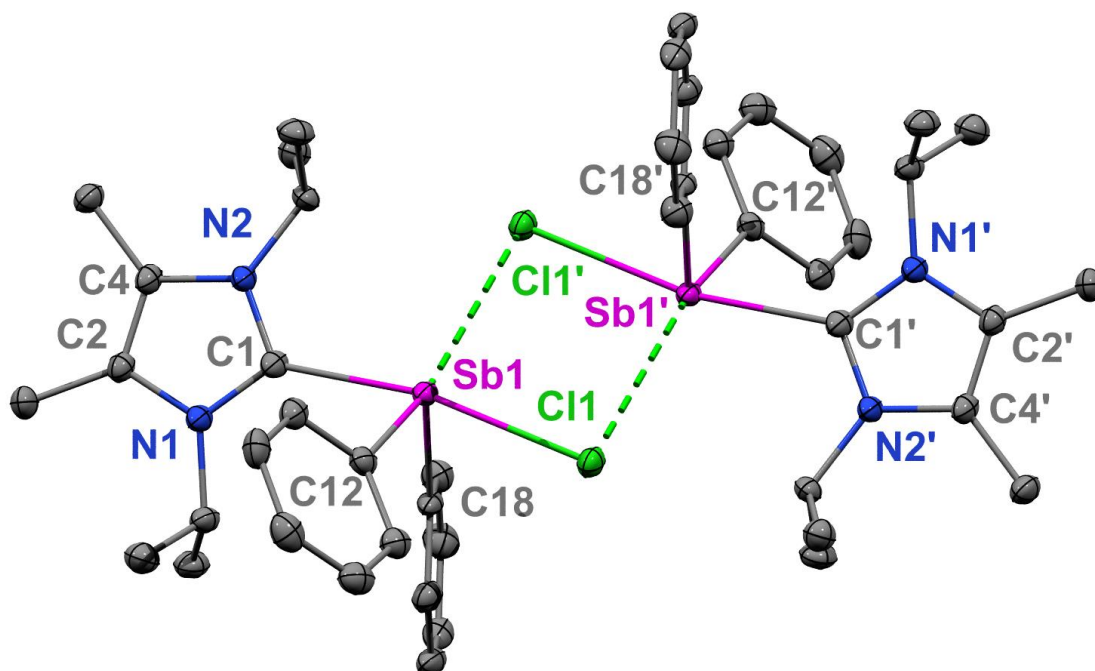


**Figure A3S27:** Molecular structure of **5.1** (thermal ellipsoids at 50% probability; H atoms omitted for clarity). Selected bond distances (Å) and angles (deg): Sb1–C1: 2.356(3); Sb1–Cl1: 2.8006(8); Sb1–Cl1': 3.9544(10); Sb1–C18: 2.168(3); Sb1–C12: 2.171(4). C18–Sb1–C12: 102.19(14); C18–Sb1–C1: 87.58(12); C12–Sb1–C1: 86.33(12); C18–Sb1–Cl1: 87.00(8); C12–Sb1–Cl1: 85.24(9); C1–Sb1–Cl1: 168.80(9).

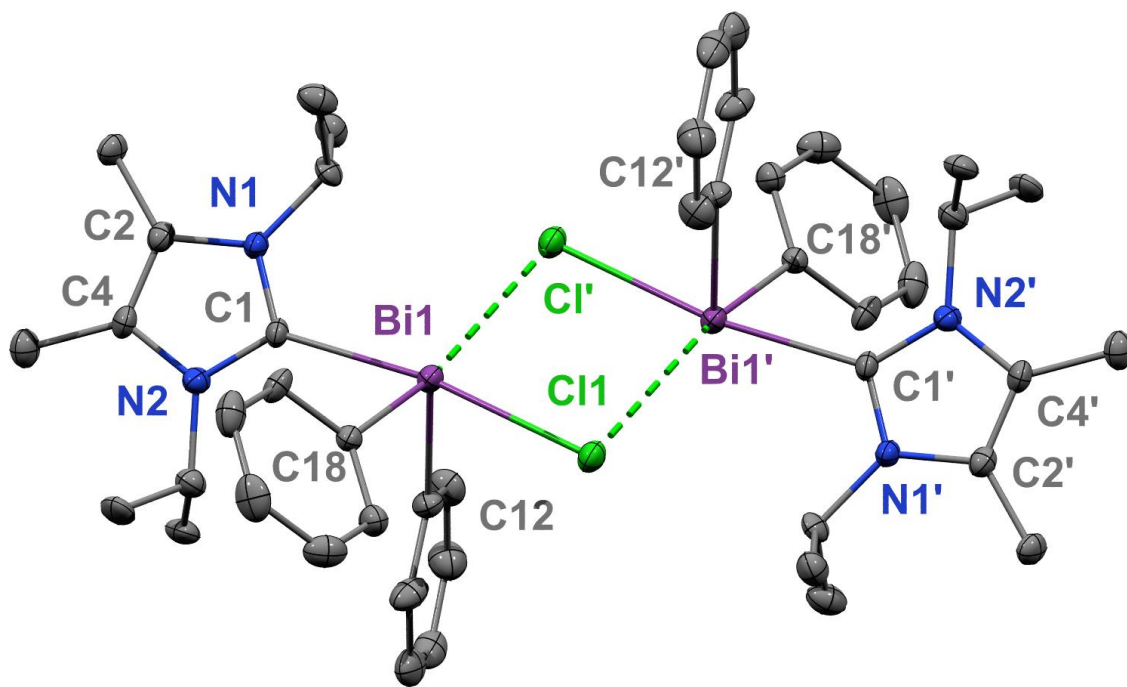


**Figure A3S28:** Molecular structure of **5.2** (also known as **4.6**) (thermal ellipsoids at 50% probability; H atoms were omitted for clarity). Selected bond distances (Å) and angles (deg): Bi1–C1: 2.489(6); Bi1–Cl1: 2.8696(16); Bi1–Cl1': 3.7211(17); Bi1–C18: 2.257(6); Bi1–C12: 2.267(6). C18–Bi1–C12: 99.0(2); C18–Bi1–C1: 86.3(2); C12–Bi1–C1: 88.1(2); C18–Bi1–Cl1: 86.26(16); C12–Bi1–Cl1: 88.26(16); C1–Bi1–Cl1: 171.05(15).

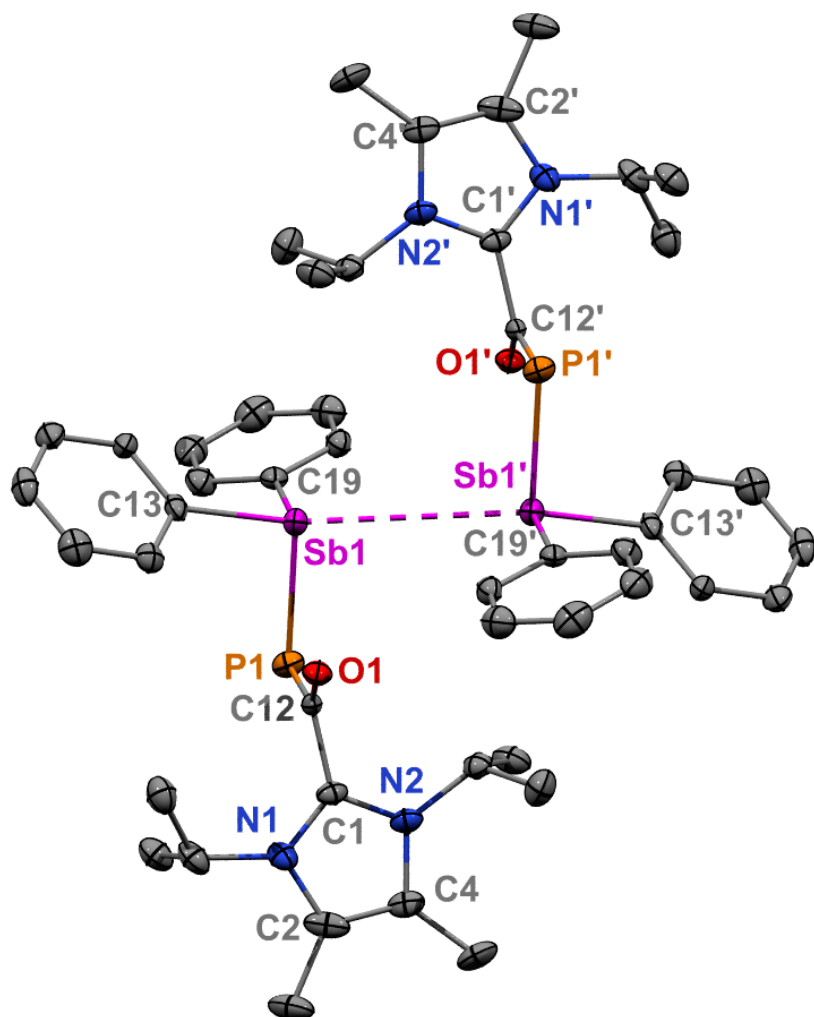


**Figure A3S29:** Molecular structure of **5.3** (thermal ellipsoids at 50% probability; H atoms omitted for clarity). Selected bond distances (Å) and angles (deg): Sb1–C13: 2.154(6); Sb1–C19: 2.155(6); Sb1–P1: 2.5042(16); Sb1–Sb1': 3.9619(17) P1–C12: 1.748(6); O1–C12: 1.264(7); C1–C12: 1.529(7). C13–Sb1–C19: 97.7(2); C13–Sb1–P1: 99.79(15); C19–Sb1–P1: 91.77(15); Sb1'–Sb1–P1: 94.602(40); Sb1'–Sb1–C19: 97.237(158); Sb1'–Sb1–C13: 158.899(168).

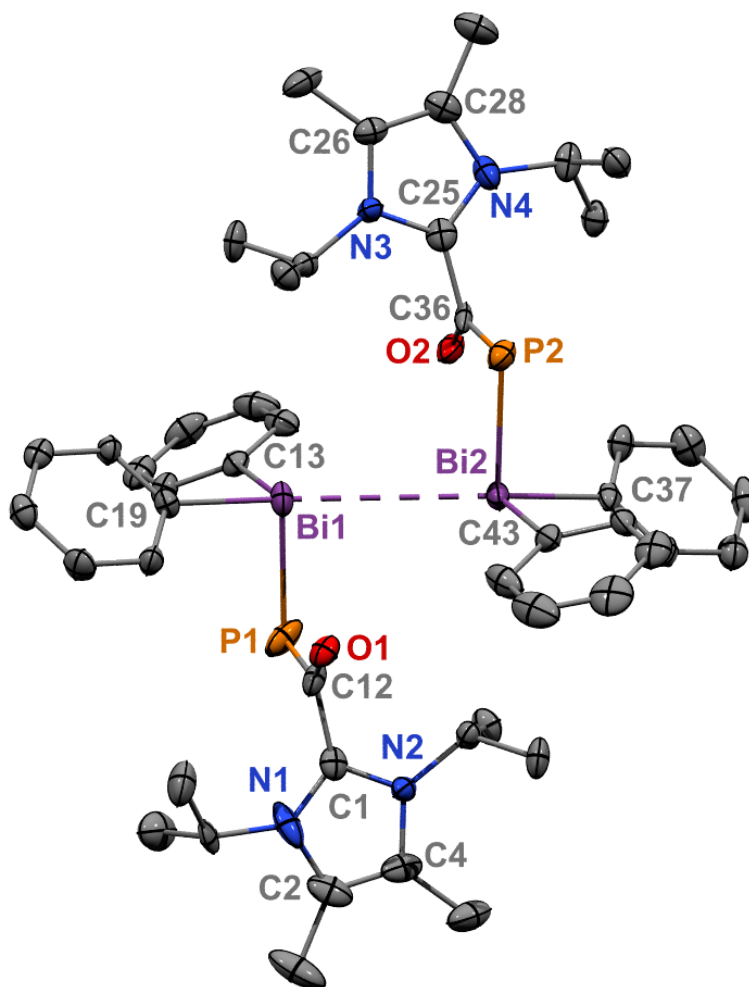


**Figure A3S30** Molecular structure of **5.4** (thermal ellipsoids at 50% probability; H atoms were omitted for clarity). Selected bond distances (Å) and angles (deg): Bi1–C19: 2.229(6); Bi1–C13: 2.272(7); Bi1–P1: 2.589(2); Bi1–Bi2: 3.8204(6); Bi2–C37: 2.251(7); Bi2–C43: 2.257(8); Bi2–P2: 2.594(2); P1–C12: 1.736(7); P2–C36: 1.746(8); O1–C12: 1.255(8); O2–C36: 1.258(8); C1–C12: 1.525(11); C25–C36: 1.515(11). C19–Bi1–C13: 94.2(2); C19–Bi1–P1: 97.38(19); C13–Bi1–P1: 87.26(19); C37–Bi2–C43: 94.8(3); C37–Bi2–P2: 98.56(19); C43–Bi2–P2: 90.99(19); Bi2–Bi1–P1: 86.913(49); Bi2–Bi1–C13: 101.940(176); Bi2–Bi1–C19: 163.528(178); Bi1–Bi2–P2: 89.365(43); Bi1–Bi2–C43: 104.176(179); Bi1–Bi2–C37: 159.346(177).

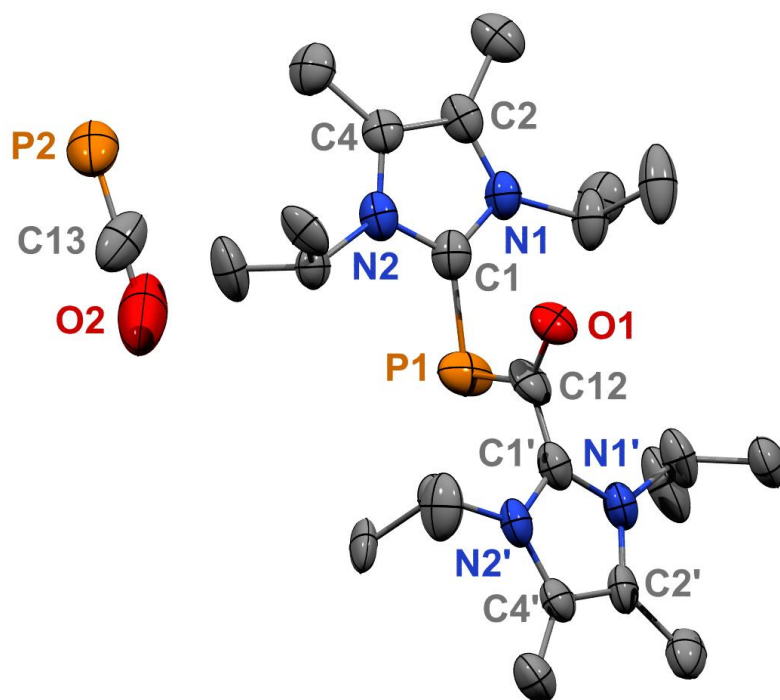


**Figure A3S31:** Molecular structure of **5.5** (thermal ellipsoids at 50% probability; H atoms omitted for clarity, only one orientation of the symmetry disordered OCP anion is shown.). Selected bond distances (Å) and angles (deg): C1–P1: 1.890(6); P1–C12: 1.755(14); C12–O1: 1.268(12); C12–C1': 1.421(16). C1–P1–C12: 98.3(5); O1–C12–C1': 117.0(14).

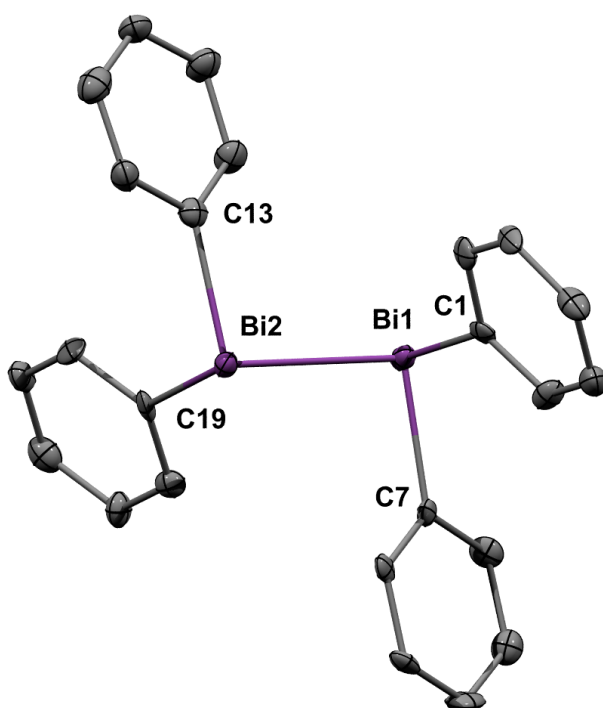


**Figure A3S32:** Molecular structure of **5.6**. Ellipsoids represent 50% probability and all hydrogen atoms have been omitted for clarity. Selected bond lengths ( $\text{\AA}$ ) and angles ( $^\circ$ ): Bi1–Bi2: 2.9867(7); Bi1–C1: 2.274(13); Bi1–C7: 2.267(12); Bi2–C13: 2.261(13); Bi2–C19: 2.261(12). C1–Bi1–Bi2: 90.5(3); C7–Bi1–Bi2: 94.0(3); C7–Bi1–C1: 92.3(4); Bi1–Bi2–C13: 95.0(3); Bi1–Bi2–C19: 91.9(3); C13–Bi2–C19: 93.0(5).

## References

1. Earnshaw, N. N. G. a. A., Beryllium, Magnesium, Calcium, Strontium, Barium, and Radium. In *Chemistry of the Elements*, First ed.; Pergamon Press Ltd.: 660 White Plains Road, Tarrytown, New York 10591-5153, USA, 1984; pp 117-153.
2. Viana, R. R.; da Costa, G. M.; De Grave, E.; Jordt-Evangelista, H.; Stern, W. B., Characterization of beryl (aquamarine variety) by Mössbauer spectroscopy. *Phys. Chem. Miner.* **2002**, *29*, 78-86.
3. Puchta, R., A brighter beryllium. *Nat. Chem.* **2011**, *3*, 416.
4. Naglav, D.; Buchner, M. R.; Bendt, G.; Kraus, F.; Schulz, S., Off the Beaten Track—A Hitchhiker's Guide to Beryllium Chemistry. *Angew. Chem., Int. Ed.* **2016**, *55*, 10562-10576.
5. Paparo, A.; Jones, C., Beryllium Halide Complexes Incorporating Neutral or Anionic Ligands: Potential Precursors for Beryllium Chemistry. *Chem. Asian J.* **2019**, *14*, 486-490.
6. Stasch, C. J. a. A., Crystal Structure of [BeI<sub>2</sub>(OEt<sub>2</sub>)<sub>2</sub>] (OEt<sub>2</sub> = diethyl ether). *Anal. Sci: X-Ray Struct. Anal. Online* **2007**, *23*, 115-116.
7. Nöth, H.; Schlosser, D., The Aminolysis of Beryllium Dichloride with Diisopropylamine and Reactions of Some Aminoberyllium Chlorides. *Eur. J. Inorg. Chem.* **2003**, 2245-2254.
8. Allred, A. L., Electronegativity values from thermochemical data. *J. Inorg. Nucl. Chem.* **1961**, *17*, 215-221.
9. Slater, J. C., Atomic Radii in Crystals. *J. Chem. Phys.* **1964**, *41*, 3199-3204.
10. Couchman, S. A.; Holzmann, N.; Frenking, G.; Wilson, D. J. D.; Dutton, J. L., Beryllium chemistry the safe way: a theoretical evaluation of low oxidation state beryllium compounds. *Dalton Trans.* **2013**, *42*, 11375-11384.
11. Arrowsmith, M.; Braunschweig, H.; Celik, M. A.; Dellermann, T.; Dewhurst, R. D.; Ewing, W. C.; Hammond, K.; Kramer, T.; Krummenacher, I.; Mies, J.; Radacki, K.; Schuster, J. K., Neutral zero-valent s-block complexes with strong multiple bonding. *Nat. Chem.* **2016**, *8*, 890.
12. Wang, G.; Walley, J. E.; Dickie, D. A.; Pan, S.; Frenking, G.; Gilliard, R. J., A Stable, Crystalline Beryllium Radical Cation. *J. Am. Chem. Soc.* **2020**, *142*, 4560-4564.
13. Speer, W.; Es-Said, O. S., Applications of an aluminum–beryllium composite for structural aerospace components. *Eng. Fail. Anal.* **2004**, *11*, 895-902.
14. Buchner, M. R., Recent Contributions to the Coordination Chemistry of Beryllium. *Chem. - Eur. J.* **2019**, *25*, 12018-12036.
15. Perera, L. C.; Raymond, O.; Henderson, W.; Brothers, P. J.; Plieger, P. G., Advances in beryllium coordination chemistry. *Coord. Chem. Rev.* **2017**, *352*, 264-290.
16. McCleskey, T. M.; Buchner, V.; Field, R. W.; Scott, B. L., Recent advances in understanding the biomolecular basis of chronic beryllium disease: a review. *Reviews on environmental health* **2009**, *24*, 75-115.
17. Mack, D. G.; Lanham, A. M.; Falta, M. T.; Palmer, B. E.; Maier, L. A.; Fontenot, A. P., Deficient and dysfunctional regulatory T cells in the lungs of chronic beryllium disease subjects. *Am. J. Respir. Crit. Care Med.* **2010**, *181*, 1241-1249.
18. McKee, A. S.; Fontenot, A. P., Interplay of innate and adaptive immunity in metal-induced hypersensitivity. *Curr Opin Immunol* **2016**, *42*, 25-30.
19. Fontenot, A. P., Immunologic Effects of Beryllium Exposure. *Ann Am Thorac Soc* **2018**, *15*, S81-S85.
20. Buchner, M. R., Beryllium coordination chemistry and its implications on the understanding of metal induced immune responses. *Chem. Commun.* **2020**, *56*, 8895-8907.

21. Buchanan, J. K.; Plieger, P. G.,  $^9\text{Be}$  nuclear magnetic resonance spectroscopy trends in discrete complexes: an update. *Z. Naturforsch. B* **2020**, *75*, 459.
22. Plieger, P. G.; John, K. D.; Keizer, T. S.; McCleskey, T. M.; Burrell, A. K.; Martin, R. L., Predicting  $^9\text{Be}$  Nuclear Magnetic Resonance Chemical Shielding Tensors Utilizing Density Functional Theory. *J. Am. Chem. Soc.* **2004**, *126*, 14651-14658.
23. Mohan, R., Green bismuth. *Nat. Chem.* **2010**, *2*, 336-336.
24. Margaretha, P., *Science of Synthesis*. Thieme Chemistry: 2007; Vol. 35, p 47.
25. Lipshultz, J. M.; Li, G.; Radosevich, A. T., Main Group Redox Catalysis of Organopnictogens: Vertical Periodic Trends and Emerging Opportunities in Group 15. *J. Am. Chem. Soc.* **2021**, *143*, 1699-1721.
26. Lichtenberg, C., Molecular Bismuth(III) Monocations: Structure, Bonding, Reactivity, and Catalysis. *Chemical Communications* **2021**.
27. Balasubramaniam, S.; Kumar, S.; Andrews, A. P.; Varghese, B.; Jemmis, E. D.; Venugopal, A., A Dicationic Bismuth(III) Lewis Acid: Catalytic Hydrosilylation of Olefins. *Eur. J. Inorg. Chem.* **2019**, *2019*, 3265-3269.
28. Bourget-Merle, L.; Lappert, M. F.; Severn, J. R., The Chemistry of  $\beta$ -Diketiminatometal Complexes. *Chem. Rev.* **2002**, *102*, 3031-3066.
29. Barry, S. T., Amidinates, guanidates and iminopyrrolidates: Understanding precursor thermolysis to design a better ligand. *Coord. Chem. Rev.* **2013**, *257*, 3192-3201.
30. Du, C. J. F.; Hart, H.; Ng, K. K. D., A one-pot synthesis of m-terphenyls, via a two-aryne sequence. *J. Org. Chem.* **1986**, *51*, 3162-3165.
31. Arduengo, A. J.; Harlow, R. L.; Kline, M., A stable crystalline carbene. *J. Am. Chem. Soc.* **1991**, *113*, 361-363.
32. Nesterov, V.; Reiter, D.; Bag, P.; Frisch, P.; Holzner, R.; Porzelt, A.; Inoue, S., NHCs in Main Group Chemistry. *Chem. Rev.* **2018**, *118*, 9678-9842.
33. Munz, D., Pushing Electrons—Which Carbene Ligand for Which Application? *Organometallics* **2018**, *37*, 275-289.
34. Lavallo, V.; Canac, Y.; Präsang, C.; Donnadiou, B.; Bertrand, G., Stable Cyclic (Alkyl)(Amino)Carbenes as Rigid or Flexible, Bulky, Electron-Rich Ligands for Transition-Metal Catalysts: A Quaternary Carbon Atom Makes the Difference. *Angew. Chem., Int. Ed.* **2005**, *44*, 5705-5709.
35. De, S.; Parameswaran, P., Neutral tricoordinated beryllium(0) compounds – isostructural to  $\text{BH}_3$  but isoelectronic to  $\text{NH}_3$ . *Dalton Trans.* **2013**, *42*, 4650-4656.
36. Dyker, C. A.; Lavallo, V.; Donnadiou, B.; Bertrand, G., Synthesis of an Extremely Bent Acyclic Allene (A “Carbodicarbene”): A Strong Donor Ligand. *Angew. Chem., Int. Ed.* **2008**, *47*, 3206-3209.
37. Tonner, R.; Frenking, G.,  $\text{C}(\text{NHC})_2$ : Divalent Carbon(0) Compounds with N-Heterocyclic Carbene Ligands—Theoretical Evidence for a Class of Molecules with Promising Chemical Properties. *Angew. Chem., Int. Ed.* **2007**, *46*, 8695-8698.
38. Petz, W.; Dehnicke, K.; Holzmann, N.; Frenking, G.; Neumüller, B., The Reaction of  $\text{BeCl}_2$  with Carbodiphosphorane  $\text{C}(\text{PPh}_3)_2$ ; Experimental and Theoretical Studies. *Z. Anorg. Allg. Chem.* **2011**, *637*, 1702-1710.
39. Herrmann, W. A.; Runte, O.; Artus, G., Synthesis and structure of an ionic beryllium-“carbene” complex. *J. Organomet. Chem.* **1995**, *501*, C1-C4.

40. Schuster, J. K.; Roy, D. K.; Lenczyk, C.; Mies, J.; Braunschweig, H., New Outcomes of Beryllium Chemistry: Lewis Base Adducts for Salt Elimination Reactions. *Inorg. Chem.* **2019**, *58*, 2652-2658.
41. Buchner, M. R.; Pan, S.; Poggel, C.; Spang, N.; Müller, M.; Frenking, G.; Sundermeyer, J., Di-ortho-beryllated Carbodiphosphorane: A Compound with a Metal–Carbon Double Bond to an Element of the s-Block. *Organometallics* **2020**.
42. Böttger, S. C.; Poggel, C.; Sundermeyer, J., ortho-Directed Dilithiation of Hexaphenyl-carbodiphosphorane. *Organometallics* **2020**, *39*, 3789-3793.
43. Hermann, M.; Frenking, G., Carbones as Ligands in Novel Main-Group Compounds  $E[C(NHC)_2]_2$  ( $E=Be, B^+, C_2^+, N_3^+, Mg, Al^+, Si_2^+, P_3^+$ ): A Theoretical Study. *Chem. - Eur. J.* **2017**, *23*, 3347-3356.
44. Gilliard, R. J.; Abraham, M. Y.; Wang, Y.; Wei, P.; Xie, Y.; Quillian, B.; Schaefer, H. F.; Schleyer, P. v. R.; Robinson, G. H., Carbene-Stabilized Beryllium Borohydride. *J. Am. Chem. Soc.* **2012**, *134*, 9953-9955.
45. Chen, W.-C.; Hsu, Y.-C.; Lee, C.-Y.; Yap, G. P. A.; Ong, T.-G., Synthetic Modification of Acyclic Bent Allenes (Carbodicarbenes) and Further Studies on Their Structural Implications and Reactivities. *Organometallics* **2013**, *32*, 2435-2442.
46. Walley, J. E.; Breiner, G.; Wang, G.; Dickie, D. A.; Molino, A.; Dutton, J. L.; Wilson, D. J. D.; Gilliard Jr, R. J., s-Block carbodicarbene chemistry:  $C(sp^3)$ -H activation and cyclization mediated by a beryllium center. *Chem. Commun.* **2019**, *55*, 1967-1970.
47. Walley, J. E.; Obi, A. D.; Breiner, G.; Wang, G.; Dickie, D. A.; Molino, A.; Dutton, J. L.; Wilson, D. J. D.; Gilliard, R. J., Jr., Cyclic(alkyl)(amino) Carbene-Promoted Ring Expansion of a Carbodicarbene Beryllacycle. *Inorg. Chem.* **2019**, *58*, 11118-11126.
48. Naglav, D.; Neumann, A.; Bläser, D.; Wölper, C.; Haack, R.; Jansen, G.; Schulz, S., Bonding situation in  $Be[N(SiMe_3)_2]_2$  – an experimental and computational study. *Chem. Commun.* **2015**, *51*, 3889-3891.
49. Arrowsmith, M.; Hill, M. S.; Kociok-Köhn, G., Activation of N-Heterocyclic Carbenes by  $\{BeH_2\}$  and  $\{Be(H)(Me)\}$  Fragments. *Organometallics* **2015**, *34*, 653-662.
50. Arrowsmith, M.; Hill, M. S.; Kociok-Kohn, G.; MacDougall, D. J.; Mahon, M. F., Beryllium-induced C-N bond activation and ring opening of an N-heterocyclic carbene. *Angew. Chem., Int. Ed.* **2012**, *51*, 2098-100.
51. Gottfriedsen, J.; Blaurock, S., The First Carbene Complex of a Diorganoberyllium: Synthesis and Structural Characterization of  $Ph_2Be(i-Pr\text{-carbene})$  and  $Ph_2Be(n-Bu_2O)$ . *Organometallics* **2006**, *25* (15), 3784-3786.
52. Buchner, M. R.; Müller, M.; Rudel, S. S., Beryllium Phosphine Complexes: Synthesis, Properties, and Reactivity of  $(PMe_3)_2BeCl_2$  and  $(Ph_2PC_3H_6PPh_2)BeCl_2$ . *Angew. Chem., Int. Ed.* **2017**, *56*, 1130-1134.
53. Bruyere, J. C.; Specklin, D.; Gourlaouen, C.; Lapenta, R.; Veiros, L. F.; Grassi, A.; Milione, S.; Ruhlmann, L.; Boudon, C.; Dagonne, S., Cyclic(Alkyl)(Amino)Carbene (CAAC)-Supported Zn Alkyls: Synthesis, Structure and Reactivity in Hydrosilylation Catalysis. *Chem. - Eur. J.* **2019**, *0*.
54. Paul, U. S. D.; Radius, U., Synthesis and Reactivity of Cyclic (Alkyl)(Amino)Carbene Stabilized Nickel Carbonyl Complexes. *Organometallics* **2017**, *36*, 1398-1407.
55. Bellemin-Laponnaz, S.; Dagonne, S., Group 1 and 2 and Early Transition Metal Complexes Bearing N-Heterocyclic Carbene Ligands: Coordination Chemistry, Reactivity, and Applications. *Chem. Rev.* **2014**, *114*, 8747-8774.

56. Wang, G.; Freeman, L. A.; Dickie, D. A.; Mokrai, R.; Benkő, Z.; Gilliard Jr., R. J., Isolation of Cyclic(Alkyl)(Amino) Carbene–Bismuthinidene Mediated by a Beryllium(0) Complex. *Chem. - Eur. J.* **2019**, *25*, 4335-4339.
57. Niemeyer, M.; Power, P. P., Synthesis,  $^9\text{Be}$  NMR Spectroscopy, and Structural Characterization of Sterically Encumbered Beryllium Compounds. *Inorg. Chem.* **1997**, *36*, 4688-4696.
58. Kovar, R. A.; Morgan, G. L., Beryllium-9 and hydrogen-1 magnetic resonance studies of beryllium compounds in solution. *J. Am. Chem. Soc.* **1970**, *92*, 5067-5072.
59. Han, R.; Parkin, G., [Tris(3-tert-butylpyrazolyl)hydroborato]beryllium hydride: synthesis, structure, and reactivity of a terminal beryllium hydride complex. *Inorg. Chem.* **1992**, *31*, 983-988.
60. Han, R.; Parkin, G., Synthesis, structure, and reactivity of  $\{\eta^3\text{-HB(3-tert-Bupz)}_3\}\text{BeCH}_3$ , a terminal beryllium alkyl complex supported by tris(3-tert-butylpyrazolyl)hydroborato ligation. *Inorg. Chem.* **1993**, *32*, 4968-4970.
61. Wilson, D. J. D.; Couchman, S. A.; Dutton, J. L., Are N-Heterocyclic Carbenes “Better” Ligands than Phosphines in Main Group Chemistry? A Theoretical Case Study of Ligand-Stabilized E2 Molecules, L-E-E-L (L = NHC, phosphine; E = C, Si, Ge, Sn, Pb, N, P, As, Sb, Bi). *Inorg. Chem.* **2012**, *51*, 7657-7668.
62. Iversen, K. J.; Wilson, D. J. D.; Dutton, J. L., Effects of the electronic structure of five-membered N-heterocyclic carbenes on insertion of silanes and boranes into the NHC C–N bond. *Dalton Trans.* **2015**, *44*, 3318-3325.
63. Chen, W.-C.; Shih, W.-C.; Jurca, T.; Zhao, L.; Andrada, D. M.; Peng, C.-J.; Chang, C.-C.; Liu, S.-k.; Wang, Y.-P.; Wen, Y.-S.; Yap, G. P. A.; Hsu, C.-P.; Frenking, G.; Ong, T.-G., Carbodicarbenes: Unexpected  $\pi$ -Accepting Ability during Reactivity with Small Molecules. *J. Am. Chem. Soc.* **2017**, *139*, 12830-12836.
64. Hill, M. S.; Liptrot, D. J.; Weetman, C., Alkaline earths as main group reagents in molecular catalysis. *Chem. Soc. Rev.* **2016**, *45*, 972-988.
65. Harder, S.; Spielmann, J.; Intemann, J.; Bandmann, H., Hydrogen Storage in Magnesium Hydride: The Molecular Approach. *Angew. Chem., Int. Ed.* **2011**, *50*, 4156-4160.
66. Mukherjee, D.; Okuda, J., Molecular Magnesium Hydrides. *Angew. Chem., Int. Ed.* **2018**, *57*, 1458-1473.
67. Kuchenbeiser, G.; Soleilhavoup, M.; Donnadiou, B.; Bertrand, G., Reactivity of Cyclic (Alkyl)(amino)carbenes (CAACs) and Bis(amino)cyclopropenylidenes (BACs) with Heteroallenes: Comparisons with their N-Heterocyclic Carbene (NHCs) Counterparts. *Chem. Asian J.* **2009**, *4*, 1745-1750.
68. Lieske, L. E.; Freeman, L. A.; Wang, G.; Dickie, D. A.; Gilliard Jr., R. J.; Machan, C. W., Metal-Free Electrochemical Reduction of Carbon Dioxide Mediated by Cyclic(Alkyl)(Amino) Carbenes. *Chem. - Eur. J.* **2019**, *25*, 6098-6101.
69. Tretiakov, M.; Shermolovich, Y. G.; Singh, A. P.; Samuel, P. P.; Roesky, H. W.; Niepötter, B.; Visscher, A.; Stalke, D., Lewis-base stabilized diiodine adducts with N-heterocyclic chalcogenamides. *Dalton Trans* **2013**, *42*, 12940-12946.
70. Arrowsmith, M.; Hill, M. S.; Kociok-Köhn, G.; MacDougall, D. J.; Mahon, M. F.; Mallov, I., Three-Coordinate Beryllium  $\beta$ -Diketiminates: Synthesis and Reduction Chemistry. *Inorg. Chem.* **2012**, *51*, 13408-13418.
71. Bonyhady, S. J.; Jones, C.; Nembenna, S.; Stasch, A.; Edwards, A. J.; McIntyre, G. J.,  $\beta$ -Diketimate-Stabilized Magnesium(I) Dimers and Magnesium(II) Hydride Complexes:

Synthesis, Characterization, Adduct Formation, and Reactivity Studies. *Chem. – Eur. J.* **2010**, *16*, 938-955.

72. Czernetzki, C.; Arrowsmith, M.; Fantuzzi, F.; Gärtner, A.; Tröster, T.; Krummenacher, I.; Schorr, F.; Braunschweig, H., A Neutral Beryllium(I) Radical. *Angew. Chem., Int. Ed.* **2021**, DOI: 10.1002/anie.202108405.

73. Mokkelbost, T.; Kaus, I.; Haugsrud, R.; Norby, T.; Grande, T.; Einarsrud, M.-A., High-Temperature Proton-Conducting Lanthanum Ortho-Niobate-Based Materials. Part II: Sintering Properties and Solubility of Alkaline Earth Oxides. *J. Am. Chem. Soc.* **2008**, *91*, 879-886.

74. Haynes, W. M., ed., *CRC handbook of chemistry and physics: a ready-reference book of chemical and physical data: 2011-2012*. 92nd ed.; CRC: Boca Raton, FL, 2011.

75. Diao, Y.; Walawender, W. P.; Sorensen, C. M.; Klabunde, K. J.; Ricker, T., Hydrolysis of Magnesium Methoxide. Effects of Toluene on Gel Structure and Gel Chemistry. *Chem. Mater.* **2002**, *14*, 362-368.

76. Bell, N. A.; Shearer, H. M. M.; Twiss, J., Dimeric tert-butoxyberyllium bromide-diethyl ether adduct,  $[\text{Be}_2\text{Br}_2(\text{C}_4\text{H}_9\text{O})_2(\text{C}_4\text{H}_{10}\text{O})_2]$ , and a comparison with the magnesium analogue. *Acta Crystallographica* **1984**, *40*, 605-607.

77. Bell, N. A.; Coates, G. E.; Schneider, M. L.; Shearer, H. M. M., Terminal beryllium-hydrogen bonding. X-Ray crystal structure of the (2-dimethylamino-N-methylethylamido)hydridoberyllium dimer. *Chem. Commun.* **1983**, 828-829.

78. Bell, N. A.; Coates, G. E.; Shearer, H. M. M.; Twiss, J.,  $\pi$ -Bonding in three-co-ordinate beryllium compounds. Structure of tetra- $\mu$ -t-butoxydichlorotriberyllium. *Chem. Commun.* **1983**, 840-841.

79. Naglav, D.; Tobey, B.; Wölper, C.; Bläser, D.; Jansen, G.; Schulz, S., On the Stability of Trimeric Beryllium Hydroxide Scorpionate Complexes. *Eur. J. Inorg. Chem.* **2016**, *2016*, 2424-2431.

80. Pietrzak, T.; Kubisiak, M.; Justyniak, I.; Zelga, K.; Bojarski, E.; Tratkiewicz, E.; Ochal, Z.; Lewiński, J., Oxygenation Chemistry of Magnesium Alkyls Incorporating  $\beta$ -Diketimate Ligands Revisited. *Chem. - Eur. J.* **2016**, *22*, 17776-17783.

81. Ruhlandt-Senge, K.; Bartlett, R. A.; Olmstead, M. M.; Power, P. P., Synthesis and structural characterization of the beryllium compounds  $[\text{Be}(2,4,6\text{-Me}_3\text{C}_6\text{H}_2)_2(\text{OEt}_2)]$ ,  $[\text{Be}\{\text{O}(2,4,6\text{-tert-Bu}_3\text{C}_6\text{H}_2)\}_2(\text{OEt}_2)]$ , and  $[\text{Be}\{\text{S}(2,4,6\text{-tert-Bu}_3\text{C}_6\text{H}_2)\}_2(\text{THF})]$ . cnddot.PhMe and determination of the structure of  $[\text{BeCl}_2(\text{OEt}_2)_2]$ . *Inorg. Chem.* **1993**, *32*, 1724-1728.

82. Arrowsmith, M.; Crimmin, M. R.; Hill, M. S.; Kociok-Köhn, G., Beryllium derivatives of a phenyl-substituted  $\beta$ -diketimate: a well-defined ring opening reaction of tetrahydrofuran. *Dalton Trans.* **2013**, *42*, 9720-9726.

83. Buchner, M. R.; Spang, N.; Müller, M.; Rudel, S. S., Formation and Properties of the Trichloroberyllate Ion. *Inorg. Chem.* **2018**, *57*, 11314-11317.

84. Bayram, M.; Naglav, D.; Wölper, C.; Schulz, S., Syntheses and Structures of Homo- and Heteroleptic Beryllium Complexes Containing N,N'-Chelating Ligands. *Organometallics* **2017**, *36*, 467-473.

85. Thiele, K.-H.; Lorenz, V.; Thiele, G.; Zönnchen, P.; Scholz, J.,  $[\text{Be}(\text{dad})_2]$ : Synthesis and Structure of a Diazabutadieneberyllium Complex. *Angew. Chem., Int. Ed.* **1994**, *33*, 1372-1373.

86. Liu, S.-F.; Wu, Q.; Schmider, H. L.; Aziz, H.; Hu, N.-X.; Popović, Z.; Wang, S., Syntheses, Structures, and Electroluminescence of New Blue/Green Luminescent Chelate Compounds:  $\text{Zn}(2\text{-py-in})_2(\text{THF})$ ,  $\text{BPh}_2(2\text{-py-in})$ ,  $\text{Be}(2\text{-py-in})_2$ , and  $\text{BPh}_2(2\text{-py-aza})$  [ $2\text{-py-in} = 2\text{-(2-pyridyl)indole}$ ;  $2\text{-py-aza} = 2\text{-(2-pyridyl)-7-azaindole}$ ]. *J. Am. Chem. Soc.* **2000**, *122*, 3671-3678.

87. Arrowsmith, M.; Hill, M. S.; Kociok-Köhn, G., Activation of N-Heterocyclic Carbenes by {BeH<sub>2</sub>} and {Be(H)(Me)} Fragments. *Organometallics* **2015**, *34* (3), 653-662.
88. Kindervater, M. B.; Marczenko, K. M.; Werner-Zwanziger, U.; Chitnis, S. S., A Redox-Confused Bismuth(I/III) Triamide with a T-Shaped Planar Ground State. *Angew. Chem., Int. Ed.* **2019**, *58*, 7850-7855.
89. Turner, Z. R., Bismuth Pyridine Dipyrrolide Complexes: a Transient Bi(II) Species Which Ring Opens Cyclic Ethers. *Inorg. Chem.* **2019**, *58*, 14212-14227.
90. Planas, O.; Wang, F.; Leutzsch, M.; Cornella, J., Fluorination of arylboronic esters enabled by bismuth redox catalysis. *Science* **2020**, *367*, 313-317.
91. Jurrat, M.; Maggi, L.; Lewis, W.; Ball, L. T., Modular bismacycles for the selective C–H arylation of phenols and naphthols. *Nat. Chem.* **2020**, *12*, 260-269.
92. Wang, F.; Planas, O.; Cornella, J., Bi(I)-Catalyzed Transfer-Hydrogenation with Ammonia-Borane. *J. Am. Chem. Soc.* **2019**, *141*, 4235-4240.
93. Engesser, T. A.; Lichtenthaler, M. R.; Schleep, M.; Krossing, I., Reactive p-block cations stabilized by weakly coordinating anions. *Chem. Soc. Rev.* **2016**, *45*, 789-899.
94. Marczenko, K. M.; Chitnis, S. S., Bismuthanylstibanes. *Chem. Commun.* **2020**, DOI: 10.1039/D0CC00254B.
95. Dostál, L., Quest for stable or masked pnictinidenes: Emerging and exciting class of group 15 compounds. *Coord. Chem. Rev.* **2017**, *353*, 142-158.
96. Tokitoh, N.; Arai, Y.; Okazaki, R.; Nagase, S., Synthesis and Characterization of a Stable Dibismuthene: Evidence for a Bi-Bi Double Bond. *Science* **1997**, *277*, 78-80.
97. Solyntjes, S.; Bader, J.; Neumann, B.; Stammler, H.-G.; Ignat'ev, N.; Hoge, B., Pentafluoroethyl Bismuth Compounds. *Chem. - Eur. J.* **2017**, *23*, 1557-1567.
98. Sasamori, T.; Takeda, N.; Fujio, M.; Kimura, M.; Nagase, S.; Tokitoh, N., Synthesis and Structure of the First Stable Phosphabismuthene. *Angew. Chem., Int. Ed.* **2002**, *41*, 139-141.
99. Whitmire, K. H.; Hoppe, S.; Sydora, O.; Jolas, J. L.; Jones, C. M., Oligomerization and Oxide Formation in Bismuth Aryl Alkoxides: Synthesis and Characterization of Bi<sub>4</sub>(μ<sub>4</sub>-O)(μ-OC<sub>6</sub>F<sub>5</sub>)<sub>6</sub>{μ<sub>3</sub>-OBi(μ-OC<sub>6</sub>F<sub>5</sub>)<sub>3</sub>}<sub>2</sub>(C<sub>6</sub>H<sub>5</sub>CH<sub>3</sub>), Bi<sub>8</sub>(μ<sub>4</sub>-O)<sub>2</sub>(μ<sub>3</sub>-O)<sub>2</sub>(μ-OC<sub>6</sub>F<sub>5</sub>)<sub>16</sub>, Bi<sub>6</sub>(μ<sub>3</sub>-O)<sub>4</sub>(μ<sub>3</sub>-OC<sub>6</sub>F<sub>5</sub>){μ<sub>3</sub>-OBi(OC<sub>6</sub>F<sub>5</sub>)<sub>4</sub>}<sub>3</sub>, NaBi<sub>4</sub>(μ<sub>3</sub>-O)<sub>2</sub>(OC<sub>6</sub>F<sub>5</sub>)<sub>9</sub>(THF)<sub>2</sub>, and Na<sub>2</sub>Bi<sub>4</sub>(μ<sub>3</sub>-O)<sub>2</sub>(OC<sub>6</sub>F<sub>5</sub>)<sub>10</sub>(THF)<sub>2</sub>. *Inorg. Chem.* **2000**, *39*, 85-97.
100. Jones, C. M.; Burkart, M. D.; Bachman, R. E.; Serra, D. L.; Hwu, S. J.; Whitmire, K. H., Hypervalent bismuth alkoxide dimer complexes: syntheses, structures, and thermal decompositions of [Bi(OCH(CF<sub>3</sub>)<sub>2</sub>)<sub>2</sub>(μ-OCH(CF<sub>3</sub>)<sub>2</sub>)(THF)]<sub>2</sub> and [Bi(OC<sub>6</sub>F<sub>5</sub>)<sub>2</sub>(μ-OCH(CF<sub>3</sub>)<sub>2</sub>)<sub>2</sub> · 2C<sub>7</sub>H<sub>8</sub>]. *Inorg. Chem.* **1993**, *32*, 5136-5144.
101. Jones, C. M.; Burkart, M. D.; Whitmire, K. H., Bismuth Alkoxide Dimer Complexes Containing Planar Bi<sub>2</sub>(μ-OR)<sub>2</sub> Cores: Syntheses and Structures of [{Bi[OCH(CF<sub>3</sub>)<sub>2</sub>]<sub>3</sub>(thf)}<sub>2</sub>] and [{Bi(OC<sub>6</sub>F<sub>5</sub>)<sub>3</sub>(C<sub>7</sub>H<sub>8</sub>)<sub>2</sub>] · 2C<sub>7</sub>H<sub>8</sub>. *Angew. Chem., Int. Ed.* **1992**, *31*, 451-452.
102. Yasui, M.; Kikuchi, T.; Iwasaki, F.; Suzuki, H.; Murafuji, T.; Ogawa, T., First X-ray structure determination of a bismuthio ylido: 4,4-dimethyl-2,6-dioxo-1-triphenylbismuthiocyclohexanide. *J. Chem. Soc., Perkin Trans. 1* **1990**, 3367-3368.
103. Frank, W.; Weber, J.; Fuchs, E., [CH<sub>3</sub>C<sub>6</sub>H<sub>5</sub>BiCl<sub>2</sub>][AlCl<sub>4</sub>] and [(CH<sub>3</sub>)<sub>6</sub>C<sub>6</sub>BiCl<sub>2</sub>][AlCl<sub>4</sub>]—Compounds containing η<sup>6</sup>-Arene-Complexed BiCl Units. *Angew. Chem., Int. Ed.* **1987**, *26*, 74-75.

104. Calderazzo, F.; Morvillo, A.; Pelizzi, G.; Poli, R., Synthesis and crystal and molecular structure of tetraphenyldibismuthine, Bi<sub>2</sub>Ph<sub>4</sub>, the first crystallographically characterized tetraorganyl derivative of bismuth(II). *Chem. Commun.* **1983**, 507-508.
105. Dikarev, E. V.; Li, B., Rational Syntheses, Structure, and Properties of the First Bismuth(II) Carboxylate. *Inorg. Chem.* **2004**, *43*, 3461-3466.
106. Zhang, X.; Yin, S.; Qiu, R.; Xia, J.; Dai, W.; Yu, Z.; Au, C.-T.; Wong, W.-Y., Synthesis and structure of an air-stable hypervalent organobismuth (III) perfluorooctanesulfonate and its use as high-efficiency catalyst for Mannich-type reactions in water. *J. Organomet. Chem.* **2009**, *694*, 3559-3564.
107. Soran, A. P.; Silvestru, C.; Breunig, H. J.; Balázs, G.; Green, J. C., Organobismuth(III) Dihalides with T-Shaped Geometry Stabilized by Intramolecular N→Bi Interactions and Related Diorganobismuth(III) Halides. *Organometallics* **2007**, *26*, 1196-1203.
108. Arduengo, A. J.; Calabrese, J. C.; Cowley, A. H.; Dias, H. V. R.; Goerlich, J. R.; Marshall, W. J.; Riegel, B., Carbene–Pnictinidene Adducts. *Inorg. Chem.* **1997**, *36*, 2151-2158.
109. Aprile, A.; Corbo, R.; Vin Tan, K.; Wilson, D. J. D.; Dutton, J. L., The first bismuth–NHC complexes. *Dalton Trans.* **2014**, *43*, 764-768.
110. Wang, G.; Freeman, L. A.; Dickie, D. A.; Mokrai, R.; Benkő, Z.; Gilliard, R. J., Highly Reactive Cyclic(alkyl)(amino) Carbene- and N-Heterocyclic Carbene-Bismuth(III) Complexes: Synthesis, Structure, and Computations. *Inorg. Chem.* **2018**, *57*, 11687-11695.
111. Olaru, M.; Duvinage, D.; Lork, E.; Mebs, S.; Beckmann, J., Heavy Carbene Analogues: Donor-Free Bismuthenium and Stibenium Ions. *Angew. Chem., Int. Ed.* **2018**, *57*, 10080-10084.
112. Lichtenberg, C.; Pan, F.; Spaniol, T. P.; Englert, U.; Okuda, J., The Bis(allyl)bismuth Cation: A Reagent for Direct Allyl Transfer by Lewis Acid Activation and Controlled Radical Polymerization. *Angew. Chem., Int. Ed.* **2012**, *51*, 13011-13015.
113. Waters, J. B.; Chen, Q.; Everitt, T. A.; Goicoechea, J. M., N-Heterocyclic carbene adducts of the heavier group 15 tribromides. Normal to abnormal isomerism and bromide ion abstraction. *Dalton Trans.* **2017**, *46*, 12053-12066.
114. Chitnis, S. S.; Robertson, A. P. M.; Burford, N.; Patrick, B. O.; McDonald, R.; Ferguson, M. J., Bipyridine complexes of E<sup>3+</sup> (E = P, As, Sb, Bi): strong Lewis acids, sources of E(OTf)<sub>3</sub> and synthons for EI and EV cations. *Chem. Sci.* **2015**, *6*, 6545-6555.
115. Dyker, C. A.; Lavallo, V.; Donnadiou, B.; Bertrand, G., Synthesis of an Extremely Bent Acyclic Allene (A “Carbodicarbene”): A Strong Donor Ligand. *Angew. Chem., Int. Ed.* **2008**, *120*, 3250-3253.
116. Klein, S.; Tonner, R.; Frenking, G., Carbodicarbenes and Related Divalent Carbon(0) Compounds. *Chem. - Eur. J.* **2010**, *16*, 10160-10170.
117. Liu, S.-k.; Shih, W.-C.; Chen, W.-C.; Ong, T.-G., Carbodicarbenes and their Captodative Behavior in Catalysis. *ChemCatChem* **2018**, *10*, 1480-1480.
118. Su, W.; Pan, S.; Sun, X.; Wang, S.; Zhao, L.; Frenking, G.; Zhu, C., Double dative bond between divalent carbon(0) and uranium. *Nat. Commun.* **2018**, *9*, 4997.
119. Vicente, J.; Singhal, A. R.; Jones, P. G., New Ylide–, Alkynyl–, and Mixed Alkynyl/Ylide–Gold(I) Complexes. *Organometallics* **2002**, *21*, 5887-5900.
120. Ramirez, F.; Desai, N. B.; Hansen, B.; McKelvie, N., HEXAPHENYLCARBODIPHOSPHORANE, (C<sub>6</sub>H<sub>5</sub>)<sub>3</sub>PCP(C<sub>6</sub>H<sub>5</sub>)<sub>3</sub>. *J. Am. Chem. Soc.* **1961**, *83*, 3539-3540.
121. Hsu, Y.-C.; Shen, J.-S.; Lin, B.-C.; Chen, W.-C.; Chan, Y.-T.; Ching, W.-M.; Yap, G. P. A.; Hsu, C.-P.; Ong, T.-G., Synthesis and Isolation of an Acyclic Tridentate

Bis(pyridine)carbodicarbene and Studies on Its Structural Implications and Reactivities. *Angew. Chem., Int. Ed.* **2015**, *54*, 2420-2424.

122. Đorđević, N.; Ganguly, R.; Petković, M.; Vidović, D., E–H (E = B, Si, C) Bond Activation by Tuning Structural and Electronic Properties of Phosphenium Cations. *Inorg. Chem.* **2017**, *56*, 14671-14681.

123. Đorđević, N.; Ganguly, R.; Petković, M.; Vidović, D., Bis(carbodicarbene)phosphenium trication: the case against hypervalency. *Chem. Commun.* **2016**, *52*, 9789-9792.

124. Gurnani, C.; Đorđević, N.; Muthaiah, S.; Dimić, D.; Ganguly, R.; Petković, M.; Vidović, D., Extending the chemistry of carbones: P–N bond cleavage via an SN2'-like mechanism. *Chem. Commun.* **2015**, *51*, 10762-10764.

125. Chen, W.-C.; Lee, C.-Y.; Lin, B.-C.; Hsu, Y.-C.; Shen, J.-S.; Hsu, C.-P.; Yap, G. P. A.; Ong, T.-G., The Elusive Three-Coordinate Dicationic Hydrido Boron Complex. *J. Am. Chem. Soc.* **2014**, *136*, 914-917.

126. Floch, P. L., Phosphaalkene, phospholyl and phosphinine ligands: New tools in coordination chemistry and catalysis. *Coord. Chem. Rev.* **2006**, *250*, 627-681.

127. Balmer, M.; Gottschling, H.; von Hänisch, C., Phosphaalkene-substituted organo-group 15 compounds: synthesis and characterisation of (NHC)P–EtBu<sub>2</sub> (E = P, As, Sb and Bi). *Chem. Commun.* **2018**, *54*, 2659-2661.

128. Wilson, D. W. N.; Hinz, A.; Goicoechea, J. M., An Isolable Phosphaethynolatoborane and Its Reactivity. *Angew. Chem., Int. Ed.* **2018**, *57*, 2188-2193.

129. Rosa, P.; Gouverd, C.; Bernardinelli, G.; Berclaz, T.; Geoffroy, M., Phosphaalkenes with Inverse Electron Density: Electrochemistry, Electron Paramagnetic Resonance Spectra, and Density Functional Theory Calculations of Aminophosphaalkene Derivatives. *J. Chem. Phys. A.* **2003**, *107*, 4883-4892.

130. Appel, R.; Knoll, F.; Ruppert, I., Phospha-alkenes and Phospha-alkynes, Genesis and Properties of the (p-p) $\pi$ -Multiple Bond. *Angew. Chem., Int. Ed.* **1981**, *20*, 731-744.

131. Morales Salazar, D.; Mijangos, E.; Pullen, S.; Gao, M.; Orthaber, A., Functional small-molecules & polymers containing P $\square$ C and As $\square$ C bonds as hybrid  $\pi$ -conjugated materials. *Chem. Commun.* **2017**, *53*, 1120-1123.

132. Hinz, A.; Hansmann, M. M.; Bertrand, G.; Goicoechea, J. M., Intercepting a Transient Phosphino-Arsinidene. *Chem. - Eur. J.* **2018**, *24*, 9514-9519.

133. Tambornino, F.; Hinz, A.; Köppe, R.; Goicoechea, J. M., A General Synthesis of Phosphorus- and Arsenic-Containing Analogues of the Thio- and Seleno-cyanate Anions. *Angew. Chem., Int. Ed.* **2018**, *57*, 8230-8234.

134. Pfeifer, G.; Papke, M.; Frost, D.; Sklorz, J. A. W.; Habicht, M.; Müller, C., Clicking the Arsenic–Carbon Triple Bond: An Entry into a New Class of Arsenic Heterocycles. *Angew. Chem., Int. Ed.* **2016**, *55*, 11760-11764.

135. Weber, L.; Meine, G.; Boese, R., Synthesis and Structure of the First Arsaalkenyl Complex with FeAs Single Bond. *Angew. Chem., Int. Ed.* **1986**, *25*, 469-471.

136. Doddi, A.; Weinhart, M.; Hinz, A.; Bockfeld, D.; Goicoechea, J. M.; Scheer, M.; Tamm, M., N-Heterocyclic carbene-stabilised arsinidene (AsH). *Chem. Commun.* **2017**, *53*, 6069-6072.

137. Bouslikhane, M.; Gornitzka, H.; Escudié, J.; Ranaivonjatovo, H.; Ramdane, H., The First Diarsaallene ArAsCAsAr (Ar = 2,4,6-Tri-tert-butylphenyl). *J. Am. Chem. Soc.* **2000**, *122*, 12880-12881.

138. Ferguson, G.; Glidewell, C.; Gosney, I.; Lloyd, D.; Metcalfe, S.; Lumbroso, H., Stibonium and bismuthonium ylides. A comparison with arsonium and other ylides, also including the crystal

structure of triphenylarsonium bis(phenylsulphonyl)methylide and triphenylarsonium and triphenylstibonium 4,4-dimethyl-2,6-dioxocyclohexylides. *J. Chem. Soc., Perkin Trans. 2* **1988**, 1829-1837.

139. Jones, C.; W. Steed, J.; C. Thomas, R., Compounds containing  $\lambda^3, \sigma^2$ -Sb-C bonds: synthesis and structural characterisation of the first stiba-enol, Mes<sup>\*</sup>C(O)Sb-C(OH)Mes<sup>\*</sup> (Mes<sup>\*</sup> = C<sub>6</sub>H<sub>2</sub>But<sub>3-2,4,6</sub>) and a 2,3-distibabutadiene, {Mes(Me<sub>3</sub>SiO)C-Sb}<sub>2</sub> (Mes = C<sub>6</sub>H<sub>2</sub>Me<sub>3-2,4,6</sub>)<sup>†</sup>. *Dalton Trans.* **1999**, 1541-1542.

140. Krüger, J.; Wölper, C.; John, L.; Song, L.; Schreiner, P. R.; Schulz, S., Syntheses, Structures, and Bonding Analyses of Carbene-Stabilized Stibinidenes. *Eur. J. Inorg. Chem.* **2019**, 2019, 1669-1678.

141. Thirumoorthi, R.; Chivers, T.; Vargas-Baca, I., S,C,S-Pnictogen bonding in pincer complexes of the methanediide [C(Ph<sub>2</sub>PS)<sub>2</sub>]<sup>2-</sup>. *Dalton Trans.* **2011**, 40, 8086-8088.

142. Hitchcock, P. B.; Jones, C.; Nixon, J. F., The First Distibabutadiene: Synthesis and Structure of trans-1,4-Bis(trimethylsiloxy)-1,4-bis(2,4,6-tri-tert-butylphenyl)-2,3-distibabutadiene. *Angew. Chem., Int. Ed.* **1995**, 34, 492-493.

143. Ishii, T.; Suzuki, K.; Nakamura, T.; Yamashita, M., An Isolable Bismabenzene: Synthesis, Structure, and Reactivity. *J. Am. Chem. Soc.* **2016**, 138, 12787-12790.

144. Sindlinger, C. P.; Stasch, A.; Wesemann, L., Heavy Group 15 Element Compounds of a Sterically Demanding Bis(iminophosphorane)methanide and -methanediide. *Organometallics* **2014**, 33, 322-328.

145. Pan, X.; Wang, X.; Zhang, Z.; Wang, X., Two phosphalkene radical cations with inverse spin density distributions. *Dalton Trans.* **2015**, 44, 15099-15102.

146. Liu, L.; Ruiz, D. A.; Dahcheh, F.; Bertrand, G., Isolation of a Lewis base stabilized parent phosphonium (PH<sub>2</sub><sup>+</sup>) and related species. *Chem. Commun.* **2015**, 51, 12732-12735.

147. Ellis, B. D.; Ragona, P. J.; Macdonald, C. L. B., Computational Insights into the Acceptor Chemistry of Phosphenium Cations. *Inorg. Chem.* **2004**, 43, 7857-7867.

148. Grützmacher, H.; Pritzkow, H., Three Independent Molecules in the Unit Cell of a Phosphorus Ylide; Changes in the Molecular Geometry on Rotation about the Phosphorus-Carbon Ylide Bond. *Angew. Chem., Int. Ed.* **1992**, 31, 99-101.

149. Heim, U.; Pritzkow, H.; Schönberg, H.; Grützmacher, H., Phosphorus lone pairs stabilization of carbocations: the synthesis and dynamics of unsymmetrical methylene phosphonium ions. *Chem. Commun.* **1993**, (8), 673-674.

150. Gamon, N.; Reichardt, C.; Allmann, R.; Waśkowska, A., Darstellung und Eigenschaften von  $\beta$ -Arsa-trimethincyanin-Farbstoffen mit Indolin-Endgruppen<sup>1</sup>). *Chem. Ber.* **1981**, 114, 3289-3305.

151. Doddi, A.; Bockfeld, D.; Zaretske, M.-K.; Bannenberg, T.; Tamm, M., Isolation of Carbene-Stabilized Arsenic Monophosphide [AsP] and its Radical Cation [AsP]<sup>+</sup>. and Dication [AsP]<sub>2</sub><sup>2+</sup>. *Chem. - Eur. J.* **2019**, 25, 13119-13123.

152. Mrutu, A.; Dickie, D. A.; Goldberg, K. I.; Kemp, R. A., A Unique Three-Dimensional Coordination Cluster Based on a Silver Carbene Complex. *Inorg. Chem.* **2011**, 50, 2729-2731.

153. Cordero, B.; Gómez, V.; Platero-Prats, A. E.; Revés, M.; Echeverría, J.; Cremades, E.; Barragán, F.; Alvarez, S., Covalent radii revisited. *Dalton Trans.* **2008**, (21), 2832-2838.

154. Rodrigues, R. R.; Dorsey, C. L.; Arceneaux, C. A.; Hudnall, T. W., Phosphaalkene vs. phosphinidene: the nature of the P-C bond in carbonyl-decorated carbene  $\rightarrow$  PPh adducts. *Chem. Commun.* **2014**, 50, 162-164.

155. Becke, A. D., Density-functional exchange-energy approximation with correct asymptotic behavior. *Phys. Rev. A* **1988**, *38*, 3098-3100.
156. Perdew, J. P., Density-functional approximation for the correlation energy of the inhomogeneous electron gas. *Phys. Rev. B* **1986**, *33*, 8822-8824.
157. Grimme, S.; Ehrlich, S.; Goerigk, L., Effect of the damping function in dispersion corrected density functional theory. *J. Comput. Chem.* **2011**, *32*, 1456-1465.
158. Grimme, S.; Antony, J.; Ehrlich, S.; Krieg, H., A consistent and accurate ab initio parametrization of density functional dispersion correction (DFT-D) for the 94 elements H-Pu. *J. Chem. Phys.* **2010**, *132*, 154104.
159. Weigend, F., Accurate Coulomb-fitting basis sets for H to Rn. *Phys. Chem. Chem. Phys.* **2006**, *8*, 1057-1065.
160. Weigend, F.; Ahlrichs, R., Balanced basis sets of split valence, triple zeta valence and quadruple zeta valence quality for H to Rn: Design and assessment of accuracy. *Phys. Chem. Chem. Phys.* **2005**, *7*, 3297-3305.
161. Ziegler, T.; Rauk, A., On the calculation of bonding energies by the Hartree Fock Slater method. *Theor. Chim. Acta* **1977**, *46*, 1-10.
162. Mitoraj, M.; Michalak, A., Applications of natural orbitals for chemical valence in a description of bonding in conjugated molecules. *J. Mol. Model.* **2008**, *14*, 681-687.
163. Mitoraj, M.; Michalak, A., Donor–Acceptor Properties of Ligands from the Natural Orbitals for Chemical Valence. *Organometallics* **2007**, *26*, 6576-6580.
164. Yang, W.; Krantz, K. E.; Freeman, L. A.; Dickie, D. A.; Molino, A.; Frenking, G.; Pan, S.; Wilson, D. J. D.; Gilliard Jr., R. J., Persistent Borafluorene Radicals. *Angew. Chem., Int. Ed.* **2020**, *59*, 3850-3854.
165. Saha, R.; Pan, S.; Merino, G.; Chattaraj, P. K., Unprecedented Bonding Situation in Viable E<sub>2</sub>(NHBMe)<sub>2</sub> (E=Be, Mg; NHBMe=(HCNMe)<sub>2</sub>B) Complexes: Neutral E<sub>2</sub> Forms a Single E–E Covalent Bond. *Angew. Chem., Int. Ed.* **2019**, *58*, 8372-8377.
166. Wang, Q.; Pan, S.; Wu, Y.-B.; Deng, G.; Bian, J.-H.; Wang, G.; Zhao, L.; Zhou, M.; Frenking, G., Transition-Metal Chemistry of Alkaline-Earth Elements: The Trisbenzene Complexes M(Bz)<sub>3</sub> (M=Sr, Ba). *Angew. Chem., Int. Ed.* **2019**, *58*, 17365-17374.
167. Wang, Q.; Pan, S.; Lei, S.; Jin, J.; Deng, G.; Wang, G.; Zhao, L.; Zhou, M.; Frenking, G., Octa-coordinated alkaline earth metal–dinitrogen complexes M(N<sub>2</sub>)<sub>8</sub> (M=Ca, Sr, Ba). *Nat. Commun.* **2019**, *10*, 3375.
168. Chi, C.; Pan, S.; Meng, L.; Luo, M.; Zhao, L.; Zhou, M.; Frenking, G., Alkali Metal Covalent Bonding in Nickel Carbonyl Complexes ENi(CO)<sub>3</sub><sup>–</sup>. *Angew. Chem., Int. Ed.* **2019**, *58*, 1732-1738.
169. Wu, X.; Zhao, L.; Jin, J.; Pan, S.; Li, W.; Jin, X.; Wang, G.; Zhou, M.; Frenking, G., Observation of alkaline earth complexes M(CO)<sub>8</sub> (M = Ca, Sr, or Ba) that mimic transition metals. *Science* **2018**, *361*, 912-916.
170. Pan, S.; Zhao, L.; Dias, H. V. R.; Frenking, G., Bonding in Binuclear Carbonyl Complexes M<sub>2</sub>(CO)<sub>9</sub> (M = Fe, Ru, Os). *Inorg. Chem.* **2018**, *57*, 7780-7791.
171. Pecher, L.; Pan, S.; Frenking, G., Chemical bonding in the hexamethylbenzene–SO<sub>2</sub><sup>+</sup> dication. *Theor. Chem. Acc.* **2019**, *138*, 47.
172. Walley, J.; Warring, L.; Wang, G.; Dickie, D. A.; Pan, S.; Frenking, G.; Gilliard, R. J., Carbodicarbene Bismaalkene Cations: Unravelling the Complexities of Carbene versus Carbene in Heavy Pnictogen Chemistry. *Angew. Chem., Int. Ed.* **2021**, *60*, 6682-6690.

173. Zhao, Y.; Truhlar, D. G., The M06 suite of density functionals for main group thermochemistry, thermochemical kinetics, noncovalent interactions, excited states, and transition elements: two new functionals and systematic testing of four M06-class functionals and 12 other functionals. *Theor. Chem. Acc.* **2008**, *120*, 215-241.
174. Appel, R.; Knoll, F., Double Bonds Between Phosphorus and Carbon. In *Advances in Inorganic Chemistry*, Sykes, A. G., Ed. Academic Press: 1989; Vol. 33, pp 259-361.
175. Escudié, J.; Ranaivonjatovo, H.; Rigon, L., Heavy Allenes and Cumulenes ECE' and ECCE' (E = P, As, Si, Ge, Sn; E' = C, N, P, As, O, S). *Chem. Rev.* **2000**, *100*, 3639-3696.
176. Appel, R.; Paulen, W., The First Stable Phosphaketene. *Angew. Chem., Int. Ed.* **1983**, *22*, 785-786.
177. Goicoechea, J. M.; Grützmacher, H., The Chemistry of the 2-Phosphaethynolate Anion. *Angew. Chem., Int. Ed.* **2018**, *57*, 16968-16994.
178. Puschmann, F. F.; Stein, D.; Heift, D.; Hendriksen, C.; Gal, Z. A.; Grützmacher, H.-F.; Grützmacher, H., Phosphination of Carbon Monoxide: A Simple Synthesis of Sodium Phosphaethynolate (NaOCP). *Angew. Chem., Int. Ed.* **2011**, *50*, 8420-8423.
179. Becker, G.; Schwarz, W.; Seidler, N.; Westerhausen, M., Acyl- und Alkylidenphosphane. XXXIII. Lithoxy-methylidenphosphan DME und -methylidinphosphan 2 DME ? Synthese und Struktur. *Z. Anorg. Allg. Chem.* **1992**, *612*, 72-82.
180. Yang, W.; Krantz, K. E.; Dickie, D. A.; Molino, A.; Wilson, D. J. D.; Gilliard Jr., R. J., Crystalline BP-Doped Phenanthryne via Photolysis of The Elusive Boraphosphaketene. *Angew. Chem., Int. Ed.* **2020**, *59*, 3971-3975.
181. Heift, D.; Benkő, Z.; Grützmacher, H., Is the phosphaethynolate anion, (OCP)<sup>-</sup>, an ambident nucleophile? A spectroscopic and computational study. *Dalton Trans.* **2014**, *43*, 5920-5928.
182. Mei, Y.; Borger, J. E.; Wu, D.-J.; Grützmacher, H., Salen supported Al–O–C≡P and Ga–P≡C≡O complexes. *Dalton Trans.* **2019**, *48*, 4370-4374.
183. Li, Z.; Chen, X.; Li, Y.; Su, C.-Y.; Grützmacher, H., N-Heterocyclic carbene phosphaketene adducts as precursors to carbene–phosphinidene adducts and a rearranged π-system. *Chem. Commun.* **2016**, *52*, 11343-11346.
184. Li, Z.; Chen, X.; Benkő, Z.; Liu, L.; Ruiz, D. A.; Peltier, J. L.; Bertrand, G.; Su, C.-Y.; Grützmacher, H., N-Heterocyclic Carbenes as Promoters for the Rearrangement of Phosphaketenes to Phosphaheteroallenes: A Case Study for OCP to OPC Constitutional Isomerism. *Angew. Chem., Int. Ed.* **2016**, *55*, 6018-6022.
185. Appel, R.; Laubach, B.; Siray, M., Einschiebungsreaktion von kohlendioxid in disilylierte phosphane. *Tetrahedron Lett.* **1984**, *25*, 4447-4448.
186. Heift, D.; Benkő, Z.; Grützmacher, H., Coulomb repulsion versus cycloaddition: formation of anionic four-membered rings from sodium phosphaethynolate, Na(OCP). *Dalton Trans.* **2014**, *43*, 831-840.
187. Gilliard, R. J.; Heift, D.; Benkő, Z.; Keiser, J. M.; Rheingold, A. L.; Grützmacher, H.; Protasiewicz, J. D., An isolable magnesium diphosphaethynolate complex. *Dalton Trans.* **2018**, *47*, 666-669.
188. Hoerger, C. J.; Heinemann, F. W.; Louyriac, E.; Maron, L.; Grützmacher, H.; Meyer, K., Formation of a Uranium-Bound η<sup>1</sup>-Cyaphide (CP<sup>-</sup>) Ligand via Activation and C–O Bond Cleavage of Phosphaethynolate (OCP<sup>-</sup>). *Organometallics* **2017**, *36*, 4351-4354.

189. Yao, S.; Xiong, Y.; Szilvási, T.; Grützmacher, H.; Driess, M., From a Phosphaketonyl-Functionalized Germylene to 1,3-Digerma-2,4-diphosphacyclobutadiene. *Angew. Chem., Int. Ed.* **2016**, *55*, 4781-4785.
190. Wu, Y.; Liu, L.; Su, J.; Zhu, J.; Ji, Z.; Zhao, Y., Isolation of a Heavier Cyclobutadiene Analogue: 2,4-Digerma-1,3-diphosphacyclobutadiene. *Organometallics* **2016**, *35*, 1593-1596.
191. Hinz, A.; Goicoechea, J. M., Limitations of Steric Bulk: Towards Phospha-germynes and Phospha-stannynes. *Chem. - Eur. J.* **2018**, *24*, 7358-7363.
192. Xiong, Y.; Yao, S.; Szilvási, T.; Ballester-Martínez, E.; Grützmacher, H.; Driess, M., Unexpected Photodegradation of a Phosphaketonyl-Substituted Germyliumylidene Borate Complex. *Angew. Chem., Int. Ed.* **2017**, *56*, 4333-4336.
193. Del Rio, N.; Baceiredo, A.; Saffon-Merceron, N.; Hashizume, D.; Lutters, D.; Müller, T.; Kato, T., A Stable Heterocyclic Amino(phosphanylidene- $\sigma$ 4-phosphorane) Germylene. *Angew. Chem., Int. Ed.* **2016**, *55*, 4753-4758.
194. Wilson, D. W. N.; Myers, W. K.; Goicoechea, J. M., Synthesis and decarbonylation chemistry of gallium phosphaketenes. *Dalton Trans.* **2020**, *49*, 15249-15255.
195. Alidori, S.; Heift, D.; Santiso-Quinones, G.; Benkő, Z.; Grützmacher, H.; Caporali, M.; Gonsalvi, L.; Rossin, A.; Peruzzini, M., Synthesis and Characterization of Terminal [Re(XCO)(CO)<sub>2</sub>(triphos)] (X=N, P): Isocyanate versus Phosphaethynolate Complexes. *Chem. - Eur. J.* **2012**, *18*, 14805-14811.
196. Mielke, Z.; Andrews, L., Infrared detection of the PCO radical and HPCO molecule. *Chem. Phys. Lett.* **1991**, *181*, 355-360.
197. Hou, G.-L.; Chen, B.; Transue, W. J.; Yang, Z.; Grützmacher, H.; Driess, M.; Cummins, C. C.; Borden, W. T.; Wang, X.-B., Spectroscopic Characterization, Computational Investigation, and Comparisons of ECX<sup>-</sup> (E = As, P, and N; X = S and O) Anions. *J. Am. Chem. Soc.* **2017**, *139*, 8922-8930.
198. Hansmann, M. M.; Bertrand, G., Transition-Metal-like Behavior of Main Group Elements: Ligand Exchange at a Phosphinidene. *J. Am. Chem. Soc.* **2016**, *138*, 15885-15888.
199. Westerhausen, M.; Schneiderbauer, S.; Piotrowski, H.; Suter, M.; Nöth, H., Synthesis of alkaline earth metal bis(2-phosphaethynolates). *J. Organomet. Chem.* **2002**, *643-644*, 189-193.
200. Do, D. C. H.; Protchenko, A. V.; Vasko, P.; Campos, J.; Kolychev, E. L.; Aldridge, S., N-nacnac Stabilized Tetrelenes: Formation of an N,P-Heterocyclic Germylene via C-C Bond Insertion. *Z. Anorg. Allg. Chem.* **2018**, *644*, 1238-1242.
201. Szkop, K. M.; Jupp, A. R.; Stephan, D. W., P,P-Dimethylformylphosphine: The Phosphorus Analogue of N,N-Dimethylformamide. *J. Am. Chem. Soc.* **2018**, *140*, 12751-12755.
202. Li, Z.; Chen, X.; Bergeler, M.; Reiher, M.; Su, C.-Y.; Grützmacher, H., A stable phosphanyl phosphaketene and its reactivity. *Dalton Trans.* **2015**, *44*, 6431-6438.
203. Mehta, M.; McGrady, J. E.; Goicoechea, J. M., B(C<sub>6</sub>F<sub>5</sub>)<sub>3</sub>-Enabled Synthesis of a Cyclic cis-Arsaphosphene. *Chem. - Eur. J.* **2019**, *25*, 5445-5450.
204. Vehkamäki, M.; Hatanpää, T.; Ritala, M.; Leskelä, M., Bismuth precursors for atomic layer deposition of bismuth-containing oxide films. *J. Mater. Chem.* **2004**, *14*, 3191-3197.
205. Conrad, E.; Burford, N.; McDonald, R.; Ferguson, M. J., Bismuthenium-pnictonium dications [R'BiPnR<sub>3</sub>]<sup>2+</sup> (Pn = As, Sb) containing carbenoid bismuth centers and rare Bi-Sb bonds. *Chem. Commun.* **2010**, *46*, 4598-4600.
206. Zhang, X.-P.; Tian, H.-R.; Yan, G.-F.; Su, Y.; Feng, Y.-L.; Cheng, J.-W., Incorporating different secondary building units of {Bi<sub>2</sub>}, {Bi<sub>8</sub>} and {Bi<sub>10</sub>} to construct diversity of luminescent bismuth-organic frameworks. *Dalton Trans.* **2013**, *42*, 1088-1093.

207. Balasanthiran, V.; Chisholm, M. H.; Durr, C. B.; Gallucci, J. C., Single-site bismuth alkoxide catalysts for the ring-opening polymerization of lactide. *Dalton Trans.* **2013**, *42*, 11234-11241.
208. Schwamm, R. J.; Day, B. M.; Coles, M. P.; Fitchett, C. M., Low-Coordinate Bismuth Cations. *Inorg. Chem.* **2014**, *53*, 3778-3787.
209. Lo, Y.-H.; Gabbaï, F. P., An Antimony(V) Dication as a Z-Type Ligand: Turning on Styrene Activation at Gold. *Angew. Chem., Int. Ed.* **2019**, *58*, 10194-10197.
210. Alič, B.; Štefančič, A.; Tavčar, G., Small molecule activation: SbF<sub>3</sub> auto-ionization supported by transfer and mesoionic NHC rearrangement. *Dalton Trans.* **2017**, *46*, 3338-3346.
211. Dorsey, C. L.; Mushinski, R. M.; Hudnall, T. W., Metal-Free Stabilization of Monomeric Antimony(I): A Carbene-Supported Stibinidene. *Chem. - Eur. J.* **2014**, *20*, 8914-8917.
212. Arduengo III, A. J.; Davidson, F.; Krafczyk, R.; Marshall, W. J.; Schmutzler, R., Carbene Complexes of Pnictogen Pentafluorides and Boron Trifluoride. *Monatsh Chem* **2000**, *131*, 251-265.
213. Li, Y.-Z.; Ganguly, R.; Leong, W. K., Oxidative Addition across Sb–H and Sb–Sb Bonds by an Osmium Carbonyl Cluster: Trapping the Intermediate. *Organometallics* **2014**, *33*, 823-828.
214. Henne, F. D.; Dickschat, A. T.; Hennersdorf, F.; Feldmann, K. O.; Weigand, J. J., Synthesis of Selected Cationic Pnictanes [LnPnX<sub>3-n</sub>]<sup>n+</sup> (L = Imidazolium-2-yl; Pn = P, As; n = 1–3) and Replacement Reactions with Pseudohalogenes. *Inorg. Chem.* **2015**, *54*, 6849-6861.
215. Ho, L. P.; Nasr, A.; Jones, P. G.; Altun, A.; Neese, F.; Bistoni, G.; Tamm, M., London Dispersion Interactions in Pnictogen Cations [EC<sub>12</sub>]<sup>+</sup> and [E=E]<sub>2</sub><sup>+</sup> (E=P, As, Sb) Supported by Anionic N-Heterocyclic Carbenes. *Chem. - Eur. J.* **2018**, *24*, 18922-18932.
216. Blom, R.; Haaland, A., A modification of the Schomaker—Stevenson rule for prediction of single bond distances. *J. Mol. Struct.* **1985**, *128*, 21-27.
217. Hennersdorf, F.; Frötschel, J.; Weigand, J. J., Selective Derivatization of a Hexaphosphane from Functionalization of White Phosphorus. *J. Am. Chem. Soc.* **2017**, *139*, 14592-14604.
218. Jupp, A. R.; Goicoechea, J. M., The 2-Phosphaethynolate Anion: A Convenient Synthesis and [2+2] Cycloaddition Chemistry. *Angew. Chem., Int. Ed.* **2013**, *52*, 10064-10067.
219. Jost, M.; Finger, L. H.; Sundermeyer, J.; von Hänisch, C., Simple access to ionic liquids and organic salts containing the phosphaethynolate (PCO<sup>-</sup>) and Zintl (Sb<sub>113</sub><sup>-</sup>) anions. *Chem. Commun.* **2016**, *52*, 11646-11648.
220. Liu, L.; Ruiz, D. A.; Dahcheh, F.; Bertrand, G.; Suter, R.; Tondreau, A. M.; Grützmacher, H., Isolation of Au-, Co-η<sup>1</sup>PCO and Cu-η<sup>2</sup>PCO complexes, conversion of an Ir-η<sup>1</sup>PCO complex into a dimetalladiphosphene, and an interaction-free PCO anion. *Chem. Sci.* **2016**, *7*, 2335-2341.
221. Doddi, A.; Bockfeld, D.; Zaretske, M.-K.; Kleeberg, C.; Bannenberg, T.; Tamm, M., A modular approach to carbene-stabilized diphosphorus species. *Dalton Trans.* **2017**, *46*, 15859-15864.
222. Wang, Y.; Xie, Y.; Wei, P.; King, R. B.; Schaefer, H. F.; Schleyer, P. v. R.; Robinson, G. H., Carbene-Stabilized Diphosphorus. *J. Am. Chem. Soc.* **2008**, *130*, 14970-14971.
223. Wang, Y.; Robinson, G. H., Carbene Stabilization of Highly Reactive Main-Group Molecules. *Inorg. Chem.* **2011**, *50*, 12326-12337.
224. Waters, J. B.; Everitt, T. A.; Myers, W. K.; Goicoechea, J. M., N-heterocyclic carbene induced reductive coupling of phosphorus tribromide. Isolation of a bromine bridged P–P bond and its subsequent reactivity. *Chem. Sci.* **2016**, *7*, 6981-6987.
225. Back, O.; Donnadiou, B.; Parameswaran, P.; Frenking, G.; Bertrand, G., Isolation of crystalline carbene-stabilized P<sub>2</sub>-radical cations and P<sub>2</sub>-dications. *Nat. Chem.* **2010**, *2*, 369-373.

226. Beil, A.; Gilliard, R. J.; Grützmacher, H., From the parent phosphinidene–carbene adduct NHC□PH to cationic P4-rings and P2-cycloaddition products. *Dalton Trans.* **2016**, *45*, 2044-2052.
227. Oehlke, E.; Kückmann, T.; Abram, U., Silver(I) Complexes of 1,3-Dialkyl-4,5-dimethylimidazol-2-ylidenes and their Use as Precursors for the Synthesis of Rhenium(V) NHC Complexes. *Z. Anorg. Allg. Chem.* **2007**, *633*, 830-834.
228. Patchett, R.; Chaplin, A. B., Coordination chemistry of a calix[4]arene-based NHC ligand: dinuclear complexes and comparison to  $\text{LiPr}_2\text{Me}_2$ . *Dalton Trans* **2016**, *45*, 8945-8955.
229. Chesnokov, G. A.; Topchiy, M. A.; Dzhevakov, P. B.; Gribanov, P. S.; Tukov, A. A.; Khrustalev, V. N.; Asachenko, A. F.; Nechaev, M. S., Eight-membered-ring diaminocarbenes bearing naphthalene moiety in the backbone: DFT studies, synthesis of amidinium salts, generation of free carbene, metal complexes, and solvent-free copper catalyzed azide–alkyne cycloaddition (CuAAC) reaction. *Dalton T* **2017**, *46* (13), 4331-4345.